Reconstructing abrupt, high-magnitude sea-level changes from near-field coastal environments

Thomas Lawrence

Thesis submitted for the degree of Doctor of Philosophy

Department of Geography

Durham University

October 2015

“One never notices what has been done;

one can only see what remains to be done”

Marie Curie, 1896

Reconstructing abrupt, high-magnitude relative sea-level changes from near-field coastal environments

Thomas Lawrence

Abrupt, high-magnitude sea-level changes pose a major challenge to society and have, in the past, been significant drivers of coastal change. Traditionally, sea-level reconstructions from near-field regions - those close to or strongly influenced by current or former ice masses - depict long-term, millennial-scale sea-level changes associated with low-amplitude ice-sheet histories. Types of abrupt sea-level change, including meltwater pulses, tsunamis and storms, are not well studied in near-field regions, but such areas have potential to provide a suitable context for recording and identifying evidence of abrupt sea-level change. For example, unusually high sedimentation rates due to the presence of glaciers might promote the development of high-resolution records, while a dominant glacio-isostatic adjustment signal might facilitate improved registration and identification of globally significant episodes of abrupt sea-level rise.

This thesis explores the efficacy of near-field regions in reconstructing abrupt sea-level change by using a combination of stratigraphic and dating methods at field sites in Scotland and Greenland. From southwest Scotland, a sub-centennially resolved, diatom-based sea-level reconstruction for the early Holocene constrains the timing and magnitude of three meltwater-induced sea-level accelerations in the c. 500 yrs prior to the 8.2 kyr BP event. Despite an inability of the ^{14}C dating technique to confirm synchroneity of events, the three sea-level jumps overlap in age with other examples of abrupt change recorded in North Atlantic non-coastal and coastal archives, lending support to a three-event model of meltwater release from the Laurentide Ice Sheet as the driving mechanism responsible for the 8.2 kyr BP event.

In Greenland, nearshore and freshwater stratigraphic records contain evidence of landslide- and iceberg-induced tsunami events in the mid and late Holocene. Field sites in Vaigat (Disko Bugt, West Greenland) preserve evidence of five tsunami events in the past 1500-2000 years, which is comparable to tsunami recurrence intervals described from sites on large subduction zone margins. A coastal lake at Innaarsuit also provides the first reported sedimentary evidence of an iceberg-generated tsunami in the mid Holocene. The thesis concludes by reflecting on the opportunities and challenges in reconstructing abrupt sea-level change from near-field settings.

Table of Contents

List of Figures

List of Tables

Declaration and copyright

I confirm that no part of the material presented in this thesis has previously been submitted by me or any other person for a degree in this or any other university. In all cases, where it is relevant, material from the work of others has been acknowledged.

Acknowledgements

At the top of the list is Antony Long. Antony provided the ideas, words of encouragement and humour that guided this thesis. Without his support, I would have learned less and branched-out less. From sitting on a lake in Greenland ("sounds like a polar bear swimming"), to a bar in Copenhagen ("they're only halves") to a nearly-missed flight, not to mention all the other quality advice you've provided along the way, thank you for everything. It really has been an immense pleasure.

I also thank my second supervisor Sarah Woodroffe. Sarah's serene calmness and guidance has been a great help, especially in the early phases of my PhD.

I thank the Durham members of staff for fruitful discussions. In particular, Jerry Lloyd, Dave Roberts, Ian Shennan, Jim Innes, Andreas Vieli, Pippa Whitehouse, Nick Rosser and Chris Stokes. Frank, Merv, Kathryn, Alison, Chris, Amanda and Neil have all been superb help within the lab. Thanks to those from outside of Durham, for contributing knowledge on all manner of topics. David Smith, Torbjorn Törnqvist, Sarah Bradley, Sophie Ward, James Wells, Eelco Rohling and Lauren Gregoire.

To international friends from INQUA; Matt Ryan, Adam Griggs, Len Martin, Naomi Riggs and Craig Sloss.

Part of this work contributed to a wider research project funded by the Polish Ministry of Science, and for this I am indebted to Witek Szczuciński and Matt Strzelecki. Thanks for the opportunity and the memories.

There are many other people who have contributed their friendship and time along the way. Huge thanks to Scott - for endless trips to the Cree, coring when you hated it, and icicles on the tent. Cheers mate. Kettle, Bailey, Matt, Lanks, Sarah, Ben, Oliver, Ed, Tasha, Tim and Sarah Clarke. You've all been there for me, at the most important times.

To my former teachers and mentors. For guidance and direction during the early stages, when I could have chosen the wrong path; Alan Hadrill and Joanne Lukas. For helping me mature and develop self-belief; Roland Gehrels, Gerd Masselink and Neil Roberts.

Finally, to my family; Mum, Dad, Nan, Grandad, Gramps and Hannah.

Thank you all.

For Mary Elizabeth Horseman

Who planted the seed

1

Introduction

1.1 Introduction

The inextricable link between Earth's temperature and sea level is reflected in the close coupling of these two variables in long-term, 10^3 to 10^6 yr records (Grant et al., 2012; Rohling et al., 2014). Traditionally, deglacial and Holocene relative sea level (RSL) records have been used to infer low amplitude ice-sheet histories (e.g. Shennan et al., 2005) and models of glacio-isostatic adjustment (GIA) (e.g. Bradley et al., 2011; Kuchar et al., 2012; Whitehouse et al., 2012), yet high-magnitude (10^{-1} to 10^1 m-scale), abrupt (10^{-1} to 10^3 yr) episodes of sea-level rise (meltwater pulses) - attributed to rapid and/or nonlinear ice-sheet retreat (e.g. Weber et al., 2014; Gregoire et al., 2012) – are poorly understood features of deglacial and early Holocene RSL records (Fairbanks, 1989; Chappell and Polach, 1991; Bard et al., 1996; 2010, Deschamps et al., 2012; Hijma and Cohen, 2010; Li et al., 2011). Such events are widely considered to be major inducers of abrupt climate change given their ability to disrupt ocean density and circulation patterns (Broecker, 1994; McManus et al., 2004; Sierro et al., 2009). Amid recent and ongoing concerns of enhanced ice-sheet retreat (e.g. Carr et al., 2015; Khan et al., 2014; Paolo et al., 2015), rapid sea-level rise (Hay et al., 2015) and a possible weakening of the Atlantic Meridional Overturning Circulation (AMOC) (Boulton et al., 2014; Rahmstorf et al., 2015), reconstructing past episodes of high-magnitude sea-level change associated with ice-sheet instability is critical for unravelling ice-ocean-climate interactions and for assessing the potential likelihood and impact of similar future events (Dutton et al., 2015).

On even shorter timescales of minutes to hours, singularities of sea-level rise of a similar magnitude (10^{-1} to 10^1 m-scale) occur as a consequence of non ice-sheet processes, in particular tsunamis. However, existing tsunami reconstructions are almost exclusively restricted to locations distal to present and former glaciation centres (so-called "far-field" regions) where tsunamis are driven principally by tectonic processes (e.g. Atwater 1987; 1991; Jankaew et al., 2008; Garrett et al., 2014; Sieh et al., 2015). A small number of studies exist from active and once-active glacial environments (near-field regions) that describe evidence of historical- and palaeo-tsunamis and whose drivers have been attributed to non-tectonic processes, including iceberg roll events (Long et al., 2011), coastal mass movements (Pedersen et al., 2002; Dahl-Jensen et al., 2004) and submarine slides (Wagner et al., 2007; Romundset and Bondevik, 2011). More rigorous study of these distinct types of events is required to extend our knowledge of abrupt sea-level change to near-field areas. Of particular value are studies that develop criteria to interpret the processes responsible (e.g. storms, tsunami or different origin; Nelson et al., 1996; Peters and Jaffe, 2010). In the simplest terms, the most important criteria for interpreting whether a deposit has regional

significance is whether it can be laterally traced across sites with sufficient spatial and temporal precision.

The types of transient, abrupt sea-level changes described above are examples of how near-field processes can generate sea-level changes that are high-magnitude. The first was how episodes of ice-sheet instability can trigger meltwater pulses that rapidly accelerate the rate of eustatic sea-level rise, while the second relates to how near-field processes can drive abrupt singularities of sea-level rise (tsunamis) of local significance. Reconstructing both types of sea-level extremes is difficult because of a number of problems related to their reconstruction and, as a result, studies that document examples of such events are rare and not without problems, including in their fidelity to identify cause (discussed in Section 1.3).

1.2 Thesis rationale

The ultimate rationale behind this research is the requirement for improved reconstructions of abrupt sea-level change that originate in near-field settings. A holistic understanding of the processes that control sea-level change can be achieved by studying relative sea-level (RSL) changes across a broad range of spatial and temporal scales. Abrupt, high-magnitude events that originate in the near-field are poorly understood extremes, both temporally and spatially. Their reconstruction is important as societal impacts of sea-level change are more likely to be wrought out of the extremes, rather than as a consequence of changes in mean sea level (MSL) over several decades (IPCC AR5, 2014). For example, in October 2012, Hurricane Sandy caused an estimated $50 billion of damage and the direct deaths of 147 people (Blake et al., 2013). What is striking is that around 700 million people, or 10% of the world population, live within 10 m of contemporaneous mean sea level (Nicholls and Cazenave, 2010).

This thesis reconstructs two contrasting examples of high-magnitude RSL changes. The first had a global impact; in which ice-dammed proglacial lakes fronting the Laurentide Ice Sheet (LIS) drained suddenly in the early Holocene, contributing metre-scale meltwater pulses to the ocean which registered detectable imprints in coastal environments globally. These freshwater episodes also contributed to abrupt climate change during the early Holocene (the so-called ‘8.2 event’). The second example focuses on the local scale; investigating how abrupt near-field processes such as coastal mass movements and iceberg-roll events can drive local singularities of sea-level rise (tsunamis) in west Greenland during the mid Holocene to present. This latter study in particular requires an assessment of the

stratigraphic signatures of tsunami versus storms deposits in High Arctic settings. By investigating two contrasting but largely overlapping and relevant themes, I have addressed separately two significant gaps in understanding relating to the reconstruction of RSL changes in near-field areas, one working in an active paraglacial environment (Greenland) and the other in a long ice-free but paraglacial setting at the time period of interest (Scotland).

The section of this thesis that reconstructs examples of meltwater pulses (Chapter 2) is funded by a Durham Doctoral Award and builds on my MRes research. Roland Gehrels (York University) was my former MRes supervisor and has remained as an (unofficial) external supervisor throughout the duration of this thesis. The radiocarbon dating aspect of this project was supported by the NERC Radiocarbon Laboratory (allocation no. 1629.0312), with scientific advice provided by Dr. Charlotte Bryant. The Arctic tsunami element of this thesis (Chapters 3, 4 and 5) has benefited from a collaborative program of funded research with scientists from the Poznan University (Dr. Witold Szczuciński) and Wroclaw University (Dr. Mateusz Strzelecki), Poland, to which this thesis contributes. Funded by Polish National Science Centre grant 2011/01/B/ST10/01553, the principle aim of the Arctic tsunami project was to undertake field and laboratory investigations of sedimentary deposits from coastal lakes in west Greenland in order to assess the evidence for large waves (tsunamis) during the Holocene. In this thesis, I expand on the initial aim of the funded project by targeting nearshore depositional environments in west Greenland for evidence of tsunamis and storms, in addition to coastal lakes. I have acquired a broad range of skills related to the reconstruction of abrupt sea-level changes in the Arctic while working as a core member of this project team.

1.3 Background

1.3.1 Reconstructing abrupt RSL changes of global significance: meltwater pulses

Significant features of the last deglaciation are meltwater pulses, the most notable of which was first identified as a sea-level jump of ~20 m between ~14 to 13.5 kyr BP in Barbados corals (meltwater pulse 1A; MWP-1A) (Fairbanks, 1989). MWP-1A has been implicated in changes in ocean circulation and climate during the deglacial period given its apparent close coincidence with notable climatic events in ice-core records (e.g. Bard et al., 1996; 2000; Stanford et al., 2006; Weaver et al., 2003; Deschamps et al., 2012), yet its precise role in

forcing abrupt climate change remains unresolved in light of a number of issues. First, the paucity of deglacial sea-level records reflects the difficulty in accessing this period during a time of low sea level (>40 m below present). These archives are mostly located offshore within submerged coral reefs that, to gain access, require costly drilling programs. Second, in the few deglacial RSL records that exist, age discrepancies in the timing of MWP-1A have invoked two competing hypotheses relating to its precise origin, with some authors favouring a Laurentide Ice Sheet (LIS) source (Bard et al., 1996; Stanford et al., 2006) and others favouring an Antarctic Ice Sheet (AIS) source (e.g. Weaver et al., 2003; Deschamps et al., 2012). In particular, a Laurentide source is conceivable on the basis of evidence where MWP-1A is temporally well-aligned with the end of the Bølling-Allerød interstadial, implying that a freshwater perturbation of North Atlantic circulation brought about the end of the Bølling warm period (Stanford et al., 2006). In contrast the case for an Antarctic source is based on the evidence where MWP-1A is coeval with onset of the Bølling warming (e.g. Deschamps et al., 2012). This scenario supports the hypothesis that a freshwater pulse from Antarctica caused reduced overturning in the southern hemisphere and, via a bipolar seesaw mechanism, a subsequent strengthening of ocean circulation in the North Atlantic (Deschamps et al., 2012). Interestingly, recent GIA modelling has suggested that during MWP-1A the LIS contributed 10 m of eustatic sea-level equivalent while the AIS only 3 m (Gomez et al., 2015), which could explain why conventional sea-level studies have been unable to conclusively rule out either source. Third, corals are unable to constrain the precise magnitude of MWP-1A because they are limited as sea-level indicators by their relatively low vertical resolution (>5 m) (Yokoyama and Esat, 2015). Although sea-level fingerprinting theory predicts a non-uniform pattern of sea-level change in response to a point source of mass loss (Mitrovica et al., 2001; Tamisiea et al., 2003), the vertical constraints on the magnitude of MWP-1A are not precise enough to robustly test competing scenarios of meltwater origins defined by geophysical (fingerprint) models (Clark et al., 2002; Mitrovica et al., 2009). Overall, these factors reflect the difficulties associated with reconstructing a known meltwater pulse with conventional sea level reconstruction methods.

Although, understandably, the term ‘meltwater pulse’ has become synonymous with the 10^1-10^2 m-scale events that occurred during a time of significant global ice-cover (i.e. the deglacial), events of a similar abruptness albeit lower magnitude (10^{-1} to 10^1 m) have occurred during periods of substantially reduced global ice-volume configuration (e.g. Hijma and Cohen, 2010; Li et al., 2011). Interestingly, the role of these lower magnitude meltwater pulses in forcing abrupt climate change is thought to be as equally significant as their higher magnitude and older counterparts (Törnqvist and Hijma, 2012). Indeed, the early to mid Holocene is a potentially important time interval where sub-metre to metre-scale

events might provide better analogues of potential future sea-level change compared to the larger (tens of metre) events of the deglacial.

RSL records developed from basal peats have bridged the gap from the deglacial into the Holocene, providing the vertical precision necessary to track the few tens of metres of sea-level rise prior to the final cessation of Laurentide melt, dated by Carlson et al. (2008) to 6.8 ± 0.3 kyr BP. A critical time period is the centuries prior to 8.2 ka, when meltwater stored in proglacial lakes Agassiz and Ojibway (LAO) is widely thought to have drained abruptly into the Labrador Sea (e.g. Barber et al., 1999), recently dated to 8609-8489 cal yr BP by Jennings et al. (2015). This 'drainage event' likely reduced the formation of North Atlantic Deep Water (NADW) and resulted in climate cooling on a northern hemispheric scale, famously recognized as a sharp $\delta^{18}O_{ice}$ excursion centred on 8.2 ka in Greenland ice-core records (the '8.2 event') (e.g. Alley et al., 1997; Thomas et al., 2007). Thus, determining the precise magnitude and timing of the drainage event and other possible meltwater pulse(s) in the centuries prior to the 8.2 event have the potential to provide critical constraints for climate models in their attempt to disentangle the response of the thermohaline circulation to freshwater forcing.

Flood hydrograph simulations of LAO prior to its final drainage determined that it contained a volume of meltwater sizeable enough to have left a detectable imprint in RSL records (Clarke et al., 2004). RSL records thus provide a potential means to constrain the precise timing and magnitude of the drainage event and therefore its role in forcing the 8.2 event. To this end, two studies have attempted to address these aims with varying success, each using basal peats to track sea level. The first record is from the western Netherlands (Rhine-Meuse Delta), where Hijma and Cohen (2010) recognized a sea-level jump of 2.1 ± 1.8 m (2σ) between 8540 to 8200 cal yr BP. A second is from the southern USA (Mississippi Delta), where Li et al. (2011) inferred a sea-level jump of 0.33 ± 0.23 m (2σ) between 8310-8180 cal yr BP. After correction for gravimetric and geoidal effects by using geophysical modelling estimates of a Laurentide meltwater source (Kendall et al., 2008), the two jumps from opposing North Atlantic sites have the potential to be reconciled, but with the caveat (assumption) that the western Netherlands jump records two separate meltwater pulses or drainage events, while the southern USA record captures a final drainage event only (Li et al., 2011). Although there is a growing body of evidence to support a two-event model of LAO drainage (e.g. Teller et al., 2002; Ellison et al., 2006; Kleiven et al., 2008), the precise number, timing and magnitude of meltwater events prior to the 8.2 event has yet to be fully resolved, which reflects the (in-)ability of basal peats to decipher sub-centennial scale RSL changes of sub-metre to metre scale. Indeed, as the vertical growth range of basal peats can

be affected by factors other than sea level, it is "inherently difficult for basal peat sequences to record any falls or short-lived fluctuations in sea level; by their nature they record millennial-scale rising sea levels" (Gehrels and Shennan, 2015; p. 134).

Over the past two decades, a theme of work has developed using high resolution techniques to constrain the pattern and timing of sea level changes in the past few centuries, with a particular focus on determining the possible existence of a 20th century sea-level acceleration (e.g. Gehrels et al., 2005; 2008; 2012; Kemp et al., 2011; Barlow et al., 2014; Saher et al., 2015; Long et al., 2014). These high resolution reconstructions employ microfossils preserved within saltmarsh sediments as sea-level indicators, and in many cases have been validated by their ability to reproduce the trends observed in nearby tide gauge records with a typical precision of ± 0.2 m (e.g. Callard et al., 2011). In addition, saltmarsh sediments can generate continuously and often contain an abundance of dating material, aiding in the development of chronologies that are precise to the multi-decadal to sub-centennial level. These factors permit the development of past sea-level records from saltmarshes with excellent vertical (sub-decimetre) and chronological (multi-decadal) resolution.

A section of this thesis (Chapter 2) reconstructs sea level during the early Holocene using the high resolution techniques outlined above. In particular, I determine the timing and magnitude of sea-level jumps (meltwater pulses) in the centuries prior to the 8.2 event using high resolution techniques to reconstruct RSL. As noted above, our understanding of this period is limited because the two existing records from this time (Hijma and Cohen, 2010; Li et al., 2011) employ the basal peat methodology. The records have been largely unable to attain decimetre- to metre-scale vertical and sub-centennial scale chronological resolution; the precision required to identify meltwater pulses prior to the 8.2 event. This is the first time that high resolution microfossil techniques have been applied to address abrupt RSL change within the timeframe of the early Holocene, with the majority of microfossil-based reconstructions being restricted temporally to the mid-late Holocene.

The focus is on estuarine and saltmarsh deposits from the Cree Estuary, SW Scotland. The site benefits from a relatively slow rate of background (millennial-scale) RSL change at the time of interest and by an abundant sediment supply. The location of the new site is also helpful; geographically positioned between the US and Dutch investigations summarised above and predicted to experience an intermediate magnitude of RSL change associated with a RSL jump, with present estimates of the 8.2-related meltwater pulses fall within the range of 0.5-3.0 m. It remains to be seen whether estuarine and saltmarsh records can reconstruct RSL jumps of this magnitude. This thesis will investigate the efficacy of

near-field regions as archives of high-magnitude, abrupt meltwater-driven RSL changes.

1.3.1 Reconstructing abrupt RSL changes of local significance: Arctic tsunamis

Palaeotsunami studies are widely described in equatorial- to mid-latitudes where the majority of events reflect seismic activity or submarine landsliding (Minoura and Nakaya, 1991; Grauert et al., 2001; Hartley et al., 2001; Smith et al., 2004; Sawai et al., 2009; Goff et al., 2010b; De Martini et al., 2010; Ramirez-Herrera et al., 2009; Bondevik et al., 1997a). Polar regions, however, are understudied areas, despite the presence of ample tsunami sources, including coastal landslides (e.g. Dahl-Jensen et al., 2004, Pedersen et al., 2002), ice-berg capsize or 'roll' events (Levermann, 2011) and glacier calving (Amundson et al., 2008; 2010). These events potentially pose considerable risk to polar communities, the majority of which are situated at the coast. A key question is whether techniques developed in lower latitude settings are able to successfully reconstruct high-latitude tsunami and palaeotsunami (e.g. Atwater, 1987; Long and Shennan, 1994; Goff et al., 2011). Also critical is the ability to distinguish between potential storms and tsunami deposits as these are notoriously difficult to differentiate (e.g. Foster et al., 1991; Switzer et al., 2005; Morton et al. 2007).

On 21st November 2000 a large landslide (rock avalanche) occurred on the northern coast of the Vaigat Strait, a large palaeofjord in Disko Bugt. It caused severe damage to buildings in a village c. 30 km across the fjord and deposited icebergs up to 800 m inland and up to 40 m above sea level (Pedersen et al., 2002; Dahl-Jensen et al., 2004). Based on geomorphological mapping of landslide back-scars and deposits, Dahl-Jensen et al. (2004) found evidence of a further c. 13 large landslides since the mid Holocene. Four of these likely entered the fjord itself, and provide an estimated average frequency of 1-2 landslide-tsunami events per 1000 years (Dahl-Jensen et al., 2004). In west Greenland, RSL fell gradually to a lowstand between 4.0 to 2.0 kyr BP and has since been rising to present. The Vaigat example thus offers a potential opportunity to study the late Holocene stratigraphic record of multiple episodes of abrupt RSL change; appraising the depositional signatures of landslide- and iceberg-tsunami events, in addition to storm deposits (Chapters 3 and 4).

An integral part of tsunami studies involves the estimation of vertical run-up heights using geologic evidence. The magnitude of a tsunami provides important constraints on the amount of energy initially released at the source and provides insights into the

environmental impact at the coast as well as inundation extent. In west Greenland, large millennial-scale changes in RSL characterise the early to mid Holocene, often measured in tens of metres per thousand years (e.g. Long et al., 2011; 2012). Unlike for the late Holocene, a rapidly falling RSL would reduce the potential of a single stratigraphic sequence to record multiple stacked sequences of low frequency, high magnitude events. This is in contrast to low or mid latitude settings where several hundred to a thousand year histories of tsunami inundation are recorded in single boreholes or exposures (e.g. Hutchinson et al., 2000; Kelsey et al., 2005; Jankaew et al., 2008). However, it is possible that high rates of RSL change in near-field settings could benefit calculations of tsunami run-up, because the height of shoreline above RSL at a single point in time can be inferred from areas with well-resolved RSL histories. In this way, constraints on the age of a tsunami could indirectly constrain its associated magnitude. I explore this potential in assessing the evidence for a mid Holocene tsunami preserved within a coastal lake (isolation basin) sequence at Innaarsuit, south Disko Bugt (Chapter 5), which formed part of a previous investigation of millennial-scale RSL changes in the area (Long et al., 2003). In doing so, I demonstrate the importance of integrating both short- and long-term RSL observations in near-field sea-level studies.

1.4. Aims and objectives

The main aim of this thesis is to **reconstruct abrupt, high-magnitude sea-level changes from near-field settings.** It will address two sub-fields of sea-level reconstruction concerning the high-magnitude, but temporally distinct, decimetre-metre scale. The first reconstructs glacio-eustatic changes (meltwater pulses) on sub-centennial timescales. The second reconstructs singularities of RSL rise (at least in the geological sense) on the order of minutes to hours. The specific examples that I target are:

(1) southwest Scotland coastal environments (saltmarsh and estuarine deposits) for evidence of early Holocene meltwater pulses and;

(2) mid-late Holocene tsunamis and storms preserved in coastal environments in Disko Bugt, west Greenland.

Paraglacial conditions were being experienced by both areas at the timescales concerned (and still are in Disko Bugt). Ballantyne (2002; p. 1938) defines the term paraglacial to reflect "non-glacial earth surface processes, sediment accumulations, landforms, landsystems and landscapes that are directly controlled by glaciation and

deglaciation". In Scotland, the late glacial ice-cap had fully retreated by 14 kyr BP (e.g. Everest et al., 2006; Ballantyne et al., 2009b; Clark et al., 2010), while in west Greenland, ice had withdrawn from Disko Bugt by 9 kyr BP (e.g. Long et al., 2011). The eventual relaxation of a paraglacial system to an equilibrium state typically takes several thousand years (Ballantyne, 2002).

In order to achieve the aim outlined above, the primary objectives were:

- To determine; using litho-, bio- and chronostratigraphy of raised salt-marsh and estuarine deposits, the timing and magnitude of sea-level changes in the Cree Estuary, SW Scotland, between a critical time period of 9000 to 8000 cal yr BP.
- To compare the timing and magnitude of sea-level changes in the Cree record with those in a range of coastal and non-coastal archives from around the globe, in order to assess the drivers responsible for such changes.
- To search for evidence of abrupt singularities of RSL rise (storm events, iceberg- and landslide-generated tsunami) using litho-, bio- and chronostratigraphy of coastal lakes and nearshore sedimentary sequences in west Greenland.
- To assess whether the patterns and signatures of deposition associated with abrupt RSL change in west Greenland can be used to infer driving (source) mechanisms.
- To reflect on the opportunities and challenges with regards to reconstructing abrupt RSL change in near-field settings and identify future research directions.

1.5 Chapter synopsis

The research presented in this thesis is presented in paper format. Each paper (chapter) represents a complete study, which reconstructs examples of abrupt sea-level change and whose origins lie in the near-field. The following sections of this chapter provide a synopsis of the chapters presented in this thesis.

1.5.1 Chapter 2: Relative sea-level data from southwest Scotland constrain meltwater-driven sea-level jumps prior to the 8.2 kyr BP event

This chapter presents a version of the first-author paper that is in review with *Quaternary Science Reviews*, co-authored by Antony J. Long (Durham University), W. Roland Gehrels (York University) and David E. Smith (Oxford University) and titled: "Relative sea-level

data from southwest Scotland constrain meltwater-driven sea-level jumps prior to the 8.2 kyr BP event".

The chapter presents a high resolution RSL record from the Cree Estuary, SW Scotland, which is sub-centennially resolved for the period 8.8 to 7.8 kyr BP. It contains three decimetre- to metre-scale episodes of enhanced sea-level rise, or sea-level jumps, occurring within the c. 500 yrs prior to the 8.2 event. I find that the timing of these RSL steps correlate closely with a variety of short-lived events expressed in North Atlantic proxy climate and oceanographic records, which I propose provides evidence of three distinct episodes of enhanced LIS meltwater discharge prior to the 8.2 event. The results presented in this chapter can be used to test the fidelity of both climate and ice-sheet models in simulating abrupt change during the early Holocene.

I undertook all field and laboratory investigations of sediments from the Cree Estuary, SW Scotland. I processed all samples at Durham University. Radiocarbon dating was performed by staff at the NERC SEURC radiocarbon facility on samples that I pre-prepared (picked, washed, and stored) at Durham University. I wrote the manuscript and compiled the figures; improved by comments of Long, Gehrels and Smith.

1.5.2 Chapter 3: Stratigraphic record of late Holocene tsunamis, Vaigat, west Greenland

This chapter presents a version of the first-authored paper to be submitted for publication to *Quaternary Science Reviews*, co-authored by Antony J. Long (Durham University) and Witold Szczuciński (Poznan University) and titled: "Stratigraphic record of late Holocene tsunamis, Vaigat, west Greenland".

The chapter presents the first record of near-field abrupt sea-level changes in the form of tsunamis from Greenland, using nearshore sedimentary sequences. It contains evidence of a maximum five tsunami events within the past 1000 to 1500 yrs, implying a maximum mean occurrence of 1 tsunami event per 250 yrs. This estimate is close to average tsunami and earthquake recurrence intervals inferred along the Earth's major subduction zones. I reflect on the wider implications of this work in understanding/reconstructing abrupt near-field sea-level changes (i.e. tsunamis) in active glacial environments. A key finding is that developing records of tsunami inundation is challenging in this high latitude environment as tsunami deposits are characteristically variable, thin, poorly preserved and reworked by post-depositional processes. It is difficult to apply criteria for the identification

of tsunami deposits developed in lower latitude settings to this example of a high latitude nearshore environment. This will likely have implications for the reconstruction of similar events elsewhere in the Arctic.

Field investigations for this work were conducted with Long and Szczuciński. I conducted laboratory investigations at Durham University. Radiocarbon dating was performed by staff at the Poznan radiocarbon facility on samples that I pre-prepared (picked, washed, and bottled) at Durham University. I wrote the manuscript; improved by the comments of Long and Szczuciński.

1.5.3 Chapter 4: Arctic coastal lake yields a c. 2000 yr history of landslide-tsunamis, Vaigat, west Greenland

This chapter presents a version of the paper submitted for publication and in review with *Journal Quaternary Science*, in a paper titled: "Arctic coastal lake yields a c. 2000 yr landslide-tsunami history, Vaigat, west Greenland".

Using a combination of litho-, bio- and chronostratigraphic techniques, I present a c. 2000 yr record of tsunami inundation from a coastal lake situated c. 5 m above present sea level. The paper reflects on the characteristics of tsunami deposition and the potential connection between coastal mass movements and climatic influences in Vaigat. I conducted laboratory analyses at Durham University and pre-prepared (picked) samples for ^{14}C dating. I wrote the manuscript, improved by the comments of Long and Szczuciński.

1.5.4 Chapter 5: Sedimentary evidence for a mid Holocene iceberg-generated tsunami in a coastal lake, west Greenland

This chapter presents a detailed re-appraisal of an anomalous sand horizon that is recorded within a coastal lake from Greenland, shortly following its isolation from the sea during the mid-Holocene. Using stratigraphic criteria developed from Norwegian coastal lakes associated with the Storegga tsunami (Bondevik et al., 1997b), we attribute the deposit to a tsunami that we propose was generated by a local iceberg roll. The paper reflects on the potential of iceberg roll-generated tsunami as a potential source of tsunami in polar regions, especially in semi-enclosed fjord areas where iceberg abundance is high.

Original field investigations for this Chapter were undertaken by Long in 1999. I completed additional microfossil (diatom) analysis of the original sample core, while new radiocarbon dating and grain-size analysis was completed by Szczuciński. Long wrote the paper, with input from myself and Szczuciński. The paper has been accepted for publication in the journal *Arktos* (doi: 10.1007/s41063-015-0007-7), titled "Sedimentary evidence for a mid Holocene iceberg-generated tsunami, west Greenland".

1.5.6 Chapter 6: Discussion

Chapter 6 synthesises the findings of the previous four chapters, reflecting on the opportunities and challenges provided by near-field sedimentary records for establishing the evidence for, and significance of, short-term abrupt changes in near-field RSL. Though based on the four papers that comprise the core of this thesis, the Chapter also includes selective new analysis and discussion of chronological issues, notably pertaining to the chronology of the Storegga tsunami. The focus of the Chapter is on assessing the potential of near-field stratigraphic records for providing insights into the driving mechanisms of local to global processes.

1.5.7 Chapter 7: Conclusions

Chapter 7 summarises the main findings of the thesis, reflecting on the extent to which the original aims and objectives have been achieved and identifying future research opportunities.

References

Alley, R. B., P. A. Mayewski, T. Sowers, M. Stuiver, K. C. Taylor, and P. U. Clark (1997), Holocene climatic instability: A prominent, widespread event 8200 yr ago, *Geology* 25, 483–486.

Amundson J.M., Fahnestock M., Truffer M., Brown J., Lüthi M.P., Motyka R.J.. 2010. Ice mélange dynamics and implications for terminus stability, Jakobshavn Isbræ, Greenland. J Geophys Res 115, DOI: 10.1029/2009JF001405.

Amundson J.M., Truffer M., Lüthi M.P., Fahnestock M., West M., Motyka R.J. 2008. Glacier, fjord, and seismic response to recent large calving events, Jakobshavn Isbra, Greenland. Geophys Res Lett 35, L22501, 10.1029/2008GL035281.

Atwater, B.F. 1987. Evidence for great Holocene earthquakes along the outer coast of Washington State. Science 236, 4804, 942-944.

Atwater, B.F., Stuiver, M., Yamaguchi, D.K. 1991. Radiocarbon test of earthquake magnitude at the Cascadia subduction zone. Nature 353, 156-158.

Jankaew, K., Atwater, B.F., Sawai, Y., Choowong, M., Charoentitirat, T., Martin, M.E., Prendergast, A. 2008. Medieval forewarning of the 2004 Indian Ocean tsunami in Thailand 455, 1228-1231. doi:10.1038/nature07373.

Barber, D.C., Dyke, A., Hillaire-Marcel, C., Jennings, A.E., Andrews, J.T., Ker- win, M.T., Bilodeau, G., McNeely, G., Southon, J., Morehead, M.D., and Gagnon, J.-M. 1999. Forcing of the cold event of 8,200 years ago by catastrophic drainage of Laurentide lake: *Nature* 400. 344–348, doi: 10.1038/22504.

Bard, E., Hamelin, B., Arnold, M., Montaggioni, L., Cabioch, G., Faure, G., Rougerie, F. 1996. Deglacial sea-level record from Tahiti corals and the timing of global meltwater discharge. Nature 282, 241-244.

Bard, E., Hamelin, B., Delanghe-Sabatier, D. 2010. Deglacial meltwater pulse 1B and Younger Dryas sea levels revisited with boreholes at Tahiti. Science, 327, 5970, 1235-1237.

Barlow, N.L.M., Long, A.J., Saher, M.H., Gehrels, W.R., Garnett, M.H., Scaife, R.G. 2014. Salt-marsh reconstructions of relative sea-level change in the North Atlantic during the last 2000 years. Quaternary Science Reviews 99, 1-16.

Blake, E.S., Kimberlain, T.B., Berg, R.J., Cangialosi, J.P., Beven II, J.L. 2013. (AL182012) Hurricane Sandy, Tropical Cyclone Report, National Hurricane Centre. [Accessed online: 06.06.15, http://www.nhc.noaa.gov/data/tcr/AL182012_Sandy.pdf].

Bondevik, S., Svendsen, J.I., Mangerud, J. 1997a. Tsunami sedimentary facies deposited by the Storegga tsunami in shallow marine basins and coastal lakes, western Norway. Sedimentology, 44, 1115–1131.

Bondevik, S., Svendsen, J.I., Johnsen, G., Mangerud, J., Kaland, P.E., 1997b. The Storegga tsunami along the Norwegian coast, age and runup. Boreas 26, 29–53.

Boulton, C. A., Allison, L.C., Lenton, T.M. 2014. Early warning signals of Atlantic Meridional Overturning Circulation collapse in a fully coupled climate model. *Nature Communications.* 5: 5752.

Bradley, S.L., Milne, G.A., Shennan, I., and Edwards, R. 2011. An improved Glacial Isostatic Adjustment model for the British Isles, *Journal of Quaternary Science* 26, 5, 541-552.

Broecker, W.S. 1994. Massive iceberg discharges as triggers for global climate change. Nature 372, 421-424.

Callard, S.L., Gehrels, W.R., Morrison, B.V. & Grenfell, H.R. Suitability of salt-marsh foraminifera as proxy indicators of sea level in Tasmania. *Marine Micropaleontology*. 2011;79:121.

Carlson, A.E., LeGrande, A.N., Oppo, D.W., Came, R.E, Schmidt, G.A., Anslow, F.S., Licciardi, J.M., Obbink, E.Z. 2008. Rapid early Holocene deglaciation of the Laurentide Ice Sheet. Nature Geoscience 1, 620-624.

Carr .J.R., Vieli, A., Stokes, C.R., Jamieson, S.S.R., Palmer, S.J., Christoffersen, P., Dowdeswell, J.A., Nick, F.M., Blankenship, D.D., Young, D.A. Basal topographic controls on rapid retreat of Humboldt Glacier, northern Greenland. *Journal of Glaciology* 2015, 61(225), 137-150.

Chappell, J., Polach, H. 1991. Post-glacial sea-level rise from a coral record at Huon Peninsula, Papua New Guinea *Nature* 349, 147 – 149.

Clark, P.U., Mitrovica, J.X., Milne, G.A., Tamisiea, M.E. 2002. Sea-level fingerprinting as a direct test for the source of global meltwater pulse 1A. Science 295, 2438-2441.

Clarke, K.C., Leverington, D.W., Teller, J.T., Dyke, A.S. 2004. Palaeohydraulics of the last outburst flood from glacial Lake Agassiz and the 8200 BP cold event. Quaternary Science Reviews 23, 389-407.

Dahl-Jensen, T., Larsen, L.M., Pedersen, S.A.S., Pedersen, J., Jepsen, H.F., Pedersen, G.K., Nielsen, T., Pedersen, A.K., Platen-Hallermund, F.V., Weng, W. 2004. Landslide and tsunami 21 November 200 in Paatuut, West Greenland. *Natural Hazards*, 31, 277-287.

De Martini, P.M., Barbano, M.S., Smedile, A., Gerardi, F., Pantosti, D., Del Carlo, P., Pirrotta, C., 2010. A unique 4000 year long geological record of multiple tsunami inundations in the Augusta Bay (eastern Sicily, Italy). Marine Geology 276, 42–57.

Deschamps, P., Durand, N., Bard, E., Hamelin, B., Camoin, G., Thomas, A.L., Henderson, G., Okuno, J., Yokoyama, Y. 2012. Ice-sheet collapse and sea-level rise at the Bølling warming 14,600 years ago. Nature 483, 559-583.

Dutton, A., Carlson, A.E., Long, A.J., Milne, G.A., Clark, P.U., DeConto, R., Horton, B.P., Rahmstorf, S., Raymo, M.E. 2015. Sea-level rise due to polar ice-sheet mass loss during past warm periods, Science 349, 6244, DOI: 10.1126/science.aaa4019.

Ellison, C.R.W., Chapman, M.R., and Hall, I.R. 2006. Surface and deep ocean interactions during the cold climate event 8200 years ago. *Science* 312, 1929–1932, doi: 10.1126/science.1127213.

Fairbanks, R.G. 1989. A 17,000-year glacio-eustatic sea level record: influence of glacial melting rates on the Younger Dryas event and deep-ocean circulation. Nature 342, 637-641.

Foster I.D.L., Dawson A.G., Dawson S., Lees J., Mansfield L. 1993. Tsunami sedimentation sequences in the Scilly Isles, southwest England. Science of Tsunami Hazards 11, 35-46.

Garrett, E., Shennan, I., Woodroffe, S.A., Cisternas, M., Hocking, E.P., Gulliver, P. 2014. Reconstructing paleoseismic deformation, 2: 1000 years of great earthquakes at Chucalen, south central Chile. Quaternary Science Reviews, 113, 112-122.

Gehrels W.R., Kirby J.R., Prokoph A., *et al.* 2005. Onset of recent rapid sea-level rise in the western Atlantic Ocean. *Quaternary Science Reviews* 24: 2083–2100.

Gehrels, W.R. & Shennan, I. 2015. Sea level in time and space: revolutions and inconvenient truths. Journal of Quaternary Science 30, 2, 131-143.

Gehrels, W.R., Callard, S.L., Moss, P.T., Marshall, W.A., Blaauw, M., Hunter, J., Milton, A., Garnett, M.H. 2012. Nineteenth and twentieth century sea-level changes in Tasmania and New Zealand.

Earth and Planetary Science Letters 315-316, 94-102.

Gehrels, W.R., Hayward, B.W., Newnham, R.M., Southall, K.E. 2008. A 20th century acceleration of sea-level rise in New Zealand. Geophysical Research Letters 35, L02717.

Goff, J., Catherine, Chagué--Fogg, Nichol, S., Jaffe, B., Dominey-Howes, D. 2011. Progress in palaeotsunami research. Sedimentary Geology 243-244, 70-88.

Goff, J., Nichol, S.L., Chagué-Goff, C., Horrocks, M., McFadgen, B., Cisternas, M., 2010b. Predecessor to New Zealand's largest historic trans-South Pacific tsunami of 1868 AD. Marine Geology 275, 155–165.

Grant, K.M., Rohling, E.J., Bar-Matthews, M., Ayalon, A., Medina-Elizalde, M., Bronk-Ramsey, C., Satow, C., Roberts, A.P. 2012. Rapid coupling between ice volume and polar temperature over the past 150,000 years, *Nature*, 491, 744-747.

Grauert, M., Bjo¨rck, S. & Bondevik, S. 2001. Storegga tsunami deposits in a coastal lake on SuDuroy, the Faroe Islands. *Boreas*, 30, 263–271.

Gregoire, L. J., Payne, A. J., Valdes, P. J. 2012. Deglacial rapid sea level rises caused by ice-sheet saddle collapses, *Nature* 487, 219–222.

Hartley, A., Howell, J., Mather, A.E., Chong, G., 2001. A possible Plio-Pleistocene tsunami deposit, Hornitos, northern Chile. Revista Geologica de Chile 28, 117–125.

Hay, C.C., Morrow, E., Kopp., R.E., Mitrovica, J.X. 2015. Probabilistic reanalysis of twentieth-century sea-level rise. Nature 517, 481-484.

Hijma, M.P and Cohen, K.M. 2010. Timing and magnitude of the sea-level jump precluding the 8200 yr event, *Geology* 38, 3, 275-278.

Hutchinson, I., Guilbault, J.P., Clauge, J.J., Borbrowski, P.T. 2000. Tsunamis and tectonic deformation at the northern Cascadia margin: a 3000 year record from Deserted Lake, Vancouver Island, British Columbia, Canada. *The Holocene* 10(4), 429-439.

IPCC, 2014: Climate Change 2014: Synthesis Report. Contribution of Working Groups I, II and III to the Fifth Assessment Report of the Intergovernmental Panel on Climate Change [Core Writing Team, R.K. Pachauri and L.A. Meyer (eds.)]. IPCC, Geneva, Switzerland, 151 pp.

Jennings, A., Andrews, J., Pierce, C., Wilson, L., Olfasdotttir, S. 2015. Detrital carbonate peaks on the Labrador shelf, a 13e7 ka template for freshwater forcing from the Hudson Strait outlet of the Laurentide Ice Sheet into the subpolar gyre, *Quaternary Science Reviews* 107, 62-80. http://dx.doi.org/10.1016/j.quascirev.2014.10.022.

Kelsey, H.M., Nelson, A.R., Hemphill-Haley, E., Witter, R.C. 2005. Tsunami history of an Oregon coastal lake reveals a 4600 yr record of great earthquakes on the Cascadia subduction zone. *Geological Society of America Bulletin* 117(7-8), 1009-1032, doi: 10.1130/B25452.1.

Kemp, A.C., Horton, B.P., Donnelly, J.P., Mann, M.E., Vermeer, M., Rahmstorf, S. 2011. Climate related sea-level variations over the past two millennia. Proceedings of the National Academy of Sciences 108, 27, 11017-11021.

Kendall, R.A, Mitrovica, J.X., Milne, G.A., Tornqvist, T.E. and Li, Y.X. 2008. The sea-level fingerprint of the 8.2 ka event, *The Geological Society of America* 35, 5, 423-426.

Khan, S.A., Kjær, K.H., Bevis, M., Bamber, J.L., Wahr, J., Kjeldsen, K.K., Bjørk, A.A., Korsgaard, N.J., Stears., L.A., van den Broeke, M.R., Liu, L., Larsen, N.K., Muresan, I.S. 2014. Sustained mass loss of the northeast Greenland ice sheet triggered by regional warming, Nature Climate Change 4, 292-299.

Kleiven, H.F., Kissel, C., Laj, C., Ninnemann, U.S., Richter, T.O., Cortijo, E. 2008. Reduced North Atlantic deep water coeval with the glacial Lake Agassiz Freshwater Outburst. *Science* 319, 5859, 60-64.

Kuchar, J., Milne, G., Hubbard, A., Patton, H., Bradley, S., Shennan, I., and Edward, R. 2012. Evaluation of a numerical model of the British-Irish ice sheet using relative sea-level data: implications for the interpretation of trimline observations, *Journal Quaternary Science* 27, 6, 597-605.

Levermann, A. 2011. When glacial giants roll over. Nature 472, 43-44.

Li, Y.X., Tornqvist, T.E., Nevitt, J.M., and Kohl, B. 2011. Synchronizing a sea-level jump, final lake Agassiz drainage and abrupt cooling 8200 years ago, *Earth and Planetary Science Letters* 315-316, 41-50.

Long, A.J. & Shennan, I. Sea-Level Changes in Washington and Oregon and the "Earthquake Deformation Cycle. *Journal of Coastal Research* 10, 4, 825-838.

Long, A.J., Barlow, N.L.M., Gehrels, W.R., Saher, M.H., Woodworth, P.L., Scaife, R.G., Brain, M.J. & Cahill, N. 2014. Contrasting records of sea-level change in the eastern and western North Atlantic during the last 300 years. *Earth and Planetary Science Letters* 388, 110-122.

Long, A.J., Strzelecki, M., Lloyd, J.M. & Bryant, C. 2012. Dating High Arctic Holocene relative sea level changes using juvenile articulated marine shells in raised beaches. *Quaternary Science Reviews* 48, 61-66.

Long, A.J., Woodroffe, S.A., Roberts, D.H., Dawson, S. 2011 Isolation basins, sea-level changes and the Holocene history of the Greenland Ice Sheet. *Quaternary Science Reviews* 30, 3748-3768.

McManus, J.F., Francois, R., Gherardi, J.M., Keigwin, L.D., Brown-Leger, S. 2004. Collapse and rapid resumption of Atlantic meridional circulation linked to deglacial climate changes. Nature 428, 834-837.

Minoura, K. and Nakaya, S., 1991. Traces of tsunami preserved in inter-tidal lacustrine and marsh deposits: some examples from northeast Japan. J. Geol., 99: 265-287.

Mitrovica, J.X., Gomez, N., Clark, P.U. 2009. The sea-level fingerprint of West Antarctic collapse, *Science* 323, 753.

Mitrovica, J.X., Tamisiea, M.E., Davis, J.L., Milne, G.A. 2001. Recent mass balance of polar ice sheets inferred from patterns of global sea-level change, *Nature* 409, 1026-1029.

Morton, R.A., Gelfenbaum, G., Jaffe, B.E., 2007. Physical criteria for distinguishing sandy tsunami and storm deposits using modern examples. Sedimentary Geology 200, 184-207.

Nicholls, R.J., Cazenave, A. 2010. Sea-level rise and its impact on coastal zones. Science 328, 1517-1520.

Nelson, A.R., Shennan, I., Long, A.J. 1996. Identifying coseismic subsidence in tidal-wetland stratigraphic sequences at the Cascadia subduction zone of western North America. *Journal of Geophysical Research* 101(B3), 6115-6135.

Paolo, F.S., Fricker, H.A., Padman, L. 2015. Volume loss from Antarctic ice shelves is accelerating. Science, 348, 6232, 327-331.

Pedersen, S.A.S., Larsen, L.M., Dahl-Jensen, T., Jepsen, H.F., Pedersen, G.P., Nielsen, T., Pedersen, A.K., Platen-Hallermund, F.V., Weng, W. 2002. Tsunami-generating rock fall and landslide on the south coast of Nuussuaq, central West Greenland. *Geology of Greenland Survey Bulletin* 191, 73-83.

Peters, R. & Jaffe, B.E., 2010. Identification of tsunami deposits in the geologic record; developing criteria using recent tsunami deposits: U.S. Geological Survey Open-File Report 2010-1239, 39 p. [http://pubs.usgs.gov/of/2010/1239/].

Ramírez-Herrera, M.-T., Cundy, A.B., Kostoglodov, V., Ortiz, M., 2009. Late Holocene tectonic land-level changes and tsunamis at Mitla lagoon, Guerrero, Mexico. Geofísica Internacional 48, 195–209.

Rohling, E.J., Foster, G.L., Grant, K.M., Marino, G., Roberts, A.P., Tamisiea, M.E. and Williams, F. 2014. Sea-level and deep-sea temperature variability over the past 5.3 million years, *Nature* 508, 477-482.

Romundset, A., Bondevik, S., 2011. Propagation of the Storegga tsunami into ice-free lakes along the southern shores of the Barents Sea. *Journal of Quaternary Science* 26, 457-462.

Saher, M.H., Gehrels, W.R., Barlow, N.L.M., Long, A.J., Haigh, I.D. & Blaauw, M. Sea-level changes in Iceland and the influence of the North Atlantic Oscillation during the last half millennium. 2015. *Quaternary Science Reviews* 108, 23-36.

Sawai, Y., Kamataki, T., Shishikura, M., Nasu, H., Okamura, Y., Satake, K., Thomson, K.H., Matsumoto, D., Fujii, Y., Komatsubara, J., Aung, T.T. 2009. Aperiodic recurrence of geologically recorded tsunamis during the past 5500 years in eastern Hokkaido, Japan. Journal of Geophysical Research, 114, B01319.

Shennan, I., Hamilton, S., Hillier, C., Woodroffe, S. 2005. A 16,000 yr record of near-field RSL changes, northwest Scotland, United Kingdom. *Quaternary International*, 133-134, 95-106.

Sieh, K., Daly, P., McKinnon, E.E., Pilarczyk, J.E., Chiang, H-W., Horton, B., Rubin, C., Shen, C-C., Ismail., N., Vane, C., Feener, R.M. 2015. Penultimate predecessors of the 2004 Indian Ocean tsunami in Aceh, Sumatra: Stratigraphic, archeological, and historical evidence. Journal of Geophysical Research: Solid Earth,120, 1, 308–325.

Sierro, F.J., Andersen, N., Bassetti, M.A., Berné, S., Canals, M., Curtis, J.H., Dennielou, B., Flores, J.A., Frigola, J., Gonzalez-Mora, B., Grimalt, J.O., Hodell, D.A., Jouet, G., Pérez-Folgado, M., Schneider, R., 2009. Phase relationship between sea level and abrupt climate change. Quaternary Science Reviews 28, 2867-2881.

Smith, D.E., Shi, S., Cullingford, R.A., Dawson, A.G., Dawson, S., Firth, C.R., Foster, I.D.L., Fretwell, P.T., Haggart, B.A., Holloway, L.K., Long, D. 2004. The Holocene Storegga slide tsunami in the United Kingdom. Quaternary Science Reviews 23, 2291-2321.

Stanford, J.D., Rohling, E.J., Hunter, S.E., Roberts, A.P., Rasmussen, S.O., Bard, E., McManus, J., Fairbanks, R.G. 2006. Timing of meltwater pulse 1a and climate responses to meltwater injections. Paeleoceanography 21, PA4103.

Tamisiea ME, Mitrovica JX, Milne GA, Davis JL. 2003. Long wave length sea level and solid surface perturbations driven by polar ice mass variations: fingerprinting Greenland and Antarctic Ice Sheet flux. *Space Science Reviews* (108) 81–93.

Teller, J. T., Leverington, D. W. & Mann, J. D. 2002. Freshwater outbursts to the oceans from glacial Lake Agassiz and their role in climate change during the last deglaciation. *Quaternary Science Reviews* 21, 879–887.

Thomas, E.R., Wolff, E.W., Mulvaney, R., Steffensen, J.P., Johnsen, S.J., Arrowsmith, C., White, J.W.C., Vaughn, B., Popp, T. 2007. The 8.2 ka event from Greenland ice cores. *Quaternary Science Reviews* 26, 1-2, 70-81.

Törnqvist, T.E., Hijma, M.P. 2012. Links between early Holocene ice-sheet decay, sea-level rise and

abrupt climate change, *Nature Geoscience* 5, 601-606. DOI: 10.1038/NGEO1536.

Wagner, B., Bennike, E, O., Klug, M., Cremer, H. 2007. First indication of Storegga tsunami deposits from East Greenland. *Journal of Quaternary Science* 22(4), 321-325.

Weaver, A.J., Saenko, O.A., Clark, P.U., Mitrovica, J.X. 2003. Meltwater Pulse 1A from Antarctica as a trigger of the Bølling-Allerød warm interval. Science 299, 1709-1713.

Weber, M.E., Clark, P.U., Kuhn, G., Timmerman, D., Sprenk, D., Gladstone, R., Zhang, X., Lohmann, G., Menviel., L., Chikamoto, T., Friedrich, T., Ohlwein, C. 2014. Millennial-scale variability in Antarctic ice-sheet discharge during the late deglaciation, Nature, 510, 134-138.

Whitehouse, P.L., Bentley, M.J. & Le Brocq, A.M. 2012. A deglacial model for Antarctica: geological constraints and glaciological modelling as a basis for a new model of Antarctic glacial isostatic adjustment. *Quaternary Science Reviews* 32, 1-24.

Yokoyama & Esat, 2015. Coral reefs. In: Shennan, I., Long, A.J., Horton, B.P. (eds.). Handbook of Sea Level Research. John Wiley & Sons. London.

2

Relative sea-level data from southwest Scotland constrain meltwater-driven sea-level jumps prior to the 8.2 kyr BP event

This chapter is under review with Quaternary Science Reviews (paper titled as above). I am lead author. It is co-authored by Roland Gehrels of York University, Antony Long of Durham University and David Smith of Oxford University.

1. Introduction

A prominent climate anomaly is centred on 8200 yr BP in Greenland ice-core records (Figs. 2.1 and 2.2) and is registered as an abrupt cooling of ~3.3 ± 1.1 °C that lasted for 160 yrs (Kobashi et al., 2007; Thomas et al., 2007). The widely cited (e.g. Alley et al., 1997; De Vernal et al., 1997; Barber et al., 1999; Törnqvist and Hijma, 2012) causal mechanism of the event is a weakening or complete shutdown of the Atlantic Meridional Overturning Circulation (AMOC) in response to the sudden drainage of Laurentide proglacial Lakes Agassiz and Ojibway (LAO) dated to 8740-8160 cal yr BP (1σ age range) in the Hudson region (Barber et al., 1999). However, it is unclear whether the drainage occurred as a standalone freshwater pulse or as several separate events. Indeed, climate modelling studies based on a single freshwater pulse of 2.5 Sv for one year (Sverdrup, 1.0 = 10^6 x m^3 s^{-1}) fail to simulate the observed 8.2 climatic response (Morrill et al., 2014) using a median estimate of forcing inferred from flood hydrograph simulations of LAO drainage (Clarke et al., 2004).

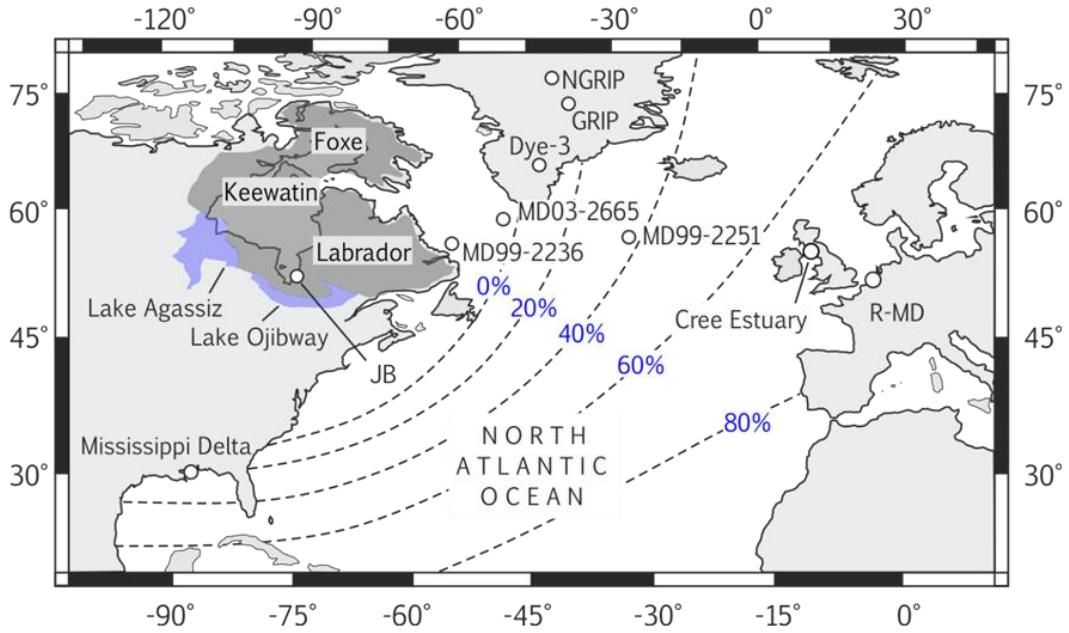

Figure 2.1 Map of circum-North Atlantic with key locations mentioned in text. Blue and dark grey shading indicates the approximate extent of Laurentide Ice Sheet and proglacial lakes Agassiz and Ojibway at ~8900 cal yr BP (after Dyke, 2004). Lines denote the spatial variability of RSL rise associated with a Laurentide source of meltwater release inferred from GIA modelling (after Kendall et al., 2008). JB = James Bay. R-MD = Rhine-Meuse Delta. The percentage contours indicate the sea-level fingerprint associated with a Laurentide source of freshwater release.

A growing body of empirical and modelling evidence is beginning to support a multi-event model of LAO drainage (Leverington et al., 2002) and/or nonlinear Laurentide Ice Sheet (LIS) collapse within a critical time interval (hereby referred to as 8900 to 8200 cal yr BP). Pronounced two-step increases in planktonic $\delta^{18}O$ and polar foraminifera abundance (*Neogloboquadrina pachyderma* s.) occur in two sub-polar North Atlantic cores, MD99-2251 and MD03-2665, situated 1250 km apart, that are interpreted as two episodes of increased surface ocean freshening and cooling within this time interval (Fig. 2.2; Ellison et al., 2006; Kleiven et al., 2008). Hematite-rich glaciolacustrine sediments in the Hudson region (the "red-bed") widely thought to represent the stratigraphic signature of LAO drainage (e.g. Barber et al., 1999; Hillaire-Marcel et al., 2007), contain two peaks of terrestrially-sourced detrital carbonate (Hillaire-Marcel et al., 2007) and two stacked sequences of reverse to normal graded sediments which could record two separate drainage events (Lajeunesse and St-Onge, 2008).

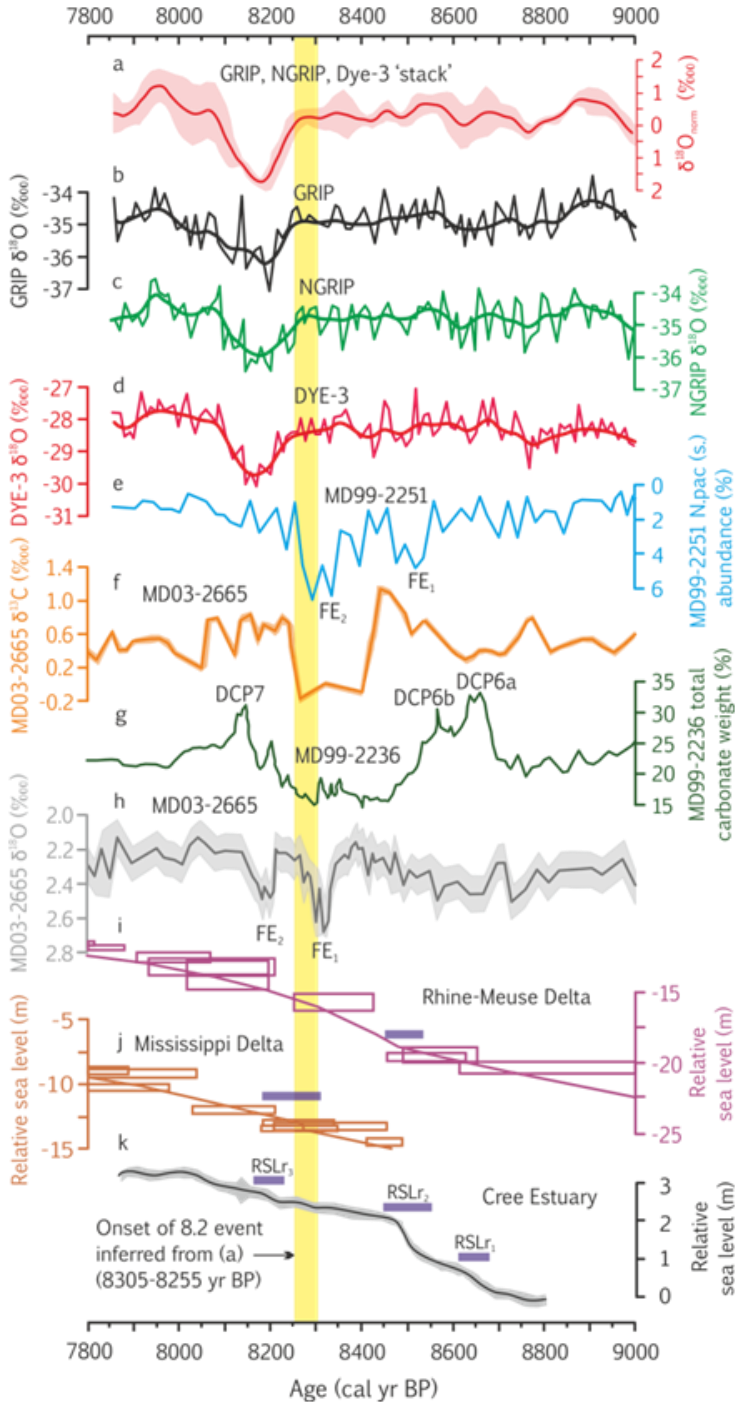

Figure. 2.2 Caption overleaf

Figure 2.2. Records of early Holocene climate, oceanographic and sea-level change in the North Atlantic. Ages are calibrated with respect to AD 1950. **a**, Composite $\delta^{18}O_{norm}$ (normalized) inferred from the GRIP, NGRIP and Dye-3 records (this study) **b**, GRIP $\delta^{18}O$ with a 50 yr moving Gaussian smoothing. **c**, NGRIP $\delta^{18}O$ with a 50 yr Gaussian smoothing **d,** Dye-3 $\delta^{18}O$ with a 50 yr Gaussian smoothing. **e**, *Neogloboquadrina pachyderma* (s.) abundance in North Atlantic deep sea sediments (Ellison et al., 2006). **f**, *Neogloboquadrina pachyderma* s. $\delta^{13}C$ in Labrador Sea sea-floor sediments (Kleiven et al., 2008), on revised chronology (this study). FE_1 = Freshening Event 1; FE_2 = Freshening Event 2 (see text). **g,** Percentage detrital carbonate by weight in Cartwright Saddle sea-floor sediments (Jennings et al., 2015). DCP events correspond to 'detrital carbonate peaks'. **h,** *Neogloboquadrina pachyderma* s. $\delta^{18}O$ record in Labrador Sea sea-floor sediments (Kleiven et al., 2008), on its revised chronology (this study). FE_1 = Freshening Event 1; FE_2 = Freshening Event 2 (see text). **i,** Relative sea-level record from the Rhine-Meuse delta defined as 2σ age and vertical uncertainty error boxes (Hijma and Cohen, 2010). Blue bar denotes 2σ age range of the start of the RSL jump (Table 2.2). **j**, Relative sea-level record from the Mississippi Delta defined as 2σ age and vertical uncertainty error boxes (Li et al., 2011). Blue bar denotes 2σ age range that encompasses the RSL jump in its entirety (Table 2.2). **k**, Relative sea-level record of the $BC421_{P\text{-}max}$ and its 95% confidence interval (grey shading). Blue bars denote 2σ age ranges which encompass the RSL jumps in their entirety (Table 2.2). Yellow bar indicates the onset of the 8.2 event inferred from the composite $\delta^{18}O_{norm}$ record in (a).

Recent evidence from shelf-sea and estuarine sediments complicate the story as these contain evidence of a third event. A well-resolved near-field record of LIS retreat is provided by Jennings et al. (2015), who observed detrital carbonate peaks (DCPs) at 8694-8609 (DCP6a), 8609-8489 (DCP6b) and 8219-7998 cal yr BP (DCP7) (Fig. 2.2g) in Cartwright Saddle core MD99-2236, which they attributed to episodes of abrupt freshwater discharge. The second event, DCP6b, is manifest as the downstream equivalent of the Hudson Bay "red-bed", which Jennings et al. (2015) re-interpret as a final phase in the abrupt 'opening' of the Tyrrell Sea following retreat of Laurentide ice – not a drainage of LAO. Recent ice-sheet modelling predicts that the dynamic separation, or "saddle-collapse" of the Keewatin and Labrador domes, which occurred over the Tyrrell Sea, produced a meltwater pulse with peak discharge rates of ~0.21 Sv between ~8800 and ~8600 yrs BP (Gregoire et al., 2012). This provides a possible mechanism for a meltwater pulse concomitant with the Tyrrell Sea 'opening' event. Jennings et al. (2015) interpret the later event, DCP7, as the signature of LAO drainage(s) due to its close coincidence with the 8.2 event. However the significance of DCP7 in forcing the 8.2 event is unclear as it post-dates the onset of the 8.2 event at 8305-8255 cal yr BP (Fig. 2.2a) by a minimum c. 30-100 yrs, albeit this could reflect chronological uncertainties within the Jennings et al. (2015) record (i.e., the 8.2 to 9.7 ka BP time interval is constrained by two ^{14}C ages). Nevertheless, this three-event model of abrupt freshwater discharge is supported by estuarine records from the Gulf of Mexico where Simkins et al. (2012) observed prominent magnetic susceptibility anomalies at ~8800, ~8600 and ~8100 cal yr BP (Simkins et al., 2012). It is thought that previous near-field records that describe evidence of one or two events (Hillaire-Marcel et al., 2007; Hoffman et al., 2012) are limited by core resolution (Jennings et al., 2015).

Notwithstanding the limited chronological control across the critical time interval, the Cartwright Saddle record arguably provides the best-resolved near-field record of final LIS retreat because of its relatively high resolution and stratigraphic continuity. The interpretation of a three-event freshwater discharge model includes the potential abrupt drainage(s) of LAO as well as a possible large ice-sheet contribution associated with the saddle collapse of the Keewatin and Labrador domes (Gregoire et al., 2012). If correct, the causal mechanisms of the 8.2 event are more complex than that suggested by the consensus view of a single- or double-event drainage of LAO. The Jennings et al. (2015) record describes a sequence of freshwater events prior to the 8.2 event but little is known regarding the magnitudes of such events, critical constraints for modelling studies of the AMOC. Understanding the pathways of freshwater routing is also critical as some authors predict

transport into the sub-tropical North Atlantic (Condron and Windsor, 2011; Hill and Condron, 2014) rather than the sub-polar gyre (Jennings et al., 2015; Kleiven et al., 2008; Ellison et al., 2006).

Relative sea-level (RSL) records provide a means to test the hypothesis that the DCP events in Cartwright Saddle core MD99-2236 (Jennings et al., 2015) were significant freshwater discharge events from the LIS. Gravimetric effects on the geoid associated with reductions in regional mass produces a pattern of sea-level change that is non-uniform across the globe, with the magnitude of local RSL rise increasing with distance away from the point source of mass loss (e.g. Mitrovica et al., 2001). The magnitudes and spatial patterning of these regional RSL signals are termed 'fingerprints' and can be corrected with geophysical modelling estimates to determine the equivalent eustatic sea-level contribution and thus the magnitude of meltwater released (e.g. Kendall et al., 2008).

Two well-dated RSL records based on radiocarbon-dated basal peats exist for the centuries prior 8.2 ka, and both contain an abrupt departure from background rates of RSL rise, or a RSL 'jump'. In the western Netherlands (Rhine-Meuse Delta), Hijma and Cohen (2010) define a eustatic equivalent sea-level jump of 3.0 ± 1.5 m at 8590-8350 cal yr BP, while in the Mississippi Delta, Li et al. (2011) identify a eustatic jump of 1.2 ± 0.2 m at 8310-8180 cal yr BP. Both jumps are corrected for a Laurentide source of mass loss using geophysical modelling predictions (Kendall et al., 2008). It has been suggested that due to differences in the timing and magnitude of the two RSL jumps, the Rhine-Meuse jump contains two separate events, while the Mississippi Delta record captures a final event only (Törnqvist and Hijma, 2012; Li et al., 2011). Indeed, the Mississippi Delta record contains a reworked pre-event stratigraphy dated to ~8400 cal yr BP which has been interpreted as possible evidence of a preceding RSL jump (Li et al., 2011).

Both the Rhine-Meuse and Mississippi Delta records lack conclusive bio- and lithostratigraphic evidence of more than one event found in continuous stratigraphic sequence. At present the sea-level data are unable to test the hypothesized three-stage LIS retreat model of Jennings et al. (2015). Resolving the full sequence, number, timing and magnitude of 8.2-related freshwater events will be an important step towards better understanding the AMOC response to freshwater perturbation(s) occurring within an unstable interglacial climate.

Here we present a stratigraphically continuous record of RSL for Blair's Croft in the Cree Estuary, SW Scotland, which is sub-centennially resolved for the period ~8800 to ~7800 cal yr BP. In particular, we test two hypotheses: (1) that RSL rose abruptly in more than one abrupt step in the several centuries prior to 8.2 event, and (2) that the RSL jump(s) correlate with other short-lived event(s) observed in various North Atlantic proxy records.

2. Field site

Our field site is located on the northern shores of the Solway Firth in the Cree Estuary (N 54°51', W 4°30'). This area offers excellent potential to provide a high-resolution reconstruction of RSL for the early Holocene for two key reasons. First, relatively high rates of GIA (crustal rebound) in response to the deglaciation of the British-Irish Ice Sheet served to dampen the rapid rate of deglacial/early Holocene sea-level rise (e.g. Fairbanks, 1989; Hijma and Cohen, 2010). Second, paraglacial conditions experienced at this time likely contributed large volumes of fine-grained sediment to the coastal zone, promoting net sediment accumulation under periods of rapid RSL rise and facilitated the development of a relatively high-resolution RSL record.

The River Cree is tidal from Newton Stewart and drains southwards through the Cree coastal lowlands into Wigtown Bay (Fig. 2.3b). The predicted present day spring tidal range in Wigtown Bay is 6.40 m (Appendix 1, Fig. S1; Ward, 2014), which is comparable to the range of 6.70 m obtained from the tide gauge in the adjacent small (up-)estuary harbour of Kirkudbright (Fig. 2.3b; Admiralty Tide Tables, 2014). The Cree coastal lowlands (i.e., the area below the 10 m OD (OD = UK geodetic datum; where 0 m OD = approximate mean tide level) contour line; Fig. 2.3c) have been the focus of several previous RSL studies (e.g. Jardine, 1975; Bishop and Coope, 1977; Smith et al., 2003a). In the most recent of these, Smith et al. (2003a) reported that RSL rose from -6 m OD at ~9500 to a mid-Holocene RSL highstand of +6 m OD at ~5500 cal yr BP before falling to present. One of the sites used to constrain this RSL history is Blair's Croft, located ~1.5 km inland of the current tidal limit and at the base of the Galloway National Park foothills, where a sequence of interbedded estuarine and salt-marsh deposits are preserved below a surface freshwater peat. These were dated by Smith et al. (2003a) using conventional bulk radiocarbon dating to within the broad timeframe of the 8.2 event, although not fully attributed to the event itself. These sediments provide the basis for this study.

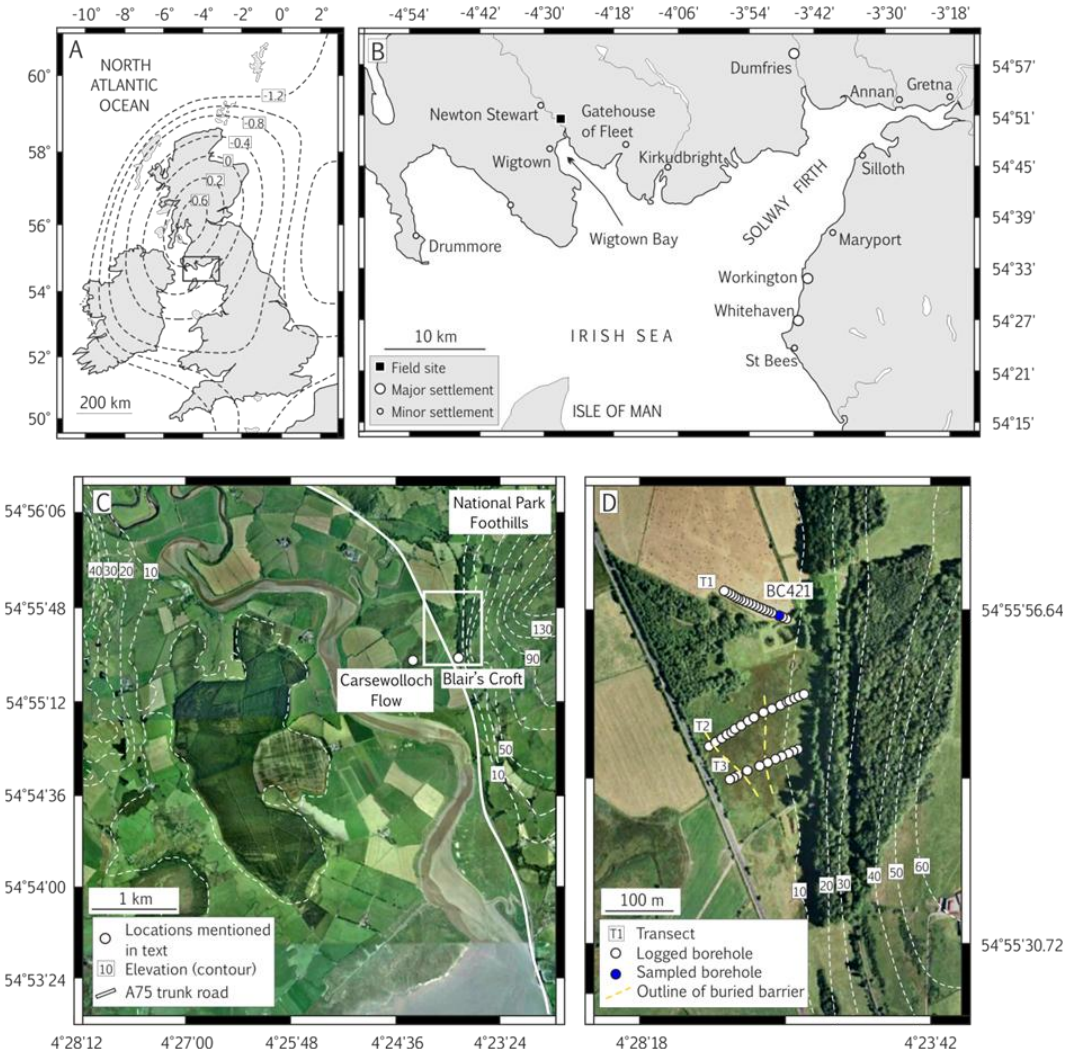

Fig. 2.3 Location maps of field site in southwest Scotland. A) Map of UK and Ireland overlain with the contour lines of the present-day vertical land motions determined by the glacio-isostatic adjustment model of Bradley et al. (2011), denoting uplift rates in mm yr^{-1}. B) Setting of Solway Firth in the Irish Sea and the location of Wigtown Bay and the Cree Estuary. C) Google Earth image of the Cree Lowlands and locations mentioned in text. D) Google Earth overview of Blair's Croft field-site and borehole locations.

3. Methods

3.1 Lithostratigraphy

We conducted further lithostratigraphic investigations at Blair's Croft, paying particular attention to the sediments that were originally dated by Smith et al. (2003a) as spanning the centuries either side of the 8.2 event, i.e. between ~8800 and 7800 cal yr BP (Figs. 2.4 and 2.5). Fifty cores were sunk along three transects with an Eijkelkamp gouge. Sediments were classified with reference to the Troels-Smith (1955) scheme of stratigraphic notation. Each transect commenced at the break of slope at the valley-side and extended westward by 100-200 m towards the A75 trunk road and the present-day estuary. No further cores were sunk on the western side of the A75 road in Carsewolloch Flow, as Smith et al. (2003a) and Wells (1997) here reported a broadly homogenous sequence of estuarine clays (i.e., no inter-bedded organic deposits). Sample core BC421 (Transect 1) was deemed representative of wider changes at Blair's Croft and was collected using a modified piston corer.

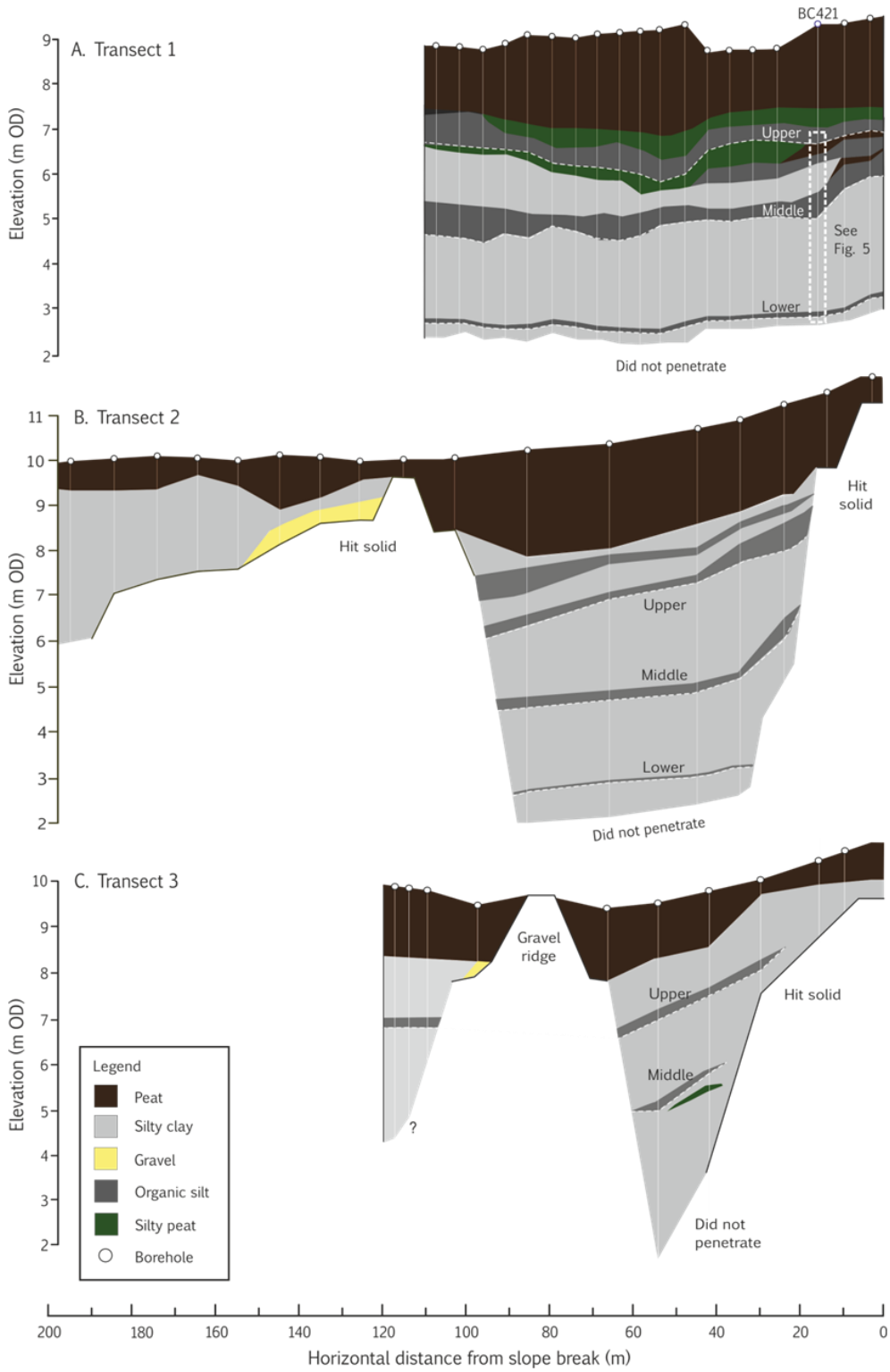

Figure 2.4. Lithostratigraphy of Blair's Croft recorded along A) Transect 1, B) Transect 2 and C) Transect 3. The reader is referred to Figures 2.3 and 2.5 for core locations and ^{14}C dating of core BC421, respectively. To aid in correlations, organic beds 'lower', 'middle' and 'upper' are illustrated, but we note that our focus is on the sedimentary sequence illustrated by the stipple white outline in Transect 1 which here encompasses the lower and middle beds and their overlying minerogenic deposits.

3.2 Laboratory methods

We conducted microfossil (diatom) analyses in order to determine estimates of past sea level. Samples were prepared using standard techniques (Palmer and Abbott, 1986), identified with reference to the taxonomy of Hartley et al. (1996) and grouped according to a simplified halobian classification scheme of Vos and de Wolf (1993). A total of 74 samples were taken at ~4 cm intervals. We counted a minimum of 200 valves, with the exception of 10 samples that contained a count of 150-200 valves. Diatom diversity was high with 170 species identified. Percentage loss-on-ignition was measured on 4 g subsamples to identify horizons with relatively high organic content (>20%) indicative of upper intertidal and supratidal conditions. Samples were weighed prior to being oven-dried overnight at 80°C, reweighed, combusted at 550°C for four hours and weighed again.

Our chronology is constrained by 13 Accelerator Mass Spectrometry (AMS) ^{14}C determinations of individual terrestrial plant macrofossils (Table 2.1). Ages are reported as 2σ ranges, calibrated (IntCal13; Reimer et al., 2013) with respect to BP (where BP = AD 1950). We do not use the radiocarbon dates of Smith et al. (2003a) as they were obtained from >3 cm-thick bulk slices which had large 1σ age errors. Our dating was performed at the Scottish Universities Environmental Research Centre, NERC radiocarbon facility in East Kilbride, UK, on cleaned, horizontally-bedded plant macrofossils (*Phragmites australis*) and wood (*Alnus*) fragments that were intact and away from the core edges. All ^{14}C samples were pre-treated using standard methods (e.g. Czernik and Goslar, 2001) in East Kilbride. Most samples were dated twice and subject to a weighted mean using the "R_combine" function of OxCal 4.2 (Bronk Ramsey, 2008) in an attempt to increase the precision of uncalibrated ^{14}C ages (i.e. the reported 1σ laboratory errors, Marshall et al., 2007; Li et al., 2012). Ages were modelled with an OxCal 4.2 "Sequence" function, which assumes that calibrated ages increase with depth, i.e., that no age reversals are allowed. Such models have shown to improve accuracy and retain precision (e.g. Bronk Ramsey, 2000). An alternative model is the Poisson sequence ("P_sequence"), which takes into account stratigraphic depth information and requires a 'k-factor' - a parameter for model rigidity. However, it is not possible to assess a reliable k-factor for the entire Blair's Croft sequence because some sections of core were inorganic and devoid of well-preserved dating material. Thus, we use the "Sequence" model as it contains fewer assumptions; rendering it the more parsimonious and cautious of the two models (Bondevik et al., 2012).

Table 2.1. Radiocarbon dates from BC421. Samples B1(a) and B1(b) (dark gray) are excluded from the age model because they are taken from the base of the 'upper' organic bed and are too young to be associated with the 8.2 kyr BP event, but provide a maximum age of barrier activity at its present position. Sample B is not included because of a minor age reversal with preceding samples (light gray). AMS = accelerator mass spectrometry. *Calibrated with the IntCal13 calibration curve (Reimer et al. 2013) in OxCal 4.2 (Bronk Ramsey, 2008).

Sample Code	Identifier	Depth (cm)	Height (m OD)	Dating method	Material dated	Reported ^{14}C age (±1σ lab error)	Calibrated* range (2σ)
SUERC-44407	B1(b)	259.5	6.90	Duplicate AMS	Phragmites australis	6890 ± 64	7917-7608
SUERC-44406	B1(a)	259.5	6.90	Duplicate AMS	Phragmites australis	6963 ± 36	7923-7694
SUERC-44405	B	294.5	6.55	Single AMS	Phragmites australis	7127 ± 26	8005-7877
SUERC-44400	C	300.5	6.49	Single AMS	Phragmites australis	7049 ± 65	7997-7730
SUERC-42712	D(b)	307	6.42	Duplicate AMS	Phragmites australis	7088 ± 26	7969-7854
SUERC-44399	D(a)	307	6.42	Duplicate AMS	Phragmites australis	7107 ± 26	7996-7865
SUERC-44371	Q(b)	389	5.60	Duplicate AMS	Wood	7409 ± 26	8318-8180
SUERC-42711	Q(a)	389	5.60	Duplicate AMS	Wood	7452 ± 25	8345-8195
SUERC-44398	R(b)	395.5	5.54	Duplicate AMS	Phragmites australis	7344 ± 65	8321-8018
SUERC-44397	R(a)	395.5	5.54	Duplicate AMS	Phragmites australis	7392 ± 39	8340-8060
SUERC-44386	T	402	5.47	Single AMS	Phragmites australis	7507 ± 25	8389-8214
SUERC-44387	U	631	3.18	Single AMS	Phragmites australis	7831 ± 65	8973-8450
SUERC-42709	V(b)	632	3.17	Duplicate AMS	Wood	7936 ± 27	8978-8640
SUERC-44385	V(a)	632	3.17	Duplicate AMS	Wood	7977 ± 26	8993-8725
SUERC-44369	W(b)	632	3.17	Duplicate AMS	Wood	7980 ± 27	8995-8725

SUERC-42708	W(a)	633	3.16	Duplicate AMS	Wood	7982 ± 27	8995-8725

3.3 Transfer function development

To reconstruct RSL from fossil diatom assemblages, we exploit the relationship between the distribution of their modern counterparts with marsh surface elevation (e.g. Zong and Horton, 1999; Barlow et al., 2013), which is primarily controlled by the frequency of tidal flooding (hence, RSL). The elevation of an assemblage relative to tide levels is termed its 'indicative meaning'. Underpinning this is the assumption that the indicative meanings of contemporary diatoms and their assemblages remain unchanged through time. We apply the Barlow et al. (2013) transfer function to our fossil assemblages using the computer software C^2 v.1.6 (Juggins, 2011). The Barlow et al. (2013) dataset, although based on nine separate modern records from western Scotland, is lacking a key taxon that forms a large component of the Blair's Croft fossil record, *Tryblionella navicularis*, and which is essential to our reconstruction. Within UK salt-marshes this taxon has only been documented in suitable abundances in Brancaster Marsh, Norfolk, eastern England, where it is found around the level of MHWST within an area characterized by *Phragmites australis* (Appendix 2, Fig. S2; Gehrels et al., 2001). In view of the abundance of *P. australis* macrofossil remains in the Blair's Croft organic beds, these appear to be analogous environments. All taxa from the Brancaster samples are included in addition to *T. navicularis*, which are integrated by standardizing their elevations (with respect to tidal range) with the standard water level index (SWLI) equation (Barlow et al., 2013):

$$SWLI_n = 100(h_n - h_{MTL}) / (h_{MHWST} - h_{MTL}) + 100 \quad (1)$$

where $SWLI_n$ is the standard water level index for a given sample *n*, h_n is the elevation of a given sample *n* (in metres OD), h_{MHWST} is the local mean height of spring tide and h_{MTL} is the local height of mean tide level. A SWLI of 100 and 200 are equivalent to MTL and MHWST, respectively.

Transfer function-based estimates of palaeo-RSL are calculated with respect to the modern tidal regime so they require correction for palaeotidal change. Estimates of the elevation of the height of MHWST for Wigtown Bay are provided by the palaeotidal model of Ward (2014), which indicates a reduction in MHWST height ($M^2 + S^2$) from 3.27 m OD at 9.0 ka BP to 3.00 m OD at 8.0 ka BP (Appendix 1, Fig. S1). As most of our record encompasses this 1 kyr interval, we correct our data points using simple linear interpolation

of the points between the 9.0 and 8.0 ka BP time-slices (Appendix 1, Fig. S1). We assume a fixed height of MTL (=0 m OD) across the time interval, such that the only fluctuating variable is MHWST height. The resulting correction applied is specific to each data point and uses the corresponding age inferred from the age model. No attempt was made to correct the few samples younger than 8.0 ka BP with a second linear function for the 8.0 to 7.0 ka BP time period; instead we extrapolate the same linear function. Uncertainties in the Ward (2014) model are yet to be rigorously quantified (Ward, pers. comm.), so we introduce a measure of uncertainty of 0.06 m for each data point (Section 3.4) which is equivalent to 2 standard error of the mean (SEM) of the Ward (2014) palaeotidal data. Transformation of the SWLI values back to OD is achieved using:

$$OD_n = (SWLI_n - 100) \times (PTH_{MHWST} - PTH_{MTL}) / 100 \quad (2)$$

where OD_n is the height of a given sample relative to ordnance datum, $SWLI_n$ is the standard water level index of a given sample, PTH_{MHWST} is the local height of mean high water of spring (palaeo)tide for the appropriate time period of interest (inferred from the age model) and PTH_{MTL} is the local height of mean (palaeo)tide level for the appropriate time period of interest (assumed zero).

3.4 Sea-level reconstruction

The combined uncertainty of each RSL data point comprises three error components (Appendix 1, Table S1); a) bootstrapped 1 SEM values of indicative meanings predicted by the modified Barlow et al. (2013) transfer function that includes *T. navicularis*, b) the uncertainty of the palaeotidal correction (0.06 m) and, c) a uniform compaction error term (0.20 m). Sampled core BC421 was compacted during extrusion in the field and has been linearly corrected for the difference between logged depths in a hand core and extruded depths from the piston core. The above error terms are expressed as bidirectional 1σ uncertainties and are propagated in a mean squared estimate using:

$$\text{Mean squared estimate} = \sqrt{(a^2 + b^2 + c^2)} \quad (3)$$

The indicative meanings for each data point are converted to RSL using: $S = H - I$, where S is the height of relative sea-level (m OD), H is the height of the given sample (m OD) and I is the indicative meaning of the fossil sample (m OD). Both the mean (μ) and uncertainties (σ) for RSL and age are then combined to construct confidence limits for RSL (Appendix 1, Table S2). We follow the method of Rohling et al. (2014) by defining probability density functions (assumed normal) for each data point by expressing their 1σ values symmetrically in both the x and y directions about their means (μ) in MATLAB software v. R2013b (where y uncertainty = the mean squared estimate for each RSL data point, and x uncertainty = the 1σ error for the relevant depth within the BC421 age model). Each probability density function was randomly perturbed 500 times using its own randomizer to produce 500 new 'iterations' for each data point in both the x and y directions. After sorting each 'sample' of 500 RSL iterations on age, we removed the iterations that overlapped in age with the adjacent 'sample'. Next we calculated cumulative density functions for each 'sample', from which we inferred 95% and 68% probability intervals for each. The histogram peak defines the "probability maximum" ($BC421_{P\text{-}max}$) and provides the most likely RSL solution (Rohling et al., 2014). To remove spurious fluctuations, the $BC421_{P\text{-}max}$ has been smoothed with a moving 50 yr Gaussian filter in PTC Mathcad v. 14 and is determined with an average precision of ± 0.15 m (95% confidence).

3.5 Developing comparative chronologies from ocean and ice core records

We test hypothesis (2); whether the timing of RSL jumps correlate with other abrupt events expressed in North Atlantic proxy records, by comparing the timing of sea-level accelerations/jumps within our record with those observed in various records from the North Atlantic. Where resolution permits, we focus on comparing the start of events rather than event maxima within their respective chronologies.

3.5.1 Inferring the timing of abrupt North Atlantic events

We infer the onset of the two-step increases recorded in the surface $\delta^{18}O$ record from the North Atlantic (FE_1 and FE_2; Fig. 2.2h) (Kleiven et al., 2008) following new age modelling of the Kleiven et al. (2008) chronology, which was previously based on simple linear interpolation of ^{14}C ages. The Kleiven et al. (2008) observations are supported by a second planktonic foraminiferal dataset retrieved some 1250 km away in core MD99-2251 which

also contains two abrupt anomalies (Figs. 2.2e and 2.2h) (Ellison et al., 2006), although the records are offset by c. 250 yrs likely because of the limited age control of MD99-2251. For instance the chronology for MD99-2251 (Ellison et al., 2006) contains only two ages within the critical time interval compared to the nine in MD03-2665 (Kleiven et al., 2008). As a result, we do not include the Ellison et al. (2006) record in our comparison, but nevertheless assume that the two-step anomalies in both records are expressions of the same events (Kleiven et al., 2008) and that the age offset reflects the limitations of the Ellison et al. (2006) chronology.

Of the nine dates between 9.0 to 8.0 kyr BP in the Kleiven et al. (2008) record, two are reversed. To correct this offset they introduced a local reservoir value (ΔR) of 23 yrs to account for an enhanced East Greenland Current coincident with North Atlantic freshwater perturbation(s). We are unable to assess the reliability of this interpretation, but it is one we follow given the internal consistency of ΔR corrected ages. To ensure chronological robustness, we model the original Kleiven et al. (2008) ^{14}C data in OxCal 4.2 using a *P_sequence* function, after conservatively doubling (arbitrarily) the local ΔR uncertainties applied to the two ages with reversals. We then propagate the original laboratory 1σ errors of each ^{14}C age in a mean squared estimate. The modelled ages of MD03-2665 demonstrate strong internal agreement (96% overall model agreement index).

Next we infer the timing of the start of the two *N. pachyderma* δ^{18}O peaks from the adjusted chronology of Kleiven et al. (2008). However, we need to determine the precise onset of each anomaly within MD03-2665 with respect to core depth. The first abrupt increase in δ^{18}O occurs at 332 cm, while the initial drop in δ^{13}C occurs at 346 cm in the same core (equivalent to ~70 yrs within the chronology). This is likely indicative of a transfer delay between ocean surface and bottom waters in registering the freshwater anomaly (Kleiven et al. 2008). The earliest manifestation of an underlying anomaly, the start of the δ^{13}C excursion, is therefore a more accurate representation of the start of the underlying freshwater event. This is supported by an increase in magnetic properties that is coeval with the onset of the δ^{13}C excursion. To infer the onset of the second anomaly, we use the δ^{18}O record because the δ^{13}C series records a broad minimum spanning several centuries rather than two distinct events.

Proximal to the former LIS margin, the timing of three DCPs observed in core MD99-2236 (Jennings et al., 2015) and the modelled collapse of the Keewatin and Labrador ice-dome saddle (Gregoire et al. 2012) are also included in our comparison. Revising the

Jennings et al. (2015) chronology in OxCal 4.2 is not necessary given the limited chronological control across the critical time interval. To tie in existing RSL observations from elsewhere, we compare age probability density functions of the onset of the Rhine-Meuse Delta RSL jump (Hijma and Cohen, 2010) and the full range of the Mississippi Delta RSL jump (Li et al., 2011).

3.5.2 Greenland $\delta^{18}O_{ice}$ 'stack' development

We determined the start of the 8.2 event from a 'stacked' Greenland ice-core $\delta^{18}O$ record (Fig. 2.2a) built from the individual records of GRIP, NGRIP and Dye-3 (Figs. 2.2b, 2.2c, 2.2d) to identify possible leads and lags. This enables us to infer a 'best-estimate' of the start of the event, within uncertainties, from the three individual ice-core records.

First, the $\delta^{18}O_{ice}$ values are standardized in order to facilitate inter-record comparison. The Greenland Ice Core Chronology (GICC05) (Rasmussen et al., 2008) was converted to yrs BP from yrs 2k, where BP=AD1950, to aid in comparison with existing records. We then developed eight new smoothed records for each ice-core record in PTC Mathcad v. 14 by filtering each record with a different degree of smoothing. More specifically, we systematically increased the degree of smoothing by 10 yrs for each record; between a minimum of 20 yrs and a maximum of 100 yrs (n=8 records). We then performed a series of regressions of the NGRIP and GRIP records on the basis that the greatest correlation is observed between these two records from the outset. The start of the 8.2 event occurs earlier in Dye-3 compared to both NGRIP and GRIP which is probably reflective of a time-latitudinal transgression of the 8.2 signal. We then plot their correlation coefficients (r) to determine an appropriate degree of smoothing (Appendix 1, Fig. S3). Where *r* values peak and cease to increase by >3% with additional smoothing, we interpret that level of smoothing to be the most appropriate. This way we minimize data loss associated with filtering time series. For the GRIP and NGRIP combination, the appropriate smoothing is 50 yrs (r=0.84) (Appendix 1, Fig S3). We then average the resulting (smoothed) records of GRIP and NGRIP to produce a composite record of these two ice-cores. We then perform a second series of regressions on the smoothed Dye-3 records, using the same >3% threshold. Similarly, 50 yrs (r=0.82) is the ideal filter value (Appendix 1, Fig. S3). Finally, we averaged the composite record of NGRIP and GRIP with Dye-3 to produce a 'stack' of all three $\delta^{18}O_{ice}$ records. Uncertainties are sample-specific and are equivalent to two standard error of the mean. The timing of the start of the 8.2 event within the composite record is

8280 yrs BP. The inaccuracies in layer counting of this part of the chronology is 49 yrs (Rasmussen et al., 2008) which we express bidirectionally around 8280 yrs BP, such that the timing of the onset of the 8.2 event is 8305-8255 yrs BP.

To infer possible leads and lags, next we calculated minimum and maximum age intervals between each event and the 8.2 event by subtracting the minimum and maximum estimates of their respective 2σ calibrated ranges. Cluster analysis (unconstrained, Euclidean distance) was performed on the 2σ calibrated age ranges in order to decipher a possible sequence of LIS freshwater events prior to the 8.2 event (Fig. 2.9; Table 2.2).

4. Results

4.1 Lithostratigraphy

Our lithostratigraphy survey confirms the original sequence of minerogenic silts and laterally extensive beds of organic silt that were mapped by Smith et al. (2003a). The individual beds onlap the foot of the eastern hillside and can be traced ~100-200 m westward towards the present estuary (Fig. 2.4). The beds dip westward towards the estuary, indicating that the shallower, valley-side sediments are less compacted than those closer to the present estuary. The organic beds contain abundant macrofossils of *Phragmites australis*, a common indicator of a fringing salt-marsh environment (>MHWST) (e.g. Zong and Horton, 1999). The most prominent organic beds (traceable across at least two transects) are those that occur at ~3 m, ~5 m and ~7 m OD which we refer to as 'lower', 'middle' and 'upper' beds, respectively. They are dated in sample core BC421 (Transect 1) to ~8800, ~8200 and ~7800 cal yr BP, respectively. The top of the lower and middle beds contain detrital, horizontally-bedded wood fragments that have been transported from the adjacent freshwater upland and are overlain by grey silty clays containing sparse well-humified flecks and minor layers (sub mm) of unidentified organic material, but probably *P. australis*. Transitions from organic to minerogenic sedimentation in each case record marsh drowning and marine transgression. In contrast, the upper organic bed is overlain by freshwater peat and records regression. LOI is high within the organic beds (20-60%) and low within the silts (5-10%; Fig. 2.6). The upper and middle beds can be correlated across all three transects based on their elevations, although the lower organic bed is not present in the south of the site (Transect 3). An additional, locally developed organic bed occurs in Transect 2 and is located above the

'upper' organic bed that rises from ~7 m OD in the west to ~9 m OD at the valley-side. To provide a rigorous test of hypothesis (1); whether RSL rose by more than one abrupt step prior to the 8.2 event, our focus is on the entire sedimentary sequence that embraces the lower and middle organic beds and their overlying minerogenic deposits within core BC421, which appear to provide a continuous depositional record for the period ~8800 to ~7800 cal yr BP.

In the south of Blair's Croft, a gravel barrier underlies the surface peat (Fig. 2.3). Wells (1997) traced this feature farther north towards the wooded part of Blair's Croft where it falls sharply in altitude and is overlain by minerogenic silts. In Transect 3, the upper organic bed at ~7 m OD is recorded on the landward and seaward sides of the barrier suggesting that it was in place at its present position after the deposition of the upper bed. Two ages from near the base of the upper bed (7917-7608 and 7923-7694 cal yr BP; Fig. 2.5) thus provide a minimum age of ~8000 cal yr BP of barrier formation, at least at its present position. The potential influence of a palaeo-barrier on the stratigraphy that pre-dates ~8000 cal yr BP is considered later in the discussion.

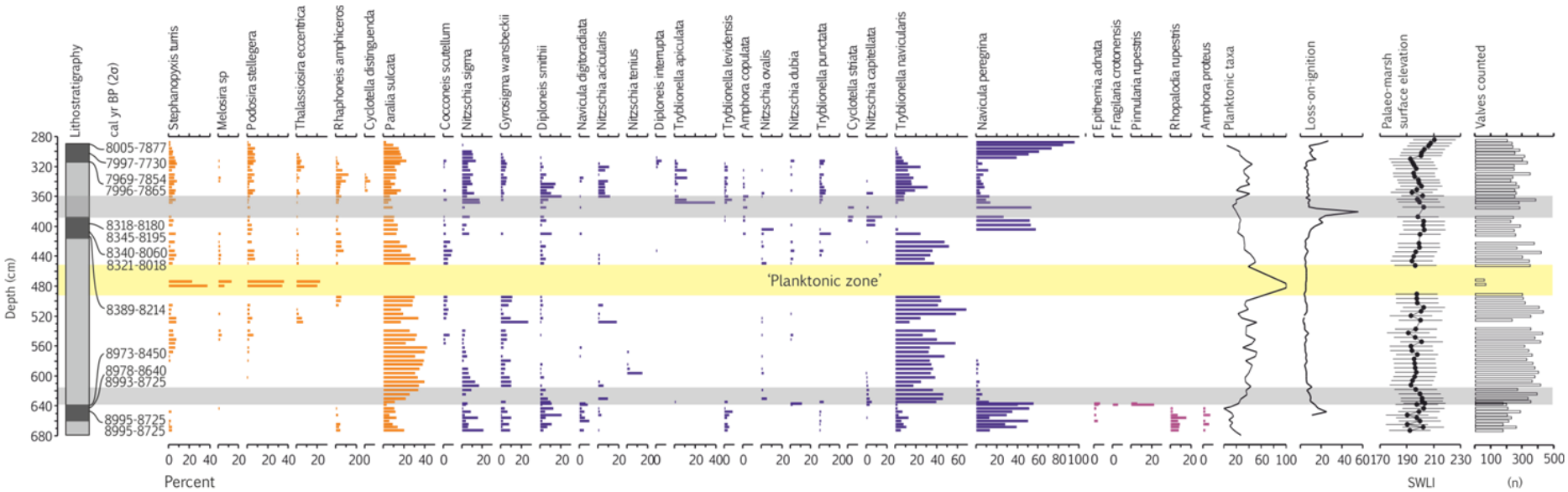

Figure 2.6. Diatom biostratigraphy, chronostratigraphy and LOI of core BC421. Diatom contributions represent >5%. Palaeomarsh surface elevation (in SWLI units) is reconstructed using the component-two model (WA-PLS) of the 'screened' training set. For a more detailed view of sample depths of ^{14}C ages, refer to Figure 2.5 and Table 2.1. Marine taxa (planktonic forms) are indicated in orange, brackish-indifferent taxa in blue and freshwater-brackish taxa in purple. Yellow shading indicates the 'planktonic zone' (RSLr^{2}). Grey shading indicates abrupt reductions in SWLI that are accompanied by stratigraphic evidence of marsh drowning (see discussion), with the stratigraphically deepest and shallowest grey shading corresponding to RSLr^{1} and RSLr^{3}, respectively.

4.2 Biostratigraphy

In general, the organic beds are dominated by high frequencies of *Navicula peregrina*, a high marsh taxon (Fig. 2.6), while the minerogenic silts contain *T. navicularis*, *Nitzschia sigma*, *Diploneis smithii*, *Gyrosigma wansbeckii*, *Cocconeis scutellum* (all epipelic or epiphytic taxa) and *Paralia sulcata* (planktonic), which are indicative of lower intertidal saltmarsh/mudflat conditions. For brevity, epipelic and epiphytic taxa are hereafter collectively referred to as 'benthic'.

The transition between the lower organic bed and the overlying silt is sharp (<2 mm), with the microfossils indicating an abrupt (but non-erosive) switch from high marsh to lower intertidal conditions (Fig. 2.6). The overlying minerogenic silt contains minor amounts of well-humified organics, including in situ roots alongside organic material washed onto the tidal flat from a higher elevation, indicating close proximity of a lower salt marsh environment. At ~530 cm the diatoms begin to record a gradual return to saltmarsh conditions, with *P. sulcata* giving way to increased frequencies of *T. navicularis*. Frequencies of *P. sulcata* undergo a second increase from 30% to 55% between 511 and 494 cm, after which benthic taxa are not present until 455 cm. This section of core is mostly barren, but two samples contain thickly silicified planktonic taxa *Thalassiosira eccentrica*, *Podosira stillegera*, *Stephanopyxis turris* and *Rhaphoneis amphiceros*. Organic content is low (<3%) and the core log records an increase in clay content. Either side of the planktonic zone, relatively low frequencies of *Cocconeis scutellum* (<10%) indicate a mudflat setting. Overall these data indicate the abrupt drowning of an already low intertidal setting. Higher up in the overlying minerogenic silt between 451 and 414 cm, *D. smithii* and *N. sigma* indicate a gradual return to lower salt-marsh conditions and the establishment of the middle bed.

Accumulation of the middle bed between 414 and 389 cm and the presence of high frequencies of *N. peregrina* indicate a full return of high marsh conditions. The contact between the middle bed and overlying minerogenic sediment is sharp (<2 mm), although there are relatively gradual microfossil involving increased frequencies of *T. navicularis*, *P. sulcata* and *D. smithii*. A final return to full high-marsh conditions is indicated by renewed deposition of organic silt at 315 cm which forms the organic silt that underlies peat and contains high frequencies of *N. peregrina* throughout.

In summary, there are three stratigraphic levels that record intertidal drowning within the Blair's Croft stratigraphic record between 8.8 and 7.8 ka BP (Appendix 1, Fig. S4). Summarised from bottom to top, these are: i) across the transition between the lower bed and its overlying minerogenic deposit (high marsh drowning), ii) within this overlying minerogenic deposit, across the full length of the 'planktonic zone' (low marsh/mudflat drowning), and, iii) across the transition between the middle bed and its overlying minerogenic deposit (high marsh drowning).

4.3 Chronology

The chronology is based on nine tie-points (a total of 13 AMS ^{14}C ages, including a mixture of duplicate and single dates) that are modelled in stratigraphic sequence in OxCal v 4.2 (Bronk Ramsey, 2009a) (Appendix 1, Fig. S5). The model builds prior (unmodelled) probability distributions of ^{14}C ages and compares them with posterior (modelled) densities using Bayesian analysis and Monte Carlo Markov Chain random sampling (Gilks et al., 2006). The agreement index provides a measure of overlap between the prior and posterior model densities, with agreement indices >60% the accepted threshold (Bronk Ramsey, 2008). In our model, there is good agreement between the prior and posterior densities; seven out of eight tie-points have an agreement index of >83%, while the one remaining tie-point has a satisfactory agreement of 68%. Posterior probability densities for each RSL (y) data-point were determined by inserting blank ages into the model at the relevant stratigraphic position using the Date() function.

4.4 Transfer function

We introduce new samples to the Barlow et al. (2013) transfer function to resolve the issue of a missing modern analogue (*T. navicularis*). The species environmental response of the data determines model selection choice; those with environmental gradients >2 standard deviation (SD) units are generally considered to respond unimodally and require a weighted averaging partial least squares (WA-PLS) regression model, while a simple weighted averaging (WA) model is appropriate for datasets with gradient lengths <2 SD (Birks, 1995). The original Barlow et al. (2013) dataset is strongly unimodal (4.08 SD units), which is retained after adding the additional samples from Brancaster Marsh. We therefore use WA-PLS regression with bootstrapping (1000 permutations) cross validation (ter Braak and

Juggins, 1993; Birks, 1995) using the C^2 software v. 1.6 (Juggins, 2011). Fig. S6 and Table S3 (Appendix 1) plots observed versus predicted and observed versus residuals of the full dataset, which now includes 27 samples from Brancaster Marsh (total = 231 samples).

To improve the predictive ability of the transfer function, the training set is 'screened' of outlying samples. We follow Gehrels et al. (2005) who remove samples with residuals >1 SD of SWLI, which removes 14 samples, leaving 217 samples. Fig. S7 and Table S3 (Appendix 1) illustrates the performance (observed versus predicted and observed versus residual plots) of the one-, two- and three-component models of the screened dataset. We select the WA-PLS model with two components over the one-component model on the basis of an improvement in R^2 and RMSEP by >5% (after Barlow et al., 2013). Good agreement of the Brancaster Marsh samples is indicated by low residuals in the observed versus residual plot (Appendix 1, Fig. S7; red crosses). Detrended correspondence analysis (DCA) also indicates a good degree of similarity between most of the Brancaster Marsh samples with the pre-existing samples (Appendix 1, Fig. S8), giving us further confidence in the decision to integrate these samples.

4.4.1 Modern analogues

Integration of the Brancaster Marsh data facilitates the inclusion of *T. navicularis* in the reconstruction but a further 27 taxa remain with no modern analogues (Appendix 1, Fig. S9). These are rare forms, however, so they have little impact on the reconstruction. For example, if we exclude these from the dataset are re-run the transfer function, we observe no change in reconstructed values when compared to a model-run that includes the no-analogue taxa (r^2 = 1).

A more important issue, however, concerns the inclusion of *P. sulcata* in the reconstruction, a highly-siliceous planktonic taxon that is present in high abundance in the minerogenic silts and indeed mudflat settings elsewhere in the U.K. (Zong and Horton, 1999; Gehrels et al., 2001; Wilson and Lamb, 2011; Hill et al., 2007). Planktonic taxa are assumed to have an imprecise relationship with RSL because they can be allochthonous (i.e., transported) although in the Cree fossil record *P. sulcata* demonstrates gradual (linear) changes in abundance across the lithological transitions between organic mud and minerogenic mud. As its ecological optimum occurs around the elevation of the upper tidal flat in the modified Barlow et al. (2013) model, the ecological information on its distribution

appears to be supported by stratigraphic changes. If not directly controlled by elevation, the distribution of *P. sulcata* likely reflects other processes that are tightly coupled to elevation such as increased/decreased tidal influence. This presents a problem as we are unable to test the robustness of the ecological optimum of *P. sulcata* in the modified Barlow et al. (2013) model. However, we have no choice but to include it in the reconstruction as it provides constraints on the indicate meanings of tidal flat deposits and extends the vertical range of our reconstruction to these environments, which are critical to constraining a minimum magnitude of drowning events (i.e., abrupt transitions from organic to minerogenic sedimentation). In doing so we recognize that accurately interpreting genuine short-lived events within our reconstruction requires careful consideration of the assemblage contributions of *P. sulcata* and whether these are supported by lithostratigraphic information (see discussion).

4.5 RSL reconstruction

Fig. 2.7 plots reconstructed RSL change at Blair's Croft for the period 8800 to 7800 cal yr BP. The record of the $BC421_{P\text{-}max}$ identifies a background rising trend of 6-5 mm yr^{-1} that undergoes a gradual slowdown and stabilizes by ~8000 cal yr BP. A second order polynomial fit captures the long-term trend well (r^2=0.96). Despite the agreement in the long-term trends, the Smith et al. (2003a) sea-level index points plot on average 1 m higher as they have been corrected for compaction after Cullingford et al. (1980), who infer that peat deposit thicknesses can be post-depositionally compressed by 40-68% of their original thicknesses and that minerogenic deposits undergo no compression. We are unable to robustly assess the impact of compaction within the Cree record, but the possible impact of compaction on the Cree observations is considered in the discussion.

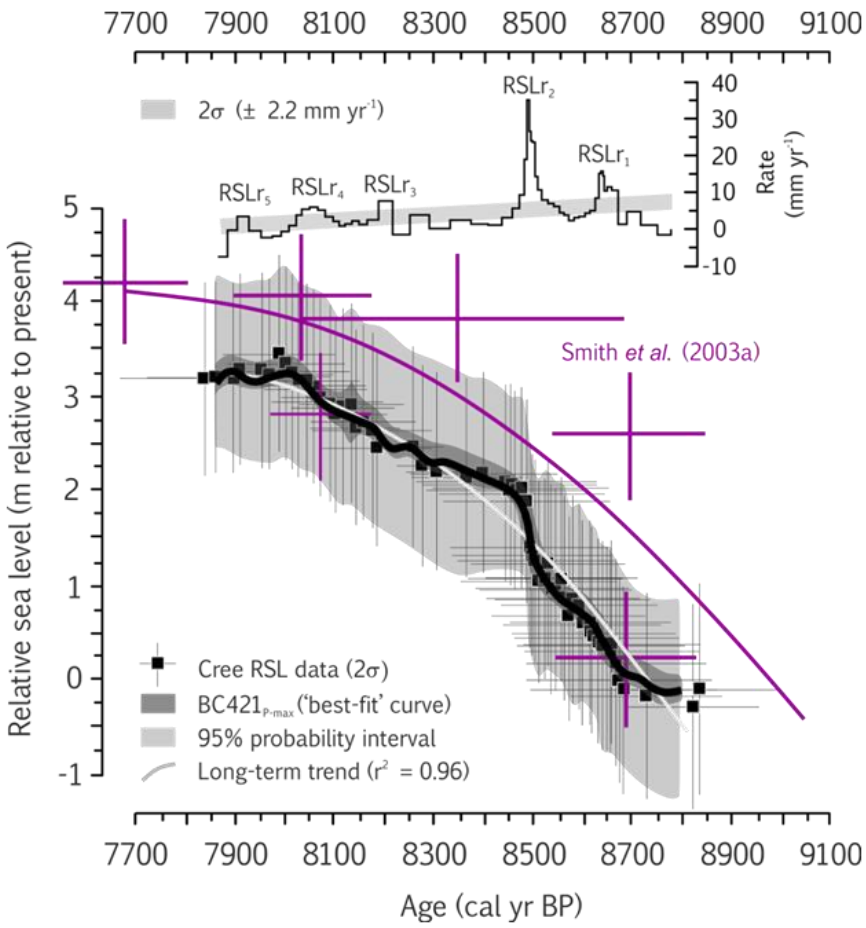

Figure 2.7. Relative sea-level reconstruction for the Cree Estuary for the period 8800 to 7800 cal yr BP. Rates (black step plot) are inferred from the probability maximum for RSL. Smith et al. (2003a) relative sea-level data (purple crosses) are expressed as 2σ vertical and 1σ age uncertainties and have been corrected with the palaeotidal model of Ward (2014). Purple line indicates second-order polynomial fit (r^2=86).

Superimposed on the background trend of the $BC421_{P\text{-}max}$ are a number of multi-decadal to century-scale accelerations in the rate of RSL rise. Here we test hypothesis (1) with the following criterion: when rates of RSL rise exceed the rate of the long-term trend by more than two standard deviations (equivalent to ± 2.2 mm yr^{-1}), these periods are deemed significant and warrant further discussion as potential RSL jumps (Appendix 1,Table S2). The dating uncertainties of each jump are determined by propagating the 2σ uncertainties of the start and end data-points of each jump (for both RSL and age) in a mean squared estimate. Applying this criterion identifies five accelerations in the rate of RSL rise (Fig. 2.7). The youngest two ($RSLr_4$ and $RSLr_5$) are not supported by lithostratigraphic information and therefore deemed insignificant. The first event ($RSLr_1$) occurred between

8680-8610 cal yr BP and measured 0.38 ± 0.19 m, which coincides with the transition from the lower organic bed to overlying minerogenic silt at 630 cm. Lithostratigraphic evidence of the second event ($RSLr_2$) is equivocal, but given that it translates to a relatively large RSL jump (decimetre scale) we accept it on a preliminary basis and subject it to further scrutiny (see discussion). It occurred between 8550-8450, measured 0.88 ± 0.19 m and corresponds to the 'planktonic zone' in the microfossil record between 495-450 cm. The third event ($RSLr_3$) is between 8231-8163 (0.22 ± 0.22 m) and coincides with the transition from the middle organic bed to overlying silt at 389 cm. Rates of rise during the third event exceed the background rate in only one data-point of the $BC421_{P\text{-}max}$, so the preceding data-point of background RSL was used to quantify the timing, duration and magnitude of this event. As such, the constraints on $RSLr_3$ are maximum estimates.

5. Discussion

5.1 Assessing the evidence for sea-level jumps in the Blair's Croft record

We infer the RSL significance of abrupt microfossil changes by considering supporting (stratigraphic) evidence of abrupt drowning and whether these could reflect local morphodynamical processes. In turn, we assess the global sea-level significance of the Cree observations.

On the basis that abrupt microfossil changes are supported by lithostratigraphic evidence, in particular abrupt switches from organogenic to minerogenic sedimentation, we accept $RSLr_1$ and $RSLr_3$ as significant RSL jumps. The notion that $RSLr_2$ is a genuine short-lived event rests heavily on the interpretation of the relatively barren 'planktonic zone'; a 45 cm unit containing only two samples of planktonic microfossils. Within the stratigraphy below the planktonic zone there is evidence of minor marsh recovery in the form of increased abundance of well-humified organic macrofossils. We therefore interpret the overlying planktonic zone as a drowning of a high mudflat or lower salt marsh environment that was in the early stages of colonization by salt marsh vegetation. Sediments within the planktonic zone are increasingly fine-grained and contain few well-humified organics. Supporting evidence of lagoonal infilling in response to enhanced freshwater runoff, such as laminations or freshwater taxa, are not present. A key observation is provided by Smith et al.

(2003a), who describe an unprecedented increase in clay content at Carsewolloch Flow towards the centre of the estuary (Fig. 2.3c) between 4.0-4.5 m OD. Its elevation is similar to the elevation of the planktonic zone which is slightly higher (4.90-4.45 m OD), which we interpret a result of variable compaction (i.e. less compaction of valley-side sediments). We therefore suggest that the 'planktonic zone' records a shift in sedimentology that extends beyond Blair's Croft towards the centre of the estuary. We propose that the lack of a distinct organogenic-minerogenic lithostratigraphic signature similar to that observed for $RSLr_1$ and $RSLr_3$ can be explained by the low intertidal height of the pre-drowned surface (high mudflat or low salt marsh). The Solway Firth and its sub-estuaries contain an abundance of fine-grained sediment, which likely supported rapid sedimentation once accommodation space was made available by sudden sea-level rise. On these grounds, we accept $RSLr_2$ as a significant RSL jump.

There are other possible explanations for the drowning events identified in the Blair's Croft sequence that could be of local origin. First, meandering tidal creeks could alter the local depositional environment and result in changes in diatom assemblages within the sample core. However, we dismiss this possibility on the basis that channel deposits are usually distinct within the litho- and biostratigraphy (e.g. Long and Innes, 1993; Zecchin et al., 2014) and do not operate over the wide areas in which the Blair's Croft organic beds are observed. Second, a gravel barrier was identified to the southwest of the sample core during the stratigraphic survey and this may have influenced the pattern of sedimentation at the sample site by providing protection from open-estuary processes and by trapping freshwater discharged from the adjacent upland. The site chronology indicates that the barrier was deposited at its present position at a minimum of c. 8000 cal yr BP. Critically there is no stratigraphic evidence for changes in the dynamics of this barrier during the timeframe of our record. For example, barrier over-wash deposits are lacking, and we find no evidence for tidal inlet deposition that one might expect in a genuine back-barrier depositional setting. Smith et al. (2002a) describe evidence of a further two barrier ridges on the opposite side of the estuary of a similar morphology, which probably attests to the abundance of glacial sediment now buried within the valley lowlands. Certainly the barrier would have provided a degree of protection for low energy conditions in its lee after c. 8000 cal yr BP, and this may have influenced the RSL record associated with $RSLr_5$ and potentially $RSLr_4$. However, we conclude that barrier dynamics is unlikely to have contributed to the changes in litho- and biostratigraphy prior to 8000 cal yr BP, which here encompasses $RSLr_{1\text{-}3}$.

A third possible explanation for surface lowering is enhanced tidal scour during a high-energy event such as a storm and subsequent infilling (e.g. Haslett and Bryant, 2007). However, this is not consistent with the biostratigraphy either side of RSL accelerations identified where we observe gradual microfossil changes instead of abrupt transitions associated with erosion (Fig. 2.6).

A final observation is that rates of RSL rise determined from sediments across the middle and upper organic beds are low. For example, long-term rates of RSL rise exceed the average rates of ~1.5 mm yr^{-1} observed within these units (Fig. 2.7). A plausible explanation for this is that the thicknesses of the organic beds have been reduced by long-term overburden pressure and are therefore underestimating rates of RSL rise. Organic (saltmarsh) sediments experience a greater degree of compressibility than minerogenic (mudflat) sediments (e.g., Brain et al. 2011). We assume that $RSLr_2$ is unaffected by the impact of compression variability across lithologies as it is recorded across one unit of minerogenic silt. On the other hand, $RSLr_1$ and $RSLr_3$ directly overlie the lower and middle beds and their onsets occur at the organogenic-minerogenic contacts. For $RSLr_1$ and $RSLr_3$ to be considered an effect of variable compaction, we require pre-event rates of RSL rise that are similar in magnitude to that observed during the RSL jumps themselves; which are on the order of 15 mm yr^{-1} during $RSLr_1$ and 7 mm yr^{-1} during $RSLr_3$ (Fig. 2.7). Estimated rates of background RSL rise in SW Scotland at this time, both modelled and observed, do not exceed such values (Smith et al., 2003a; Bradley et al., 2011; Kuchar et al., 2012). Whilst we cannot determine the influence of compaction, if indeed present, we note that the microfossil changes observed are independent of potential compaction variability across lithologies. Hence, we conclude that there is evidence that RSL rose in three steps prior to the 8.2 event and, on this basis, accept hypothesis (1), that RSL rose in more than one abrupt step in the centuries leading up to the 8.2 event.

5.2 Comparison with existing chronologies: testing hypothesis (2)

There is debate regarding the potential routing and impact of freshwater discharge at the time interval of interest, with some authors suggesting routing into the sub-tropical North Atlantic and not the sub-polar gyre (e.g. Condron and Windsor 2011; Hill and Condron, 2014). Nevertheless, the strong polar foraminiferal and $\delta^{18}O$ signal in records from the sub-polar North Atlantic (Ellison et al., 2005; Kleiven et al., 2008) indicates a significant impact

in this region and provides a basis for chronological comparison with the three Cree Estuary RSL jumps.

Fig. 2.8 plots the age probability density functions and 2σ ranges (bars) computed for the start of each respective North Atlantic event. We observe ages that cluster in three largely distinct time intervals, with mid-points that are separated by up to two centuries. A first group contains $RSLr_1$, DCP6a and modelled peak meltwater discharge concomitant with LIS saddle collapse, which all occur between ~8800 to ~8600 cal yr BP. A second group of events contains $RSLr_2$, DCP6b; the downstream equivalent of the Hudson Bay "red-bed", the Rhine-Meuse Delta RSL jump and the earliest North Atlantic surface freshening event (FE_1) in MD99-2665, which occur between ~8600 to ~8300 cal yr BP. The final group of events occurred between ~8300 and ~8100 cal BP, where $RSLr_3$, the Mississippi Delta RSL jump and the youngest North Atlantic surface freshening event (FE_2) in MD99-2665 indicate strong overlap at the 1σ probability level. The 2σ range of DCP7 (Jennings et al., 2015) and the LAO drainage deposit recorded in James Bay (Roy et al., 2010) overlaps with the 2σ range of this final age group. In addition, they all overlap with the onset of the 8.2 event at 8305-8255 cal yr BP inferred from the stacked Greenland $\delta^{18}O$ record. Table 2.2 provides the age determinations of these individual estimates.

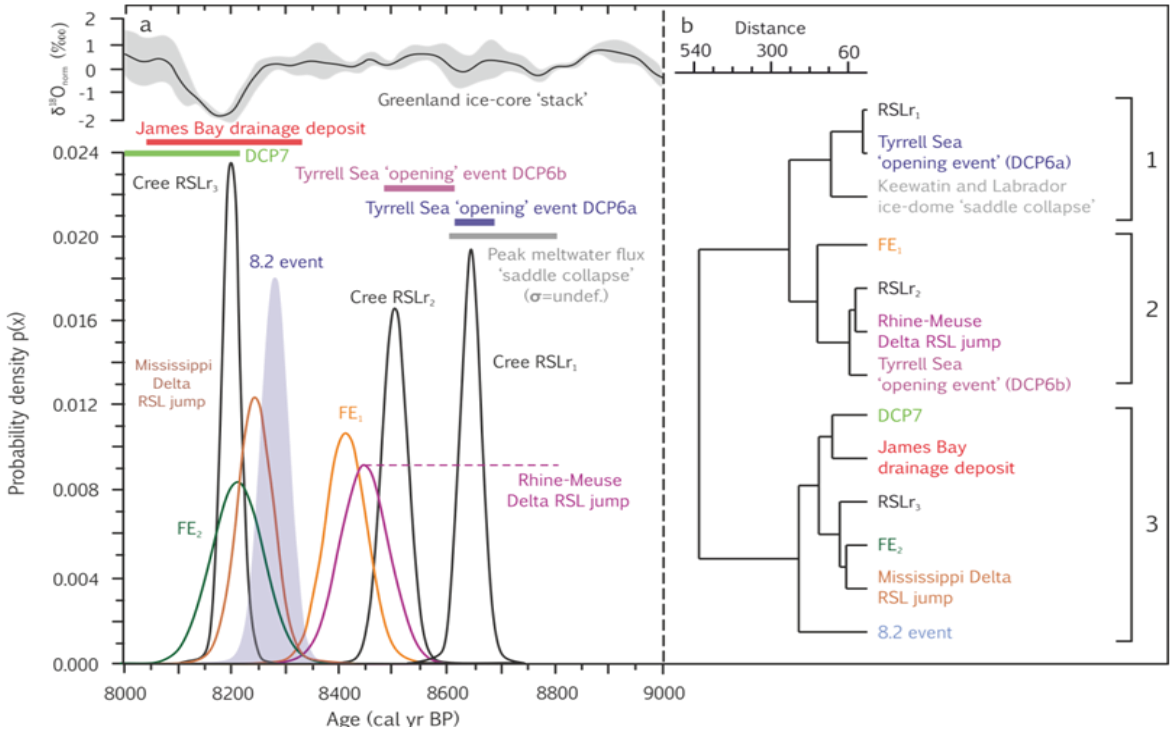

Figure 2.8. Timing and sequence of climate, ocean and sea-level events in the North Atlantic between 9000 and 8000 cal yr BP. a. Timing of events are expressed as age probability density functions (3σ), except for the Cree RSL jumps that represent the 95% confidence interval of the $BC421_{P\text{-}max}$ expressed symmetrically around mean values. Horizontal bars indicate 2σ probability ranges from existing studies. Age probability density functions of $RSLr_1$, $RSLr_2$ and $RSLr_3$ (black curves) in the Cree estuary from this study are plotted alongside DCP6a (blue bar) and DCP6b (purple bar) from Jennings et al. (2015), the James Bay drainage deposit (red bar; Roy et al., 2005), the onset of sudden sea-level rise in the Rhine-Meuse Delta (purple curve; Hijma and Cohen, 2010) and Mississippi Delta (brown curve; Li et al., 2012) and the two North Atlantic surface cooling and freshening events (FE_1; orange curve, FE_2 light blue curve) inferred from revised chronology of Kleiven et al. (2008). Peak meltwater discharge (modelled) associated with separation of Keewatin and Labrador 'saddle' (Gregoire et al., 2012) is shown as a gray bar (note that the full uncertainty range is undefined). The onset of the 8.2 event (shaded blue curve) is inferred from the Greenland ice-core $\delta^{18}O_{norm}$ (normalized) 'stack' (gray record; this study). **b.** Cluster plot of the events illustrated in (a) based on an analysis of age gaps between each event and the 8.2 event. Three clusters are recognised (labelled 1, 2, 3). The units of the x-axis are Euclidean distance units.

Table 2.2. Timing of abrupt events within the critical time interval. Ages presented are 2σ calibrated ranges with respect to BP (AD 1950), except for the 8.2 event (derived from GICC05 with respect to BP; Appendix 1).

	Position in stratigraphy / record	**Minimum age (cal yr BP)**	**Maximum age (cal yr BP)**	**Minimum age (yrs BP) from start of 8.2 event**	**Maximum age (yrs BP) from start of 8.2 event**	**Reference**
8.2 event	Start	8255	8305	0	0	This study
Cree Estuary $RSLr_3$	All	8163	8231	-142	-24	This study
FE_2	Start	8114	8308	-191	53	Kleiven et al. (2008); this study
Mississippi Delta	All	8180	8310	-125	55	Li et al. (2011)
James Bay drainage deposit	All	8032	8323	-273	68	Roy et al. (2011)
FE_1	Start	8338	8492	33	237	Kleiven et al. (2008); this study
Cree Estuary $RSLr_2$	All	8450	8550	145	295	This study
Rhine-Meuse Delta	Start	8455	8587	150	332	Hijma and Cohen (2010)
Cree Estuary $RSLr_1$	All	8610	8680	305	425	This study
DCP6b	Peak	8489	8609	184	354	Jennings et al. (2015)
Keewatin and Labrador saddle	Peak	8600	8800	295	545	Gregoire et al. (2012)

collapse						
DCP6a	Peak	8609	8694	304	439	Jennings et al. (2015)

Interpreting an accurate sequence of freshwater events is strongly dependent on the accuracy of the underpinning chronologies. Maximizing chronological accuracy and precision is critical given the short timescale under consideration and because of the limitations imposed by variable ^{14}C production across the time interval. In particular, minor plateaus in ^{14}C production occur between 8550-8400, 8300-8200 and 8150-8050 cal yr BP, while a much larger plateau occurs at 8950-8650 cal yr BP and could be implicated in the strong correlations in Fig. 2.8. To some extent however, this potential biasing effect is mitigated where age models incorporate stratigraphic information; such is the case with the Cree record. Further, the estimates derived from marine chronologies depend strongly on the magnitude of local marine reservoir corrections which are difficult to define. These problems are inherent to the process of ^{14}C calibration and demonstrate the limitations of the technique on these timescales. We are therefore unable to fully determine whether events within the critical time interval were synchronous but suggest that events are likely to have been synchronous when ages overlap, especially at the 1σ probability level.

The Cree observations demonstrate significant overlap in timing with existing estimates of short-lived events (Fig. 2.8); in particular those within the best resolved near-field record of final LIS retreat on the Cartwright Saddle (Jennings et al., 2015). We infer that local / regional processes are unable to explain the changes observed in the Cree stratigraphy. However, interpreting the wider significance of the Cree RSL jumps in the context of global sea-level change via direct comparison with existing RSL records from the Mississippi and Rhine-Meuse deltas is not straightforward (Tables 2.2 and 2.3). First, the second event in the Cree Estuary ($RSLr_2$) overlaps in timing with the Rhine-Meuse RSL jump but their magnitudes do not match following correction for a Laurentide source of freshwater release. Based on the record of the $BC421_{P\text{-}max}$, $RSLr_2$ had a eustatic equivalent magnitude of 1.25 ± 0.30 m (2σ), whereas the eustatic-corrected Rhine-Meuse Delta RSL jump measured 3.0 ± 1.3 m (1σ; Hijma and Cohen, 2010). It is possible that the maximum magnitude of $RSLr_2$ has not been fully constrained given that our reconstruction is restricted to the upper fringe of the tidal flat by the optimum of *P. sulcata* (Appendix 1, Fig. S10). Alternatively, the Rhine-Meuse Delta RSL jump could contain the signal of $RSLr_1$ in addition to $RSLr_2$, an explanation that we prefer given the short age gap between these two events within the Cree record. We hypothesize that the two episodes of freshwater release occurred in quick succession and were registered in the Rhine-Meuse record as a single RSL jump. Summing the fingerprint-corrected values of $RSLr_1$ and $RSLr_2$ generates a value of

1.8 ± 0.4 m (2σ) which sits comfortably within the vertical range of the Rhine-Meuse Delta RSL jump of 3.0 ± 2.6 m (2σ).

Table 2.3. Magnitude of abrupt sea-level change within the critical time interval. The correction for eustatic sea-level equivalent, assuming a LIS source of freshwater release with fingerprint values of 20% for the Mississippi Delta and 70% for the Cree Estuary and Rhine-Meuse Delta, respectively (after the geophysical model predictions of Kendall et al. (2008). *MSE = uncertainty is based on a mean squares estimate of the $RSLr_1$ and $RSLr_2$ uncertainties.

	Relative sea level change		**Eustatic sea-level equivalent**	
Sea-level jump	Mean (m)	2σ (m)	Mean (m)	2σ (m)
Cree Estuary $RSLr_3$ ($BC421_{P\text{-}max}$)	0.22	0.22	0.32	0.32
Mississippi Delta	0.33	0.23	1.65	1.15
Cree Estuary $RSLr_2$ ($BC421_{P\text{-}max}$)	0.88	0.19	1.26	0.28
Rhine-Meuse Delta	2.11	$0.89^{*1\sigma}$	3.01	2.53
Cree Estuary $RSLr_1$ ($BC421_{P\text{-}max}$)	0.38	0.19	0.55	0.27
Cree Estuary $RSLr_1$ and $RSLr_2$ summed (for comparison with Rhine-Meuse Delta RSL jump)			1.81	0.38^{*MSE}

The Mississippi Delta RSL jump coincides with $RSLr_3$, although again their associated magnitudes do not match following correction for a LIS source. $RSLr_3$ measures a eustatic-equivalent magnitude of 0.3 ± 0.3 m (2σ); while the Mississippi Delta RSL jump measures 1.7 ± 1.2 m (2σ), potentially placing $RSLr_3$ within the lower end of the Mississippi Delta uncertainty range. It is possible that the Mississippi Delta record contains unquantified background RSL rise, although this is difficult to determine as much depends on the perceived (i.e., assumed) rapidity of the RSL jumps. Here, for example, we assume that the Cree RSL jumps record near-instantaneous episodes of freshwater discharge such that the removal of the background signal is not necessary (i.e., the jumps contain no background signal). Indeed, if we detrend our estimates of the inferred background signal, which we note compare well with existing empirical observations (Smith et al., 2003a) and modelled estimates (Bradley et al., 2011; Kuchar et al., 2012) from our field-site, the magnitudes of the RSL jumps become smaller and less compatible with the Rhine-Meuse and Mississippi Delta observations. Our inability to resolve this is another indication that we are near the limit of the ^{14}C dating technique. Equally, the magnitudes of the Cree RSL jumps could be underestimated given the smoothing in our record and/or the possible influence of compaction. Also, our interpretations of RSL are based on the probability maximum and not the uncertainties of the full dataset.

Alternatively, the contrasts in the eustatic magnitudes of the final event may imply that a different meltwater source is required to explain the discrepancies. In particular, the local magnitudes of $RSLr_3$ and the Mississippi Delta RSL jump are remarkably similar which makes them more compatible as fingerprints of mass loss from the Antarctic Ice Sheet (Tamisiea et al., 2003; Mitrovica et al., 2009). Until this final event is reconciled with further sea-level data, we accept this as the most parsimonious explanation. We therefore suggest that this event was not implicated in the forcing of the 8.2 event (see further discussion below).

5.3 Deriving a sequence of events between 8900 to 8200 cal yr BP

In light of the Cree and existing observations, we propose the following three-event model of freshwater forcing from the LIS between 8900-8200 cal yr BP.

First, collapse of the Keewatin and Labrador ice-dome saddle (Gregoire et al., 2012) was swiftly followed by the opening of the Tyrrell Sea (Jennings et al., 2015). It coincides closely with detrital carbonate event DCP6a in core MD99-2236 from the Cartwright Saddle, dated to 8694-8609 cal yr BP (Jennings et al. 2015). This first event at ~8650 cal yr BP registered a RSL rise in SW Scotland of

0.38 ± 0.19 m, which translates to a eustatic-equivalent magnitude of 0.6 ± 0.3 m. There is no evidence of this event within sub-polar North Atlantic proxy records which could reflect low rates of freshwater discharge during this event, relative to the events that followed. However, it overlaps with a possible cold event at 8.75 ka BP exemplified by Rasmussen et al. (2007) in Greenland ice-core records. It could also have been responsible for the onset of the broad climatic anomaly that starts around this time (Rohling and Pälike, 2005).

A second episode of enhanced freshwater forcing followed shortly after at ~8500 cal yr BP and this registered a surface and deep ocean signal (FE_1; Kleiven et al., 2008; Ellison et al., 2005 Fig. 2.2) along with RSL jumps in SW Scotland ($RSLr_2$) and the western Netherlands. It was likely responsible for the reworked stratigraphy in the Mississippi Delta record (Li et al., 2011). The event agrees in timing with DCP6b, which Jennings et al. (2015) date to 8609-8489 cal yr BP and correlate with the Hudson Bay "red bed" deposit (e.g. Barber et al., 1999). We propose that $RSLr_2$ records the first and largest drainage of LAO. As it swiftly followed $RSLr_1$, we suggest that the collapse of the Keewatin and Labrador ice-domes reached a critical threshold whereby sufficient thinning forced the drainage of LAO subglacially under buoyant ice (Lajeunesse and St Onge, 2008; Clarke et al., 2004; Teller et al., 2002). The notion of a negligible time gap between these two events is supported by two lines of evidence; first, DCP6 has been subdivided into two remarkably close but largely separate events (DCP6a and DCP6b) by Jennings et al. (2015). Second, the Rhine-Meuse Delta RSL record (Hijma and Cohen, 2010) was unable to capture two distinctly separate events.

The final event within the Cree Estuary ($RSLr_3$) occurred at 8231-8163 cal yr BP and correlates broadly with DCP7; dated to 8219-7998 cal yr BP, which Jennings et al. (2015) interpret as representing the possible two-staged release of LAO and the cause of the 8.2 event. The LIS was the most likely source of this event given its registration in sub-polar North Atlantic proxy records (Ellison et al. 2006; Kleiven et al., 2008). It is therefore unlikely that the majority of freshwater was routed south into the sub-tropical gyre (Condron and Windsor, 2011; Hill and Condron, 2014), although it remains possible that this region received a portion of the total discharge volume. In view of the James Bay drainage deposits, which provide strong overlap at the 1σ probability level (Roy et al. 2011), we interpret this event as the second and final drainage of LAO following a century-scale phase of partial lake recharge (Teller et al., 2002).

5.4 Implications for AMOC sensitivity

The differences in the magnitudes of RSL jumps have implications for AMOC sensitivity. The

relatively large and abrupt freshwater pulses at ~8650 and ~8500 cal yr BP associated with the opening of the Tyrrell Sea and first drainage of LAO respectively could have preconditioned the AMOC (e.g. Carlson and Clark, 2012), with a relatively modest freshwater perturbation at ~8270 yrs BP triggering its eventual reorganization. If this final event was indeed low-magnitude, beyond the detection of RSL data, then it is possible that sea-ice-albedo feedbacks (Wiersma and Jongma, 2010; Otto-Bliesner and Brady, 2010) and freshwater fluxes were important in forcing the 8.2 event (Teller et al., 2002; Törnqvist and Hijma, 2012), as was the relative impact of the preconditioning event(s). In contrast, the apparent time lag between the closely-tied DCP7 and $RSLr_3$ (dated to ~8200-8000; Figs 2.2g and 2.2k) and the start of the 8.2 event (dated to 8305-8255; Fig. 2.2a) could imply that the final event had little bearing on the forcing of the 8.2 event. Indeed, it is conceivable that the first and largest LAO drainage at ~8500 cal yr BP was sufficient to trigger the 8.2 event as, although some models predict a near-instantaneous response to freshwater forcing (LeGrande et al. 2006; Wiersma and Renssen, 2006), some predict a climate overshoot and decadal-scale lagged response (Wiersma et al. 2011). While it is difficult to correlate single events across independently ^{14}C-dated chronologies on these short timescales, proxy records appear to demonstrate a time-transgressive signal (Alley and Ágústsdóttir, 2005), with the onset of the 8.2 event appearing to commence later with distance north. This might well suggest that the first and largest LAO drainage at ~8500 cal yr BP was the critical freshwater pulse, with the final RSL jump in the Cree Estuary ($RSLr_3$) and the third and final freshwater event had little impact on AMOC forcing. Clearly, resolving this with better time resolution is important for understanding the linkages between high magnitude sea-level and climate changes during an interglacial climate state.

6. Conclusions

The exceptionally well-mapped 8.2 event was originally thought to have been triggered by an AMOC freshwater perturbation associated with the drainage of LAO, but studies based on empirical data and modelling have increasingly speculated that the single-event model of freshwater forcing is an oversimplification of the 8.2 event's causal mechanism. RSL records provide one of the few means to calculate the magnitude of freshwater released and to determine a likely sequence of freshwater events prior to the 8.2 event.

We present the first microfossil-based RSL record that is continuous from 8800 to 7800 cal yr BP. It contains three decimetre- to metre-scale RSL jumps that overlap in age with a range of abrupt

events expressed in existing North Atlantic records, lending significant support to a three-event model of Laurentide freshwater release within the c. 500 yr window prior to the 8.2 event.

Our observations provide support of a two-event model of LAO drainage which was preceded by a dynamical ice-sheet contribution at ~8650 cal yr BP (0.55 ± 0.25 m). The first drainage was at ~8500 cal yr BP (1.25 ± 0.3 m). A second was coeval with the start of the 8.2 event but this was of a much lower magnitude (0.32 ± 0.32 eustatic sea-level equivalent). We advocate that in order to better understand this largely unresolved turbulent interval of the Holocene, future work should focus on developing and testing higher resolution climate and ocean models with new and existing empirical data.

References

Alley, R. B., P. A. Mayewski, T. Sowers, M. Stuiver, K. C. Taylor, and P. U. Clark (1997), Holocene climatic instability: A prominent, widespread event 8200 yr ago, *Geology* **25**, 483–486.

Alley, R.B and Agustdottir, A.M. 2005. The 8k event: causes and consequences of a major Holocene abrupt climate change, *Quaternary Science Reviews* **24**, 1123-1149.

Barber, D.C., Dyke, A., Hillaire-Marcel, C., Jennings, A.E., Andrews, J.T., Ker- win, M.T., Bilodeau, G., McNeely, G., Southon, J., Morehead, M.D., and Gagnon, J.-M. 1999. Forcing of the cold event of 8,200 years ago by catastrophic drainage of Laurentide lake: *Nature* **400**. 344–348, doi: 10.1038/22504.

Barlow N. L. M., Shennan I., Long A.J., Gehrels, W.R., Saher, M.H., Woodroffe, S.A., Hillier, C. H. 2013. Salt marshes as late Holocene tide gauges. *Global and Planetary Change* **106**, 90–110.

Birks, H.J.B., 1995. Quantitative palaeoenvironmental reconstructions. In: Maddy, D., Brew, J.S. (Eds.), Statistical Modelling of Quaternary Science Data. Quaternary Research Association, Cambridge, 161–254.

Bishop, W. W. & Coope, G. R. 1977. Stratigraphical and faunal evidence for Lateglacial and early Flandrian environments in south-west Scotland. In Gray, J. M. & Lowe, J. J. (eds), *Studies in the Scottish Late glacial environment*, 61±88. Oxford: Pergamon Press.

Bradley, S.L., Milne, G.A., Shennan, I., and Edwards, R. 2011. An improved Glacial Isostatic Adjustment model for the British Isles, *Journal of Quaternary Science* **26**, 5, 541-552.

Brain, M.J., Long, A.J., Petley, D.N., Horton, B.P. and Allison, R.J. Compression behaviour of minerogenic low energy intertidal sediments. *Sedimentary Geology* **233**, 28-41.

Bronk Ramsey, C. 2000. Comment on 'The Use of Bayesian Statistics for 14C dates of chronologically ordered samples: a critical analysis'. *Radiocarbon, **42***, 2, 199-202.

Bronk Ramsey, C. 2008. Deposition models for chronological records. *Quaternary Science Reviews, **27***, 1-2, 42-60.

Bronk Ramsey, C. 2008. Deposition models for chronological records. *Quaternary Science Reviews, **27***, 1-2, 42-60.

Bronk Ramsey, C. 2009a. Bayesian analysis of radiocarbon dates. *Radiocarbon, **51***, 1, 337-360.

Carlson, A.E., and Clark, P.U., 2012, Ice-sheet sources of sea-level rise and freshwater discharge during the last deglaciation, *Reviews of Geophysics* **50**, doi: 10.1029/ 2011RG000371.

Clarke, G. K. C., Leverington, D. W., Teller, J. T. & Dyke, A. S. 2004. Paleohydraulics of the last outburst flood from glacial Lake Agassiz and the 8200 BP cold event. *Quaternary Science Reviews* **23,** 389–407.

Condron, A., Windsor, P. 2011. A subtropical fate awaited freshwater discharged from glacial Lake Agassiz, *Geophysical Research Letters* **38**, 3, 10.1029/2010GL046011.

Cullingford, R. A., Caseldine, C. J. and Gotts, P. E. 1980. Early Flandrian land and sea level changes in Lower Strathearn. *Nature* **284**, 159-61.

Czernik, J., Goslar, T. 2001. Preparation of graphite targets in The Gliwice Radiocarbon Laboratory for AMS 14C dating. *Radiocarbon* **43**, 283–291.

de Vernal, A., Hillaire-Marcel, C., von Grafenstein, U., Barber, D., 1997. Researchers look for links among paleoclimate events: EOS (Transactions, American Geophysical Union) **78**, 247–249.

Ellison, C.R.W., Chapman, M.R., and Hall, I.R. 2006. Surface and deep ocean interactions during the cold climate event 8200 years ago. *Science* **312**, 1929–1932, doi: 10.1126/science.1127213.

Gehrels W.R., Kirby J.R., Prokoph A., *et al.* 2005. Onset of recent rapid sea-level rise in the western Atlantic Ocean. *Quaternary Science Reviews* **24**: 2083–2100.

Gehrels, W.R., Roe, H.M., Charman, D.J. 2001. Foraminifera, testate amoebae and diatoms as sea-level indicators in UK saltmarshes: a quantitative multiproxy approach, *Journal Quaternary Science* **16**, 3, 201-220. DOI: 10.1002/JQS.588.

Gilks, W., Richardson, S., Spiegelhalter, D. (Eds.) 1996. Markov Chain Monte Carlo in Practice. Chapman & Hall, London.

Gregoire, L. J., Payne, A. J., Valdes, P. J. 2012. Deglacial rapid sea level rises caused by ice-sheet saddle collapses, *Nature* **487,** 219–222.

Hartley, B., Barber, H.G., Carter, J.R. 1996. An Atlas of British Diatoms. Sims, P.A (ed). Biopress, London.

Haslett, S.K., and Bryant, E.A. 2007. Reconnaissance of historic (post-AD 1000) high-energy deposits along the Atlantic coasts of southwest Britain, Ireland and Brittany, France. *Marine Geology* **242**, 207-220.

Hijma, M.P and Cohen, K.M. 2010. Timing and magnitude of the sea-level jump precluding the 8200 yr event, *Geology* **38**, 3, 275-278.

Hill, J.C., Condron, A. 2014. Subtropical iceberg scours and meltwater routing in the deglacial western North Atlantic, *Nature Geoscience* **7**, 806-810. DOI: 10.1038/NGEO2267.

Hill, T.C.B., Woodland, W.A., Spencer, C.D., and Marriot, S.B. 2007. Holocene sea-level change in the Severn Estuary, southwest England: a diatom-based sea-level transfer function for macrotidal settings. *The Holocene*, **17**, 5, 639-648.

Hillaire-Marcel, C. de Vernal, A. Piper, D.J.W. 2007. Lake Agassiz final drainage event in the North Atlantic. *Geophysical Research Letters* **34**, doi:10.1029/2007GL030396.

Hoffman, A.S., Carlson, A.E., Windsor, K., Klinkhammer, G.P., Le Grande, A.N., Andrews, J.T., Strasser, J.C. 2012. Linking the 8.2 ka event and its freshwater forcing in the Labrador Sea, *Geophysical Research Letters* **39**, doi:10.1029/2012GL053047.

Hydrographic Office (2011) Admiralty Tide Tables: United Kingdom and Ireland including European and Channel Ports: Hydrographer of the Navy, Taunton, Somerset, 1, 1-364.

Jardine, W. G. 1975. Chronology of Holocene marine transgression and regression in south-western Scotland. *Boreas* **4**, 173 96.

Jennings, A., Andrews, J., Pierce, C., Wilson, L., Olfasdotttir, S. 2015. Detrital carbonate peaks on the Labrador shelf, a 13e7 ka template for freshwater forcing from the Hudson Strait outlet of the Laurentide Ice Sheet into the subpolar gyre, *Quaternary Science Reviews* **107**, 62-80. http://dx.doi.org/10.1016/j.quascirev.2014.10.022.

Juggins, S. (2011) C^2 Version 1.6: Software for Ecological and Palaeoecological Data Analysis and Visualisation: Department of Geography, University of Newcastle, Newcastle upon Tyne, U.K.

Kendall, R.A, Mitrovica, J.X., Milne, G.A., Tornqvist, T.E. and Li, Y.X. 2008. The sea-level fingerprint of the 8.2 ka event, *The Geological Society of America* **35**, 5, 423-426.

Kleiven, H.F., Kissel, C., Laj, C., Ninnemann, U.S., Richter, T.O., Cortijo, E. 2008. Reduced North Atlantic deep water coeval with the glacial Lake Agassiz Freshwater Outburst. *Science* **319**, 5859, 60-64.

Kobashi, T., Severinghaus, J.P., Brook, E.J., Barnola, J.M., and Grachev., A.M. 2007. Precise timing and characterization of abrupt climate change 8200 years ago from air trapped in polar ice. *Quaternary Science Reviews* **26**, 1212–1222, doi:10.1016/j.quascirev.2007.01.009.

Kuchar, J., Milne, G., Hubbard, A., Patton, H., Bradley, S., Shennan, I., and Edward, R. 2012. Evaluation of a numerical model of the British-Irish ice sheet using relative sea-level data: implications for the interpretation of trimline observations, *Journal Quaternary Science* **27**, 6, 597-605.

Lajeunesse, P., and St-Onge, G. The subglacial origin of the Lake Agassiz-Ojibway final outburst flood, *Nature Geoscience* **1**, 184-187. doi:10.1038/ngeo130.

LeGrande, A.N., Schmidt, G.A., Shindell, D.T., Field, C.V., Miller, R.L., Koch, D.M., Faluvegi, G. and Hoffman, G. 2006. Consistent simulations of multiple proxy responses to an abrupt climate change event, *Proceedings of the National Academy of Sciences* **103**, 4, 837-842. doi: 10.1073/pnas.0510095103.

Leverington, D. W., J. D. Mann, and J. T. Teller. 2002. Changes in the bathymetry and volume of glacial Lake Agassiz between 9200 and 7700 14C yr B.P. *Quaternary Research* **57**, 244–252.

Li, Y.X., Tornqvist, T.E., Nevitt, J.M., and Kohl, B. 2011. Synchronizing a sea-level jump, final lake Agassiz drainage and abrupt cooling 8200 years ago, *Earth and Planetary Science Letters* **315-316**, 41-50.

Long, A.J. and Innes, J.B. 1993. Holocene sea-level and coastal sedimentation in Romney Marsh, southeast England, UK.*The Proceedings of the Geologists' Association*, 104, 223-237.

Marshall, W.A., Gehrels, W.R., Garnett, M.H., Freeman, S.P.H.T., Maden, C., Xu, S., 2007. The use of 'bomb spike' calibration and high-precision AMS 14C analyses to date salt-marsh sediments deposited during the past three centuries. *Quaternary Research*, **68**, 325–337.

Mitrovica, J.X., Gomez, N., Clark, P.U. 2009. The sea-level fingerprint of West Antarctic collapse, *Science* **323**, 753.

Mitrovica, J.X., Tamisiea, M.E., Davis, J.L., Milne, G.A. 2001. Recent mass balance of polar ice sheets inferred from patterns of global sea-level change, *Nature* **409**, 1026-1029.

Morrill, C., Ward, E.M., Wagner, A.J., Otto-Bliesner, B.L., Rosenbloom, N. 2014. Large sensitivity to freshwater forcing location in 8.2 ka simulations. *Paleoceanography* **29**, doi:10.1002/2014PA002669.

Otto-Bliesner, B.I. and Brady, E.C. 2010. The sensitivity of the climate response to the magnitude and location of freshwater forcing: last glacial maximum experiments, *Quaternary Science Reviews* **29**, 56-73.

Palmer, A.J.M., and Abbott, W.H. 1986. Diatoms as sea-level indicators. In: Van de Plassche O (ed) Sea level research: A manual for the collection and evaluation of data. Geo Books, Norwich.

Rasmussen, S. O., Seierstad, I. K., Andersen, K. K., Bigler, M., Dahl-Jensen, D., and Johnsen, S. J 2008. Synchronization of the NGRIP, GRIP, and GISP2 ice cores across MIS 2 and palaeoclimatic implications, *Quaternary Science Reviews* **27**, 18–28, doi:10.1016/j.quascirev.2007.1001.1016.

Reimer, P. J., Bard, E., Bayliss, A., Beck, J. W., Blackwell, P. G., Bronk Ramsey, C., Grootes, P. M., Guilderson, T. P., Haflidason, H., Hajdas, I., HattŽ, C., Heaton, T. J., Hoffmann, D. L., Hogg, A. G., Hughen, K. A., Kaiser, K. F., Kromer, B., Manning, S. W., Niu, M., Reimer, R. W., Richards, D. A., Scott, E. M., Southon, J. R., Staff, R. A., Turney, C. S. M., & van der Plicht, J. 2013. IntCal13 and Marine13 Radiocarbon Age Calibration Curves 0-50,000 Years cal BP, *Radiocarbon **55***.

Rohling, E.J., Foster, G.L., Grant, K.M., Marino, G., Roberts, A.P., Tamisiea, M.E. and Williams, F. 2014. Sea-level and deep-sea temperature variability over the past 5.3 million years, *Nature* **508**, 477-482.

Roy, M., Dell'Oste, F., Veillette, J.J., de Vernal, A., Helie, J.-F., Parent, M., 2011. Insights on the events surrounding the final drainage of Lake Ojibway based on James Bay stratigraphic sequences. *Quaternary Science Reviews* **30**, 682-692.

Simkins, L.M., Simms, A.R., Cruse, A.M., Troiani, T. Atekwana, E.A., Puckette, J., Yokayama, Y. 2012. Correlation of early and mid-Holocene events using magnetic susceptibility in estuarine cores from bays along the northwestern Gulf of Mexico, *Palaeogeography, Palaeoclimatology, Palaeoecology* **346-347**, 95-107.

Smith, D.E., Wells, J.M., Mighall, T.M., Cullingford, R.A., Holloway, L.K., Dawson, S., Brooks, C.L. 2003a. Holocene relative sea levels and coastal changes in the lower Cree valley and estuary, SW Scotland, UK. *Transactions of the Royal Society of Edinburgh: Earth Sciences*, **93,** 301-331.

Tamisiea ME, Mitrovica JX, Milne GA, Davis JL. 2003. Long wave length sea level and solid surface perturbations driven by polar ice mass variations: fingerprinting Greenland and Antarctic Ice Sheet flux. *Space Science Reviews* (108) 81–93.

Teller, J. T., Leverington, D. W. & Mann, J. D. 2002. Freshwater outbursts to the oceans from glacial Lake Agassiz and their role in climate change during the last deglaciation. *Quaternary Science Reviews* **21,** 879–887.

ter Braak, C.J.F., Juggins, S., 1993. Weighted averaging partial least squared regression (WA-PLS): an improved method for reconstructing environmental variables from species assemblages. *Hydrobiologia* **269**, 270, 485–502.

Thomas, E.R., Wolff, E.W., Mulvaney, R., Steffensen, J.P., Johnsen, S.J., Arrowsmith, C., White, J.W.C., Vaughn, B., Popp, T. 2007. The 8.2 ka event from Greenland ice cores. *Quaternary Science Reviews* **26**, 1-2, 70-81.

Törnqvist, T.E., Hijma, M.P. 2012. Links between early Holocene ice-sheet decay, sea-level rise and abrupt climate change, *Nature Geoscience* **5**, 601-606. DOI: 10.1038/NGEO1536.

Troels-Smith, J. 1955. Karakterisering af lose jordarter.Characterisation of unconsolidated sediments, *Geological Survey of Denmark*, **4**, 3, 1-73.

Vos, Peter C., de Wolf, H., 1993. Diatoms as a tool for reconstructing sedimentary environments in coastal wetlands; methodological aspects. In: Twelfth International Diatom Symposium. Springer, Netherlands, 285-296.

Ward, S. L., 2014. A new proxy for constraining palaeotidal model simulation of the Northwest European Shelf Seas. Doctoral thesis, Bangor University.

Wells, J. M. 1997. Flandrian relative sea level changes in the Cree estuary region, southwest Scotland. Doctoral thesis. Coventry University.

Wiersma AP, Renssen H. 2006. Model–data comparison for the 8.2 ka BP event: confirmation of a forcing mechanism by catastrophic drainage of Laurentide lakes. *Quaternary Science Reviews* **25**, 63–88.

Wiersma, A.P., Jongma, J.I. 2010. A role for icebergs in the 8.2 ka climate event, *Climate Dynamics* **35**, 535-549.

Wilson, G.P., and Lamb, A.L. 2011. An assessment of the utility of regional diatom-based transfer functions. *Journal Quaternary Science* **27**, 4, 360-370. DOI: 10.1002/jqs.1553.

Zecchin, M., Tosi, L., Caffau, M., Baradello, L., Donnici, S. 2014. Sequence stratigraphic significance of tidal channel systems in shallow lagoon (Venice, Italy). *The Holocene* **24**, 6. doi:10.1177/0959683614526903.

Zong, Y., Horton, B.P. 1999. Diatom-based tidal-level transfer functions as an aid in reconstructing Quaternary history of sea-level movements in the UK. *Journal Quaternary Science* **14**, 2, 15

Appendix 1

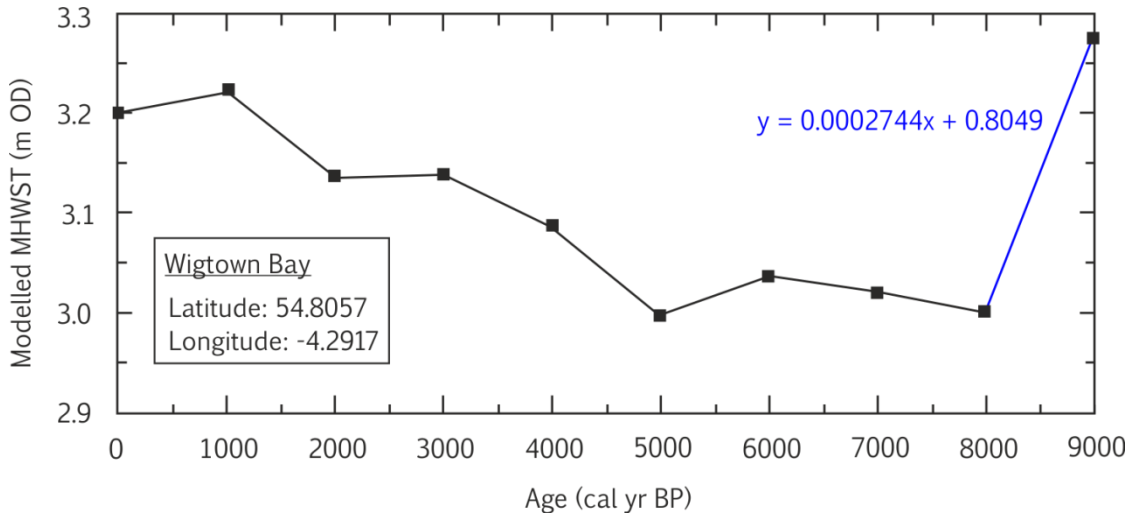

Fig. S1. The variable height of MHWST as quantified by the palaeotidal model of Ward (2014) for the outer Cree Estuary (coordinates shown). Sample-specific palaeotidal corrections are applied using a simple linear interpolation of the 8.0 to 9.0 kyr BP timeslices (blue). The correction applied assumes a constant MTL of 0 m (relative to OD).

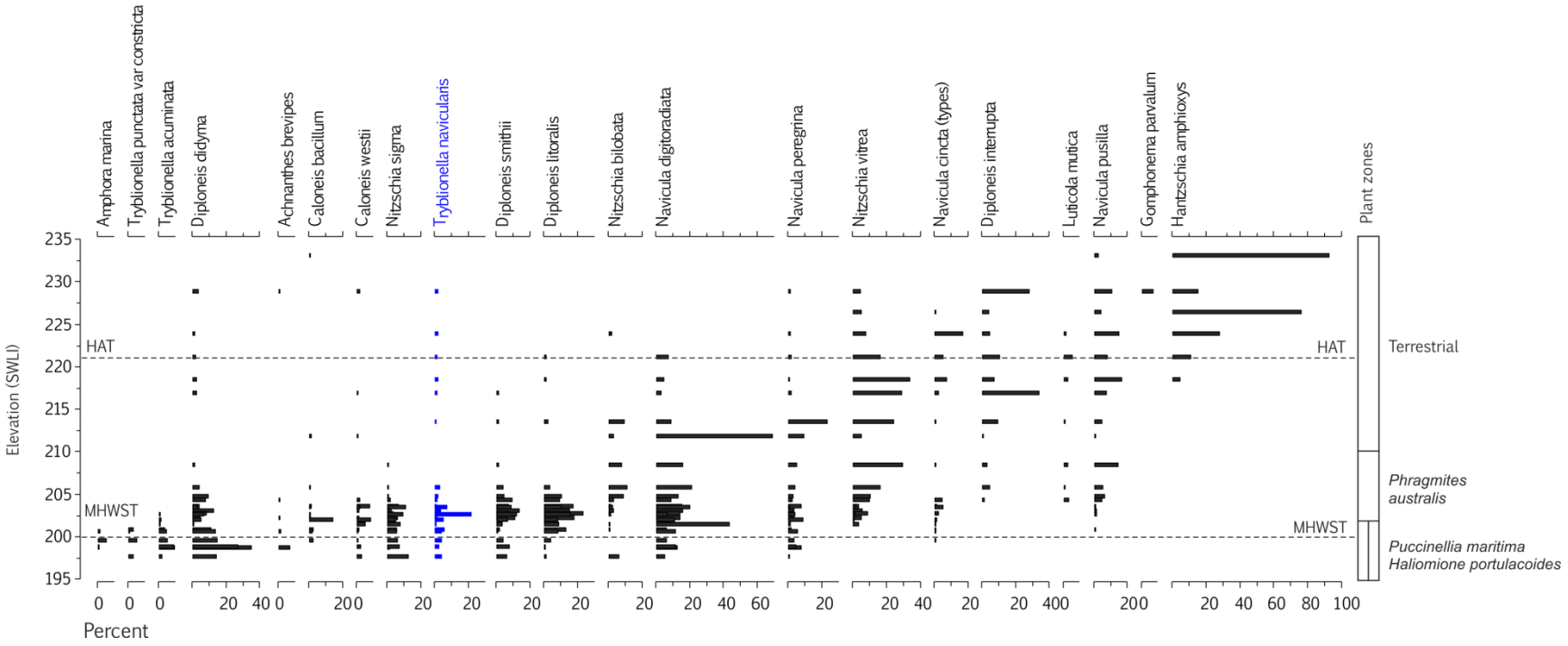

Fig. S2. Biostratigraphy and floral zonation at Brancaster Marsh (after Gehrels et al., 2001). *Tryblionella navicularis* is highlighted in blue.

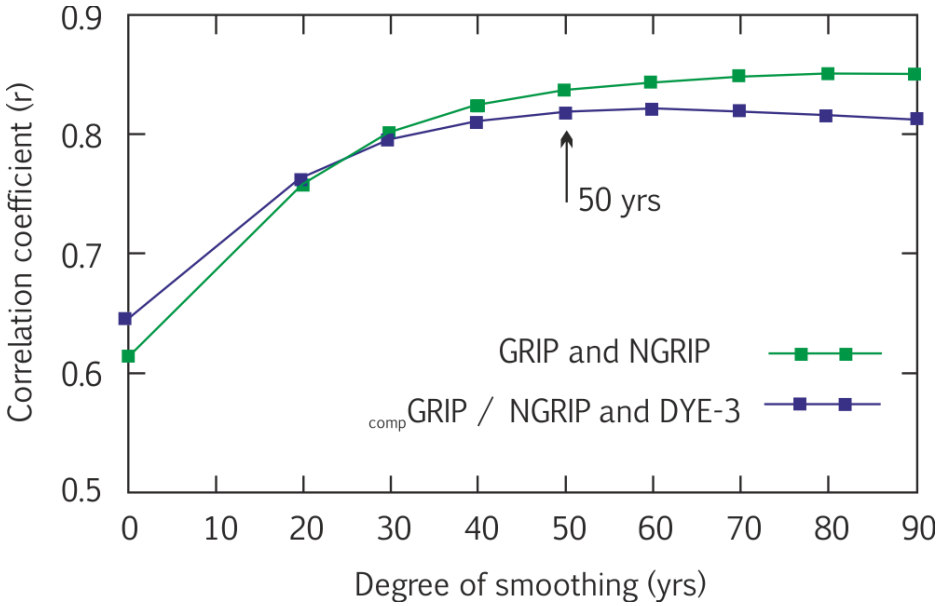

Fig. S3. Correlation coefficients of smoothed regressed records of GRIP, NGRIP and DYE-3 $\delta^{18}O_{ice}$.

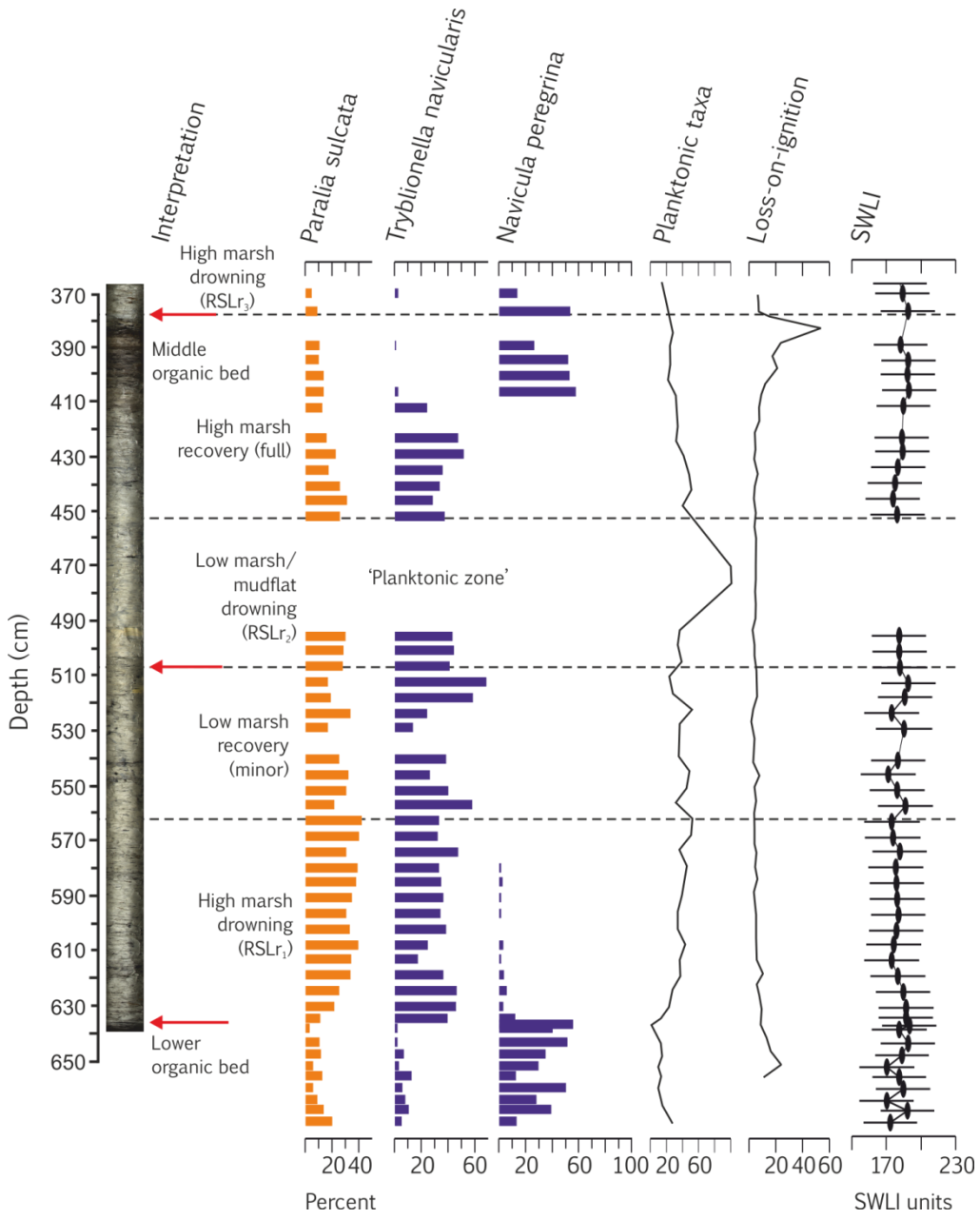

Figure S4. Summary plot and palaeoenvironmental interpretation of core BC421 stratigraphy, with a particular focus on the two lower drowning events. Taxa shown are the three most abundant. We interpret three stages of intertidal drowning, summarised from bottom to top: a high-marsh drowning, a low-marsh/mudflat drowning and a high-marsh drowning (red arrows).

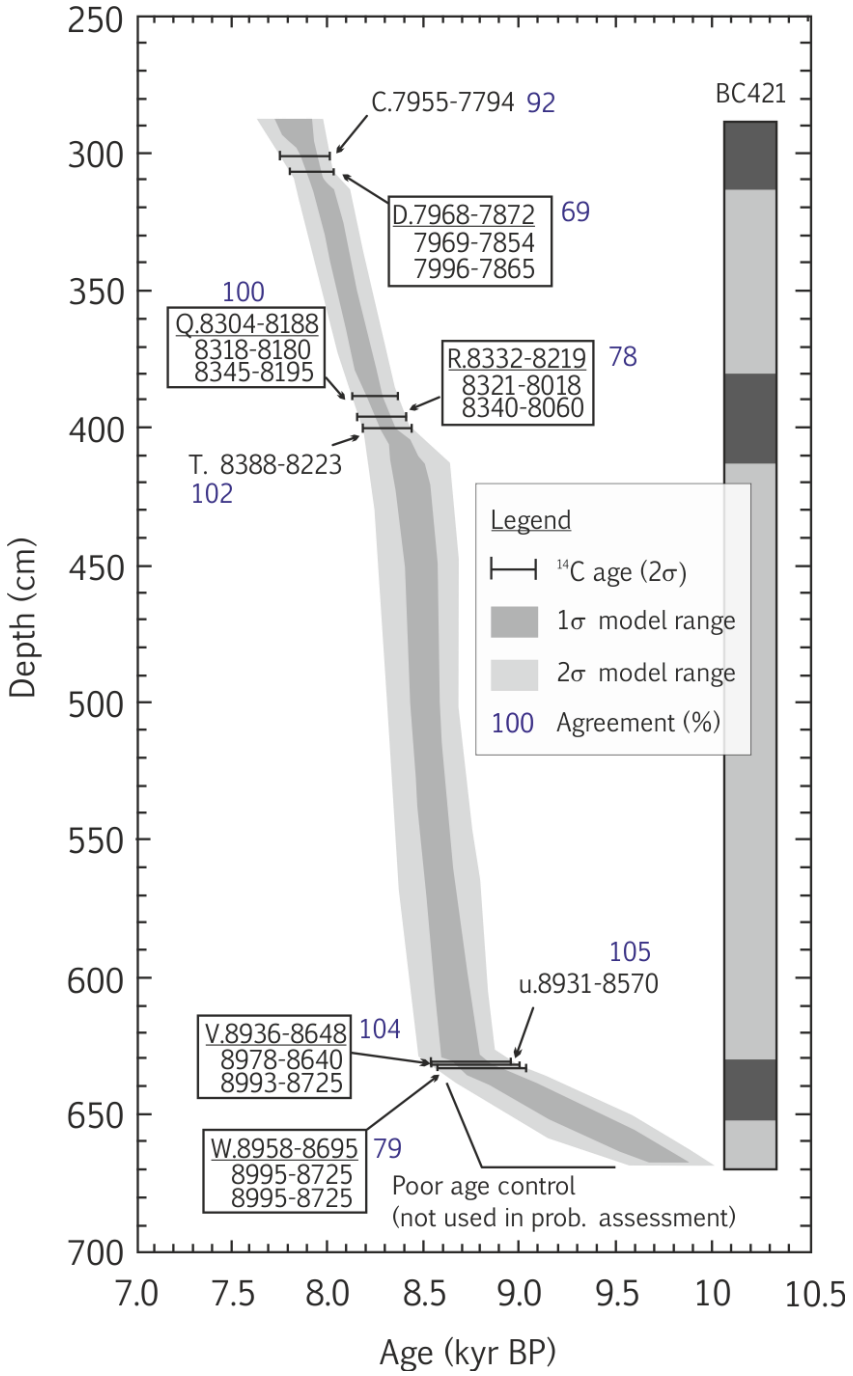

Fig. S5. OxCal 4.2 "Sequence" model alongside the simplified lithostratigraphy of core BC421. Boxed ages indicate duplicate ages that have been averaged (resulting weighted average age in underlined).

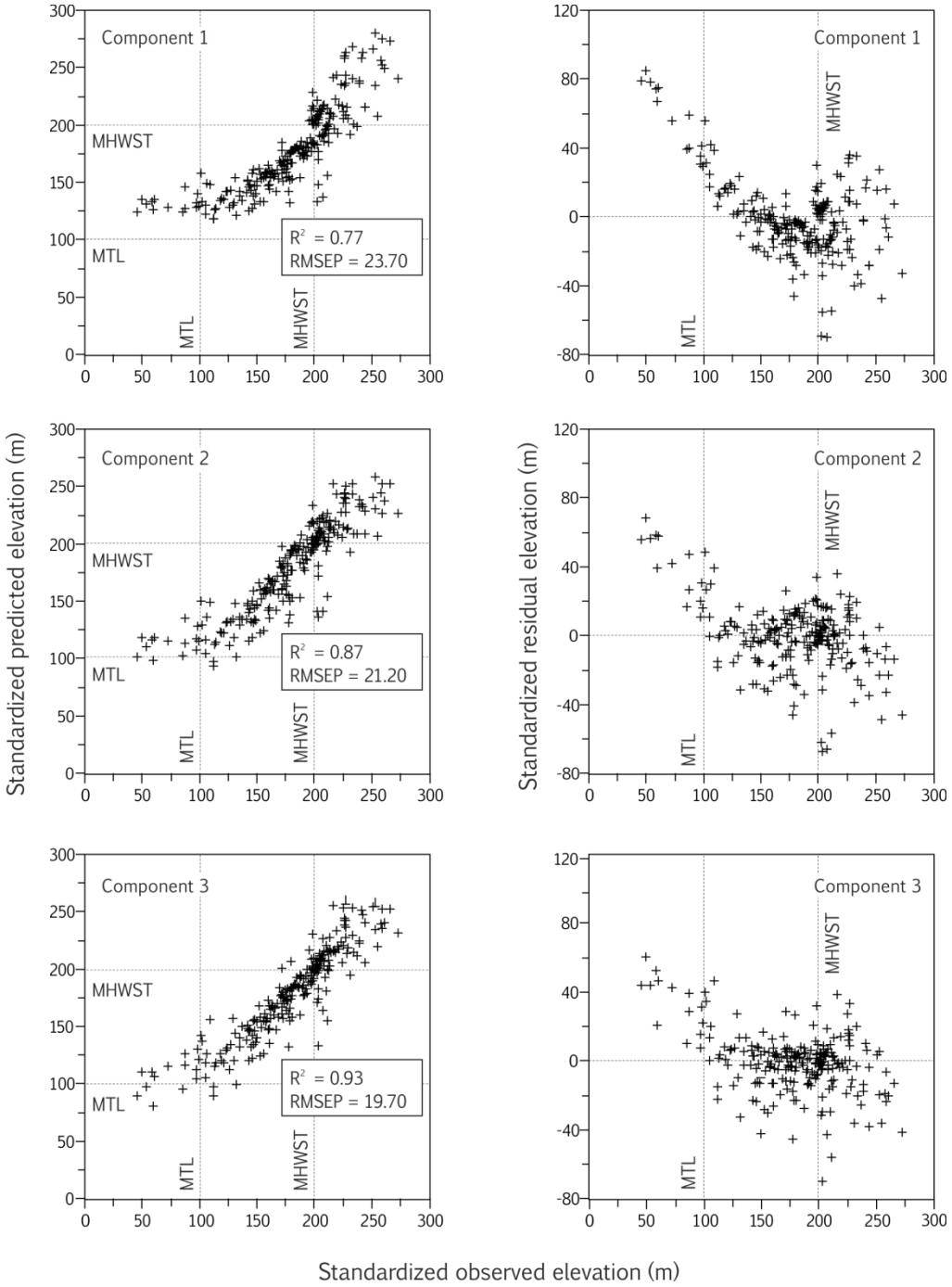

Fig. S6. Plots of observed versus predicted (left) and observed versus residual (right) palaeo-marsh surface elevation (SWLI) for the 'full' one-, two- and three-component WA-PLS model comprising n=231 samples. Transfer function developed in C2 software (Juggins, 2006). Statistics R^2 and RMSEP and tidal data are illustrated.

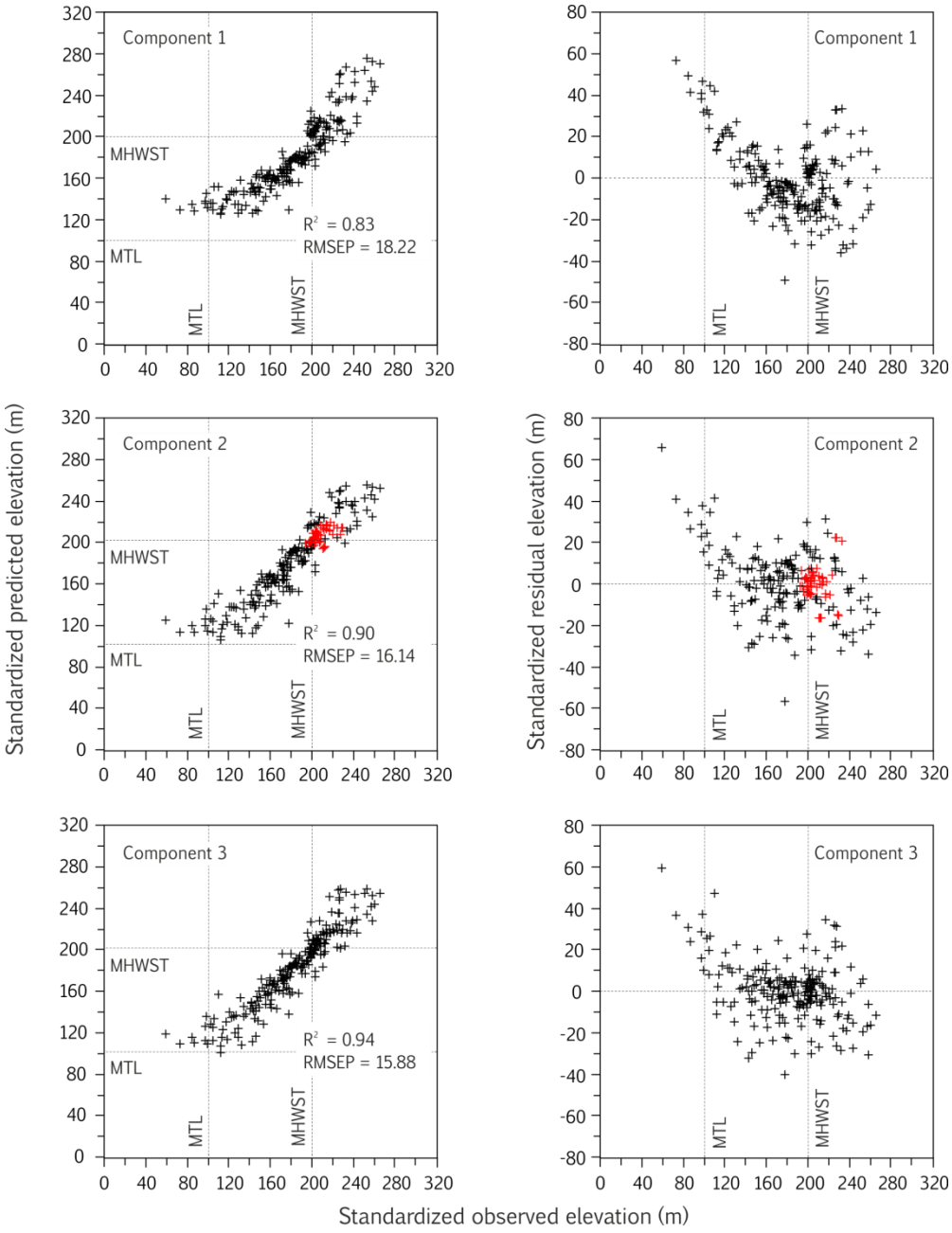

Fig. S7. Plots of observed versus predicted (left) and observed versus residual (right) palaeo-marsh surface elevation (SWLI) for the 'screened' one-, two- and three-component WA-PLS model comprising n=217 samples. Transfer function developed in C^2 software (Juggins, 2006). Brancaster samples are highlighted (red) on the chosen component 2 model. Statistics R^2 and RMSEP and tidal data are illustrated.

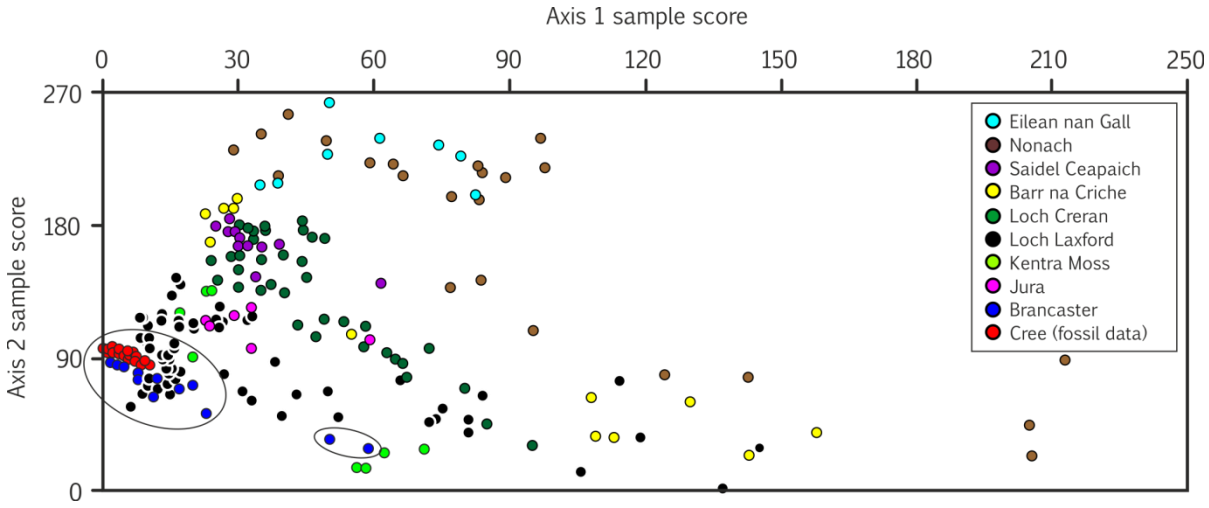

Fig. S8. Detrended correspondence analysis (DCA) sample plot of the 'full' model of Barlow et al. (2013) which now includes Brancaster marsh samples (blue). The Cree fossil samples (red) are not dissimilar to the Brancaster marsh and Loch Laxford modern samples. Ellipses mark the Cree fossil and Brancaster Marsh samples.

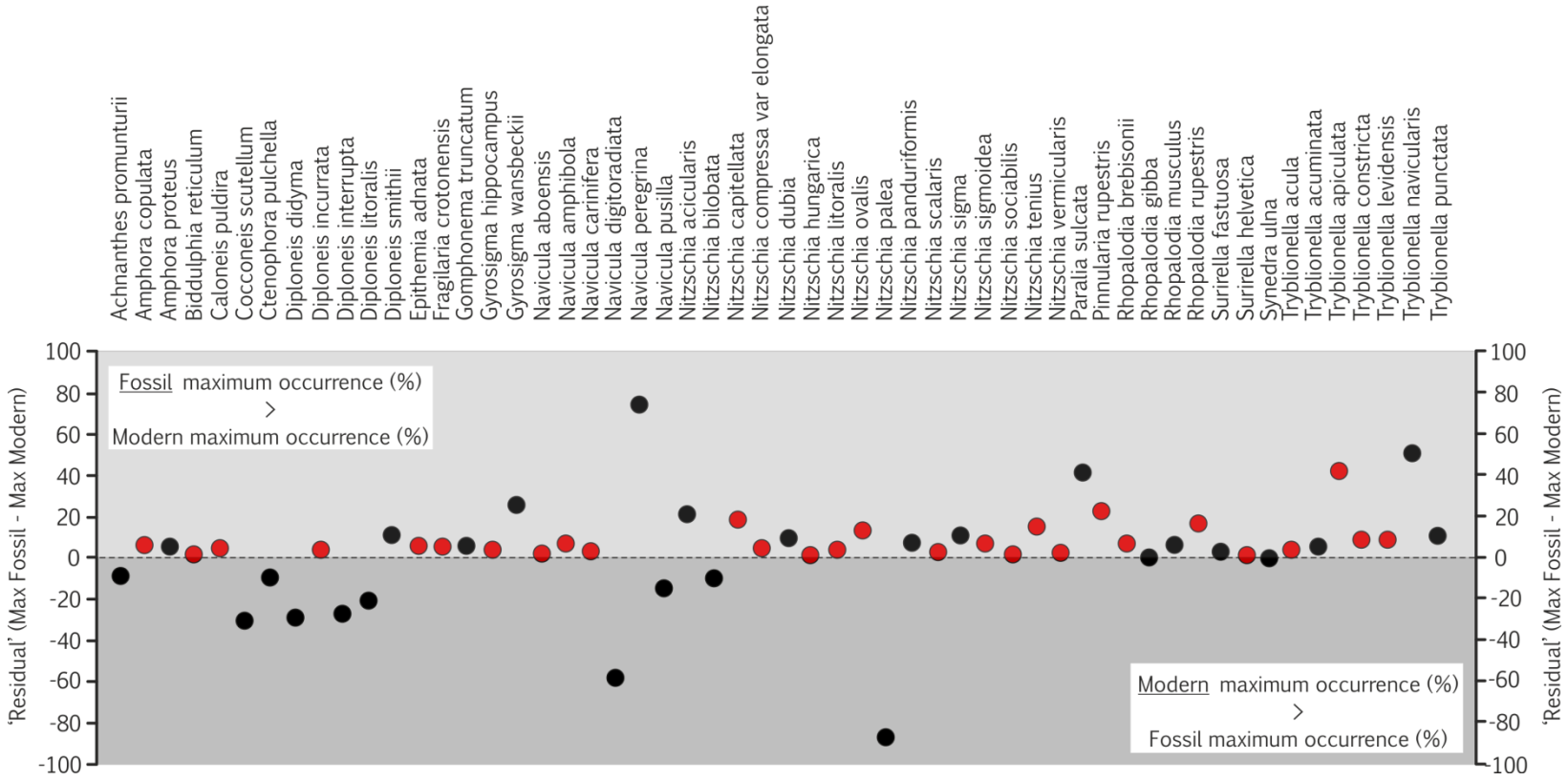

Fig. S9 Plot of maximum fossil versus maximum modern occurrences ('residuals') of all species found at Blair's Croft. Minus values indicate taxa that are more abundant in the modern than in the fossil record, vice versa for the positive values (hence, the positive values are the most important in terms of the reconstruction). Taxa with no modern analogues are shown in red, which are typically rare forms within either the assemblage and/or core.

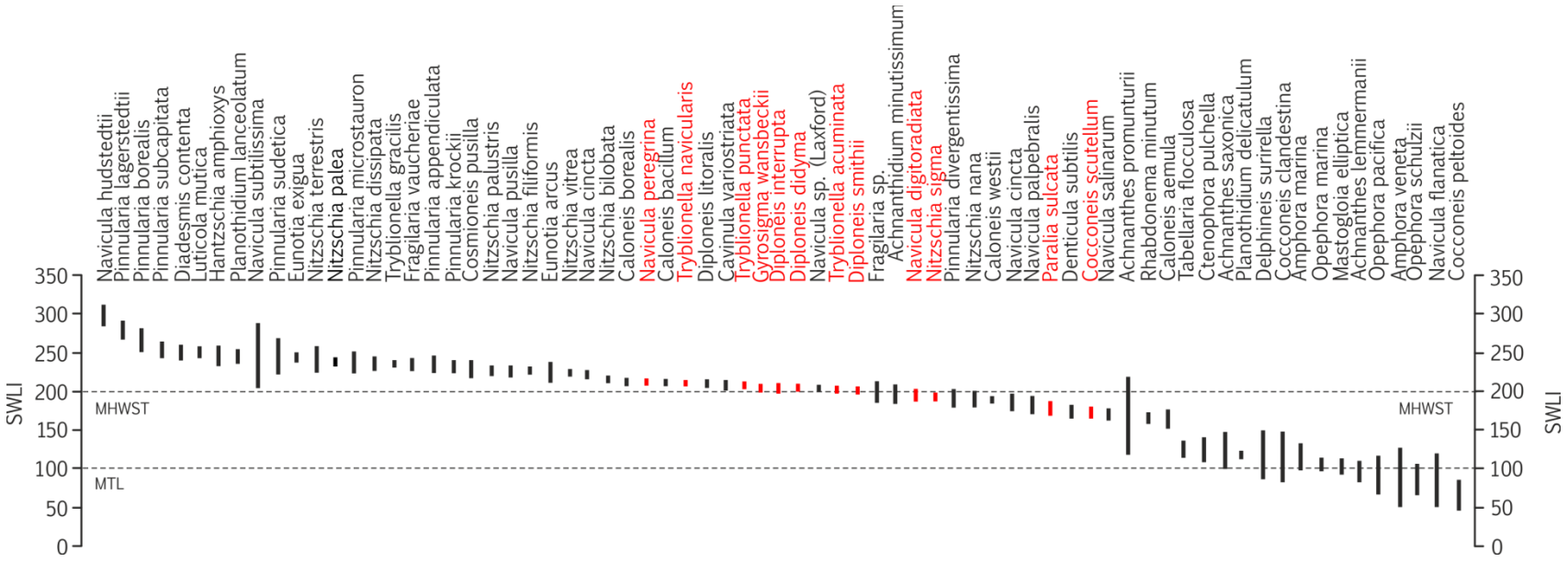

Fig. S10. Species coefficients and bootstrapped standard errors (1000 permutations) of taxa present in the modern training set (>10% abundance, with the exception of *P. sulcata, G. wansbeckii, T. punctata* and *T. acuminata* that comprise <10% of modern assemblages. These are also included because of their representation in the fossil record). Key fossil taxa (>10%) from the Cree Estuary are illustrated in red.

Table S1. RSL reconstruction data from BC421 (mean points and uncertainties). $1SE_{boot}$ = bootstrapped one standard error of the reconstruction (component 2 – WA-PLS model). Individual errors used in the calculation of total uncertainty (mean squares estimate (MSE); a, b, c) are indicated in red. Blue shading highlights data-points with poor age control (not included in RSL interpretations and probabilistic assessment). Grey shading highlights the "planktonic zone" within the microfossil record.

Sample code	OD (m)	Depth (cm)	Age (μ)	Age (1σ)	Palaeotidal correction (MHWST - MTL) (m) (Section 6)	Palaeo-marsh surface elevation (SWLI)	Palaeo-marsh surface elevation $1SE_{boot}$ (SWLI)	RSL (m)	RSL $1SE_{boot}$ (m) (a)	Palaeotidal range correction error (m) (b)	Core compaction error (m) (c)	MSE (m) (1σ)
J	2.72	668	9781	103	3.49	192.3	15.6	-0.50	0.55	0.06	0.2	0.58
I	2.76	664	9667	137	3.46	202.1	15.6	-0.77	0.54	0.06	0.2	0.58
H	2.80	660	9553	156	3.43	190.2	15.8	-0.29	0.54	0.06	0.2	0.58
F	2.84	656	9439	167	3.39	199.6	15.7	-0.54	0.53	0.06	0.2	0.57
E	2.88	652	9325	169	3.36	197.4	15.6	-0.40	0.53	0.06	0.2	0.57
D	2.92	648	9210	164	3.33	190.2	15.8	-0.09	0.53	0.06	0.2	0.57
C	2.96	644	9096	151	3.30	199.1	15.6	-0.31	0.51	0.06	0.2	0.55
B	3.00	640	8982	129	3.27	202.5	15.6	-0.35	0.51	0.06	0.2	0.55
1	3.05	635	8847	77	3.23	197.4	16.0	-0.10	0.52	0.06	0.2	0.56
2	3.06	634	8826	67	3.23	203.2	15.7	-0.27	0.51	0.06	0.2	0.55
4	3.09	631	8734	77	3.20	201.3	15.6	-0.15	0.50	0.06	0.2	0.54
5	3.13	627	8692	95	3.19	201.4	15.8	-0.10	0.50	0.06	0.2	0.54
6	3.19	621	8684	93	3.19	199.7	15.7	0.01	0.50	0.06	0.2	0.54

7	3.24	616	8675	91	3.19	196.6	15.8	0.16	0.50	0.06	0.2	0.54
8	3.30	610	8666	89	3.18	193.0	15.8	0.34	0.50	0.06	0.2	0.54
9	3.35	605	8658	88	3.18	194.4	15.8	0.35	0.50	0.06	0.2	0.55
10	3.41	599	8649	86	3.18	195.8	15.7	0.36	0.50	0.06	0.2	0.54
11	3.46	594	8640	84	3.18	196.9	15.8	0.39	0.50	0.06	0.2	0.54
12	3.52	588	8632	83	3.17	196.1	15.8	0.47	0.50	0.06	0.2	0.54
13	3.57	583	8623	82	3.17	196.0	15.8	0.53	0.50	0.06	0.2	0.54
14	3.63	577	8614	81	3.17	195.3	15.8	0.61	0.50	0.06	0.2	0.54
15	3.68	572	8606	80	3.17	197.7	15.8	0.59	0.50	0.06	0.2	0.54
16	3.74	566	8597	79	3.16	193.7	15.9	0.77	0.50	0.06	0.2	0.55
17	3.79	561	8588	78	3.16	193.2	15.9	0.85	0.50	0.06	0.2	0.55
18	3.85	555	8580	78	3.16	201.0	15.7	0.66	0.50	0.06	0.2	0.54
19	3.90	550	8571	77	3.16	196.3	15.8	0.86	0.50	0.06	0.2	0.54
20	3.96	544	8563	77	3.15	191.1	15.9	1.09	0.50	0.06	0.2	0.54
21	4.01	539	8554	77	3.15	196.7	15.8	0.96	0.50	0.06	0.2	0.54
22	4.12	528	8545	78	3.15	200.2	16.2	0.97	0.51	0.06	0.2	0.55
23	4.18	522	8537	78	3.15	193.1	15.9	1.25	0.50	0.06	0.2	0.54

24	4.23	517	8528	79	3.14	200.8	15.7	1.07	0.49	0.06	0.2	0.54
25	4.29	511	8519	79	3.14	202.7	15.7	1.06	0.49	0.06	0.2	0.54
26	4.34	506	8511	80	3.14	197.8	15.7	1.27	0.49	0.06	0.2	0.54
27	4.40	500	8502	81	3.14	197.5	15.7	1.34	0.49	0.06	0.2	0.54
28	4.45	495	8499	81	3.14	197.3	15.7	1.40	0.49	0.06	0.2	0.54
29		489										
30		484										
31		478										
32		473										
33		467										
34		462										
35		456										
36	4.89	451	8493	83	3.14	196.3	15.7	1.87	0.49	0.06	0.2	0.54
37	4.95	445	8485	84	3.13	193.7	15.8	2.01	0.49	0.06	0.2	0.54
38	5.01	439	8476	86	3.13	194.9	15.7	2.03	0.49	0.06	0.2	0.53
39	5.06	434	8467	87	3.13	196.7	15.7	2.04	0.49	0.06	0.2	0.53
40	5.12	428	8459	89	3.13	199.2	15.7	2.01	0.49	0.06	0.2	0.53

41	5.17	423	8450	91	3.12	198.9	15.7	2.08	0.49	0.06	0.2	0.53
42	5.28	412	8408	74	3.11	199.7	15.6	2.18	0.49	0.06	0.2	0.53
43	5.34	406	8374	54	3.10	203.1	15.7	2.14	0.49	0.06	0.2	0.53
44	5.39	401	8312	30	3.09	202.3	15.7	2.23	0.48	0.06	0.2	0.53
45	5.45	395	8283	26	3.08	202.7	15.7	2.29	0.48	0.06	0.2	0.53
46	5.50	390	8263	30	3.07	198.1	15.6	2.49	0.48	0.06	0.2	0.52
47	5.62	378	8194	55	3.05	202.4	15.7	2.49	0.48	0.06	0.2	0.52
78	5.68	372	8180	54	3.05	199.2	15.6	2.65	0.48	0.06	0.2	0.52
79	5.72	368	8166	53	3.05	197.8	15.6	2.74	0.47	0.06	0.2	0.52
80	5.76	364	8151	53	3.04	201.7	15.8	2.67	0.48	0.06	0.2	0.52
81	5.80	360	8137	52	3.04	193.7	15.7	2.95	0.48	0.06	0.2	0.52
82	5.84	356	8123	52	3.03	197.3	15.7	2.89	0.48	0.06	0.2	0.52
83	5.88	352	8108	52	3.03	200.8	15.7	2.82	0.47	0.06	0.2	0.52
84	5.92	348	8094	52	3.03	199.2	15.6	2.92	0.47	0.06	0.2	0.52
85	5.96	344	8080	52	3.02	198.5	15.8	2.98	0.48	0.06	0.2	0.52
86	6.00	340	8065	53	3.02	195.7	15.6	3.11	0.47	0.06	0.2	0.51
87	6.04	336	8051	53	3.01	195.2	15.6	3.17	0.47	0.06	0.2	0.51

91	6.10	330	8037	54	3.01	197.2	15.7	3.17	0.47	0.06	0.2	0.52
92	6.14	326	8022	55	3.01	195.3	15.9	3.28	0.48	0.06	0.2	0.52
93	6.18	322	8008	57	3.00	194.2	15.8	3.35	0.48	0.06	0.2	0.52
94	6.22	318	7994	58	3.00	192.6	15.7	3.44	0.47	0.06	0.2	0.51
95	6.26	314	7979	59	2.99	200.5	15.6	3.25	0.47	0.06	0.2	0.51
96	6.30	310	7957	59	2.99	201.2	15.6	3.28	0.47	0.06	0.2	0.51
97	6.34	306	7918	31	2.98	202.8	15.7	3.28	0.47	0.06	0.2	0.51
98	6.38	302	7902	38	2.97	206.0	15.7	3.23	0.47	0.06	0.2	0.51
99	6.42	298	7865	66	2.96	207.8	15.8	3.23	0.47	0.06	0.2	0.51
100	6.46	294	7844	85	2.96	210.4	15.9	3.20	0.47	0.06	0.2	0.51

Table S2. Confidence limits and rates of change inferred from the record of the $BC421_{P\text{-}max}$. RSL jumps ($RSLr_1$-$RSLr_5$) are indentified where rates of rise exceed long-term rates as indicated by the second-order polynomial fit (± 2.2 mm; equivalent to 2 standard deviations of the long-term trend; highlighted by gray shading).

RSL (y) and Age (x) data					Confidence limits				Rates of change (mm yr^{-1})	
Sample code	Age (μ)	Age (2σ)	$BC421_{P\text{-}max}$	$BC421_{P\text{-}max}$ (95%)	Upper 95%	Upper 68%	Lower 68%	Lower 95%	Rate ($BC421_{P\text{-}max}$)	Rate of long-term trend
1	8801	25	-0.07	0.15	0.86	0.37	-0.75	-1.21	NA	NA
2	8779	15	-0.11	-0.07	0.87	0.34	-0.79	-1.26	0.0	7.4
3	8750	25	-0.06	-0.11	0.84	0.39	-0.69	-1.17	-1.3	7.2
4	8718	25	0.08	-0.06	0.93	0.45	-0.59	-1.09	1.4	7.0
5	8690	25	0.11	0.08	1.14	0.62	-0.45	-0.93	5.0	6.7
6	8671	25	0.25	0.11	1.33	0.80	-0.34	-0.77	1.6	6.6
7	8658	25	0.35	0.25	1.42	0.90	-0.24	-0.73	10.8	6.5
8	8649	25	0.42	0.35	1.40	0.92	-0.24	-0.78	11.7	6.4
9	8643	25	0.46	0.42	1.41	0.91	-0.17	-0.69	10.7	6.3
10	8640	25	0.49	0.46	1.45	0.97	-0.06	-0.65	14.7	6.3
11	8638	20	0.52	0.49	1.47	1.03	0.01	-0.40	16.0	6.3
12	8633	20	0.57	0.57	1.60	1.11	0.06	-0.36	15.4	6.3

13	8626	20	0.63	0.63	1.62	1.14	0.11	-0.39	8.7	6.2
14	8615	20	0.69	0.69	1.73	1.22	0.18	-0.26	5.3	6.2
15	8604	40	0.74	0.74	1.90	1.39	0.30	-0.20	4.6	6.1
16	8593	20	0.78	0.78	1.84	1.33	0.23	-0.27	3.5	6.0
17	8582	20	0.81	0.81	1.76	1.27	0.20	-0.25	3.3	5.9
18	8571	20	0.84	0.84	2.06	1.50	0.41	-0.09	2.7	5.8
19	8562	25	0.88	0.88	2.10	1.60	0.49	0.04	4.1	5.8
20	8553	20	0.93	0.93	2.08	1.54	0.43	0.00	5.0	5.7
21	8542	25	1.00	1.00	2.19	1.68	0.59	0.11	6.5	5.6
22	8530	20	1.08	1.08	2.27	1.70	0.65	0.14	7.3	5.6
23	8518	20	1.18	1.18	2.09	1.58	0.53	0.02	8.2	5.5
24	8509	20	1.28	1.28	2.15	1.69	0.61	0.15	11.0	5.4
25	8503	15	1.37	1.37	2.31	1.84	0.82	0.25	14.5	5.4
26	8499	20	1.46	1.46	2.39	1.93	0.88	0.28	24.0	5.3
27	8495	15	1.56	1.56	2.72	2.20	1.10	0.60	24.3	5.3
28	8491	20	1.67	1.67	2.94	2.44	1.42	1.03	26.8	5.3

29	8488	20	1.77	1.77	3.01	2.53	1.51	1.12	35.3	5.2
30	8483	20	1.87	1.87	3.01	2.54	1.53	1.17	19.2	5.2
31	8473	20	1.97	1.97	2.99	2.54	1.49	1.16	9.6	5.2
32	8459	25	2.05	2.05	2.97	2.55	1.55	1.16	5.9	5.1
33	8437	20	2.12	2.12	3.07	2.62	1.61	1.19	3.3	4.9
34	8409	20	2.16	2.16	3.20	2.66	1.63	1.14	1.5	4.8
35	8374	15	2.22	2.22	3.23	2.73	1.61	1.10	1.7	4.5
36	8333	10	2.33	2.33	3.31	2.82	1.68	1.14	2.7	4.3
37	8291	10	2.35	2.35	3.44	2.91	1.86	1.28	0.4	4.0
38	8251	10	2.51	2.51	3.50	3.01	2.00	1.45	4.1	3.7
39	8216	15	2.47	2.47	3.68	3.12	2.05	1.55	-1.2	3.4
40	8188	25	2.69	2.69	3.75	3.22	2.22	1.66	7.9	3.2
41	8166	15	2.75	2.75	3.74	3.23	2.24	1.73	2.8	3.0
42	8149	15	2.78	2.78	3.89	3.37	2.29	1.80	1.7	2.9
43	8134	15	2.82	2.82	3.92	3.46	2.42	1.89	2.5	2.8
44	8120	15	2.84	2.84	3.81	3.35	2.30	1.80	1.6	2.7

45	8108	15	2.86	2.86	3.87	3.36	2.32	1.86	1.2	2.6
46	8096	15	2.89	2.89	4.02	3.48	2.45	1.98	2.4	2.5
47	8081	15	2.94	2.94	4.08	3.59	2.51	2.05	3.7	2.4
48	8065	15	3.03	3.03	4.12	3.66	2.66	2.20	5.4	2.3
49	8049	15	3.13	3.13	4.17	3.68	2.69	2.18	6.2	2.2
50	8034	10	3.21	3.21	4.19	3.71	2.71	2.20	5.6	2.1
51	8021	15	3.26	3.26	4.28	3.81	2.79	2.28	4.1	2.0
52	8008	10	3.28	3.28	4.39	3.91	2.91	2.37	1.2	1.9
53	7993	15	3.27	3.27	4.34	3.88	2.87	2.32	-0.4	1.8
54	7974	15	3.24	3.24	4.18	3.73	2.77	2.26	-1.6	1.7
55	7952	15	3.20	3.20	4.23	3.76	2.77	2.30	-1.9	1.5
56	7928	10	3.20	3.20	4.18	3.74	2.74	2.32	0.0	1.4
57	7904	10	3.29	3.29	4.18	3.73	2.74	2.37	3.7	1.2
58	7884	15	3.29	3.29	4.25	3.74	2.76	2.44	-0.1	1.0
59	7868	20	3.18	3.18	4.27	3.71	2.77	2.45	-7.1	0.9

Table S3. Transfer function model performance statistics for the 'unscreened' and 'screened' training sets. RMSE = root mean squared error, RMSEP = root mean squared error of prediction. Gray shading highlights the chosen model (WA-PLS component 2 of the screened dataset).

Full dataset (n=231):						
Name	**RMSE**	**R^2**	**R^2 (bootstrapped)**	**Average bias (bootstrapped)**	**Maximum bias (bootstrapped)**	**RMSEP**
WA-PLS Component 1	21.28	0.77	0.73	0.69	76.58	23.70
WA-PLS Component 2	15.90	0.87	0.79	0.15	55.96	21.17
WA-PLS Component 3	11.64	0.93	0.84	0.41	44.58	19.67
'Screened' dataset (n=217):						
Model	**RMSE**	**R^2**	**R^2 (bootstrapped)**	**Average bias (bootstrapped)**	**Maximum bias (bootstrapped)**	**RMSEP**
WA-PLS Component 1	16.37	0.83	0.80	0.16	68.44	18.22
WA-PLS Component 2	12.32	0.90	0.85	-0.19	53.34	16.14
WA-PLS Component 3	9.61	0.94	0.87	-0.07	47.92	15.88

3

Reconstructing abrupt near-field sea-level changes of local significance: nearshore stratigraphic records from west Greenland

This chapter will be submitted to the journal *Quaternary Science Reviews*, in a paper titled "*Stratigraphic record of late Holocene tsunamis, Vaigat, West Greenland*". I am lead-author. It is co-authored by Antony Long of Durham University and Witold Szczuciński of Poznan University.

1. Introduction

Submarine slides and coastal landslides that enter the sea can generate exceptional tsunamis. The largest of the historic era was caused by a landslide in 1958 at the head of Lituya Bay, Alaska, and attained a maximum run-up height of 518 m (Miller, 1960), while at c. 8150 cal yr BP the Storegga submarine slide in the North Sea generated a tsunami with a run-up that exceeded 20 m (e.g. Bondevik et al., 2005). A characteristic of these events is that they occurred on or near glaciated or recently formerly glaciated coastal margins (paraglacial coasts), where glacial loading/unloading (e.g. Solheim et al., 2005) and the enhanced action of physical processes inherent to glaciated environments (e.g. freeze-thaw weathering) provide mechanisms that can cause slope failure. Further, the constraining topography of fjord systems that are common features of glaciated landscapes can enhance the destructive capacity of landslide-tsunami by amplifying wave heights at the local scale (e.g. Fritz et al., 2009; Harbitz et al., 2014).

Aerial photographs and coastal geomorphological mapping of the northern Vaigat shoreline (Nuussuaq peninsula), a large fjord located in west Greenland, has identified a zone of high landslide activity (Fig. 3.1; Pedersen et al., 2002), with four out of 14 landslides having been ascribed tsunamigenic potential in the mid to late Holocene (Pedersen et al., 2002). A large rock avalanche (90 million m^3) that triggered a submarine slide at Paatuut on November 21, 2000, generated a tsunami that propagated c. 20 km longitudinally up-fjord to the village of Saqqaq and ~30 km across-fjord to the abandoned town of Qullissat, where buildings below +25 m mean tide level (MTL) were damaged or destroyed (Fig. 3.1; Dahl-Jensen et al., 2004). The landslide registered a seismic signal in monitoring stations at the Summit camp c. 550 km to the east on the ice sheet (Pedersen et al., 2002) and according to local testimony generated modest seiches in the harbour at Ilulissat c. 125 km to the southeast. Dahl-Jensen et al. (2004) suggest that the Paatuut landslide was the largest event in at least the last 500 years. Previously, on December 15, 1952, a landslide c. 10 km west of Tupaasat generated a smaller tsunami of unknown vertical run-up that damaged buildings and killed one person at Qullissat (Fig. 3.1) (Pedersen et al., 2002).

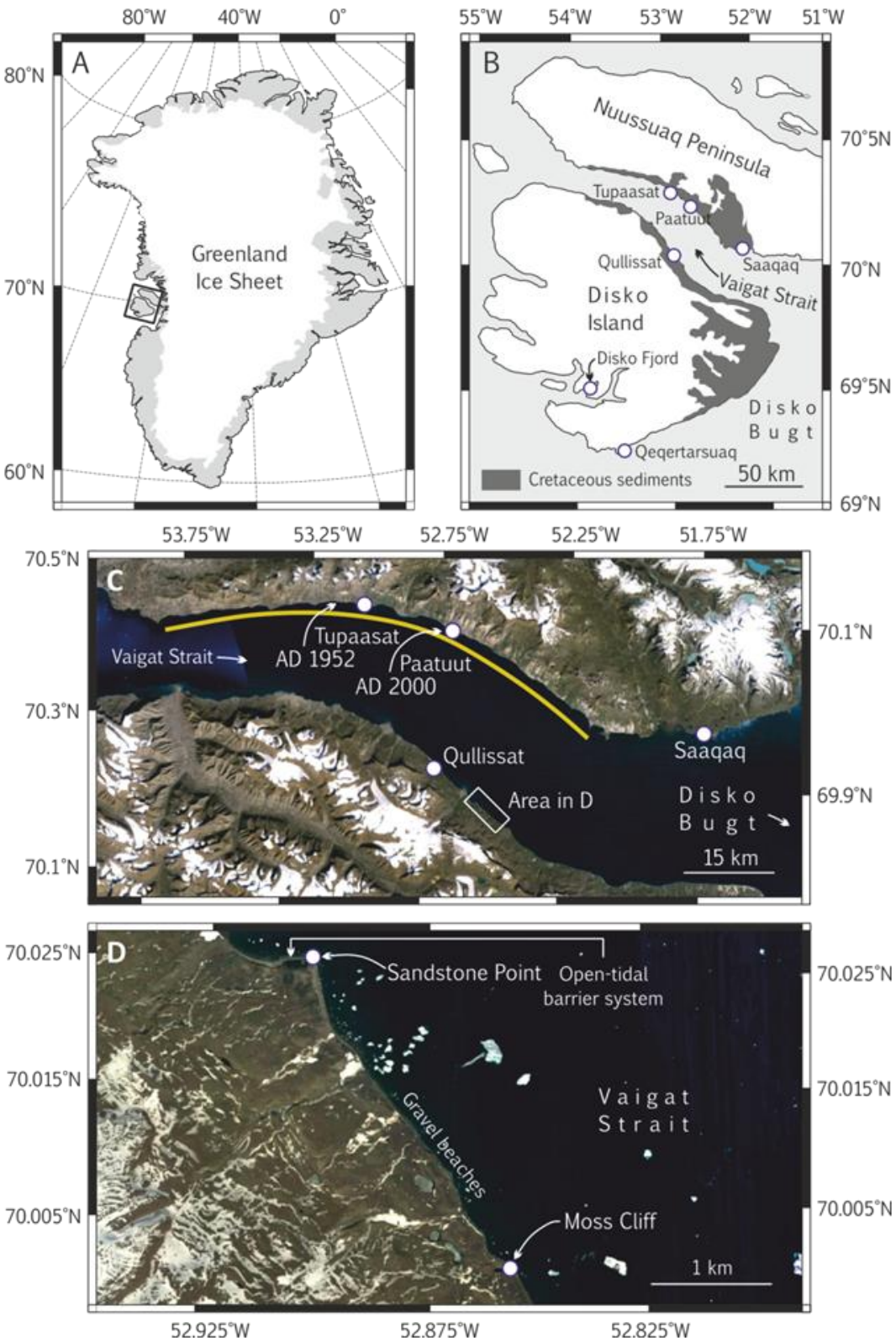

Figure 3.1 Overview maps of places mentioned in text. a, Greenland. **b,** Disko Island and the Nuussuaq Peninsula, west Greenland. **c,** Google Earth image of the Vaigat Strait; with locations of AD 2000 and 1952 landslides and c. 70 km landslide-prone escarpment (yellow line). **d,** Google Earth image of study sites Sandstone Point and Moss Cliff in southeast Vaigat.

Despite several lines of evidence attesting to the potential for large tsunami in high-latitude environments, our understanding of the stratigraphic imprints of such events is limited to coastal lake records of the Storegga tsunami (Bondevik et al., 1997a; Romundset and Bondevik, 2011; Wagner et al., 2007). There is a need, therefore, for further stratigraphic records of high-latitude tsunami developed from a range of morpho-depositional settings in order to extend our knowledge of abrupt sea-level and coastal change (tsunamis) to these regions. Both the AD 2000 and 1952 tsunamis in Vaigat present ideal opportunities to explore the tsunami archive-potential of an Arctic nearshore sedimentary environment and its subsequent response to tsunami inundation.

In this paper, we adopt a litho-, bio- and chronostratigraphic approach to reconstruct tsunami history in Vaigat, using the techniques and criteria for identification of tsunami deposits developed in lower-latitude settings (e.g. Nelson et al., 1996; Peters and Jaffe, 2010). Our aims are fourfold: (1) to establish whether Vaigat nearshore environments record evidence of tsunamis, (2) to determine the characteristics of tsunami deposits, (3) to constrain the average frequency and magnitude (vertical run-up) of tsunami events in the late Holocene, and (4) to reflect on the wider implications of this work for our understanding of tsunami in glaciated landscapes.

2. Field site

The Vaigat Strait (Inuktitut: 'Sullorsuaq'), west Greenland, is a large fjord located in northwest Disko Bugt between 69°52'N, 51°58'W and 70°24'N, 54°18'W (Fig. 3.1). The fjord is approximately 100 km long, 25 km wide and 300 m deep, with depths extending to 500 m locally (Andersen, 1981). It acts as an important circulation pathway for the West Greenland Current in Disko Bugt (Perner et al., 2013) and is a conduit for the discharge of icebergs and meltwater originating from tidewater glaciers in eastern Disko Bugt.

The bedrock geology of wider Disko Bugt and its coastal margins is characterized by Precambrian orthogneisses and granites (Escher et al., 1976; Larsen and Pulvertraft, 2000). Westward, the geology of Disko Island and the Nuussuaq Peninsula is formed of Palaeogene basaltic rocks with outcrops of Cretaceous deposits that include sandstones, shales and coal seams (Henriksen et al., 2000). This geological configuration generates slope instability (Pedersen et al., 2002), especially on the northern coast of Vaigat (Nuussuaq Peninsula) where previous geomorphological mapping of the c. 1.5 km-high coastal escarpment identified at least 14 landslides of assumed mid to late Holocene age (Pedersen

et al., 2002). In comparison, the relatively stable south coast of the fjord (north coast of Disko Island) has areas of coastal lowland, well-vegetated slopes and a small number of coastal lakes and raised beaches, although it too has evidence of slope instability. Tidal modelling at the port of Qeqertarsuaq on the south coast of the island predicts a spring tidal range of 2.50 m (DMI, 2014). The modern climate of the Disko Bugt region is low Arctic maritime with a mean annual temperature of -5.2°C and a mean summer temperature of 4.8°C (Fredskild, 1996).

In this study, our focus is on the sampling sites located on the southeastern shores of the Vaigat Strait, generally southeast of the many landslide scars that are so prominent along the Nuussuaq Peninsula coast (Figs. 3.1 and 3.2). Our sites are situated up-fjord (east) from the AD 2000 and AD 1952 landslides. The coastal lowlands of southeast Vaigat comprise active depositional environments that include areas of waterlogged freshwater marshland and open-tidal lagoons located behind narrow gravel and sandy beaches (Fig. 3.2). Relative sea level (RSL) data from Avreprinsens Eijland; ~65 km to the east (Long et al., 1999), and from Disko Fjord; ~65 km to the southwest (Long et al., 2011), indicate that RSL fell from c. +75 m MTL at c. 10000 cal yr BP and intersected present MTL at c. 4500 cal yr BP. It then continued to fall to a low-stand of c. -5 m below MTL at c. 2200 cal yr BP, after which it rose to present. As rising sea levels promote the creation of accommodation space and favour deposition over erosion, we anticipate that the Vaigat coastal environments contains a sequence of deposits that extends to at least c. 2200 cal yr BP; the approximate time at which RSL started to rise to present.

Our focus is on two sites situated c. 3.5 km apart (Fig. 3.2). The first is Sandstone Point (unofficial name); a low rocky peninsula that juts into the Vaigat Strait and provides a southeast anchor for a gravel barrier system that extends farther west but encompasses a tidal lagoon behind its southeastern extent. The peninsula supports *Empetrum nigrum* (shrub) and *Festuca rubra* (grass) on its seaward side (‘fjord-side’ Fig 3.2b,c) and *E. nigrum* on its leeward side (‘lee-side’ Fig 3.2d). Depths of Holocene sediment of variable thickness and continuity are preserved on both flanks. On the fjord-side, sediments are preserved within a small area (2 x 10 m) between +2.5 and +3.5 m MTL and c. 20 m from the present gravel beach within a shallow bedrock depression. On its opposite flank (‘lee-side’) sediments are restricted to a small area (<0.25 m^2) between +3.4 to +3.7 m MTL at the head of a salt-marsh within the back-barrier lagoon environment. Based on field observations in July 2011, tidal exchange into the back-barrier area occurs only on the spring tidal cycle (i.e., neap tides are unable to penetrate this far inland).

Our second site is Moss Cliff (unofficial name) situated c. 3.5 km east of Sandstone Point (Fig. 3.1, 3.2e,f) and comprises an area of vegetated lowland surrounding the mouth of a small freshwater lake (the focus of Chapter 4). The slopes that surround the lake have raised beach deposits on their surfaces at maximum elevations of c. +11 m MTL that were likely deposited during the mid Holocene as RSL fell (e.g. Long et al., 2011). The lake outflow is vegetated by an area of shrub swamp, through which the water from the lake drains to the sea. A low cliff (<0.5 m high) and gravel beach defines the seaward extent of this wetland. The wetland vegetation is characterized by *Eriophorum chamissonis* (cotton grass) and *Betula nana* (dwarf birch) and *E. nigrum*. Our focus in this chapter is the sediments exposed in the low cliff between +3.0 and +3.5 m MTL that comprise an alternating sequence of organic and inorganic deposits that may be of tsunami origin.

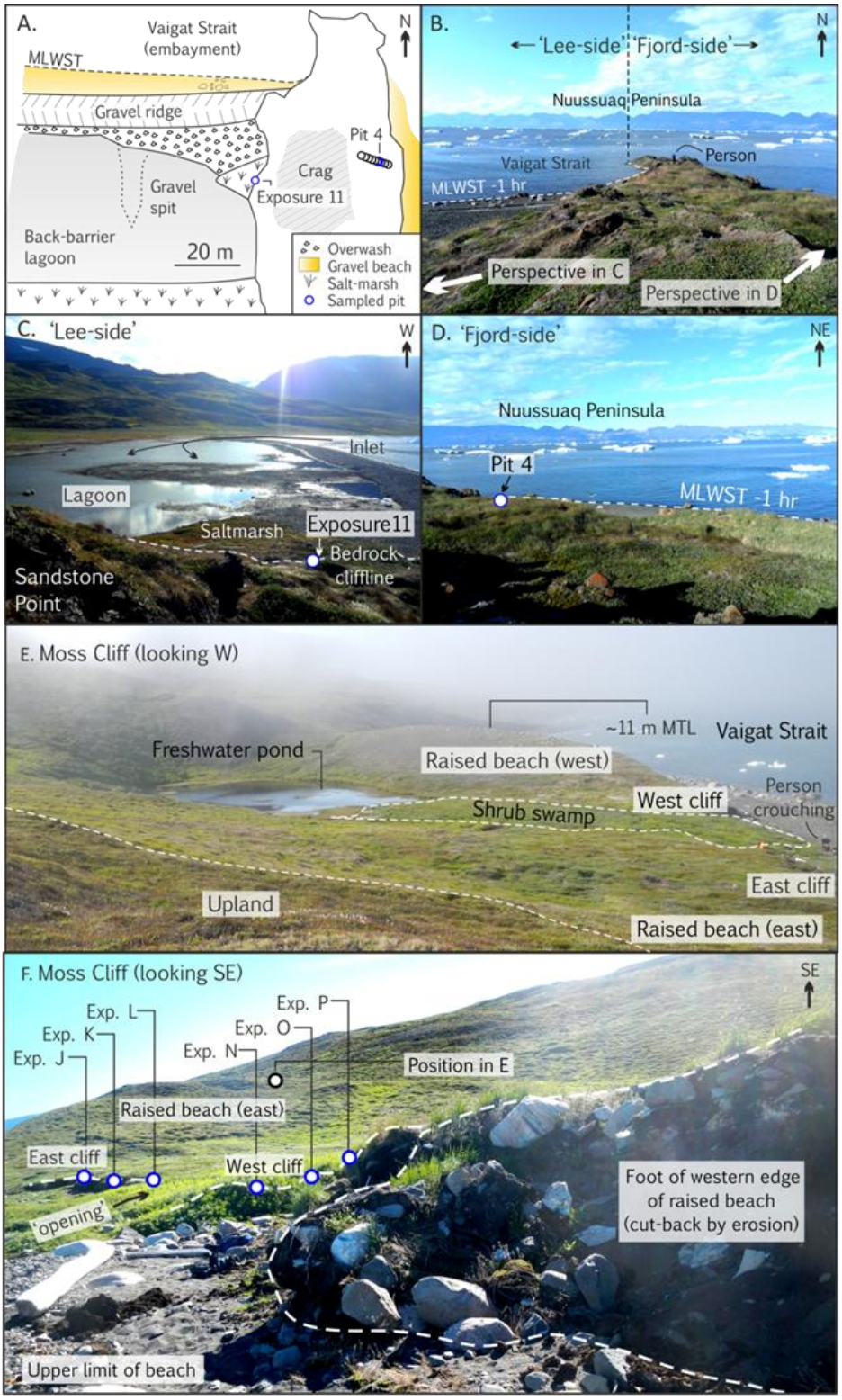

Figure 3.2. Overview of study sites. a, Illustration of Sandstone Point, with key morphological features and core locations. **b,** Sandstone Point looking north. **c,** Sandstone Point looking west ("Lee-side"). **d,** Sandstone Point looking northeast ("Fjord-side"). **e,** Moss Cliff looking west, with key morphological aspects and core locations. **f,** Moss Cliff looking southeast with core locations.

3. Methodology

3.1 Stratigraphy

Coastal environments provide an essential source of information used to constrain tsunami frequency (e.g. Atwater, 1987). Lithologic units that are stratigraphically anomalous are used as the primary basis for further analyses with a range of proxy methods (e.g. Chague-Goff et al., 2011). We sampled and logged marsh exposures and hand-dug pits with reference to Long et al. (1999), which is a modification of Troels-Smith (1955) scheme of stratigraphic notation. Elevations of deposits were surveyed to sea level with a Sokkisha level and converted to MTL using tide tables.

3.2 Biostratigraphy and sedimentology

Microfossil (diatom) analysis was conducted in order to identify evidence for marine deposits. Diatom analyses are sensitive to ambient environmental factors such as salinity, substrate and tidal exposure (Sherrod, 2001) and can assist in the identification of tsunami-lain sands and gravels as well as storms (e.g. Dawson et al., 1996; Hemphill-Haley, 1996). Diatoms were prepared using standard methods (Palmer and Abbott, 1986), identified with reference to Hartley (1996) and grouped according to the halobian classification scheme of Vos and de Wolf (1988; 1993). The total count contained a minimum of 100-200 diatom valves. The low diversity of diatom assemblages (maximum of four taxa in one section, for example) justifies low total counts (Fatela and Taborda, 2002), which reflects low diatom concentrations and/or poor preservation in many of the samples analysed. Assemblage diagrams were plotted in the computer software C2 version 1.6 (Juggins, 2011). Percentage loss-on-ignition (LOI) and grain size analysis was measured on ~4 g sediment subsamples. Samples for LOI were weighed prior to being oven-dried overnight at 80°C, reweighed, combusted at 550°C for four hours and then reweighed. Grain size analysis was performed using a Beckman Coulter laser diffraction grain-size analyzer following removal of organics in a 30% solution of H_2O_2 and submersion in a water bath at 85°C. Magnetic susceptibility was measured using a GeoTek core scanner at 0.2 cm resolution. We used magnetic and grain size information to aid in the precise correlation of core overlaps.

3.3. Chronostratigraphy

Our chronology is based on AMS ^{14}C dating of terrestrial plant macrofossils and, where these are absent, bulk peat samples. Where possible, we targeted whole delicate plant macrofossils (e.g. leaves and seeds) on the premise that significant transportation will cause them to disintegrate. Samples for ^{14}C analysis were pre-treated using standard methods (e.g. Czernik and Goslar, 2001) and dating was performed at the Poznan radiocarbon laboratory in Poznan, Poland. Ages are calibrated (IntCal13; Reimer et al., 2013) with respect to AD unless otherwise stated and given as 2σ ranges. Recent ages (last <65 yrs) that contained >100% modern carbon are calibrated with the 13NH1 bomb-spike curve (Hua et al., 2013). Age modelling was conducted in Bayesian age modelling software OxCal 4.2 (Bronk Ramsey, 2009a) using the P_sequence function, which allows for random fluctuations in deposition rate. The model builds prior densities for each point (priors) before building posterior (modelled) densities for each point using stratigraphic information, Bayesian algorithms and a Monte Carlo Markov Chain random sampling approach (Gilks et al., 2006). Model agreement is provided by an "agreement index" (AI), with AI >60% the accepted threshold for good agreement (Bronk Ramsey, 2009). Elevated ^{137}Cs concentrations provide a chronological marker for ~1963 associated with atmospheric fallout of the radionuclide following nuclear weapons testing (e.g. Pennington et al., 1973). Samples were freeze dried, ball-milled and homogenized prior to sample equilibration for 7 days and measured with a well-type gamma spectrometer with a counting time of 6-8 days.

4. Results

4.1 Sandstone Point (fjord-side)

4.1.1 Stratigraphy

Nine shallow pits dug along a 9 m-long transect document the stratigraphy of the fjord-side of Sandstone Point (Fig. 3.3). The stratigraphy above bedrock comprises peaty soils that contain four interbedded coarse sandy peat horizons of variable thickness. The present sediment surface is draped by a 0.02-0.04 m-thick unit of coarse sand and fine gravel that was deposited by the AD 2000 Paatuut landslide-tsunami and has been recolonized by thickets of *F. rubra*. The stratigraphy is continuous along the transect length, despite minor local variability with respect to thickness of deposits. Pit 4 was sub-sampled for further analyses. The sandy peat units are referred to as Units A, C, E and G (base to top), and are described in order in relation to their underlying soils.

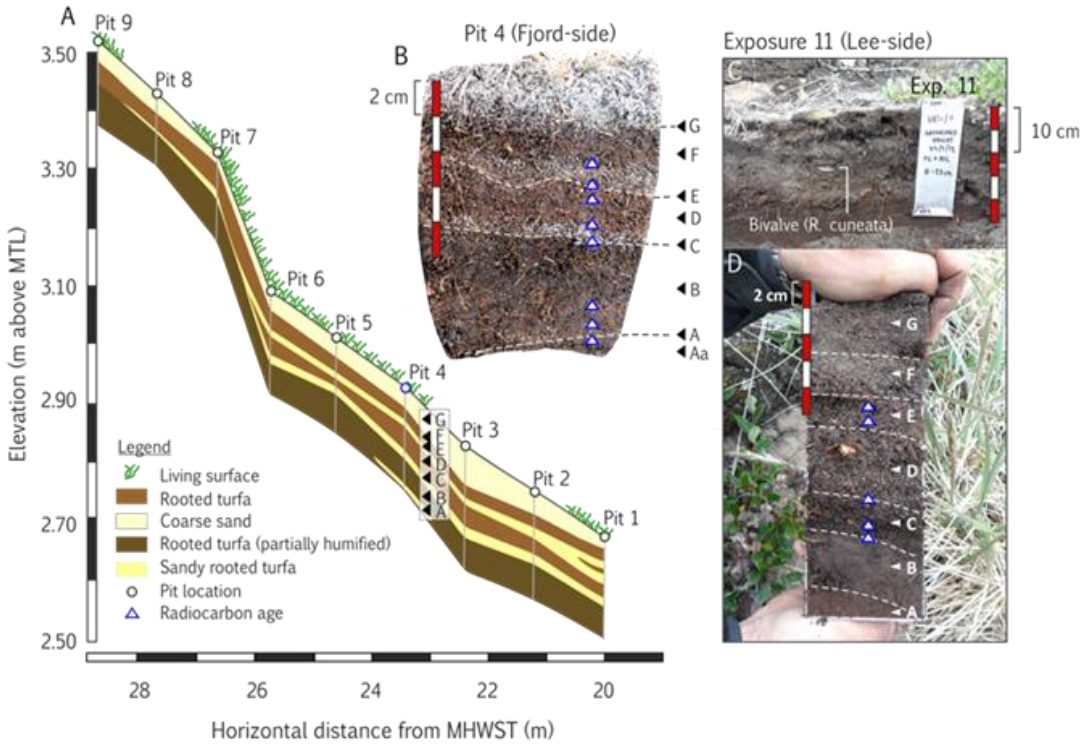

Figure 3.3. Lithostratigraphy at Sandstone Point. a. Transect on the fjord-side of the peninsula. **b,** Pit 4; the sampled pit from this transect. **c,** the small area of sediment on the lee-side of the peninsula. **d,** photograph of Exposure 11 (monolith in c).

Unit A is a thin (0.5 cm-thick) dark brown peat containing fine yellow sand which is local to Pit 4 (Fig 3.3a). It overlies a thin (1.5 cm-thick) partially humified dark brown basal peaty soil (Unit Aa) that contains herbaceous plant remains, which is also local to Pit 4. Unit C is a 1 cm-thick sandy rooted peat that overlies a dark brown peat (Unit B) and is indistinguishable from the basal soil. LOI in the lower half of the peat is high (80%) and drops abruptly within the upper half (to 30%) where the peat becomes partially humified (Fig. 3.4). A well-rooted, sandy peat (Unit D) to peat (Unit E) couplet overlies Unit C. LOI is 60% within the peat and <10% within the sandy peat. The thickness of Unit E varies both locally within the pit and along-transect. Evidence of erosion to the underlying soil is found in a seaward position in Pit 1 where an intervening 1 cm-thick brown peat occurs within Unit E, indicating the presence of an older, stratigraphically separate, coarse-grained unit. Overlying this is a brown peat containing herbaceous and woody plant remains of *E. nigrum* (Unit F). The sequence is capped at the present land surface by a laterally continuous, partially-vegetated coarse sand (Unit G) that was deposited by the Paatuut tsunami of AD 2000.

4.1.2 Biostratigraphy

The diatom assemblages analysed from a representative profile, Pit 4, indicate alternating freshwater and marine conditions throughout the sample profile (Fig. 3.4a). Species diversity was low with 10 taxa identified (percentage contributions are provided in Appendix 2; Fig. S1). Three of the four sandy peat horizons contain a mixed assemblage of thickly silicified marine and freshwater taxa. Marine taxa include *Achnanthes promunturii* and *Cocconeis pinnata* in Units G, while *Meridion circulare* is found in Units A and G alongside higher frequencies of *A. promunturii*. The freshwater *Hantzschia amphioxys* and *Pinnularia borealis* dominate the peats and are also found alongside marine taxa within sandy peats. However, there are variations to this pattern. First, a sandy peat horizon (Unit E) does not contain marine microfossils, in contrast to the remaining sandy peat units. Second, sparse marine taxa are found in three instances within peat deposits (i.e. not accompanied by coarse-grained material). These are at 2.81 m MTL within Unit B; where three valves of *Meridion circulare* were found, at 2.85 m MTL in Unit D and at 2.88 m MTL in Unit F where a sample contained two *A. promunturii* valves. Despite relatively high resolution sampling of Pit 4 (0.5 cm-slices), the stratigraphically well-incorporated, rooted and thin nature of sandy peat units (~0.5 cm thick) precludes a more detailed examination of the abruptness of palaeoenvironmental change across unit transitions.

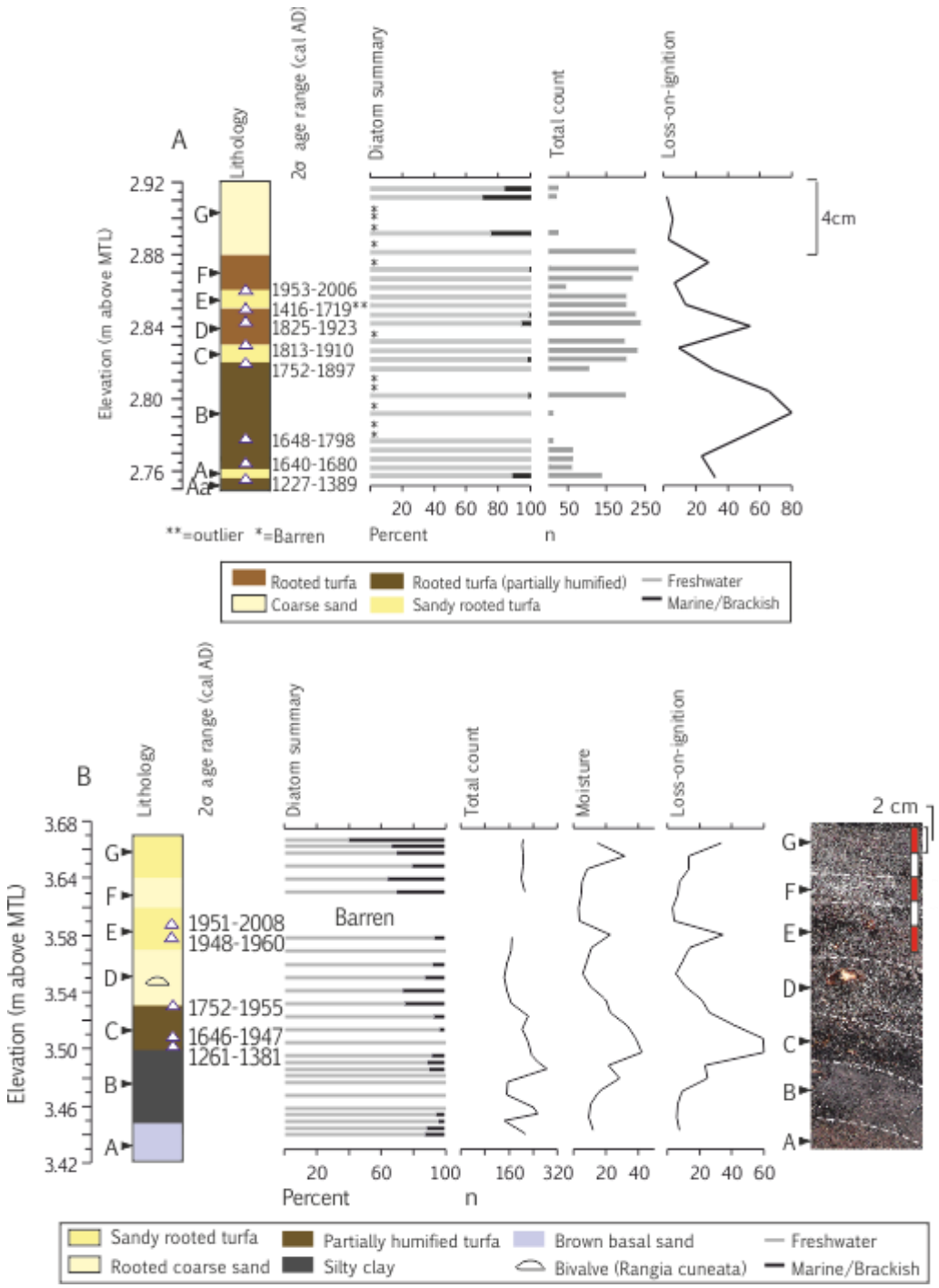

Figure 3.4. Diatom summary, loss-on-ignition, lithostratigraphy and dating at Sandstone Point. a, Pit 4 from the fjord-side of the peninsula. **b,** Exposure 11 from the lee-side of the peninsula. Note that ages presented are 2σ posterior (modelled) ages, except for one outlying age in Pit 4 which is presented as a 2σ unmodelled range (two asterisks). Single asterisk = barren of diatoms.

4.1.3 Chronology

Eight AMS ^{14}C samples constrain the chronology for Pit 4 (Table 3.1; Fig. 3.5). We mostly targeted material directly below and above sandy peat horizons for dating. Dating was performed on two samples of *E. nigrum* seeds and, where macrofossils were lacking, on six 0.5 cm-thick slices of bulk peat. Because the sandy peat horizons are thin and well incorporated into the stratigraphy, which we interpret as post-depositional reworking (see discussion), we do not adjust our age-modelled depths to exclude sandy peat horizons. Ages span the past 800 calibrated years, although we note a significant hiatus at the base of the record between Units A and Ab. In the age model, the top of Unit A is dated to AD 1640-1680, the top of Unit C to AD 1813-1910 and the top of Unit E to AD 1953-2006. Good internal consistency of modelled ages is indicated by a high age model agreement index of 87% (Figure S2).

Table 3.1. Radiocarbon dates in this study. AMS = accelerator mass spectrometry. Ages are calibrated with the IntCal13 calibration curve (Reimer et al. 2013) in OxCal 4.2 (Bronk Ramsey, 2008), except modern ages which are calibrated with the 13NH1 bomb curve of Hua et al. (2013). *=Where year of fieldwork provides absolute minimum age constraint (2012). **=Outlier.

Sample Code	Identifier	Mid depth (cm)	Height (m MTL)	Material dated	Stratigraphic position	Reported 14C age (± 1σ lab error)	Calibrated range (2σ) AD	Modelled range (2σ) BC/AD
Poz-53437	VA5C/4-A	16.25	2.3575	Bulk peat (0.5 cm)	Within 0.5 cm of sandy peat (base)	725 ± 35	1224 - 1382	1227 - 1389
Poz-53438	VA5C/4-1	15.25	2.3675	Bulk peat (0.5 cm)	Within 0.5 cm of sandy peat (top)	220 ± 25	1644 - 2012*	1640 - 1680
Poz-57632	VA5C/4-B	14.25	2.3775	Empetrum nigrum seeds and Betula nana catkin	Within peat	210 ± 30	1646 - 2012*	1648 - 1798
Poz-53439	VA5C/4-2	10.25	2.4175	Empetrum nigrum seeds and Betula nana catkin	Base of sand	240 ± 80	1470 - 2012*	1752 - 1897
Poz-53440	VA5C/4-3	9.25	2.4275	Bulk peat (0.5 cm)	Top of sand	60 ± 25	1695 - 1919	1813 - 1910
Poz-57633	VA5C/4-C	8.25	2.4375	Empetrum nigrum seeds	Within peat	55 ± 25	1695 - 1919	1825 - 1923

Poz-53442	VA5C/4-4	7.25	2.4475	Empetrum nigrum seeds and Betula nana catkin	Base of sand	360 ± 80	1416 - 1719**	Not modelled**
Poz-53443	VA5C/4-5	6.25	2.4575	Bulk peat (0.5 cm)	Top of sand	1.0889 ± 0.0037 (modern)	1953-2012*	1953 - 2006
Poz-57626	VA5C/11-5	17.75	3.493	Bulk peat (0.5 cm)	Top of silty clay	710 ± 25	1261 - 1381	1261 - 1381
Poz-57625	VA5C/11-4	16.25	3.508	Empetrum nigrum leaves and seeds	2 cm into sandy peat	180 ± 40	1648 - 2012*	1646 - 1947
Poz-57624	VA5C/11-3	14.25	3.528	Empetrum nigrum leaves and seeds	Top of sandy peat	170 ± 40	1655 - 2012*	1752 - 1955
Poz-57623	VA5C/11-2	8.75	3.583	Empetrum nigrum leaves and seeds	3 cm into sandy peat	1.0016 ± 0.0034 (modern)	1710 - 1960	1948 - 1960
Poz-57622	VA5C/11-1	7.25	3.598	Empetrum nigrum leaves and seeds	1.5 cm into sandy peat	1.0572 ± 0.0036 (modern)	1951 - 1959	1951 - 2008
Poz-53394	VA1/Ob-1	35.75	3.193	Bulk peat (0.5 cm)	Base of basal peat	3250 ± 40	1611 BC - 1453 BC	1613 BC - 1455 BC
Poz-57640	VA1/Ob-B	25.25	3.298	Bulk organic mud(0.5 cm)	In organic mud	1560 ± 30	420 - 565	423 - 568
Poz-	VA1/Ob-	24.25	3.308	Bulk organic mud (0.5	In organic mud	1440 ± 30	566 - 655	563 - 653

57636	A			cm)				
Poz-57635	VA1/Oa-1	16.25	3.388	Bulk peat (0.5 cm)	Base of peat	1.0306 ± 0.0033	1955 - 1957**	Not modelled**
Poz-53394	VA1/Oa-B	16.25	3.388	Empetrum nigrum seeds	Base of peat	575 ± 25	1306 - 1418	1308 - 1418
Poz-57634	VA1/Oa-A	14.5	3.405	Empetrum nigrum seeds	Within silty peat	365 ± 30	1449 - 1634	1446 - 1662
Poz-53395	VA1/Oa-2	10.25	3.448	Bulk peat (0.5 cm)	Base of sandy peat	230 ± 30	1530 - 2012*	1646 - 1807
Poz-93397	VA1/Oa-3	9.5	3.455	Bulk peat (0.5 cm)	Within sandy peat	85 ± 35	1682 - 1935	1700 - 1940
Poz-93398	VA1/Oa-4	8.75	3.463	Bulk peat (0.5 cm)	Above sandy peat	1.0152 ± 0.0042 (modern)	1714 - 1960	1896 - 1960
Poz-53399	VA1/Jb-1	20.25	3.3075	Bulk peat (0.5 cm)	Base of peat	2000 ± 50	161 BC - 121 AD	156 BC - 121 AD
Poz-53400	VA1/Jb-2	19.25	3.3175	Bulk peat (0.5 cm)	Within peat	130 ± 40	1670 - 1944**	Not modelled**
Poz-57641	VA1/Jb-A	17.75	3.3325	Empetrum nigrum leaves (well decayed)	Within peat	760 ± 70	1050 - 1393	1466 - 1953
Poz-93401	VA1/Jb-3	15.75	3.3525	Empetrum nigrum seeds	Within peat	290 ± 50	1458 - 1949	1948 - 1958

Poz-93403	VA1/Jb-4	13.25	3.3775	Bulk peat (0.5 cm)	Base of sand unit	1.0181 ± 0.0051 (modern)	1951 - 1959	1951 - 1959
Poz-93404	VA1/Jb-5	5.75	3.4525	Bulk peat (0.5 cm)	Top of sand unit	1.0241 ± 0.0042 (modern)	1951 - 1959	1951 - 1959
Poz-93405	VA1/Jb-6	5.5	3.455	Bulk peat (0.5 cm)	Above main sand	1.0486 ± 0.0042 (modern)	1951 - 1959	1951 - 1959

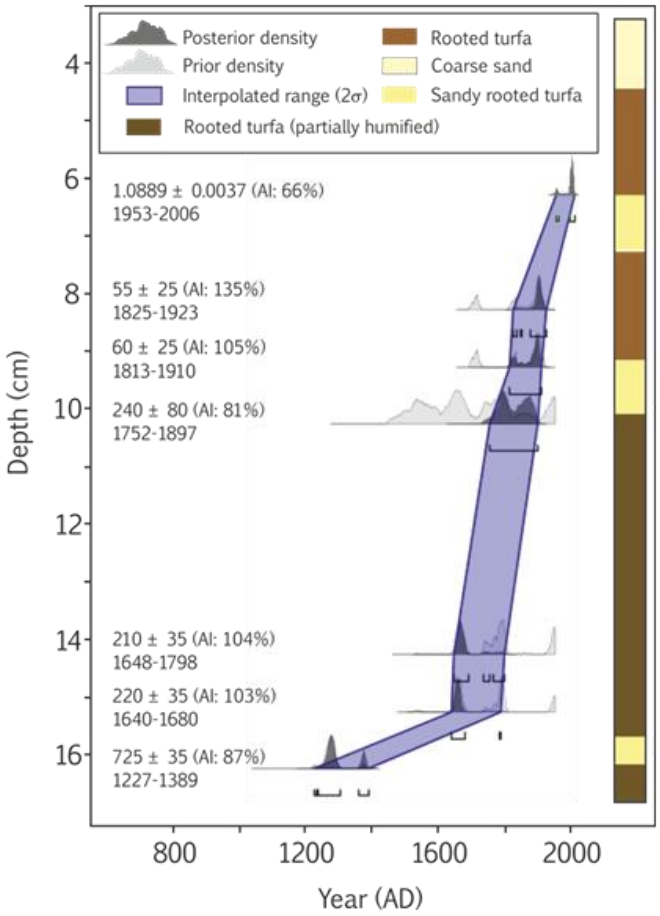

Figure 3.5. P_sequence age-depth model for Pit 4. Ages prior to AD 1950 are calibrated with the IntCal13 calibration curve (Reimer et al., 2013); while the post AD 1950 age is calibrated with the 13NH1 bomb curve (Hua et al. 2013). In this instance, depths are not adjusted to exclude sand layers as they are stratigraphically well-incorporated.

4.2 Sandstone Point (lee-side)

4.2.1 Stratigraphy

The stratigraphy of the lee-side of Sandstone Point (Fig. 3.2b, c and 3.3c, d) contains a sequence of dry (average moisture content: 17%) minerogenic, coarse and organic sediment that is described from bottom to top (Units A-G) (Fig. 3.4). Unit A is a brown sand that field reconnaissance suggests is near-ubiquitous in the nearshore intertidal zone between Sandstone Point and Moss Cliff. Overlying this is Unit B; a fine-grained purple-grey silty clay containing poorly preserved fine rootlets. Unit C is a partially humified mid-brown peat containing herbaceous macrofossils and appears analogous in lithology to Unit B found on the seaward side of the peninsula. Units A and B contain little organic matter (<5%). Organic content rises sharply across the transition to Unit C (~60%). Unit D is the first of two rooted coarse sand horizons that grade gradually into underlying peat. It is relatively thick (0.04 m) and has been disturbed by downward penetration of thick woody roots of *E. nigrum*. We found a single unarticulated *Rangia cuneata* bivalve shell horizontally embedded within this unit (Fig. 3.4) that we chose not to date due to potential reworking. Organic content is low and the gradual changes across this transition demonstrate post-depositional reworking (see discussion). Unit E is a rooted sandy peat with LOI indicating gradual transitions to under- and overlying units. The second rooted coarse sand horizon (Unit F) overlies this and grades gradually into sandy rooted peat at the top of the sequence (Unit G) that was deposited by the Paatuut tsunami.

4.2.2 Biostratigraphy

Diatom analysis reveals a sequence of alternating marine and freshwater conditions (Fig. 3.4), overall with high diversity (27 taxa present). Species percentage contributions are provided in Appendix 2, Fig. S2. *A. promunturii* is indicative of marine conditions, while *Achnanthes didyma*, *H. amphioxys* and *P. borealis* are indicative of freshwater conditions. The brown basal sand (Unit A) is dominated by *P. borealis* (~80%) and *A. promunturii* (~20%). The centre of Unit B (silty clay) containing a mono-specific assemblage of *A. didyma*, while the transitions to under- and overlying units signify gradual changes or post-depositional reworking of near-contact sediments. Across the transition to overlying *turfa* above this unit (Unit C), the marine diatom *A. promunturii* in present in low abundances (10%), while the remainder of Unit C is dominated by *H. amphioxys* and *P. borealis*. Unit D contains a mixed assemblage with high frequencies of *A. promunturii*, *A. didyma* and *P.*

borealis. A gradual transition or post-depositional reworking of near-contact sediments between Units D and E is suggested by reduced frequencies of *A. promunturii* that are replaced by *P. borealis*. The top 3 cm of Unit E is barren of diatoms. Units F and G that cap the sequence contain mixed marine and freshwater assemblages with *A. promunturii* peaking in abundance on top (60%).

4.2.3 Chronology

Five AMS ^{14}C dates constrain a chronology for Exposure 11 (Table 3.1; Fig. 3.6). Dating was performed on seeds and leaves of *E. nigrum* (4 dates) and bulk sediment (1 date) found within organic Units D and E. Our age model is based on depths that have been adjusted to remove the two coarse horizons (Units D and F), which we interpret as being deposited abruptly (see discussion). The age model agreement is satisfactory (AI=61%). The base of Unit C yields an age of AD 1261-1381 and constrains the chronology to a minimum of 750 yrs. Due to a lack of suitable material for dating, we are unable to extend the chronology to the two lowermost units of silty clay and brown basal sand, although extrapolation to the top of the basal sand (Unit A) provides an approximate date for this contact of AD 423-1056. In the age model, the first coarse sand (Unit D) is dated to AD 1752-1955 (following adjustment of age-modelled depths), while the top of the second coarse sand (Unit F) is dated to AD 1953-2011.

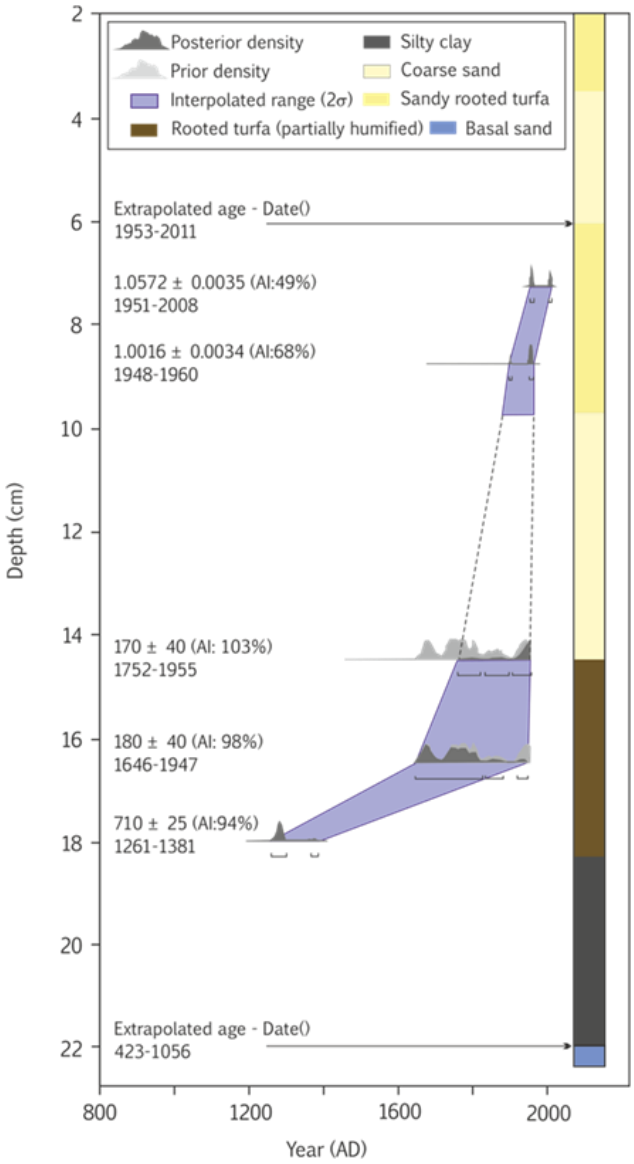

Figure 3.6 P_sequence age-depth model for Exposure 11. Ages prior to AD 1950 are calibrated with the IntCal13 calibration curve (Reimer et al., 2013); while the post AD 1950 age is calibrated with the 13NH1 bomb curve (Hua et al. 2013). We adjust the depths to exclude the sand layers in this instance, which we interpret as tsunamis and possibly storm deposits (see discussion).

4.3 Moss Cliff

4.3.1 Stratigraphy

Six exposures document the stratigraphy at Moss Cliff (Figs. 3.2e and F; Fig. 3.7). The sediments exposed in the shallow coastal cliff contain a variable stratigraphy of buried soils, coarse horizons and organogenic muds. To the west of the stream outflow the stratigraphy is more continuous and better preserved in comparison to the east. As such it is described first and used as a basis for correlation with the eastern exposures.

Underlying the entire cliff-line is a soft brown sand with occasional cobbles (Unit A). Above this is Unit B, a well-humified rooted silty peat that gradually grades into an organic mud (Unit C) that is abruptly overlain by a partially- humified peat containing rootlets and few macrofossils of *E. nigrum* (Unit D). Organic content and mean grain size is low within the organic mud (~20% and 20 μm) but at +3.33 m MTL there is a minor increase in mean grain size (to ~100 um) and fall in organic content (to ~15%) alongside an abrupt increase in magnetic properties (Fig. 3.8). The top of Unit D exhibits a gradual transition to light brown, mottled, well-rooted peat (Unit F). At the base of the peat is a thin sub-centimetre thick sandy peat (Unit E) that grades gradually upwards into Unit F. A thin sandy peat is locally preserved in Exposure O but is not stratigraphically continuous and is associated with minor increases in magnetic susceptibility and mean grain size and a slight reduction in organic content. Unit F grades up into living rhizomes of *E. nigrum* and coarse sandy peat.

The stratigraphy to the eastern side of the cliff-line is simpler; the brown basal sand is overlain by peat, rather than minerogenic mud (Units B and C) in the west. The depth of the basal sand to peat contact is locally variable and is punctuated by flame structures. In Exposures J and K, the peat is sharply overlain by a rooted coarse sand with a thickness of 0.03-0.08 m. This is the stratigraphic equivalent of Unit E in the west; preserved as a thin veneer. Above Unit E is a light brown peat which is heavily rooted by the rhizomes of *E. nigrum*. The top 0.01 m comprises living *E. nigrum* surface and coarse sandy peat.

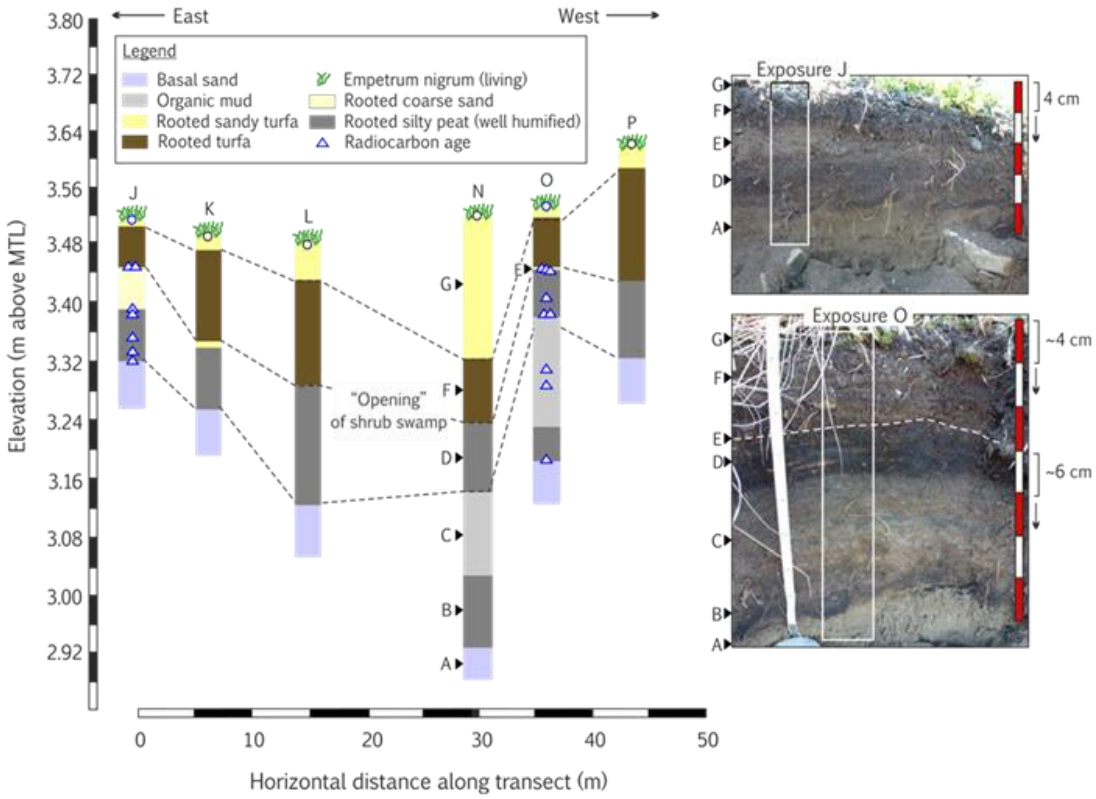

Figure 3.7. Lithostratigraphy at Moss Cliff. Western exposures contain a lower organic mud (Unit C) that is not found in the east. In contrast, in the west, Unit E is a sub-centimetre thick unit of sandy peat that can be traced along the same stratigraphic contact to the east in Exposure J where it is registered as a thicker unit of coarse sand.

4.3.2 Biostratigraphy

Diatom analysis of the sediments in the west of the cliff-line (Exposure O) reveals a largely freshwater sequence that is punctuated by three minor and one more significant increase in marine taxa (Fig. 3.8). Contributions of individual taxa are provided in Appendix 2, Fig. S3, and diatom diversity is relatively high with 24 individual taxa identified. The brown basal sand (Unit A) contains *A. promunturii* in high numbers (~50%). *Meridion circulare* (marine plankton) was found in low frequencies within the overlying partially humified peat (Unit B). Across Unit B and into the organic mud (Unit C), the freshwater taxa *Eunotia exigua*, *P. borealis* and *Fragilaria brevistriata* dominate the assemblage (>80%) and are gradually replaced within the centre of the organic mud by *Fragilaria construens* (also freshwater) which peaks in abundance (>60%) at +3.30 m MTL. To the top of the organic mud at +3.39 m MTL, *P. borealis*, *H. amphioxys* and *E. exigua* reclaim the assemblage from *F.*

construens. The first subtle increase in marine taxa is within the organic mud between +3.33 to +3.38 m MTL where low numbers of *M. circulare* and *A. promunturii* are found (<10%) alongside an abrupt change in magnetic properties and a minor fluctuations of mean grain size and LOI. The remainder of the sequence is mostly dominated by freshwater taxa, although *A. promunturii* and *M. circulare* are found within across the thin sandy peat (Unit E), which is also marked by a change in magnetic properties and mean grain size. Low numbers of *A. promunturii* demonstrate a third and final signature of marine conditions at the top (living surface) of the sequence within sandy peat.

The diatom assemblages outlined above are supportive of those observed in the east within Exposure J (Fig. 3.8; Appendix 2, Fig. S7). In particular, the brown basal sand contains marine taxa (Unit A) and the peats contain freshwater taxa. In contrast to the subtle signature of Unit E in the west, the rooted coarse sand (Unit E) contains the marine taxa *A. promunturii* in abundance (>60%) alongside the brackish *Navicula pusilla*. Once again, the transitions across these units demonstrate relatively gradual changes that we attribute to post-depositional mixing of near-contact sediments (see discussion).

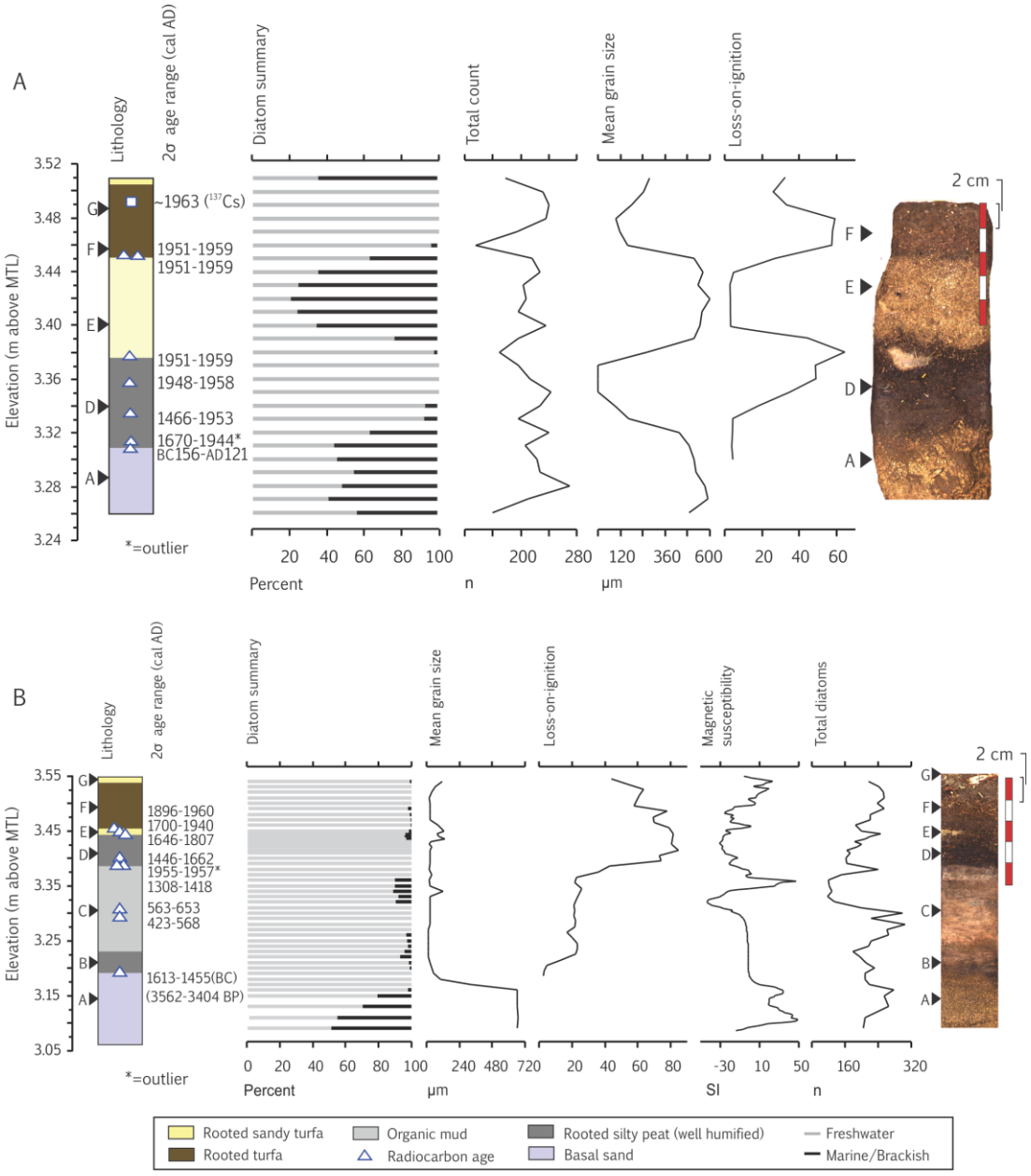

Figure 3.8. Diatom summary, lithostratigraphy, sediment properties and dating at Moss Cliff. a, Exposure J. **b,** Exposure O. Note that ages presented are 2σ posterior (modelled) ages, except for two outlying ages that are presented as a 2σ unmodelled ranges (asterisks).

4.3.3 Chronology

Eight AMS ^{14}C determinations constrain the chronology for Exposure O based on a six bulk ages and two samples of *E. nigrum* seeds and leaves (Table 3.1; Fig. 3.9). A bulk date from the base of Unit D yielded an anomalously modern age and has been excluded on the assumption that it contains carbon introduced from a higher level by plant roots. We do not adjust the depths of sand deposits as they are very thin and stratigraphically well-incorporated into under- and overlying units. Overall, the age model has good agreement (AI=87%). The contact between Units A and B yields an age modelled solution of BC 1613-1455 (equivalent to 3562-3404 cal yr BP) which is the oldest age observed across the two sites. The model dates the horizon containing the first subtle marine signature at +3.34 m MTL to AD 686-1167. The transition from organic mud to partially humified peat (Units C and D) has a modelled age of AD 1308-1418, while the top of the sandy peat (Unit E) dates to AD 1896-1960.

The chronology for Exposure J is based on seven AMS ^{14}C age determinations and ^{137}Cs concentrations (Table 3.1; Fig. 3.10). A peak in ^{137}Cs concentrations at 2 cm depth has been assigned an age of AD 1961-1965 in line with peak nuclear weapons testing (1963 ± 2; 2σ). We have adjusted the section depths following the removal of Unit E, which we interpret as a tsunami deposit (see discussion). A young age from the base of Unit D has also been excluded from the age model because it appears anomalously young for its depth and is out of sequence with the adjacent dates. Overall the resulting model has good agreement (AI=76%). It dates the top of the basal sand (Unit A) to BC 156 to AD 121 (equivalent to 2107-1807 cal yr BP) and the rooted coarse sand to AD 1951-1959.

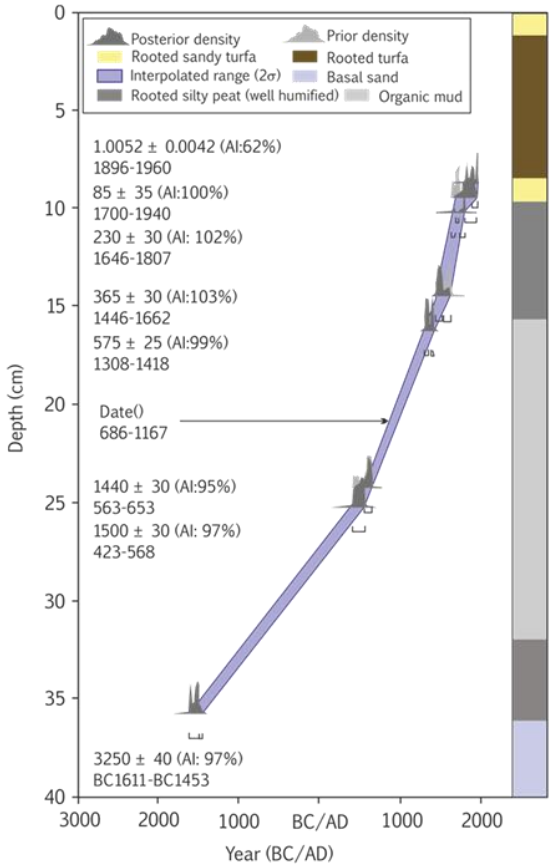

Figure 3.9. P_sequence age-depth model for Exposure O. Ages prior to AD 1950 are calibrated with the IntCal13 calibration curve (Reimer et al., 2013); while the post AD 1950 age is calibrated with the 13NH1 bomb curve (Hua et al. 2013). In this instance, depths are not adjusted to exclude sand layers as they are stratigraphically well-incorporated. We use the Date() function to infer the age of a tsunami deposit within the organic mud at 21 cm (+3.34 m MTL).

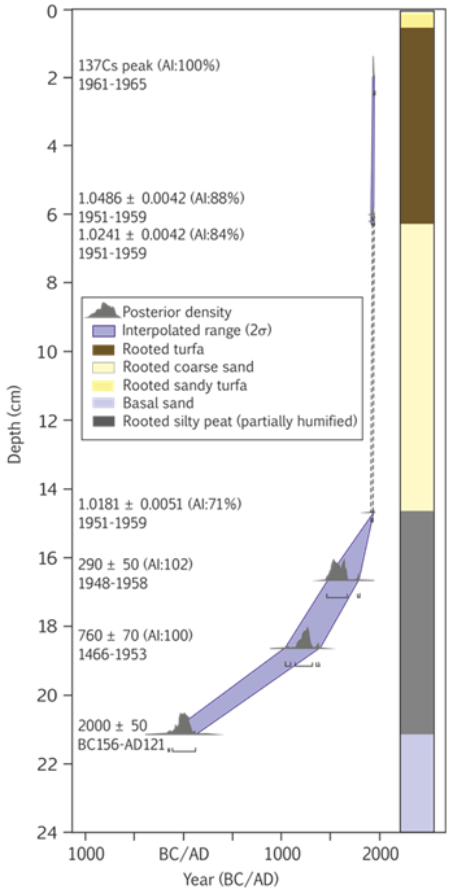

Figure 3.10 P_sequence age-depth model for Exposure J. Ages prior to AD 1950 are calibrated with the IntCal13 calibration curve (Reimer et al., 2013); while the post AD 1950 age is calibrated with the 13NH1 bomb curve (Hua et al. 2013). We adjust the depths following exclusion of the coarse-grained deposit, which we interpret as a tsunami (see discussion).

5. Discussion

5.1 Assessing the evidence for tsunami inundation in south Vaigat

The stratigraphic, radiocarbon and sedimentological data from Vaigat provide evidence of deposits emplaced by waves associated with landslide-generated tsunamis and possible iceberg-generated tsunamis and/or storm events. However, it is difficult to determine the precise mechanism responsible in each case. For example, if we encounter evidence of the AD 2000 and AD 1952 tsunamis, we know on *a priori* grounds that they were triggered by landslides. In contrast we have no known examples where waves associated with iceberg rolls or storm events made landfall, and therefore we have no modern analogues with which to compare. As such, each anomalous deposit requires critical evaluation on a case-by-case basis in order to accurately interpret the mechanism of its emplacement.

To this end, first we assess the evidence for the known AD 2000 and 1952 landslide-driven tsunami events. We then infer the environment of additional anomalous deposits based on microfossil content, age correlation of (potential) equivalent deposits and information from the AD 2000 and 1952 modern analogues. To aid in age correlations, we performed cluster analysis (unconstrained, Euclidean distance) on the (modelled) ages of anomalous deposits from multiple pits/exposures (Fig. 3.11). We discuss the resulting three groups of age similarity individually.

As a minor note, where we find marine diatoms within the stratigraphy that are unaccompanied by supporting stratigraphic evidence of marine inundation (i.e., coarse-grained deposits), we interpret that such occurrences have been deposited by wave-spray, likely during storms. Cooper and Jackson (1999) found that fine sand deposits can be sporadically emplaced several metres inland by wave-spray during storms. It is feasible that the same mechanism could deposit low frequencies of marine microfossils inland, whilst being unable to entrain the heavier coarse sands and gravels that comprise the beaches within close proximity of our sampled pits/exposures. Indeed, in such instances when marine taxa are found without accompanying coarse deposits, these examples are completely constrained to the fjord-side of the peninsula (Pit 4); a location within 25 meters of the mean high water mark.

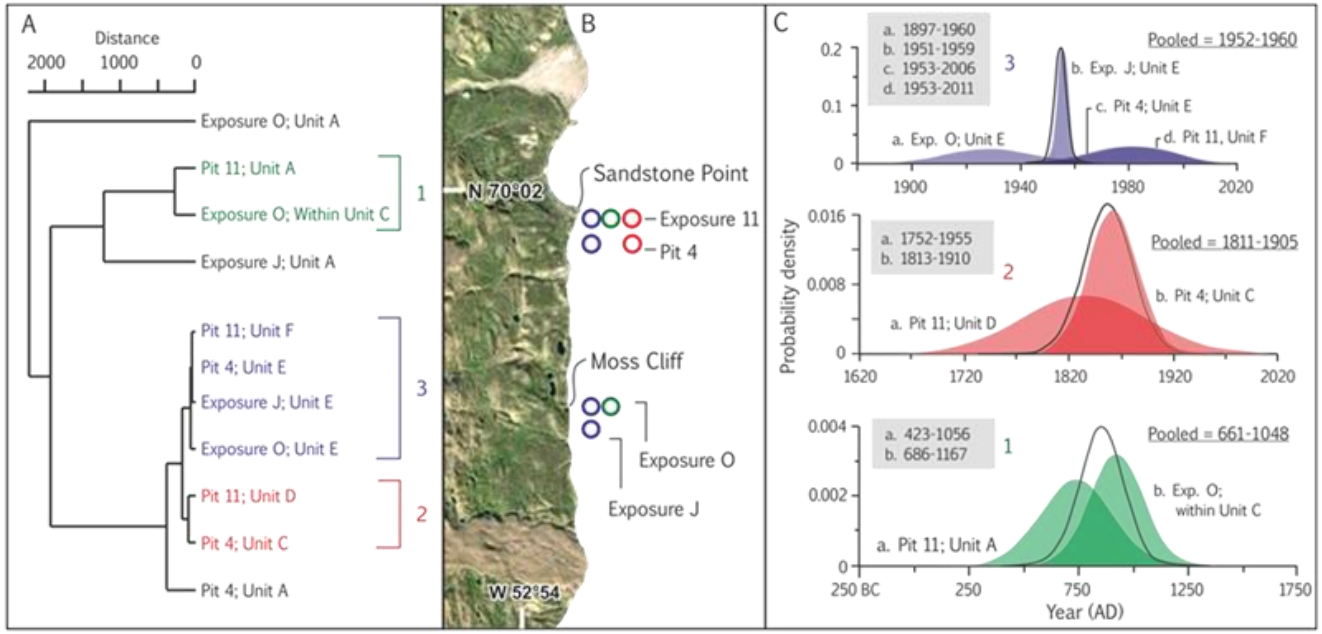

Figure 3.11. a, Cluster analysis of ages of tsunami deposits (upper contacts), see text for interpretations. **b,** Inter- and intra-site age correlation of stratigraphic units based on cluster analysis, superimposed on Google Earth image of study area. **c,** Age probability density functions and pooled means of ages that cluster on the same branches.

5.1.1 21 November 2000 tsunami

A prominent feature of the stratigraphy at both sites is a fragmented cap of coarse sand of variable thickness. At Moss Cliff it is present as a sub-centimetre thick layer that drapes the surface and in the majority of places is being reworked into the underlying soil by the roots of the colonizing *E. nigrum* (Fig. 3.7). However, there are small patches where *E. nigrum* has yet to recolonize. On the fjord-side of Sandstone Point, the deposit is relatively thick (0.04 m) and has been variably recolonized by *F. rubra* (Fig. 3.3). On the lee-side, evidence of a well-defined coarse sand deposit is more equivocal as the section here contains a sandy peat that has an increased coarse-grain and marine diatom content throughout (Fig. 3.4). In all cases the coarse-grained deposits are highly porous. In a recent paper, Buchwal et al. (2015) found surface coarse sand and gravel deposits that demonstrate similar variability along the coastal plain of our field site, which they attribute as deposits of the landslide-tsunami that occurred at Paatuut on 21 November 2000 AD (Fig. 3.1; Pedersen et al. 2002; Dahl-Jensen et al. 2004). Further, they inferred using dendrochronology that dwarf shrubs immediately recolonized the AD 2000 tsunami deposit (Buchwal et al., 2015). On the basis that the deposits observed here share the same variability and surface stratigraphic position as those presented by Buchwal et al. (2015), we attribute these to the AD 2000 landslide-generated tsunami at Paatuut. We hypothesise that these variations reflect deposition on frozen and snow-covered ground during late autumn/winter. Post-depositional reworking would have occurred during the following spring as a result of fluvial activity (snowmelt) and by recolonizing vegetation.

5.1.2 15 December 1952 tsunami

Deposits dated to around the early-mid 20th century are found at both sites (Fig. 3.11) which are directly analogous to the AD 2000 tsunami deposits. On the eastern edge of Moss Cliff (Exposure J) a prominent ~0.08 m-thick, well-rooted and highly porous coarse sand horizon containing abundant marine diatoms is dated to AD 1951-1959. It correlates strongly with the timing of a known landslide-tsunami that originated near Tupaasat on 15 December 1952; which resulted in the death of one person at Qullissat (Fig. 3.1; Pedersen et al. 2002). On the western end of the cliff-line, a sub-centimetre thick layer of sandy peat containing marine diatom taxa is recorded on the same stratigraphic contact (at the transition from partially humified peat to rooted peat), with the top yielding an age of AD 1896-1960. It was difficult to precisely date this deposit as it is thin (sub-centimetre thick) and displays evidence of being reworking into under- and overlying peat. Thus we are unable to

unequivocally attribute this deposit to the AD 1952 tsunami on the basis of age. However, because it occupies the same stratigraphic position as the AD 1952 tsunami deposit positioned to the east in Exposure J, we infer that this represents an equivalent deposit emplaced by the same tsunami. In an analogous situation to the AD 2000 tsunami event, these characteristically variable deposits probably reflect post-depositional reworking by spring snow melt and the variable recolonization of woody shrubs (Buchwal et al., 2015). The angle of wave-impact might also have contributed to this observed variability (see discussion; Section 5.2).

On the fjord-side of Sandstone Point, a laterally continuous sandy peat is dated to AD 1953-2006. The lower bound of this age range correlates in timing with the AD 1952 landslide-tsunami. Despite the generally low diversity and poor preservation of microfossils throughout Pit 4, we found marine taxa within 1 cm of its lower contact and not within the deposit itself (Fig. 3.4). These deposits are directly analogous to the highly porous AD 1952 and AD 2000 tsunami deposits described at Moss Cliff and elsewhere along the coastal plain by Buchwal et al. (2015), respectively. It is feasible that the gentle inclination of the peninsula slope facilitated rapid water percolation; washing marine diatoms from the thin drape of tsunami sediment lower into the profile. We attribute these deposits to the AD 1952 tsunami.

Towards the coast in Pit 1, the AD 1952 tsunami deposit is dissected by a thin peat (<2 cm thick). As the AD 1952 tsunami deposit appears to be preserved as a coherent coarse deposit along the entire length of the transect, the AD 1952 tsunami could have eroded a unit of underlying peat; now restricted to Pit 1, and amalgamated with a slightly older coarse-grained deposit. Alternatively, it could imply that a slightly older coarse-grained deposit is spatially constrained to Pit 1 only, an explanation that we prefer given its seaward proximity. We are unable to provide any further information of this anomalous coarse-grained deposit.

On the lee-side of the peninsula, the identification of tsunami deposits is more difficult because vertical sediment mixing has significantly disturbed the sediment profile. Exposure 11 contains a rooted coarse sand unit with diffuse upper and lower contacts yet containing marine taxa, dated to AD 1953-2011 (Figs. 3.4 and Appendix 2, Fig. S2). Marine diatom taxa are found across these contacts and likely reflect vertical mixing of sediments and diatom assemblages by bioturbation. Alternatively, it is feasible that post-depositional reworking could have been promoted by frost-heave or pressure differentials between two stratigraphic units of opposing sediment type (coarse sand and peat). Indeed, although not present here, flame structures are found elsewhere (Moss Cliff; Exposure J) and are common

indications of the latter (e.g. Bockheim and Tarnocai, 1998). Given its stratigraphic position and age, this deposit likely reflects inundation by the AD 1952 tsunami.

A pooled mean of the four ages from both sites yields an age of AD 1952-1960 (Group A) (Fig. 3.11), which coincides closely with the landslide-tsunami that originated near Tupaasat on 15 December 1952 (Fig. 3.1; Pedersen et al. 2002).

5.1.3 AD 661-1048 event (Group 1)

Exposure 11 (Sandstone Point; lee-side) and Exposure O (Moss Cliff) contain fine-grained deposits that are unique to both sites (units of silty clay and organic mud) (Figs. 3.7 and 3.8). At Sandstone Point, a unit of silty clay contains the dominant freshwater taxon *A. didyma*, which we consider implies a lagoon that was deeper than present and not open to tidal exchange (Appendix 2, Fig. S2). At Moss Cliff, *F. construens* found within organic mud provides evidence of a similar freshwater pond, likely a larger predecessor to the current pond that formed when the coastline was seaward of its present position (Appendix 2, Fig. S3). The upper contacts of these deposits overlap in age: AD 1261-1381 (Exposure 11) and AD 1308-1418 (Exposure O) and imply a signal of synchronous coastal change across sites (see Section 5.4).

Within the fine-grained sediments are distinct microfossil and sedimentological changes of similar age (Group 1) (Fig. 3.11). At Moss Cliff (Exposure O) within organic mud, there are peaks in magnetic susceptibility, grain size and a reduction of LOI values alongside the presence of marine diatom taxa at +3.34 m MTL, dated within the age model to AD 686-1167 (Fig. 3.9). This deposit must be associated with a large wave, as RSL was between -2.29 to -3.49 m MTL at this time; based on interpolated RSL data from Avreprinsens Eijland (Long et al. 1999) and the south coast of Disko Island (Long et al., 2011). Considering the height of MHWST, a minimum wave run-up height of 4.29 m was required to deposit this anomalous deposit, which we consider too large to be associated with a storm event.

At Sandstone Point (Exposure 11), the lower contact of the silty clay yields a similarly wide yet overlapping 2σ range (AD 423-1056). These age ranges are imprecise for two reasons, first; there is a plateau in the ^{14}C calibration curve at this point in time and, second, because these ages are inferred from extrapolation to undated sections of age model. It is possible that the broadly similar ages in Exposures O and 11 reflect the impact of the same event, albeit manifested differently. It is intriguing to find an abrupt lithostratigraphic

change in a back-barrier setting (Exposure 11) that appears coincident with the timing of a well-defined tsunami deposit elsewhere (Exposure O). Despite further chronological refinement, we tentatively infer that these record the same event and that these reflect the landslide-tsunami inundation. In turn, this rules out an iceberg-generated tsunami as a driving mechanism. A pooled age for this event is AD 661-1048 (Fig. 3.11). We interpret the soft brown basal sand which underlies Exposure 11 and the stratigraphy at Moss Cliff as a relic mid-late Holocene beach, given that a maximum age of deposition in Exposure O at 3562-3404 cal yr BP (BC 1613-1455) is consistent with the time that falling RSL intersected present at c. 3800 cal yr BP (Long et al., 1999; 2011).

5.1.4 AD 1640-1680 event

An anomalous event is present at the base of Pit 4 from the fjord-side of the peninsula which has no chronological equivalent in the study area. The evidence comprises a sub-centimetre thick unit of coarse sand containing marine diatom taxa (Unit A) and dates to AD 1640-1680 (modelled age). A date from below its lowermost contact within peat yields an age of AD 1227-1389, which reveals a ~450 yr hiatus between the coarse sand and underlying peat. Although it is possible that the hiatus was caused by a period where sediment accumulation ceased entirely, it more likely reflects erosion to underlying soil by a tsunami or storm event.

5.1.5 AD 1811-1905 event (Group 2)

Two coarse horizons are spatially limited to sections either side of Sandstone Point but also overlap in age (Group 2) (Fig. 3.11). On the lee-side in Exposure 11, a rooted coarse sand (Unit D) is dated to AD 1752-1955; while on the fjord-side in Pit 4, an age of AD 1813-1910 is derived from the top contact of a sub-centimetre thick unit of sandy peat (Unit C) (Appendix 2, Figs. S1 and S2). Embedded within the rooted coarse sand on the lee-side is a single bivalve of *Rangia cuneata* which indicates transportation from a sub- or inter-tidal environment. As with the remainder of the stratigraphy here, Unit E is not stratigraphically continuous (Fig. 3.3). On the fjord-side the lateral continuity of the deposit is difficult to determine as a younger coarse horizon merges with this deposit in a landward direction after cutting into overlying peat (Section 5.1.2). A pooled mean of the two ages (above) yields an age of AD 1811-1905, which does not correlate in timing with any other coarse deposits or abrupt sedimentological changes within the stratigraphy observed at Moss Cliff (Fig. 3.11). Therefore the most probable mechanism for the emplacement of these coarse horizons is

either a landslide- or iceberg-generated tsunami or storm event that did not impact or left no evidence at Moss Cliff.

5.2 Characteristics of tsunami deposition

Vaigat tsunami deposits are fragmentary, subtle and caused variable erosion to pre-tsunami surfaces. The fjord-side of Sandstone Point is well-vegetated yet we find no evidence of flattened or encased vegetation on pre-tsunami surfaces here (as observed elsewhere), suggesting complete removal of vegetation and erosion of soil. At Moss Cliff, the AD 2000 tsunami deposit is registered as a layer of sandy peat; a result of bioturbation by *E. nigrum* which has reworked the tsunami deposit into underlying soil. At Sandstone Point, the AD 2000 tsunami sand is penetrated by thick *F. rubra* rhizomes on the fjord-side, while in its lee *E. nigrum* has had difficulty recolonizing (Fig. 3.3). Conversely, there are examples from within 100 m of Sandstone Point where *E. nigrum* has recolonized without causing significant disturbance to underlying tsunami sediment (Appendix 2, Fig. S5). Tsunami deposits that are preserved as units of sandy peat may reflect where *E. nigrum* survived the wave inundation and where tsunami sands and gravels were deposited irregularly within gaps between widely-spaced rhizomes (Fig. S5). Alternatively, thawing of underlying peats during spring may unevenly incorporate the deposits of tsunami that occurred in winter, with both the AD 2000 and AD 1952 tsunamis occurring on frozen ground in late autumn/winter months. We also find evidence where *E. nigrum* has been flattened and encased in tsunami sediment (Fig. S5), with the orientation of flattened rhizomes reflecting direction of wave flow (Morton et al., 2011). Comparable variability of tsunami deposits are reported by Garrett et al. (2013) and Nelson et al. (2009).

The deposit of the AD 2000 event is preserved as a relatively continuous layer at both sites, despite being variably disturbed and incorporated into stratigraphy by bioturbation as discussed above. Where we find evidence of the AD 1952 event, it is preserved as a fragmented horizon with variable continuity and thickness. At Moss Cliff, it is found in a 2 x 0.5 m area on the eastern edge of the cliff where it is preserved as a 0.03-0.08 m thick deposit of coarse sand, while in the west it is preserved as a discontinuous thin veneer within peat (i.e., in Exposure O only). On the lee-side of Sandstone Point, it is present as a discontinuous 0.05 cm thick sand, which is in contrast to the fjord-side where it is preserved as a laterally coherent unit of coarse sandy peat (sub-centimetre thick). Similar differences in continuity and deposit thicknesses on both sides of Sandstone Point are observed for the older event dated to AD 1811-1905. We attribute these contrasts to the

angle of wave impact, with the barrier beach (lee-side) occupying a perpendicular, direct-facing angle to waves propagating up-fjord from the zone of high landslide activity. In contrast, Exposure O at Moss Cliff is offered relative shelter by the foot of the adjacent marine terrace and is angled obliquely to waves originating down-fjord. The sediments in Exposure O were accessed by cutting into a small sheltered inlet in the cliff-face (Fig. 3.7) which likely explains the continuity and good preservation of the sequence here. Similar to the lee-side of Sandstone Point, however, the eastern cliff-face angles the northwest more directly, which likely explains the contrasting patterns of deposition here.

A characteristic of the diatom content of tsunami deposits is that they consistently contain the same marine taxa within a low diversity assemblage. Low nutrient availability in Arctic environments can suppress microbe diversity (e.g. Carmack and MacDonald, 2002; Lovejoy et al., 2002; 2006) meaning that only the most robust individuals can thrive. Post-depositional preservation of thinly silicified valves is also a key issue. The thickly-silicified *A. promunturii* is the most common marine taxon and is found within a mixed assemblage containing other thickly-silicified taxa such as the freshwater *H. amphioxys* and *P. borealis*. Occasionally marine taxa are preserved in low numbers and without an accompanying tsunami deposit, especially on the more exposed fjord-side of the peninsula. Freshwater and planktonic taxa such as *A. didyma* and *M. circulare* are more delicate and generally found within quiet-water deposits (fine-grained silty clays and organic muds), but can occasionally be reworked into tsunami deposits (e.g. Pit 11; Units C and E). Similar mixed and chaotic diatom assemblages are reported by Kokocinski et al. (2009) in tsunami deposits from Thailand.

5.3 Tsunami frequency and run-up

The coastal stratigraphic record of southeast Vaigat contains evidence of five tsunami events within the last 1000-1400 yrs. At least two of these reflect landslide activity in Vaigat in the last century. For the remainder, evidence is equivocal and could reflect deposition by storms, landslide-tsunami or iceberg roll. On average these constitute a minimum mean frequency of 1 tsunami event per 450 yrs and a maximum mean frequency of 1 event per 270 yrs. Regardless of which estimate, however, the frequency of events is relatively high when compared to tectonically active sites from lower latitudes. For example, the maximum estimate is comparable to that inferred from stratigraphic records of earthquake and tsunami on the Chilean megathrust (Garrett et al., 2014) and the minimum closer to average tsunami recurrence on the Cascadia (e.g. Kelsey et al., 2005), Alaskan-Aleutian (Shennan et al.,

2014) and perhaps the Sunda (Sieh et al., 2015; Dura et al., 2011; Jankaew et al., 2008; Monecke et al., 2008) megathrust.

There are three reasons why the stratigraphic record of tsunami frequency could be an underestimate of the real frequency of tsunami events in Vaigat. First, the absence of tsunami deposits cannot be used to infer periods of no tsunami activity (Nelson et al., 1996), a problem that is universal to stratigraphic records of tsunami. A second issue is that the stratigraphic record is spatially limited to southeast Vaigat such that we have no record of tsunamis that were unable to propagate up-fjord to our location.

A specific problem of sites with complex RSL histories, however, is that RSL fluctuations alter the probability of tsunami inundation at a fixed position on the coast over time. From old to recent, tsunami events within our record have intervening age intervals (based on mid-points of modelled ranges) of 805, 199, 94 and 48 yrs - demonstrating an apparent increase in frequency over the last millennium. A temporally and vertically constrained model for tsunami run-up during periods of RSL rise illustrates how RSL rise affects the probability of tsunami inundation (Fig. 3.12). We consider tsunami run-up height at three hypothetical time-slices where RSL was lower than present (t1, t2, t3) and derive the probability of tsunami run-up height based on random sampling (1000 permutations) of two independent boundary controls: i) the Vaigat spring tidal range of 2.5 m (expressed bidirectionally as ± 1.25 m) and, ii) tsunami run-up height of 3.0 ± 2.0 m (2σ), which we consider a minimum estimate (range) of tsunami run-up in Vaigat (defining a minimum mathematical range of 1-5 m; 2σ). We do not account for atmospheric contributions to tidal levels.

At t1 when RSL stood ~3 m below present, the probability of tsunami inundation at a fixed point on the coast (e.g. the location of present MTL) is ~50%, which increases to ~90% at t3 with a rise of 2 m (Fig. 3.12). As the shortening of intervening age gaps within the Vaigat stratigraphic record likely reflects this phenomenon, it is misleading to infer (over-)precise estimates of tsunami run-up from stratigraphic records that are fixed in space, given the controls of millennial-scale RSL changes in the long-term and tidal oscillations in the short-term. In addition, temporal constraints also arise in areas of fluctuating RSL change, in particular because the creation of accommodation space controls the preservation potential of tsunami deposits (e.g. Dura et al., 2011).

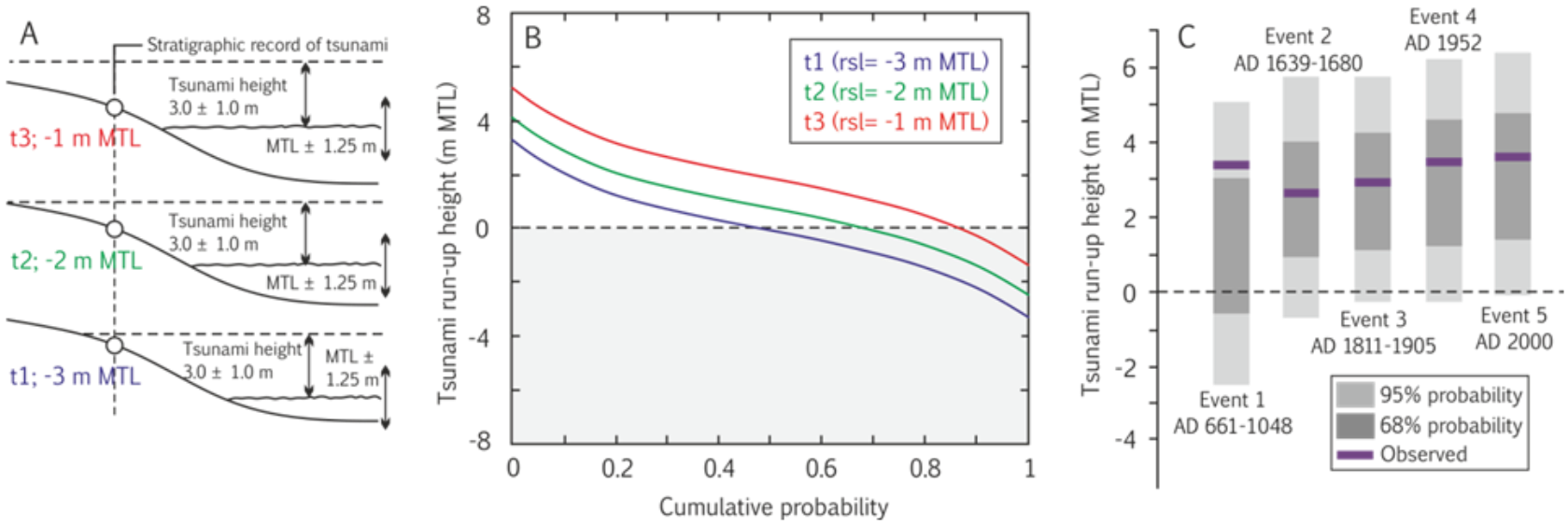

Figure 3.12. Determining tsunami run-up heights probabilistically. a, Schematic illustration of the two principle controls on tsunami run-up height when observed at a fixed position on the coast: tidal range with respect to palaeo-RSL (expressed as the spring tidal range at Qeqertarsuaq) and absolute wave height (expressed as an estimated minimum 1-5 m range). Ranges permit a probabilistic assessment of run-up height for three hypothetical time-slices where RSL was lower than present. **b,** Cumulative probability distributions of tsunami run-up height for the three hypothetical time-slices, based on random sampling of the boundary controls. **c,** Upper and lower bounds for tsunami run-up height (95% and 68% confidence) for events within the Vaigat stratigraphic record, based on random sampling of the boundary controls outlined in a. RSL positions and age estimates are inferred from interpolated RSL records of Long et al. (1999; 2011) and mid-points of event ages outlined in c, respectively. Observed run-up heights (purple bars) correspond to the elevation of deposits inferred in the stratigraphic record and are therefore minimum estimates.

5.4 Late Holocene controls on the coastal stratigraphic record in Vaigat

As mentioned in Section 5.1, there are rare instances where signals of long-term RSL and coastal change are preserved. The date of 3562-3404 cal yr BP (BC1613-BC1455) from the base of basal peat at +3.19 m MTL in Exposure O provides a minimum age on the timing of emergence of the present day coastal zone (i.e., when RSL fell below present), with brackish sediments beginning to accumulate on top of the relic mid to late Holocene beach. The height of the soft brown basal sand is lower in Exposure O than in Exposure J and could reflect erosion by fluvial activity and subsequent infilling by (high-)salt-marsh sedimentation prior to the final regression of RSL and emergence of the coastal zone. As RSL fell, fine-grained sediments at both sites record freshwater lakes which ceased to exist by c. 1000 cal yr BP. At Moss Cliff, percentage increases of *F. construens* in Exposure O document a continuous record of lake-level change throughout the 2 k yr history of the lake, with greater abundances implying a shallow pool c. 1-2 m deep (e.g. Brugam et al., 1998). Increased water depths promoted lacustrine accumulation (organic mud) over terrestrial freshwater accumulation (peat). Interestingly, the abundance of *F. construens* records a signal that mimics long-term RSL movements and could demonstrate the control of RSL on coastal sedimentation (Appendix 2, Fig. S3). At c. 3800 cal yr BP, RSL intersected present and fell by ~4 m to a still-stand at c. 2200 cal yr BP, whereupon it rose by an equivalent amount to present (e.g. Long et al., 1999; 2011). When plotted, the structure and timing of RSL changes display a strong inverse correlation with the relative abundance of *F. construens* (r=-0.93). We assume this reflects a relationship between RSL and groundwater levels, but counter-intuitively this implies a rise in groundwater in response to RSL fall, which at present we are unable to resolve. What is certain is that a tsunami event is unlikely to have been implicated in coastal geomorphological and pond-level changes given the gradualness of microfossil changes (Appendix 2, Fig. S3).

There is evidence elsewhere to suggest that climate can exert a positive control on long-term coastal evolution. A recent sea-ice reconstruction from the Vaigat Strait contains a period of reduced sea-ice formation between c. 1400-600 cal yr BP associated with the delivery of warmer surface waters to west and southwest Greenland (Sha et al., 2012; Jensen et al., 2004). At the same time, freshwater clays found on the lee-side of Sandstone Point were deposited up to a height of +3.5m MTL. This implies that the current back-barrier lagoon was 2-3 m deeper than present during a pronounced warm period characterized by increased precipitation. Following this at c. 600 cal yr BP (AD 1400), sea-ice cover in Vaigat increased in response to the Little Ice Age (LIA) cooling (Sha et al., 2014). In our record this coincides with the synchronous disappearance of freshwater pools and lakes

across our two sites, with accumulation of fine-grained freshwater muds being replaced by the accumulation of freshwater peats. This strongly supports the hypothesis that paraglacial coastal evolution is influenced strongly by alterations in the rate of sediment delivery to the coastal zone by climatic processes (e.g. Strzelecki, 2012; Strzelecki et al., 2015). However, given the short-lived increase in *A. promunturii* at the transition from freshwater mud to freshwater peat at Sandstone Point, an alternative hypothesis is that the barrier was breached by a high-energy event, resulting with the draining of the back-barrier lagoon and morpho-sedimentary changes.

5.5 Implications for reconstructing Arctic tsunami

The thin, variable and fragmentary nature of tsunami deposits outlined in Section 5.2 has made reconstructing these events a challenge. Several decades of research in lower latitude settings has resulted in the development of criteria for the identification of tsunami deposits (e.g. Nelson et al., 1996; Peters and Jaffe, 2010), which have been difficult to robustly test in Vaigat. In particular, the absence of well-defined tsunami deposits presented in this paper makes a robust hypothesis-testing exercise and deductive approach difficult to implement. It is difficult to robustly confirm the existence of a tsunami deposit when sedimentary evidence is minimal or lacking. Indeed, in Thailand, Szczuciński et al. (2010) recognized that the initial thickness of a tsunami deposit determines its preservation potential. They found that bioturbation and post-depositional reworking completely removed evidence of the 2005 Indian Ocean tsunami within 5 yrs at 50% of sites studied (Szczuciński, 2012). This may also be applicable to Arctic settings where ambient environmental factors are also extreme, exacerbating post-depositional reworking. Indeed, the Arctic maritime climate of Vaigat is subject to significant seasonal air temperature and precipitation swings, while robust dwarf shrubs that dominate the floral ecosystem have thick woody roots which can cause significant disturbance to underlying strata. These factors appear to substantially reduce the preservation potential of tsunami deposits in Vaigat, and could be applicable to studies of tsunami elsewhere in the Arctic.

The fragmented and thin nature of tsunami deposits precludes a rigorous assessment of well-documented criteria for the identification of tsunami deposits (e.g. Peters and Jaffe, 2010; Engel and Bruckner, 2011). In Vaigat tsunami deposits are limited in terms of spatial extent; often found preserved in small ~2 x 0.5 m^2 areas. Hence it is not possible to measure horizontal trends in grain size such as landward thinning or thickening of tsunami-lain sediments (Bondevik et al., 1997b; Matsumoto et al., 2012; Srisutam and Wagner, 2010).

Similarly, the thinness of tsunami deposits precludes an analysis of vertical trends in grain size (e.g. Morton et al., 2007). The only example of a sufficiently thick (>3 cm) deposit is associated with the AD 1952 tsunami (Exposure J at Moss Cliff), although this has been disturbed by thick rhizomes of overlying *E. nigrum*. This example illustrates a uniform grain size, which again could reflect post-depositional reworking (vertical sediment mixing) by bioturbation and frost-heave. Equally, where thin tsunami deposits are often found reworked into peaty soils, it is not possible to assess the degree of layering with the aims of interpreting multiple waves (e.g. Richmond et al., 2006; Szczuciński et al., 2006). Information on the sharpness of the lower contact is also lost when tsunami sands are found reworked into under- and overlying soils (Szczuciński, 2012; Goto et al., 2011).

Two criteria for the identification of tsunami deposits arise from this work. First, marine diatoms will be transported inland and deposited regardless of latitude. Here we find marine diatoms within mixed assemblages, suggesting erosion of terrestrial and marine sediments by tsunami, similar to lower latitude settings (e.g. Garrett et al., 2013). In exceptional cases, marine taxa are missing or found within 1 cm below tsunami deposits, but these examples are exceptions. Indeed, tsunami deposits devoid of marine microfossils have been identified on the Japanese coast (Szczuciński et al., 2012). In such cases, low abundances of marine taxa probably reflect low absolute concentrations within the Vaigat Strait or perhaps the seasonality of phytoplankton blooms. Delicate valves can also disintegrate once deposited, especially during summer months when soil moisture decreases. Indeed, some sediment profiles encountered contain exceptionally low levels of moisture (e.g. Pit 11; Sandstone Point). Second, dating permits age correlation of deposits from multiple sites (Nelson et al., 1996). In this study we have been able to determine the timing of the known AD 1952 tsunami with a precision of 8 yrs (2σ) using ^{14}C data from a number of stratigraphic profiles. However, as ever there remains a need to carefully consider the stratigraphic position and type of material dated because of the problems associated with erosion and reworking (e.g. Bondevik et al. 1997b).

6. Conclusions

Previous mapping of coastal landslide deposits on the northern shores of the Vaigat Strait, west Greenland, have been used to predict an average tsunami recurrence of 1-2 per thousand years (Pedersen et al., 2002). The most recent was in AD 2000 and had a maximum run-up height of 30 m directly opposite the landslide source (Dahl-Jensen, 2004).

We are able to present the first stratigraphic evidence of late Holocene tsunami events from west Greenland. Our key conclusions are:

Predecessors of the AD 2000 tsunami occurred in AD 1952, AD 1811-1905, AD 1640-1680 and AD 661-1048. Evidence for the second and third events is equivocal, and could reflect deposition by storms. A minimum mean frequency is 1 event per 450 yrs, while a maximum mean frequency is 1 per 250 yrs. These estimates are close to average tsunami and earthquake recurrence intervals inferred along the Earth's major subduction zones.

Tsunami deposits are fragmentary, variable in composition, thickness and grain size, and contain the same diatom taxon within a low diversity assemblage. The AD 2000 tsunami deposit is variably reworked into underlying soils by plants that have variably recolonized the drape of tsunami sediment. Pre-tsunami surfaces can be eroded and stripped of living vegetation, while there is evidence that some flora prior to the AD 2000 tsunami survived the inundation intact. In contrast, pre-tsunami surfaces can be flattened and encased in tsunami sediment. The AD 1952 tsunami deposits are analogous to those deposited by the AD 2000 event.

The fragmentary and thin nature of tsunami deposits precludes a rigorous assessment of criteria for the identification of tsunami deposits developed in lower latitude settings. Vaigat tsunami deposits are not well defined and this makes it difficult to determine with full confidence the mechanisms of their emplacement with a robust hypothesis testing exercise. These problems relate to the fact that deposits are mostly very thin upon being laid-down (sub-centimetre). Tsunamis occurring during winter months, such as the AD 2000 and 1952 events, deposit material on snow-covered ground and this likely contributes to the fragmented patterns of deposition. In spring, they are further disturbed by post-depositional reworking associated with fluvial activity (snowmelt) and bioturbation. Attempts to reconstruct similar events elsewhere in the Arctic will likely be met by the same challenges.

Small pockets of relatively sheltered coastal lowland preserve evidence of longer-term coastal evolution in Vaigat. An age of c. 3.5 kyr BP from the base of peat that overlies a mid to late Holocene relic beach provides a minimum age on the timing of RSL fall in the area and is consistent with RSL data from elsewhere in Disko Bugt (e.g. Long et al., 1999; 2011).

References

Andersen O.G.N. 1981. The annual cycle of temperature, salinity, currents and water masses in Disko Bugt and adjacent waters, West Greenland. *Meddelelserom Grønland, Bioscience* 5: 1–36.

Atwater, B.F. 1987. Evidence for Great Holocene earthquakes along the outer coast of Washington State, *Science*, 236, 942-944.

Bockheim, J.G., Tarnocai, C. 1998. Recognition of cryoturbation for classifying permafrost-affected soils. Geoderma, 81, 281-293.

Bondevik S, Svendsen JI, Mangerud J (1997a) Tsunami sedimentary facies deposited by the Storegga tsunami in shallow marine basins and coastal lakes, western Norway. Sedimentology 44: 1115-1131

Bondevik, S., Svendsen, J.I., Johnsen, G., Mangerud, J., Kaland, P.E., 1997b. The Storegga tsunami along the Norwegian coast, age and runup. Boreas 26, 29–53.

Bondevik, S., Mangerud, J., Dawson, S., Dawson, A., Lohne, Ø. 2005. Evidence for three North Sea tsunamis at the Shetland Islands between 8000 and 1500 years ago, Quaternary Science Reviews, 24, 1757-1775.

Bronk Ramsey, C. 2008. Deposition models for chronological records. *Quaternary Science Reviews* 27(1-2), 42-60.

Bronk Ramsey, C. 2009a. Bayesian analysis of radiocarbon dates. *Radiocarbon, 51*, 1, 337-360.

Brugam, R.B., Mckeever, K. & Kolesa, L. 199. A diatom–inferred water depth reconstruction for an Upper Peninsula Michigan Lake. Journal of Paleolimnology 20: 267–276.

Buchwal A, Szczuciński W, Strzelecki M, Long AJ (2015) Tree-ring structure of *Salix glauca* reveals evidence of a 2000 AD tsunami event in west Greenland: implications for Arctic paleotsunami and paleoecological studies. Polish Polar Res 36: 51-65

Carmack, E., and R. W. MacDonald. 2002. Oceanography of the Canadian shelf of the Beaufort Sea: A setting for marine life, Arctic, 55, suppl. 1, 29 – 45.

Chague-Goff, C., Schneider, J-L., Goff, J.R., Dominey-Howes, D. & Strotz, L. 2011. Expanding the proxy toolkit to help identify past events: Lessons from the 2004 Indian Ocean Tsunami and the 2009 South Pacific Tsunami. Earth-Science Reviews 107, 107-122 - See more at: http://www.ansto.gov.au/ResearchHub/StaffProfiles/CHAGUE-GOFF-CATHERINE#sthash.WuX8n4FZ.dpuf

Cooper, J.A.G. & Jackson, D.W.T. (1999) Wave-spray deposits and processes during a coastal storm. Marine Geology, 161, 377-383.

Czernik J., Goslar T., 2001. Preparation of graphite targets in the Gliwice Radiocarbon Laboratory for AMS 14C dating. *Radiocarbon* 43, 283-291.

Dahl-Jensen, T., Larsen, L.M., Pedersen, S.A.S., Pedersen, J., Jepsen, H.F., Pedersen, G.K., Nielsen, T., Pedersen, A.K., Platen-Hallermund, F.V., Weng, W. 2004. Landslide and tsunami 21 November 200 in Paatuut, West Greenland. *Natural Hazards*, 31, 277-287.

Dawson, A.G., 1996. The geological significance of tsunamis. Zeitschrift f .ur Geomorphologie 102, 199–210

DMI. 2012. Danish Meteorological Institude. Illulissat tides. Retreived June 2012 [http://www.dmi.dk/en/groenland/]

Dura, T., Rubin, C.M., Kelsey, H.M., Horton, B.P., Hawkes, A., Vane, C.H., Daryono, M., Grand Pre, C., Ladinsky, T., Bradley, S. 2011. Stratigraphic record of Holocene coeseismic subsidence,

Padang, West Sumatra, Journal Geophysical Research 116, B11306, doi:10.1029/2011JB008205

Engel, M., & Bruckner, H. 2011. The identification of palaeo-tsunami deposits – a major challenge in coastal sedimentary research. Karius, Hadler, Deicke, von Eynatten, Brückner & Vött (eds.): Dynamische Küsten – Prozesse, Zusammenhänge und Auswirkungen Coastline Reports 17.

Escher A., Sørensen K., Zeck H.P. 1976. Nassugtoqidian mobile belt, West Greenland. In *Geology of Greenland*, Escher A, Watt S(eds). Geological Survey of Greenland: Copenhagen; 77–103.

Fatela, F. & Taborda, T. 2002. Confidence limits of species proportions in microfossil assemblages. Marine Micropaelontology 45(2), 169-174. DOI: 10.1016/S0377-8398(02)00021-X

Fredskild, B. 1996: A phytogeographical study of the vascular plants of West Greenland (62°20'-74°00'N). Meddelelser om Grønland, Bioscience 45, 157 pp

Fritz, H.M.F., & Mohammed, A., Yoo, J. 2009. Lituya Bay landslide impact generated mega-tsunami 50th anniversary. Pure App. Geophys. 166: 153-175

Garrett, E., Shennan, I., Watcham, E.P., Woodroffe, S.A. 2013. Reconstructing palaeoseismic deformation, 1: modern analogues from the 1960 and 2010 Chilean great earthquake. Quaternary Science Reviews, 75, 11-21.

Garrett, E., Shennan, I., Woodroffe, S.A., Cisternas, M., Hocking, E.P., Gulliver, P. 2014. Reconstructing paleoseismic deformation, 2: 1000 years of great earthquakes at Chucalen, south central Chile. Quaternary Science Reviews, 113, 112-122.

Gilks, W., Richardson, S., Spiegelhalter, D. (Eds.) 1996. Markov Chain Monte Carlo in Practice. Chapman & Hall, London.

Goto, K., Chague-Goff, C., Fujino, S., Goff, J., Jaffe, B., Nishimura, Y., Richmond, B., Suguwara, D., Szczucinksi, W., Tappin, D.R., Witter, R., Yulianto, E. 2011. New insights into tsunami risk from the 2011 Tohoku-oki event. *Marine Geology* 290: 46-50

Harbitz, C.B., Glimsdal., Lovholt, F., Kveldvik, V., Pedersen, G.K., Jensen, A. 2014. Rockslide tsunamis in complex fjords: From an unstable rock slope at Åkerneset to tsunami risk in western Norway. Coastal Engineering 88, 101-122.

Hartley B., Barber H.G., Carter J.R., Sims P.A. 1996. An Atlas of British Diatoms. Biopress, Bristol, England, 601 pp

Hemphill-Haley, E., 1996. Diatoms as an aid in identifying late-Holocene tsunami deposits. The Holocene 6 (4), 439–448.

Henriksen N., Higgins A.K., Kalsbeek F., *et al*. 2000. Greenland from Archaean to Quaternary: Descriptive Text to the Geological Map of Greenland 1:2,500,000. *Geology of Greenland Survey Bulletin* 185.

Hua, Q., Barbetti, M., & Rakowski, A. J. (2013). Atmospheric Radiocarbon for the Period 1950-2010. *Radiocarbon*, *55*(4).

Jankaew, K., Atwater, B.F., Sawai, Y., Choowong, M., Charoentitirat, T., Martin, M.E., Prendergast, A. 2008. Medieval forewarning of the 2004 Indian Ocean tsunami in Thailand 455, 1228-1231. doi:10.1038/nature07373.

Juggins, S. (2011) C^2 Version 1.6: Software for Ecological and Palaeoecological Data Analysis and Visualisation: Department of Geography, University of Newcastle, Newcastle upon Tyne, U.K.

Kelsey, H.M., Nelson, A.R., Hemphill-Haley, E. & Witter, R.C. 2005. Tsunami history of an Oregon coastal lake reveals a 4600 yr record of great earthquakes on the Cascadia subduction zone, 117(7-8), 1009-1032, doi: 10.1130/B25452.1.

Kokociński, M., Szczuciński, W., Zgrundo, A., Ibragimow A., 2009. Diatom assemblages in 26 December 2004 tsunami deposits from coastal zone of Thailand as sediment provenance indicators. Polish Journal of Environmental Studies 18, 93-10

Larsen J.G., Pulvertraft T.C.R. 2000. The structure of the Cretaceous/Palaeogene sedimentary-volcanic area of Svartenhuk Halvø, central West Greenland. *Geology of Greenland Survey Bulletin* 188.

Long, A.J., Roberts, D.H., Wright, M.R. 1999. Isolation basin stratigraphy and Holocene relative sea-level change on Avreprinsen Eijland, Disko Bugt, West Greenland, Journal of Quaternary Science, 14, 4, 323-345.

Long, A.J., Woodroffe, S.A., Roberts, D.H., Dawson, S. 2011. Isolation basins, sea-level changes and the Holocene history of the Greenland Ice Sheet, Quaternary Science Reviews, 30, 3748-3768.

Lovejoy, C., L. Legendre, and N. M. Price. 2002. Prolonged diatom blooms and microbial food web dynamics: experimental results from an Arctic polynya. Aquat. Microb. Ecol. 29:267-278

Lovejoy, C., Massana, R., Pedros-Alio, C. 2006. Diversity and distribution of marine microbial eukaryotes in the Arctic Ocean and adjacent seas. Applied Environmental Microbiology 72, 5, 3085-3095.

Matsumoto, D., H. Naruse, S. Fujino, A. Surphawajruksakul, T. Jarupongsakul, N. Sakakura & M. Murayama. 2008. Truncated flame structures within a deposit of the Indian Ocean Tsunami: evidence of synsedimentary deformation. Sedimentology 55: 1559–1570.

Miller, D.J. 1960. Giant Waves in Lituya Bay, Alaska, *Geological Survey Professional Paper 345-C, US Government Printing Office*, Washington.

Monecke, K., Finger, W., Klarer, D., Kongko, W., McAdoo, B.G., Moore, L.A., Sudrajat, S.U. 2008. A 1,000-year sediment record of tsunami recurrence in northern Sumatra. Nature 455, 1232-1234

Morton, R.A., Gelfenbaum, G. & Jaffe, B.E. 2007. Physical criteria for distinguishing sandy tsunami and storm deposits using modern examples. Sedimentary Geology 200, 184–207.

Nelson, A.R., Shennan, I., Long, A.J. 1996. Identifying coseismic subsidence in tidal-wetland stratigraphic sequences at the Cascadia subduction zone of western North America. *Journal of Geophysical Research* 101(B3), 6115-6135.

Pedersen, S.A.S., Larsen, L.M., Dahl-Jensen, T., Jepsen, H.F., Pedersen, G.P., Nielsen, T., Pedersen, A.K., Platen-Hallermund, F.V., Weng, W. 2002. Tsunami-generating rock fall and landslide on the south coast of Nuussuaq, central West Greenland. *Geology of Greenland Survey Bulletin* **191**, 73-83.

Pennington, W., Tutin, T.G., Cambray, R.S., Fisher, E.M. 1973. Observations on Lake sediments using fallout 137Cs as a tracer. Nature 242, 324 – 326. doi:10.1038/242324a0

Perner, K., Moros, M., Snowball, I., Lloyd, J.M., Kuijpers, A., Richter, T. 2013. Establishment of modern circulation pattern at *c*. 6000 cal a BP in Disko Bugt, central West Greenland: opening of the Vaigat Strait. J. Quaternary Sci., 28: 480–489. doi: 10.1002/jqs.2638

Peters, R. & Jaffe, B.E., 2010. Identification of tsunami deposits in the geologic record; developing criteria using recent tsunami deposits: U.S. Geological Survey Open-File Report 2010-1239, 39 p. [http://pubs.usgs.gov/of/2010/1239/].

Reimer, P.J., Bard, E., Bayliss, A., Beck, J.W., Blackwell, P.G., Bronk Ramsey, C., Buck, C.E., Cheng, H., Edwards, R.L., Friedrich, M., Grootes, P.M., Guilderson, T.P., Haflidason, H., Hajdas, I., Hatte, C., Heaton, T.J., Hoffman, D.L., Hogg, A.G., Hughen, K.A., Kaiser, K.F., Kromer, B., Manning, S.W., Niu, M., Reimer, R.W., Richards, D.A., Scott, E.M., Southon, J.R., Staff, R.A., Turney, C.S.M., van der Plicty, J. 2013. Intcal13 and Marine13 radiocarbon age calibration curves 0-50,000 years cal BP. *Radiocabon* 55(4) 1669-1667.

Richmond, B.M., B.E. Jaffe, G. Gelfenbaum & R.A. Morton. 2006. Geologic Impacts of the 2004 Indian Ocean Tsunami on Indonesia, Sri Lanka, and the Maldives. In: Zeitschrift für Geomorphologie, Suppl. Vol. 146: 235–251.

Romundset, A., Bondevik, S., 2011. Propagation of the Storegga tsunami into ice-free lakes along the southern shores of the Barents Sea. *Journal of Quaternary Science* 26, 457-462.

Sha, L., Hui, J., Marit-Solveig, S., Olsen, K.L., Kuijpers, J., Liu, A.Y. 2014. A diatom-based sea-ice reconstruction for the Vaigat Strait (Disko Bugt, West Greenland) over the last 5000yr. *Palaeogeography, Palaeoclimatology, Palaeoecology*, 403, 66-79.

Shennan, I., Barlow, N., Carver, G., Davies, F., Garrett, E., Hocking, E. 2014. Great tsunamigenic earthquakes during the past 1000 yr on the Alaska megathrust, Geology, doi:10.1130/G35797.1

Sherrod, B.L., 2001. Evidence for earthquake-induced subsidence about 1100 yr ago in coastal marshes of southern Puget Sound, Washington. Geol. Soc. Am. Bull. 113 (10), 1299e1311.

Sieh, K., Daly, P., McKinnon, E.E., Pilarczyk, J.E., Chiang, H-W., Horton, B., Rubin, C., Shen, C-C., Ismail., N., Vane, C., Feener, R.M. 2015. Penultimate predecessors of the 2004 Indian Ocean tsunami in Aceh, Sumatra: Stratigraphic, archeological, and historical evidence. Journal of Geophysical Research: Solid Earth,120, 1, 308–325.

Solheim, A., Berg, K., Forsberg, C.F., Bryn, P., 2005. The Storegga Slide Complex: repetitive large scale sliding with similar cause and development. Marine and Petroleum Geology, 22 doi:10.1016/j.marpetgeo.2004.10.013.

Srisutam, C. & F.-F. Wagner (2010): Tsunami sediment characteristics at the Thai Andaman coast. In: Pure and Applied Geophysics 167: 215–232.

Strzelecki, M.C. 2012. 2012. High Arctic Paraglacial Coastal Evolution in Northern Billefjorden, Svalbard, Durham theses, Durham University. Available at Durham E-Theses Online: http://etheses.dur.ac.uk/7363/

Strzelecki, M.C. and Long, A.J. and Lloyd, J.M. (in press). Post-Little Ice Age development of a High Arctic paraglacial beach complex. *Permafrost and periglacial processes.*

Szczucinksi, W., Chaimanee, N., Niedzielski, P., Rachlewicz, G., Saisuttichai, D., Tepsuwan, T., Lorenc, S., Siepak, J. 2006. Environmental and geological impacts of the 26 December 2004 tsunami in coastal zone of Thailand – overview of short and long-term effects. *Polish Journal of Environmental Studies* 15(5): 793-810.

Szczucinski, W. 2012. The post-depositional changes of the onshore 2004 tsunami deposits on the Andaman Sea coast of Thailand. *Natural Hazards 60, 115-133.*

Troels-Smith, J. 1955. Karakterisering af lose jordarter.Characterisation of unconsolidated sediments, *Geological Survey of Denmark*, 4, 3, 1-73.

Vos, P.C., de Wolf, H. 1988. Methodological aspects of paleoecological diatom research in coastal areas of the Netherlands. *Geol en Mijnb* 67: 31-40

Vos, P.C., de Wolf, H. 1993. Diatoms as a tool for reconstructing sedimentary environments in coastal wetlands; methodological aspects. Hydrobiol 267/270: 285-296

Wagner B., Bennike O., Klug M., Cremer H. 2007. First indication of Storegga tsunami deposits from East Greenland. J Quat Sci 22: 321-325

Appendix 2

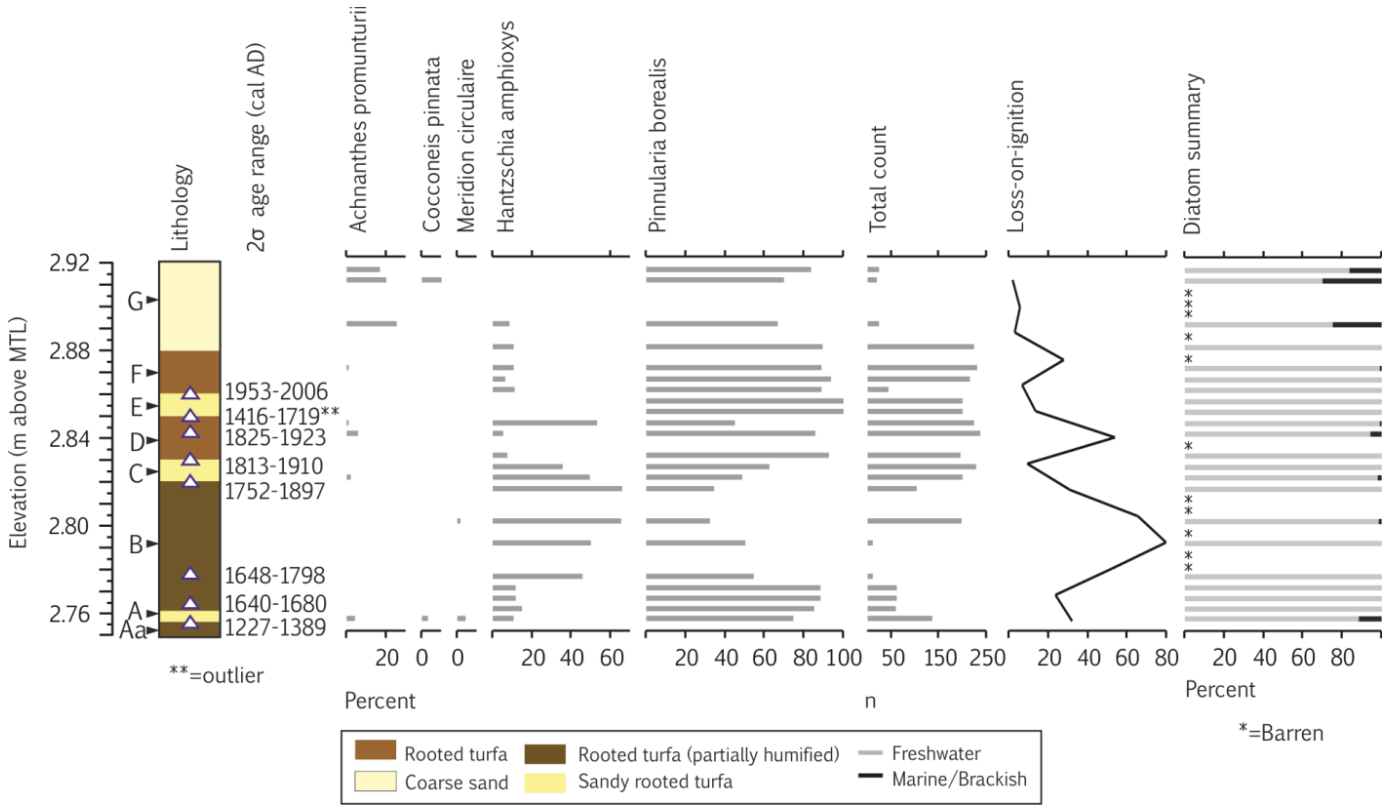

Figure S1. Diatoms, dating and loss-on-ignition of Pit 4 from the fjord-side of Sandstone Point. Diatom contributions represent >10%. Note that ages presented are 2σ posterior (modelled) ages, except for one outlying age in Pit 4 which is presented as a 2σ unmodelled range (two asterisks). Single asterisk = barren of diatoms.

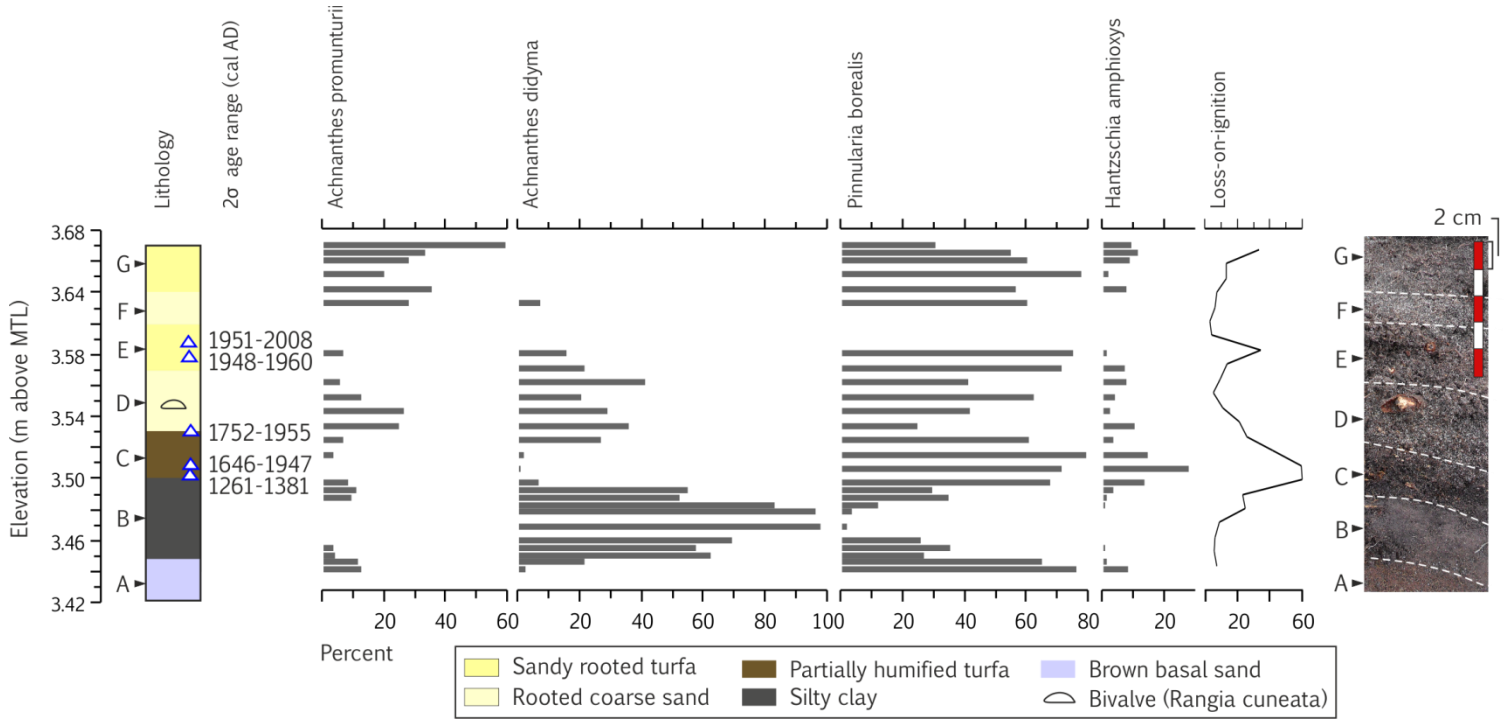

Figure S2. Diatoms, dating and loss-on-ignition of Exposure 11 from the lee-side of Sandstone Point. Diatom contributions represent >10%. Presented age ranges are 2σ posterior (modelled) ages.

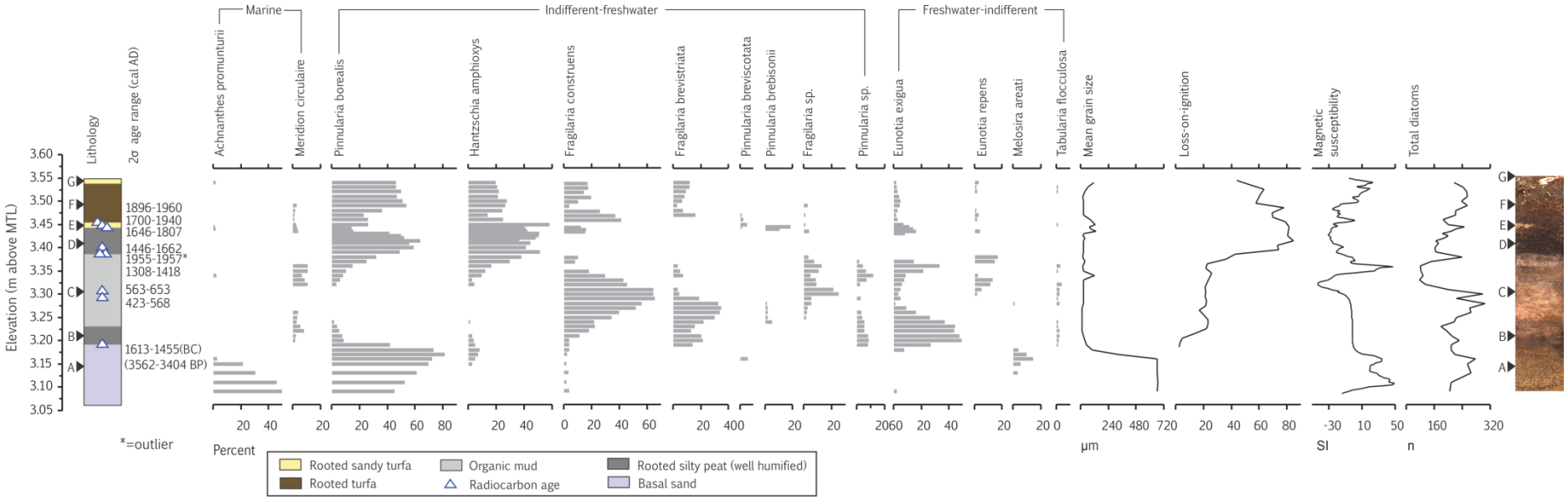

Figure S3. Diatoms, sediment properties and dating of Exposure O from Moss Cliff. Diatom contributions represent >10%. Note that ages presented are 2σ posterior (modelled) ages, except for one outlying age which is presented as a 2σ unmodelled range (asterisk).

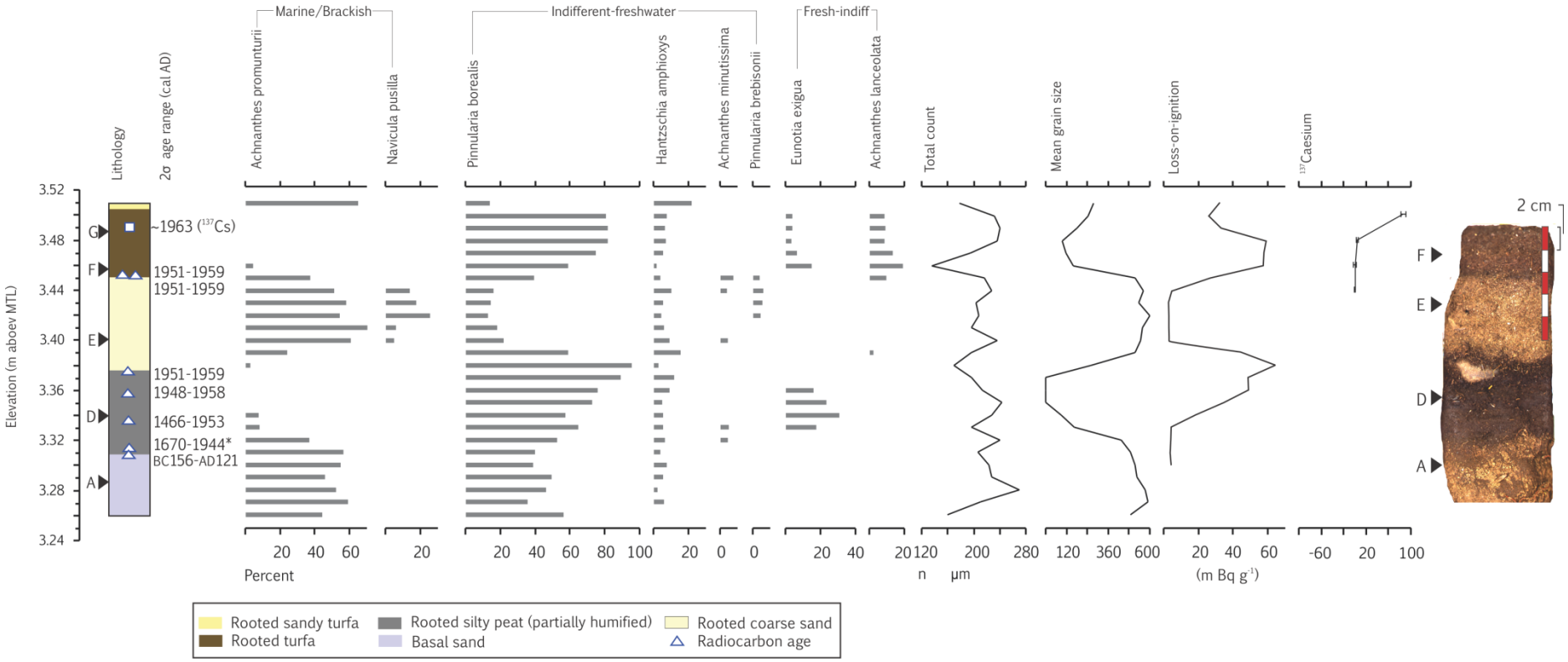

Figure S4. Diatoms, sediment properties and dating of Exposure J from Moss Cliff. Diatom contributions represent >10%. Note that ages presented are 2σ posterior (modelled) ages, except for one outlying age which is presented as a 2σ unmodelled range (asterisk).

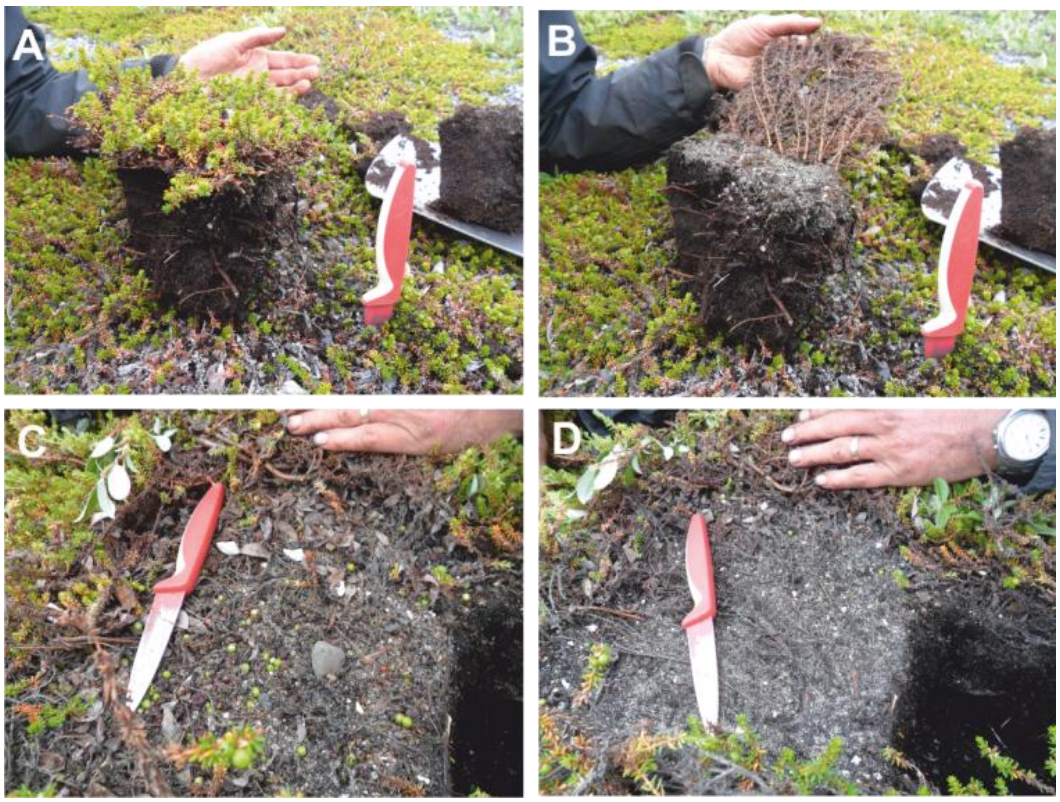

Figure S5. Excavation of the coastal lowland and living *Empetrum nigrum* surface near Sandstone Point. a, Hand-dug pit revealing *E. nigrum* in growth position and thickly-rooted underlying peat. **b,** Removal of *E. nigrum* surface reveals AD 2000 tsunami deposit comprising sands and gravels that have not been worked into underlying soil by thick *E. nigrum* rhizomes. In this example, *E. nigrum* has rooted surrounding soil. **c,** Second example AD 2000 tsunami deposit, following removal of *E. nigrum* surface. **d,** Removal of the AD 2000 tsunami deposit reveals flattened pre-tsunami E. nigrum rhizomes.

4

Arctic coastal lake yields a c. 2350 yr history of landslide-tsunamis, Vaigat, west Greenland

This chapter is in review for the journal *Journal of Quaternary Science*, in a paper titled "*Greenland coastal lake records evidence of late Holocene tsunami, Vaigat, West Greenland*". I am the lead author. It is co-authored by Antony Long of Durham University and Witold Szczuciński of Poznan University.

1. Introduction

Reconstructions of Arctic coastal evolution and relative sea-level (RSL) change have focused almost exclusively on gradual changes that operate on millennial and centennial timescales (e.g. Corner et al., 1999; Eronen, 1983; Ten Brink and Weidick, 1975; Long et al., 1999; Rasch, 2000; Romundset et al., 2010). Few studies have analysed the role and impact of short-term (minutes-hours) abrupt events in shaping coastal evolution, despite the presence of potent sources of abrupt change in these areas, including landslide- and iceberg-generated tsunami (e.g. Miller, 1960; Wagner et al., 2007; Long et al., 2011; Leonard et al., 2013). In Greenland, knowledge of this is important given that population, industry and infrastructure are situated almost exclusively in coastal settings.

Two key questions are whether multi-event sequences of abrupt change can be successfully reconstructed from Arctic coastal environments, as they have been from lower latitude settings (e.g. Atwater and Hemphill-Haley, 1997; Hutchinson et al., 1997; 2000; Jankaew et al., 2008; Kelsey et al., 2008, Nanayama et al., 2003), and whether this information can be used as a basis for Arctic coastal hazard assessment. The best-documented records of Arctic tsunami inundation are from coastal lake and nearshore sedimentary sequences in Greenland and Norway (Wagner et al., 2007; Romundset and Bondevik, 2011). These studies were successful in documenting the timing and magnitude of one notable event; the early Holocene Storegga tsunami (e.g. Bondevik et al., 2007; Dawson et al., 1998). However, it is unclear whether Arctic coastal environments can be used to reconstruct multi-event sequences of tsunamis over century to millennial timescales.

The Vaigat Strait in west Greenland is an exit route for many of the calved icebergs and meltwater from the western portion of the Greenland Ice Sheet (Andresen et al., 2011). The central ~80 km-long stretch of the strait has high landslide-generated tsunami risk, enhanced by the unstable geological configuration of the northern shoreline – the Nuussuaq Peninsula. Geomorphological mapping of landslide back-scars in this area has identified c. 20 former large mass-movements of the Holocene, with at least four of these extending into the fjord itself and providing potential tsunami sources (Pedersen et al., 2002). These mass movement events are likely younger than 5000-4000 cal a BP because of a general absence of raised beaches on the north shoreline, which have presumably been destroyed by landslides and palaeotsunami (Pedersen et al., 2002). The landslides post-date c. 5000 cal a BP because RSL was falling in the early- to mid-Holocene in east Disko Bugt and intersected present day levels at c. 5000 cal a BP (Long et al., 1999; 2011). Pedersen et al. (2002) estimate that there is an average frequency of ~1 tsunami event per thousand years,

which could be higher if older landslides have been reworked by younger landslides. Consequently, the area is an ideal testing ground to study multiple episodes of abrupt coastal forcing in the Arctic.

Local testimony, geomorphological mapping of landslide deposits and seismic monitoring have been used to interpret a large rock avalanche and landslide (c. 90 million m^3) at Paatuut at 18:04 local time, 21 November AD 2000 (Pedersen et al., 2002; Dahl-Jensen et al., 2004). A resultant tsunami extended ~25 km across-fjord and at least ~25 km longitudinally up-fjord to the village of Saqqaq (Fig. 4.1). This event provides a direct analogue for interpreting past events, in the same way that, for example, the AD 1964 Alaskan-Aleutian megathrust earthquake has provided a historical baseline for interpreting past events (e.g. Plafker, 1965). Directly opposite the Paatuut slide, ~25 km away at the abandoned coal-mining town of Qullissat (Fig 4.1), the majority of buildings below 30 m above sea-level were completely destroyed, as were Eskimo burial sites that suggest that the event was the largest of the past several hundred years (Dahl-Jensen et al., 2004). Moreover, in AD 1952, the town was hit by a smaller tsunami that "caused some material damage and the loss of one life" (Dahl-Jensen et al., 2004; p. 286).

Of particular interest is whether the Vaigat landslides are random, isolated events, or whether they are a result of external forcing. One hypothesis is that repeated freeze-thaw occurring in quick succession (i.e. multiple cycles over a short period of days-weeks-months) could cause slope failure (Dahl-Jensen et al., 2004). An alternative hypothesis is that these events could be controlled by longer-term (decadal-centennial scale) climate change, in particular by changes in temperature and precipitation. For example, meteorological data from Qeqertarsuaq on the south of Disko Island (Fig. 4.1) indicates that AD 2000 was an exceptionally warm year, with rainfall the highest since AD 1990 (Hansen et al., 2006). In Vaigat, dendrochronological analysis of a specimen of the dwarf shrub *Salix glauca* identified an injury to the AD 2000 growth ring, likely a result of solifluction due to exceptional seasonal rainfall (Buchwal et al., 2015).

Here we reconstruct the minimum frequency and magnitude of tsunami events in the Vaigat Strait, west Greenland, to provide the first multi-event record of tsunami inundation from an Arctic environment. Our reconstruction is based on stratigraphic data collected from a coastal freshwater lake situated 5 m above present day sea level on the north shore of Disko island, opposite the landslide-prone slopes of the Nuussuaq Peninsula. To elucidate potential linkages between the frequency of events and climate fluctuations, we compare the timing of tsunami events to a well-resolved, air temperature record for the past 150 years

from nearby Ilulissat (Vinther et al., 2006) and to the GISP2 ice core oxygen isotope series (Grootes et al., 1997; Meese et al., 1994) to extend our comparison back into the late Holocene.

2. Site description

The Vaigat Strait is located in northwest Disko Bugt between 69°52'N, 51°58'W and 70°24'N, 54°18'W (Fig. 4.1). The fjord is ~25 km wide and on average 300 m deep (Andersen, 1981). Seasonal sea-ice cover in the strait is between January and May, comparable with the conditions observed in wider Disko Bugt (Mosbech et al., 2000). The bedrock geology of east Disko Bugt is characterized by Precambrian orthogneisses and granites (Escher et al., 1976; Larsen and Pulvertraft, 2000) while Disko Island and the western extent of Nuussuaq is comprised mostly of Palaeogene basalt formations, with underlying outcrops of Cretaceous clastic sediments including intercalated mudstones, sandstones and coal seams (Henriksen et al., 2000). It is this latter configuration that has a propensity for slope failure (Pedersen et al., 2002). On the northern coast of Disko Island, raised beaches, well-vegetated slopes and a small number of freshwater lakes indicate that this area has been comparatively stable for much of the Holocene. Nevertheless, there is evidence for slope instability associated with rotational slides, debris flows and rock glaciers.

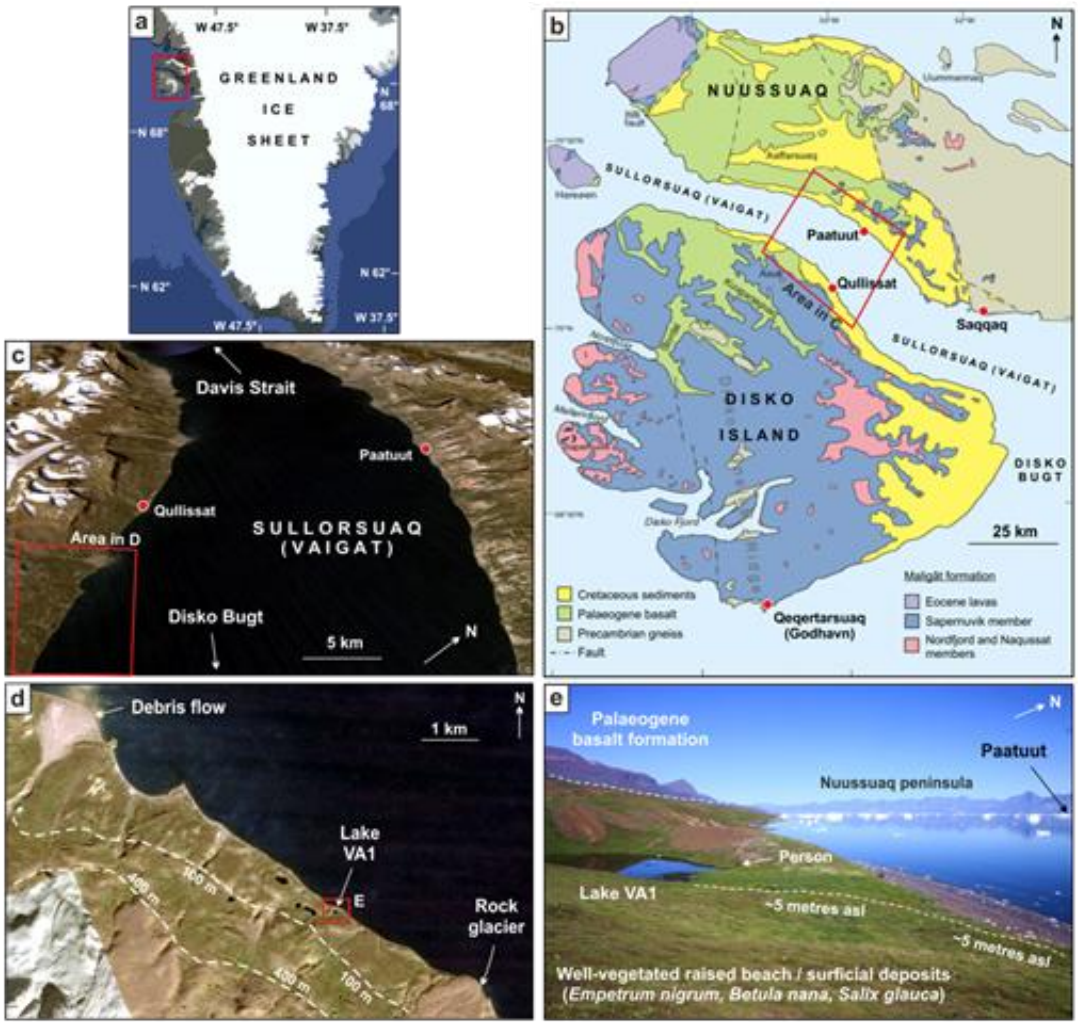

Figure 4.1. (a) Location of the study area within Greenland. Red rectangle marks location of (b); (b) Geological setting of Disko Island and the Nuussuaq peninsula adapted from Larsen and Pedersen (2009). (c) Oblique view of the Vaigat Strait looking northwest (Google Earth model). (d) Google Earth image of northern coast of Disko Island and location of VA1. (e) Overview of study site VA1 (looking northwest). asl = above sea level.

Our study site is a freshwater coastal lake (c. 60 x 30 m, unofficially named: Lake VA1) located in a small rock-bound depression on the northern coast of Disko Island, about 10 km southeast of Qullissat (Figs. 4.1 and 4.2). It is the only low-lying (<10 m above sea level) coastal lake situated throughout the entire Vaigat Strait. A peat-covered raised beach separates the lake from the sea (~50 m horizontal distance) and gradually flattens eastward onto a narrow strip of coastal plain that has a well-vegetated living surface of *Empetrum nigrum* and dwarf shrubs *Salix glauca* and *Betula nana*. The raised beach protects the lake from storm overwash; wave set-up and fetch is limited and the lake is only slightly exposed to the sea and prevailing northerlies at its northeastern extent. The basin sill of VA1 is 5.0 ± 0.1 m above mean tide level (MTL), while the mean spring tidal range in the area is 2.5 m. These factors place the lake beyond the present range of inundation by storm events. Because of the lower position of RSL in the late Holocene, the probability of storm overwash during this time is further reduced.

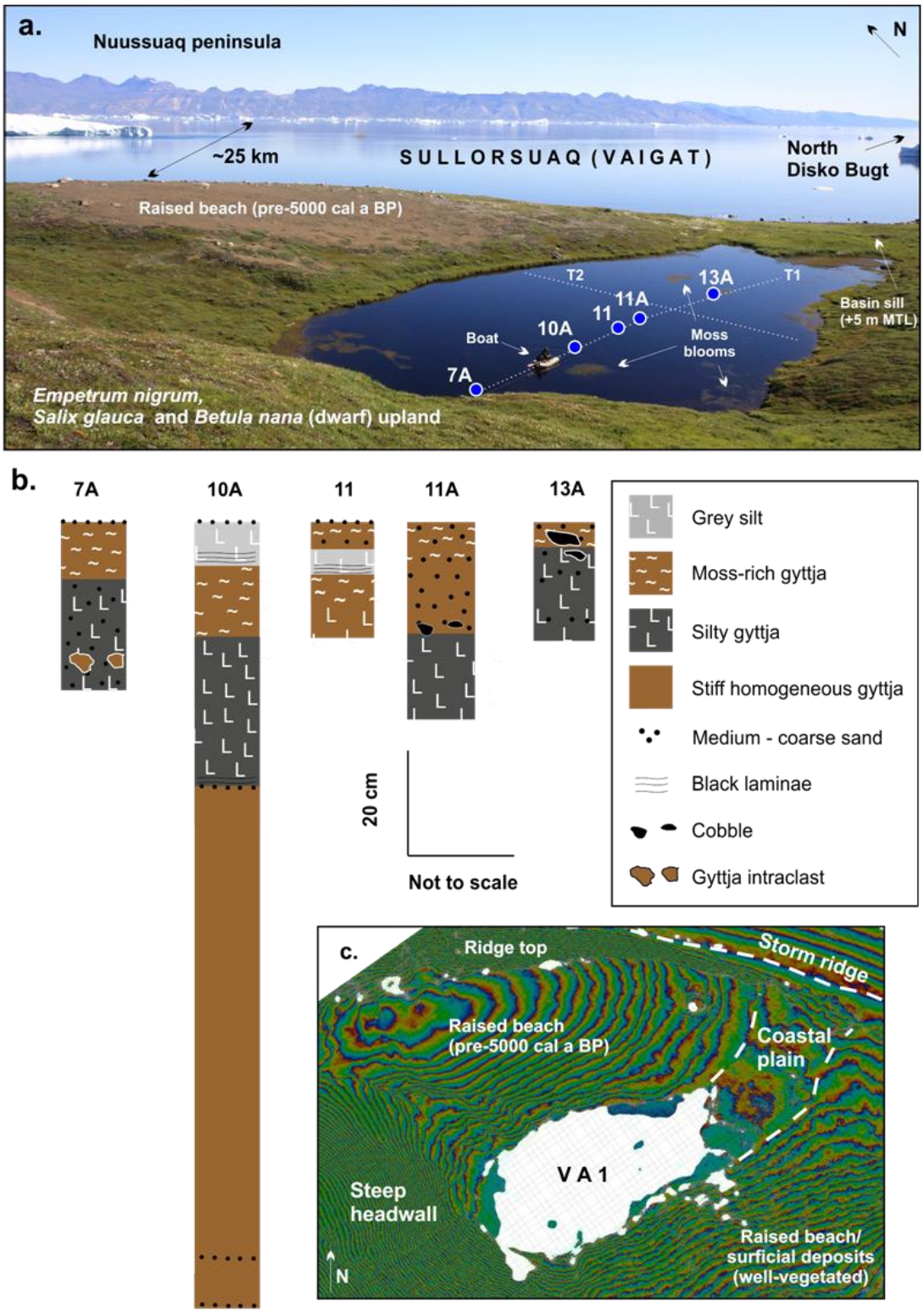

Figure 4.2. (a) The setting of VA1 on the north coast of Disko Island with marked locations of the discussed sediment cores. T1 and T2 stand for the investigated coring transects (b) Simplified stratigraphy of cores sampled along transect 1 (T1), normalized to depth below sediment surface. (c) Elevation of the area in (a) based on terrestrial laser scanning survey. Each colour fringe is 0.5 m (courtesy of N. Rosser).

Despite protection from storms, Lake VA1 has significant potential to harbour evidence of larger waves associated with past tsunami events. Evidence of tsunami inundation (tsunami deposits, erosional and depositional landforms, shrub tree-rings) associated with the most recent AD 2000 event is spatially widespread between the site and Qullissat (Buchwal et al. 2015). Proximal to the lake, significant erosion of the terrestrial surface likely due to the AD 2000 tsunami is indicated by isolated blocks of peat (>0.5 m) that have been torn from the land surface and redeposited close by (Fig. 4.3), as well as by the barren top of the raised beach (Figure 4.2). The narrow strip of low-lying coastal plain between the lake and shoreline (Figure 4.2c and 'basin sill' on Figure 4.2a) is partly covered with AD 2000 tsunami deposits composed of poorly sorted sandy gravel to gravelly sand up to 15 cm thick (Fig. 4.3). Isolated cobbles and rounded boulders up to 45 cm in diameter are also present in front of the lake. Adjacent to the seaward lake shores there are 2 to 4 cm-thick tsunami deposits (Fig. 4.3). There is no clear evidence of tsunami deposits on the relatively steep slopes surrounding the lake and the coastal plain. However, it is possible that they have been redeposited by snowmelt streams. The barren top of the raised beach, if associated with tsunami erosion in AD 2000, provides a maximum minimum vertical run-up estimate of ~11 m above MTL. Inundation by the AD 2000 tsunami into the lake is therefore highly probable and presents an excellent opportunity to constrain a modern analogue for interpreting past events.

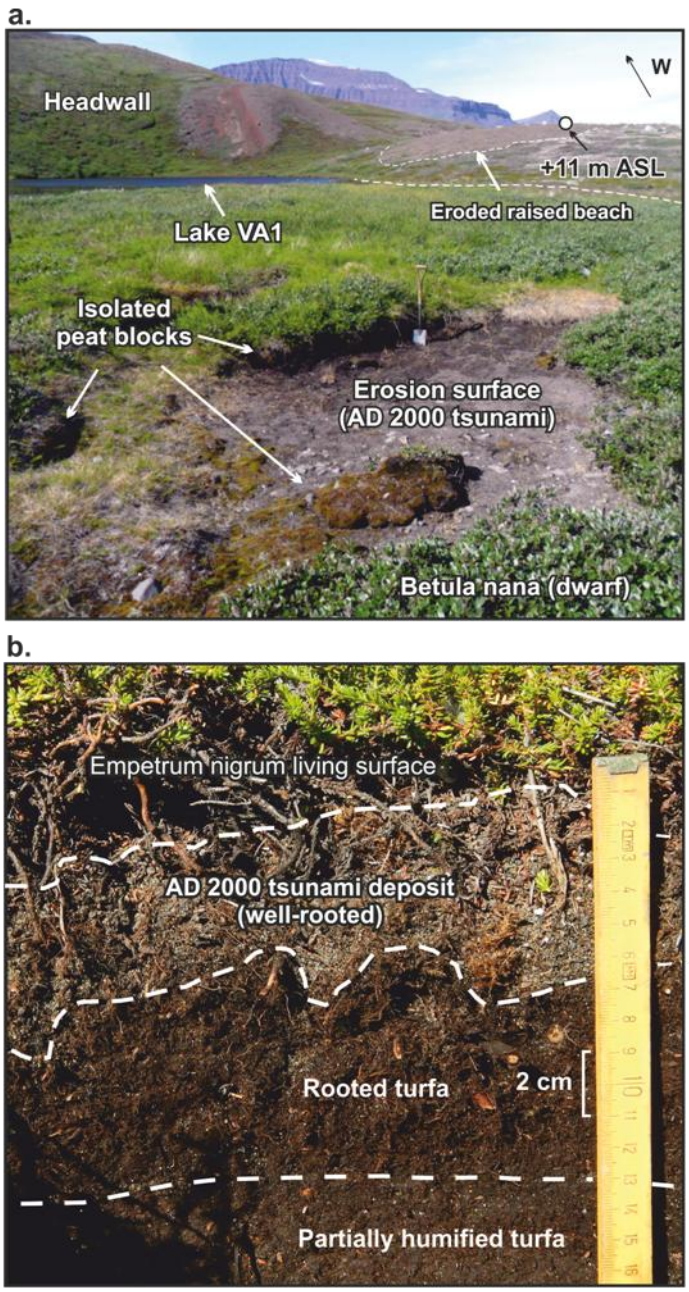

Figure 4.3. (a) Evidence of erosion of the narrow strip of low-lying coastal plain and raised beach vegetation by the AD 2000 tsunami. (b) Typical example of terrestrial stratigraphy of the coastal plain, with the AD 2000 tsunami deposit unconformably overlying turfa peat and recolonization of *Empetrum nigrum* on top of the AD 2000 tsunami sands and gravels.

3. Materials and methods

3.1 Field survey

We mapped the stratigraphy of VA1 along two transects and sampled using a Russian corer from a small inflatable boat tethered to the lake shore (Fig. 4.2). Samples were stored in plastic tubes and made airtight before shipping (by sea), upon being cold stored at 4°C on arrival at Durham ~1 month later. The elevation of the lake basin (the 'basin sill') was determined using a Sokkisha level with reference to mean high water of spring tides (MHWST) at the site, subsequently reduced to MTL at Ilulissat with tide tables (DMI, 2012).

3.2 Biostratigraphic and sedimentological techniques

Samples for diatom analysis were prepared using standard techniques (Palmer and Abbott, 1986), identified with reference to Hartley (1996) and grouped according to a simplified halobian classification scheme of Vos and de Wolf (1993). We analysed samples for diatoms to determine the environmental provenance of anomalous stratigraphic units (i.e. coarse sand horizons that might be indicative of tsunami inundation). Diatom diversity was relatively low for a lacustrine setting, with 28 taxa identified. A minimum count of 200 valves was made per sample, with frequencies expressed as a percentage of the total diatom count (%TDC). The count included broken valves where more than half a valve can be identified. Marine taxa were present in exceptionally low abundances so the entire slide (2 x coverslips) was scanned once the count had reached 200 to maximise their chance of recovery. This was important as the identification of even low frequencies of marine taxa provides objective evidence for tsunami inundation in an otherwise freshwater setting. These low frequency occurrences of marine taxa are expressed as raw counts per two coverslips. Sampling resolution varied from 0.25 cm to 4 cm.

Sediment property changes within the basin stratigraphy were determined by measuring grain-size (GS) and the magnetic susceptibility (MS). GS analysis was conducted using a Coulter laser analyser with sampling resolutions that mimicked that of diatoms. Sediment blocks (~0.5 cm^3) were pre-treated with a 30% solution of H_2O_2 and placed in a water bath for 5 hours at 85°C to remove organic matter. If organic material remained, the process was repeated with a second solution of 30% H_2O_2. Centrifuged solutions were discarded and remaining sediment was topped up with water in preparation for laser GS

analysis. MS measurements were conducted at 0.2 cm resolution using a GeoTek core scanner. X-ray radiographs were obtained from Royal Victoria Infirmary, Newcastle upon Tyne, in order to aid the identification of sedimentary structures.

3.3 Age control

Our chronology is based on Accelerator Mass Spectrometry (AMS) ^{14}C, ^{137}Cs and ^{210}Pb dating techniques. AMS ^{14}C ages were used to develop a model in the radiocarbon age modelling software OxCal 4.2 (Bronk Ramsey, 2009a). The *P_sequence* function generates a Poisson deposition model that allows for random fluctuations in accumulation rate (Bronk Ramsey, 2008). The model compares the stratigraphic position and probability distributions of each ^{14}C sample in a prior model before building posterior (modelled) densities for each point using Bayesian algorithms and Monte Carlo Markov Chain analysis (Gilks et al., 2006). The Agreement Index (AI) provides a measure of overlap between the prior and posterior models, with AIs >60% the accepted threshold (Bronk Ramsey, 2008). Measurements of ^{137}Cs act as a marker for sediments younger than c. AD 1952 because of atmospheric fallout of the radionuclide following nuclear weapons testing (e.g. Pennington et al., 1973). ^{210}Pb is a natural radionuclide and is used to date sediments ~100 years old (e.g. Robbins and Edgington, 1975).

AMS ^{14}C analyses were conducted at the Poznań Radiocarbon Laboratory in Poznań, Poland. We mostly dated allochtonous, short-lived plant macrofossils of *Betula nana* and *Empetrum nigrum* that were intact and away from the core edges (Table 4.1). All ^{14}C samples were pre-treated using standard methods (Czernik and Goslar, 2001). The ^{14}C ages were calibrated using the computer software OxCal 4.2 (Bronk Ramsey, 2009a) with the IntCal13 calibration curve (Reimer et al., 2013). Calibrated ages are given as two standard deviations (2σ).

^{137}Cs and ^{210}Pb analyses were conducted for upper parts of cores 10A and 11 on contiguous 3 to 4 cm samples that were dried and homogenized. Activities were measured using a well-type gamma spectrometer with a counting time of 6-8 days following equilibration of the samples for 7 days. The linear sediment accumulation rate was determined from the excess ^{210}Pb activities that decreased below the surface, using the model of Robbins and Edgington (1975).

4. Results

4.1 Lithostratigraphy, sediment properties and diatom content

The margins of Lake VA1 are shallow (~1 m) but water depths increase towards the centre (~2.5 m). Large moss blooms (*Calliergon scorpidium drepanocladus*) grow to the water surface in patches (Fig. 4.2). We sampled to impenetrable substrate in all cores, although the basal sediment in core 10A was difficult to penetrate and it is not certain whether total depth (i.e. solid substrate) was reached. The sediment package is relatively thin (average ~0.4 m) apart from in the central deepest portion of the lake where there is a complex ~1.5 m-thick sediment suite (core 10A). We analysed five cores from the lake, selecting core 10A as our main core for dating (Table 4.1). Cores from the shallower margins are more disturbed with greater components of coarse angular material that have likely been sourced from the adjacent bank and slopes.

Table 4.1. AMS radiocarbon dates in this study (core 10A). Ages are calibrated with the IntCal13 calibration curve (Reimer et al. 2013) in OxCal 4.2 (Bronk Ramsey, 2008),

Sample code	Lab code	Min depth (cm)	Mid depth (cm)	Max depth (cm)	Species	^{14}C age	^{14}C error (1σ)	Cal age (2σ)	Posterior (modelled) age (2σ)	Agreement Index (AI) %
VA1/10 a-1	Poz-57627	25.5	25.75	26	Betula nana, Empetrum nigrum	390	70	529 - 305	534 - 305	100
VA1/10 a-2	Poz-57628	58.5	58.75	59	Betula nana, Empetrum nigrum	960	35	933 - 792	953 - 801	98
VA1/10 a-4	Poz-57629	104.5	104.75	105	Betula nana, Empetrum nigrum	1290	25	1285 - 1181	1271 - 1175	99
VA1/10 a-5	Poz-57631	150.25	150.5	150.75	Betula nana, Empetrum nigrum	1665	30	1668 - 1454	1696 - 1536	74
VA1/10 a-1a	Poz-53408	158.25	158.5	158.75	Calliergon scorpidium drepanocladus	2240	35	2341 - 2153	2338 - 2149	100

4.1.2 Core 7A

Core 7A comprises a lower unit of brown coarse sandy gyttja between 30 and 10 cm that is overlain by an upper unit of moss-rich gyttja with some sand that extends to surface (Fig. 4a). The lower unit contains a high fine to medium sand component, comprising 50-70% of the sediment matrix, while the upper unit contains only minor sand contributions (2-5%). Major changes in MS are coupled to mean GS, with a large fluctuation in both occurring in the basal 20 cm. X-ray analysis reveals two intraclasts of homogeneous gyttja at 25 cm. Diatom content reveals an overall decline of *Fragilaria construens* var. *venter* from 40 to 10% TDC, and an increase in *Achnanthes sonyda* from 10 to 60% TDC. The top of the sequence is capped by a single grain-thick layer of medium sand that contains a few specimens of the polyhalobous taxon *Achnanthes promunturii*. Occasional specimens of this taxon are also present in the basal 5 cm of the core.

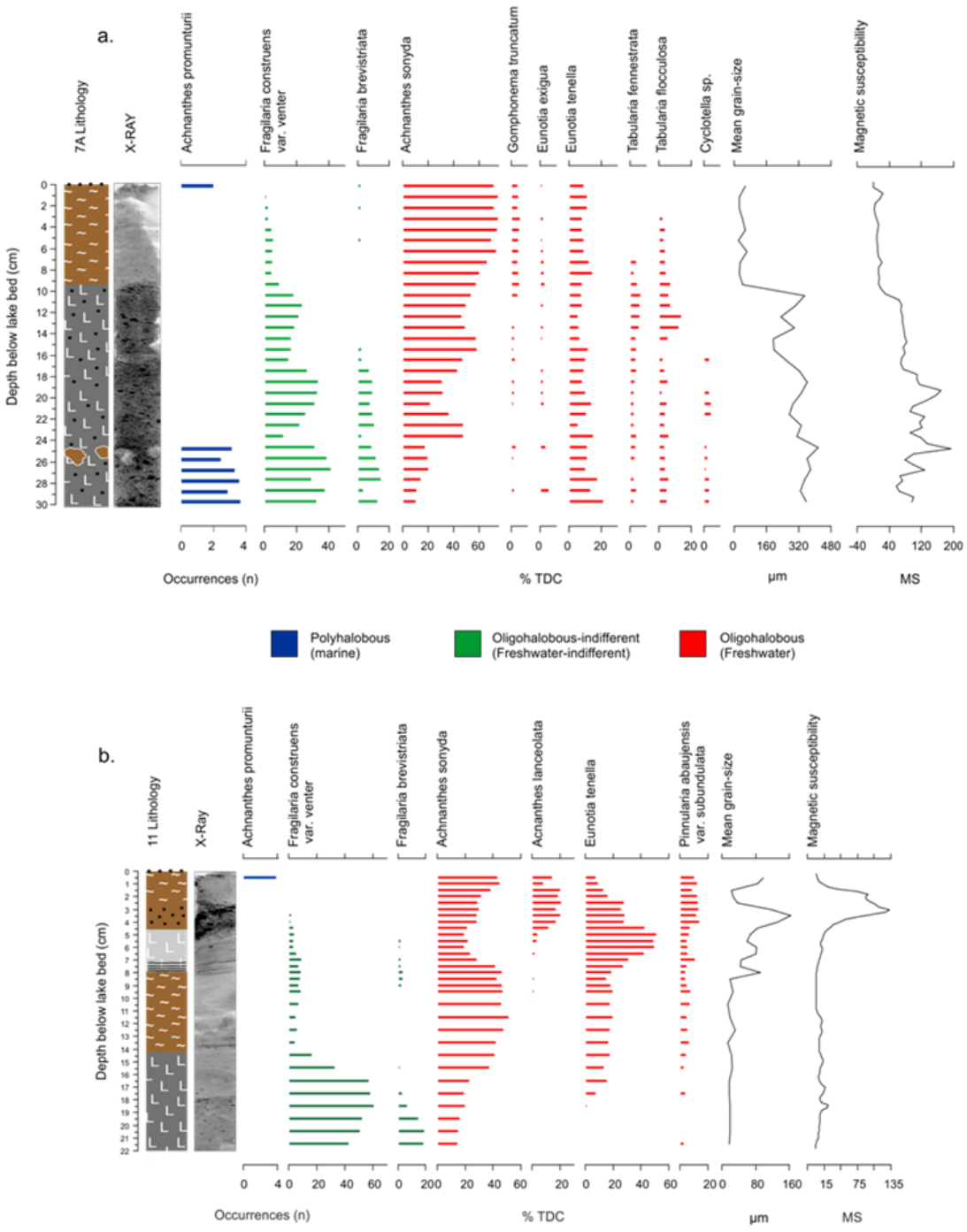

Figure 4.4. Lithology, x-ray, biostratigraphy and sediment properties of core 7A (a), core 11 (b), core 11A (c) and core 13A (d). Diatoms are colour coded based on their salinity preferences (key in between a and b). Only key taxa comprising >5% of the total count are shown, except for polyhalobous taxa which are presented in number of occurrences. For the lithology legend, see Fig. 4.2.

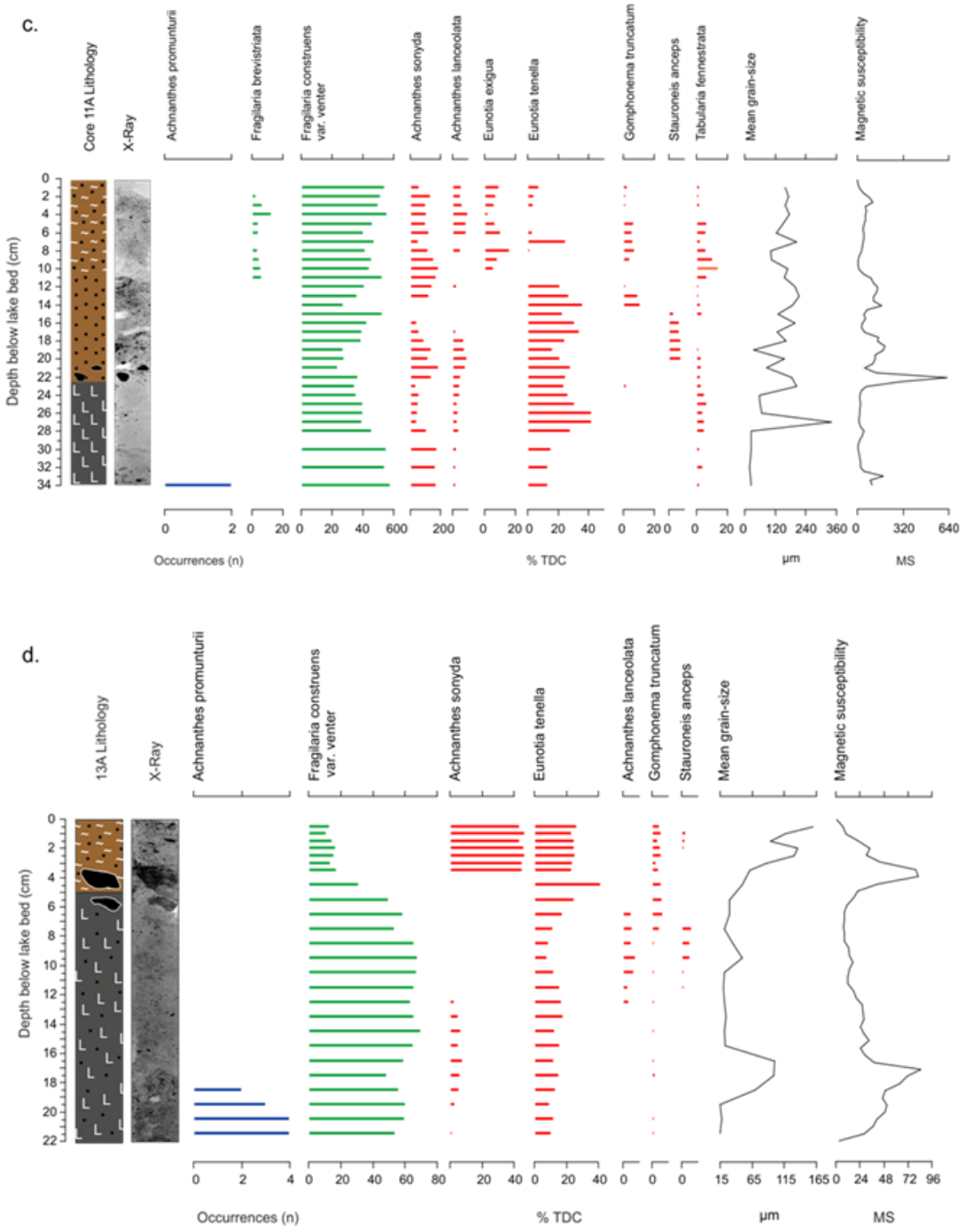

Figure 4.4, continued.

4.1.3 Core 10A

The basal unit of core 10A comprises a well-consolidated homogeneous gyttja with abundant fragments of *Calliergon scorpidium drepanocladus*, requiring a 2.5-cm diameter gouge corer to penetrate (Fig. 4.5). The base of the sampled sequence at 158 cm was dated to 2341-2153 cal a BP and contains minor occurrences of *Achnanthes promunturii*. Two thin (1-cm thick) deposits of coarse sand interrupt this unit; a first appears at 148 cm and a second overlies a homogeneous gyttja at 55 cm. Both of these deposits contain occasional specimens of *Achnanthes promunturii*. A ^{14}C date from 3 cm below the lower coarse sand unit yields an age of 1692-1444 cal a BP, while a second date from 3 cm below the upper coarse sand deposit provides an age of 933-792 cal a BP. Within the middle of the homogeneous gyttja between the two coarse sand deposits, a ^{14}C date at 105 cm yields an age of 1285-1181 cal a BP. Overlying the upper coarse sand deposit is a sequence of grey brown silty gyttja to a depth of 25 cm that is overlain by brown moss-rich gyttja to a depth of 12 cm. The transition between these two units dates to 529-305 cal a BP. Diatoms reveal a gradual decline of the dominant taxon *Fragilaria construens* var. *venter* from 70% to 1% TDC within the silty gyttja to 30 cm, becoming abruptly replaced by *Achnanthes sonyda* whose frequencies rise from 20 to 60% TDC. The top 12 cm of the sequence contains a thin section of grey silt with fine black laminae at the base. The sequence is capped by a thin mantle of medium to coarse sand containing minor frequencies of *Achnanthes promunturii*, as does a single sample from the very base of the grey silt with black laminae.

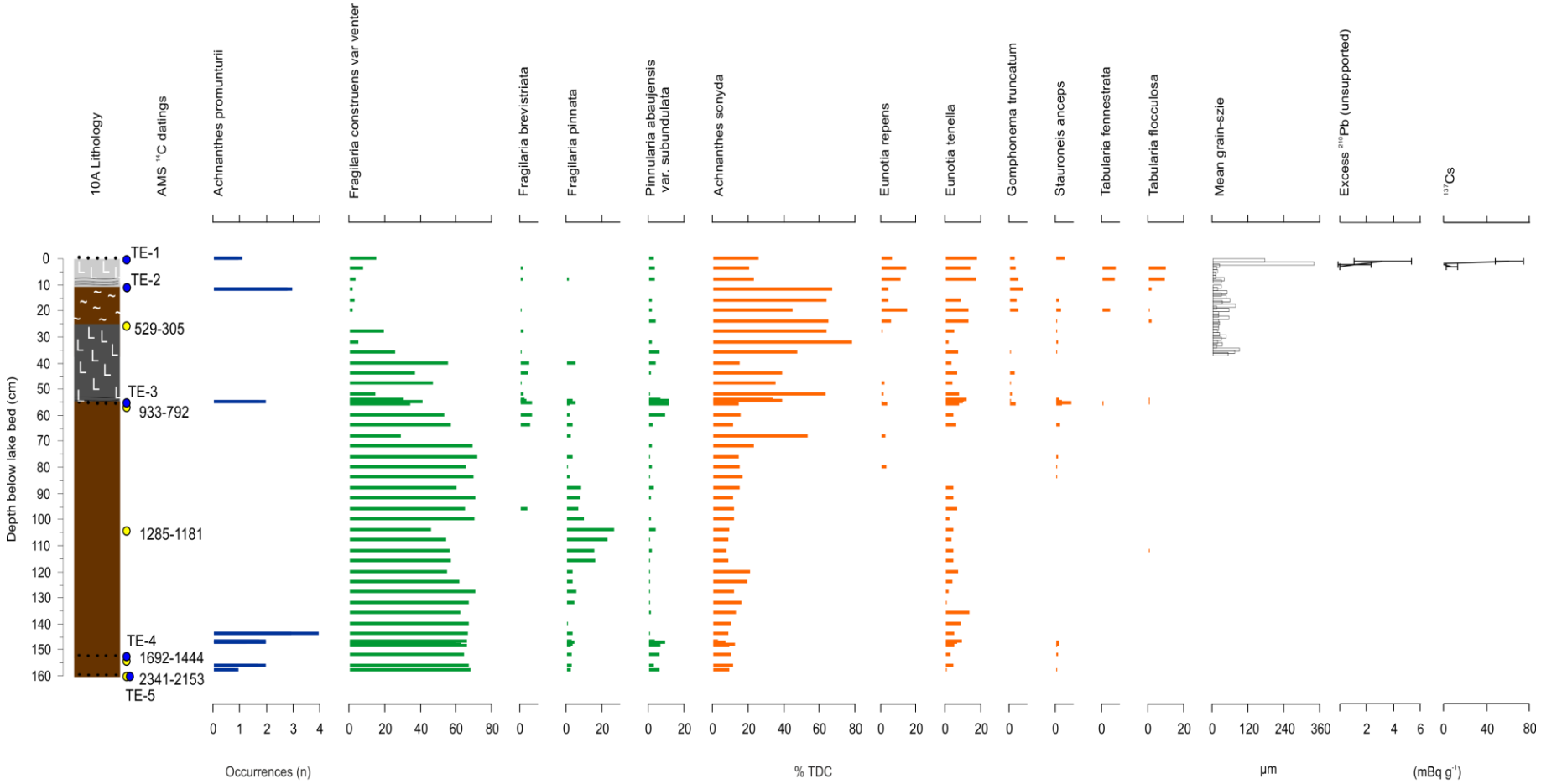

Figure 4.5. Lithology, sediment grain size, bio- and chronostratigraphy of the master core 10A. Diatoms are colour coded based on their salinity preferences (see Fig. 4.4 for the key). Only key taxa comprising >5% of the total count are shown except for polyhalobous taxa which are presented as number of occurrences. For lithology legend, see Fig. 2. The depths of calibrated (2σ) AMS ^{14}C ages are marked with yellow circles. Depths of inferred tsunami events are marked by blue circles and labelled 'TE-1 to TE-5'.

4.

4.1.4 Core 11

Core 11 contains a lower unit of silty gyttja dominated by an assemblage of *Fragilaria construens* var. *venter* (50%) that is abruptly overlain by a brown moss-rich gyttja that has high frequencies of *Achnanthes sonyda* (40%) between 14 and 8 cm (Fig. 4.4b). Between 8 and 5 cm there is a thin unit of grey silt with a few fine black laminae at the base, with an accompanying increase in mean GS from 10 to 80 µm. This unit is abruptly overlain by a 3 cm thick red gyttja containing medium-coarse sand, whose mean grain size is closely coupled with an increase in MS. The top of the sequence contains a 3 cm-thick sequence of brown moss-rich gyttja that is capped by a thin layer of medium-coarse sand containing the marine taxon *Achnanthes promunturii*. The ^{137}Cs activities in the uppermost 3 cm section are below the detection level. The laminated grey silt and overlying red sandy gyttja deposits are dominated by the freshwater taxa *Eunotia tenella*, *Achnanthes lanceolata* and *Achnanthes sonyda*. Despite the abrupt stratigraphic transitions between these units, diatoms exhibit gradual changes across these contacts.

4.1.5 Core 11A

The stratigraphy of core 11A is highly variable, albeit with no clear biostratigraphic changes throughout the profile (Fig. 4.4c). The sequence contains a lower unit of grey silty gyttja with sub-rounded pebbles that is overlain by a unit of sandy gyttja between 23 and 11 cm. The top 11 cm is comprised of a moss-rich sandy gyttja and mean GS fluctuates but steadily increases to the top of the core. *Fragilaria construens var. venter* maintain frequencies of 40-60% TDC. Minor fluctuations *of Achnanthes sonyda* and *Eunotia tenella* interrupt this pattern within the central part of sandy gyttja. There are also infrequent pulses of minor taxa; *Eunotia exigua* in the top 10 cm of the core and *Fragilaria brevistriata* throughout. A sample at the very base of the section contains a few occurrences of *Achnanthes promunturii* (2 specimens counted in two slides).

4.1.6 Core 13A

The core at the front of the lake (seaward) comprises a lower unit of silty gyttja between 22 and 17 cm containing *Achnanthes promunturii* and high frequencies of *Fragilaria*

construens var. *venter* (Fig. 4.4d). Silty gyttja extends up to 3 cm and contains a minor sand fraction (5%). The top of the sequence comprises a brown sandy moss-rich gyttja from 3 cm to top with small cobbles at the base. Diatoms here reveal a marked increase of *Achnanthes sonyda* to 40% TDC, while *Fragilaria construens* var. *venter* reduces from 60% to 15% TDC. MS and mean GS are coupled throughout with each displaying two large increases; a first within the basal silty gyttja unit and a second at the transition to the moss-rich gyttja.

4.2 Tsunami timing and frequency

Objective evidence of abrupt marine inundation events within a freshwater environment is primarily provided by the presence of marine diatom taxa within medium to coarse sand intercalations. We assume that horizons containing low frequencies of *Achnanthes promunturii* likely correspond to tsunami events (as storms are excluded due to lake position and short fetch length), providing a minimum frequency of events. There are five of these events within core 10A, spanning a maximum period of c. 2350 years. Where they have not been directly dated, interpolated ages have been determined from the age model. Overall the posterior model shows good agreement with the prior information, indicating an Agreement Index of 86%.

The sediment accumulation history in core 10A is divided into three periods based on changes in accumulation rates (Fig. 4.6). The lower stratigraphic section is represented by a well-compacted gyttja between 158 and 147 cm. The first probable tsunami event (TE) is at the very base of the section and is dated to 2339-2150 cal a BP (TE-5), while the second is at the top (147 cm), dated to 1593-1380 cal a BP (TE-4). The sediment accumulation rate between these two events was ~0.15 mm yr, which is the slowest of the entire sequence. This relatively low rate (which takes no correction for changes in bulk sediment density) might be a result of sediment compaction, which is likely given the stiffness of the basal sediment. Alternatively, the basal ^{14}C age is obtained from the only sample that comprised aquatic moss as dating material, so the age might be older due to unknown local reservoir effect. In a second period, accumulation increased to ~0.79 mm yr and is constrained by a third likely tsunami event (TE-3) at 55 cm, dated to 931-775 cal a BP. The third and final period of sedimentation is between this unit and the top of the sequence, where sediments accumulated at an average rate of ~0.66 mm/yr. TE-2 is at 12 cm at the base of the grey laminated silt and is dated to AD 1540-1940, while a final marine signature in the diatom count corresponds to the thin blanket of medium-coarse sand on the lake bed (TE-1). The

top 8 cm of sediment (i.e. 2 samples) contains ^{137}Cs and excess ^{210}Pb, implying recent accumulation (last ~60 years) at a rate of between 0.67 mm/yr and 1.33 mm/yr (Fig. 4.5).

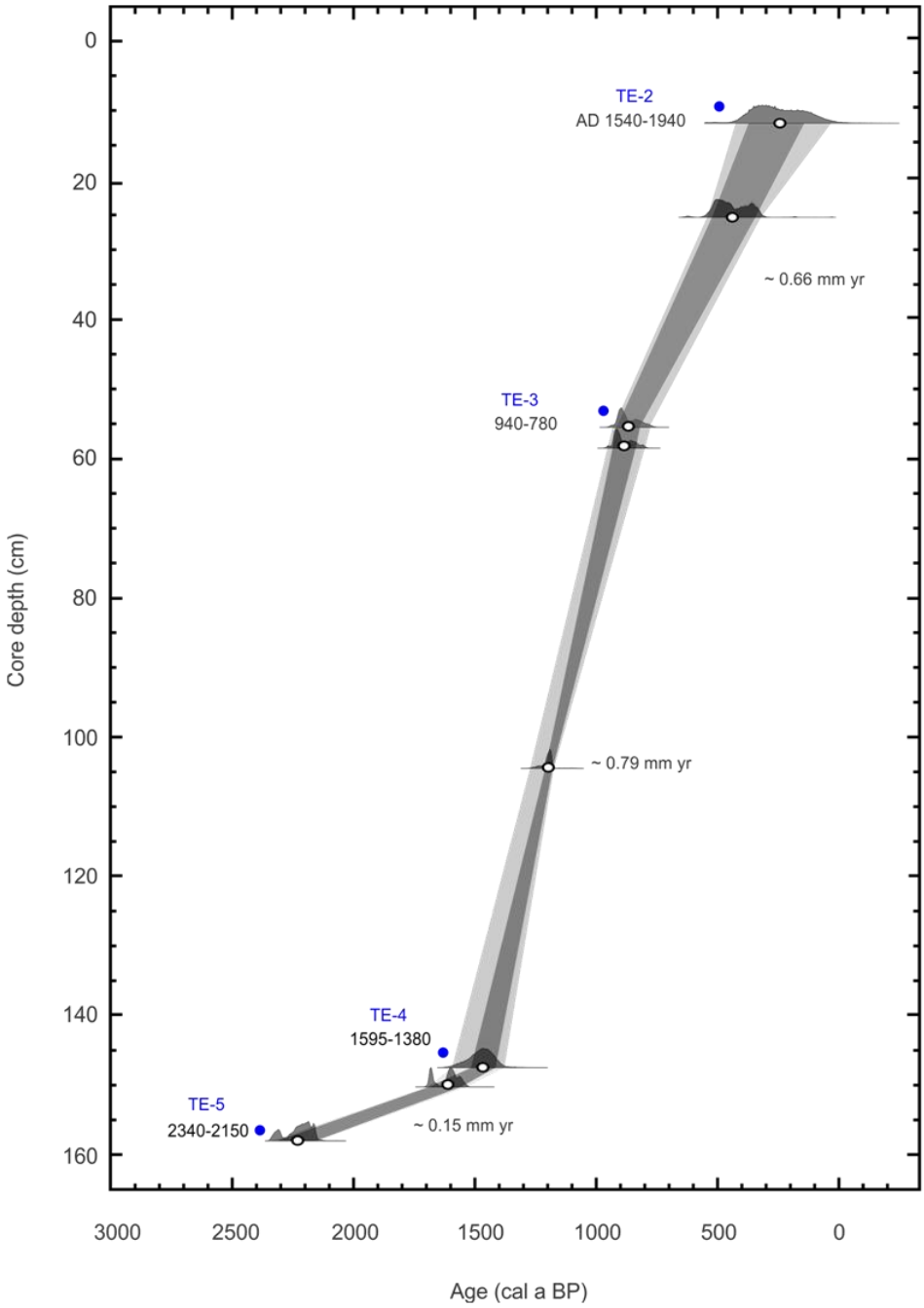

Figure 4.6. OxCal Poisson sequence deposition model for VA1 for radiocarbon dates from core 10A (Table 4.1), calibrated with the IntCal13 calibration curve (Reimer et al., 2013). The envelope indicates 2σ (light grey) and 1σ (dark grey) calibrated ranges. Tsunami events (TEs) 2-5 are labelled in blue. Model reveals a three periods of distinctly different rates of sediment accumulation.

5. Discussion

The data from core 10A provides the first multi-event record of tsunami minimum frequency and their minimum size from the Arctic. In the following discussion we provide a holistic interpretation of the history of VA1 by assessing the litho-, bio- and chronostratigraphy from multiple cores.

5.1 Interpreting tsunami events using lake-wide stratigraphy

Lake VA1 has been likely inundated by five tsunami events in the past c. 2350 years implying an average of one event per c. 600 yrs (Fig. 4.5). This is a minimum estimate because although presence of marine diatom taxa provides unequivocal evidence of marine inundation, the absence of marine taxa cannot be used to infer periods of no tsunami activity. For example, Szczuciński et al., (2012a) found that marine microfossils are not always present. Indeed, Davies and Haslett (2000) used a simple model to calculate that there is an exceptionally low probability of recovering a single marine specimen within a freshwater lake sequence. Therefore, it is possible that some tsunami events have not been identified within the stratigraphy because the probability of recovering a single marine specimen in a freshwater lake is exceptionally low (Davies and Haslett, 2000).

The nature of the Vaigat tsunami deposits is characteristically variable, fragmented and subtle. The gravel deposit associated with TE-1 is a single grain-thick; while the deposits associated with TE-5, TE-4, and TE-3 are typically ~1 cm-thick. In contrast, the deposit associated with TE-2 contains no coarse material (i.e. sand or gravel) but is marked by grey silt with fine black laminations in two cores (10A and 11). The presence of black laminae has been previously interpreted as short-lived bottom water anoxia following tsunami landfall (e.g. Kelsey et al., 2008). They are also common in laminated transitional units that record the final phases of basin isolation (Long et al., 2011), most likely a result of bottom water anoxia during the gradual mixing and filtering out of stagnant saline bottom water. Elsewhere, within the stratigraphy there are sand and gravel units containing no marine microfossils. The apparent random deposition of these deposits could reflect reworking of coarse material from the adjacent banks onto frozen lake ice by fluvial activity. Indeed, it is reasonable to assume that episodic break-up of lake-ice during preceding spring months would lead to uneven deposition of coarse-grained material (Romundset and Bondevik, 2011). As a result, they could also reflect tsunami deposition.

An enlightening feature is the lake-wide biostratigraphic shift from an assemblage dominated by tychoplanktonic *Fragilaria construens* var. *venter* to one dominated by the epiphytic *Achnanthes sonyda*, traceable in all but one of the sampled cores (core 11A). This provides a useful chronostratigraphic marker to help explain the complexity of the lake stratigraphy. In core 10A the biostratigraphic shift is coincident with the stratigraphic transition from silty gyttja to moss-rich gyttja at 25 cm that we date to within the Little Ice Age (LIA) cooling at 530-300 cal a BP (AD 1420-1650). Enhanced moss growth implies an increase in lake productivity (e.g. Riis and Sand-Jensen et al., 1997). Elsewhere in west Greenland, lake productivity proxy records document evidence of increased productivity at almost precisely the same time (Willemse and Tornqvist, 1999; Aelby and Fritz, 2009).

We use the biostratigraphic shift as recorded in core 10A as a chronostratigraphic marker to correlate, where possible, deposits in surrounding cores (Fig. 3.7). In core 10A, TE-3 pre-dates the biostratigraphic transition by a few centuries (940-780 cal a BP). At the most seaward extent of the lake (core 13A) the biostratigraphic shift occurs at a shallow depth of 3 cm. Similarly it occurs at a shallow depth (10 cm) in core 7A on the opposite landward bank. This probably reflects the impact of erosion to the stratigraphy around the lake margins by terrestrial processes. The basal part of core 7A is comprised of sandy gyttja (sand component: 50-70%) containing marine diatom taxa and occasional intraclasts of homogeneous gyttja. The homogeneous gyttja forms the lowermost (oldest) sequence of the master core, implying the erosion and reworking of surrounding lake sediments and their subsequent deposition at the margins. The same deposit, albeit without intraclasts, is present at the base of core 13A at the seaward extent of the lake. As TE-3 was the event that occurred prior to the biostratigraphic shift within the lake stratigraphy, our hypothesis is that the lower unit of sandy gyttja in cores 7A and 13A reflects tsunami deposition associated with this event (TE-3; 930-780 cal a BP). Core 11A complicates the interpretations. While its biostratigraphy reflects accumulation in the post-biostratigraphic shift time period, its lithology, comprised of silty gyttja, is not consistent with the wider lake stratigraphy (where cores are comprised of moss-rich gyttja). Although it is unlikely that such a small basin would experience localized variations in sediment supply and accumulation, at present we are unable to propose alternative reasons to explain the unique lithology of core 11A. Instead we accept the microfossil evidence that core 11A accumulated after the post biostratigraphic shift and tentatively propose that the marine signal at the base of 11A corresponds to TE-2 in core 10A (AD 1540-1940). Clearly, these are more speculative points than solid interpretations and require testing with further dating control. Finally, we attribute TE-1 to the landslide-tsunami that originated at Paatuut on November 21st 2000 AD, which is

patchily preserved as a single grain-thick layer. This would have been deposited onto a frozen lake surface before being subsequently redeposited onto the lake bed some 3-4 months later in the following spring. Based on a simple comparison of the thickness of the equivalent layer in the surrounding terrestrial environment (Fig. 4.2), it appears that a large proportion of the sediments laid onto the lake surface were subsequently reworked by terrestrial processes (aeolian and fluvial activity). This has highlights the difficulty with reconstructing winter tsunami events. Indeed, this offers a plausible explanation as to why evidence of the 15 December AD 1952 event is lacking (alternative to the explanation that the run-up height of the AD 1952 event was insufficient to ingress the basin).

Whilst at present there is a lack of criteria that can distinguish different types of tsunami event (i.e., landslide or iceberg-roll), we find it more likely that the record from Lake VA1 largely contains evidence of landslide-tsunami. It is logical to propose that iceberg-roll events are lower magnitude events with shorter run-up heights. For example a modern iceberg-roll event would require a minimum run-up height of 4.95 m to ingress the basin. In the earlier part of the record when RSL was lower, the probability of inundation by iceberg-roll events is further reduced. The same reasoning applies to storm events. We therefore suggest that the deposits are attributed to landslide-tsunami in Vaigat.

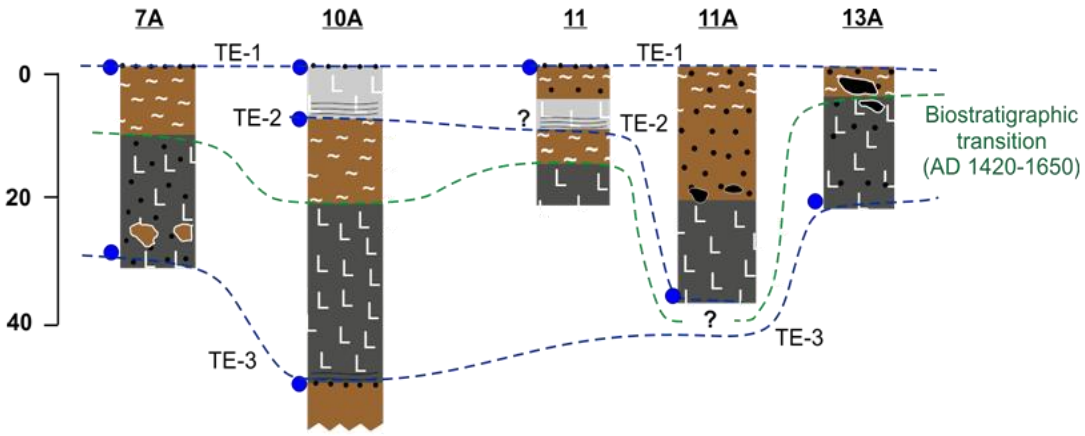

Figure 4.7. Correlation of cores and potential tsunami horizons along transect T1. Depths correspond to cm below the sediment-freshwater interface. Blue circles indicate horizons containing marine diatom taxa. We use the lake-wide biostratigraphic shift as a relative chronostratigraphic marker to interpret wider lake stratigraphy (green stippled line). Question marks illustrate uncertain stratigraphic correlation.

5.2 Tsunami run-up height

The minimum run-up height of the AD 2000 tsunami can be constrained precisely because the precise time of the event is well known (Dahl-Jensen et al., 2004). Seismic stations designed to monitor earthquake-induced crustal movements are installed across Greenland (Dahl-Jensen et al., 2003). Six stations detected seismic perturbations associated with the impact of the Paatuut landslide at 18:04 local time on 21 November 2000. We inferred the historical tidal height for the nearest tide gauge (Qeqertarsuaq; Fig. 4.1) using tidal modelling software WXTide32 v4.7 (Hopper, 2006). At the time of the event, local tides were about 5 cm above MTL, assuming no atmospheric contribution to tidal levels (Fig. 4.8a). This places the height of the Lake VA1 basin sill at 4.95 m above the modelled harmonic tidal level at the time of the event and provides a minimum run-up height for the AD 2000 tsunami of 4.95 ± 0.10 m, on the basis of the lake data alone. However, the nearby evidence of likely tsunami erosion (i.e., barren top of raised beach ridge, Fig. 4.2a) could imply a minimum run-up height of 11 m.

For the remaining historical and palaeotsunami events within our record, we estimate their minimum run-up heights by comparing the height of the basin sill above MTL to reconstructed changes in RSL over the study timescale (c. 2300 yrs) (Fig. 4.8b). The uncertainties equal the spring tidal range at the site (± 2.5 m), assuming no change in tidal range in the late Holocene. For the past c. 500 yrs, we estimate the position of palaeo RSL using an existing reconstruction from Nagtoralinguaq to the south of Disko Bugt (Long et al., 2010) which identifies a stable or slowly rising sea-level during this time. This is the closest reconstruction to our study site for this time period. For the late Holocene, we use interpolated isolation basin data from Disko Fjord (Fig. 4.1; Long et al., 2011) and Arveprinsens Ejland (Long et al., 1999), which indicate that RSL has risen by ~2 m over the past c. 2500 yrs. Despite possible spatio-temporal differences in the mode and rate of recent RSL rise in west Greenland (Long et al., 2010), we emphasise that this uncertainty will be accounted for in our wide uncertainty limits associated with the spring tidal range in Vaigat (± 2.5 m).

Fig. 4.8 illustrates the minimum run-up of tsunami events (i.e. minimum vertical height) superimposed on late Holocene RSL change in south central Vaigat. Because RSL has been rising in the late Holocene, there is a tendency to note that minimum run-up heights have decreased from c. 2500 yrs to present although, given the uncertainties associated with

the spring tidal range, event run-ups could have been variable size. They are also minimum estimates because of variations in the positions of the landslide source relative to site VA1.

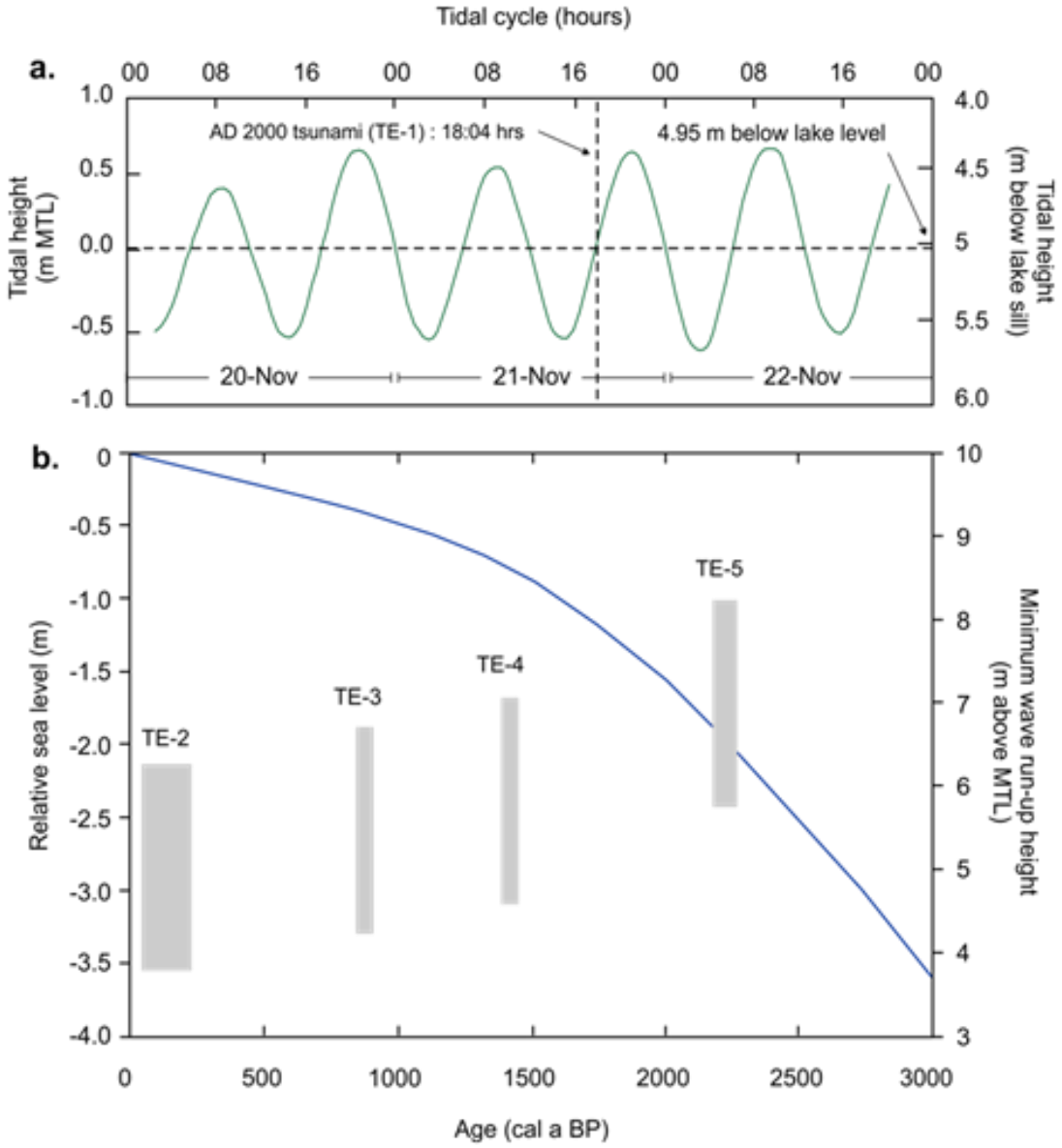

Figure 4.8. (a) Modelled neap tidal cycle at Qeqertarsuaq for the period 20-22 November AD 2000, illustrating the tidal height at the time of the AD 2000 tsunami (18:04 local time, 21 November, 2000). The event occurred at approximately mean tide level (MTL). (b) Estimated minimum vertical run-up of palaeotsunami events (right-hand axis; grey error boxes) superimposed on an interpolated record of RSL change for Vaigat (blue line; left-hand axis) for the past 3000 yrs. RSL curve combines recent sea-level data (past c. 500 yrs; Long et al., 2010) with an interpolation from two late Holocene isolation basin RSL records (Long et al., 1999; 2011). Vertical error is based on a spring tidal range of 2.5 m, horizontal errors indicate 2σ calibrated ranges of posterior ^{14}C data.

5.3 Testing the hypothesis of climate-related tsunami generation

We compare the timing of likely tsunami events recorded in Lake VA1 to the GISP2 oxygen isotope record (Grootes et al., 1997; Meese et al., 1994) for the late Holocene and to a local instrumental air temperature record for Illulissat, located to the southeast of Lake VA1 by ~100 km, for the past 160 years (Vinther et al., 2006). Fig. 4.9 illustrates the 2σ age ranges of tsunami events superimposed on the detrended centennial-millennial scale oxygen isotope record of GISP2 spanning the period 2500 cal a BP to present (i.e. AD 1950) and the shorter-term annual instrumental temperature (°C) record for Illulissat from AD 1855 to AD 2005. For the long term series (Fig. 4.9b), we calculated the average (detrended) $\delta^{18}O‰$ of each time period presented by each 2σ age range associated with TE-2 to TE-5. Despite an element of smoothing associated with averaging $\delta^{18}O‰$ within a defined 2σ age range, TE-3 and TE-4 occurred in periods where average oxygen isotope $\delta^{18}O‰$ was slightly above the mean, while TE-2 and TE-5 occurred during a period of slightly below average $\delta^{18}O‰$ values. The latter two should be treated with caution because of the large age uncertainties associated with TE-2 and the unknown additional age uncertainty associated with TE-5 (undetermined basin hardwater effect on the ^{14}C age of aquatic moss and/or unaccounted for sediment compaction at the base of the core).

The observed timing of TE-1 (21 November, 2000) and the AD 1952 event (15 December) within the instrumental era (Pedersen et al., 2001; Dahl-Jensen et al., 2004) is precise enough explore possible correlations with temperature change on seasonal timescales. We calculated seasonal average temperatures using monthly data from the Illulissat temperature record (Vinther et al., 2006). In both years, seasonal temperatures were above average, with the exception of spring in AD 1952 that experienced below average temperatures of 0.4°C. The highest amplitude temperature change is observed in autumn, where temperatures were 1.88°C and 0.67°C above detrended values in AD 1952 and AD 2000, respectively. Meteorological data from Qeqertarsuaq in southern Disko Island also indicates that precipitation in AD 2000 was the highest since AD 1990 (Hansen et al., 2006).

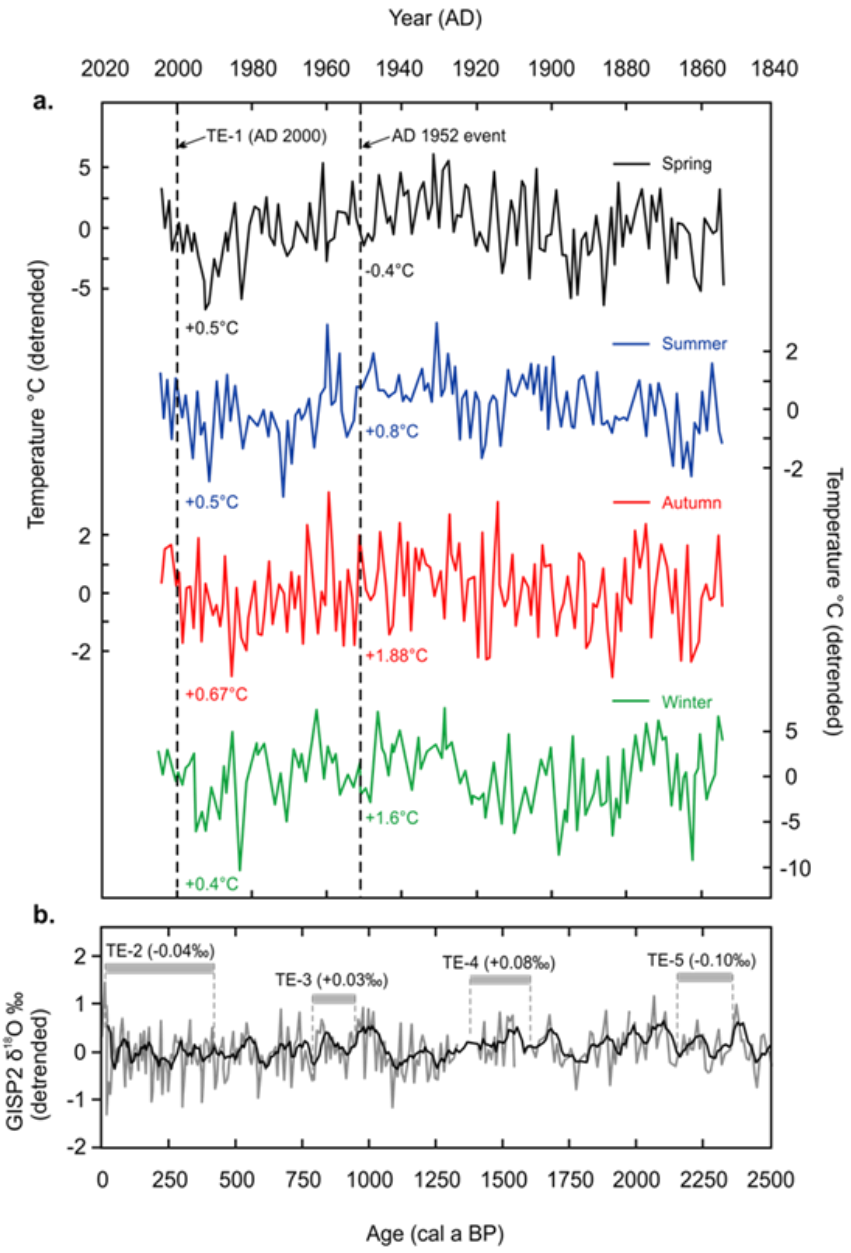

Figure 4.9. Timing of historical and palaeotsunami in Vaigat superimposed on detrended air temperature and oxygen isotope records for the late Holocene. (a) Seasonal instrumental air temperatures at Ilulissat (Vinther et al., 2006). Seasonal averages are calculated using average data for March-May (spring), June-August (summer), September-November (autumn) and December-February (winter). Seasonal mean temperature deviations for years 1952 and 2000 are also highlighted. (b) Sub-decadal (grey line) oxygen isotope ($\delta^{18}O$) record from the GISP2 ice-core (Grootes et al., 1997; Meese et al., 1994) for the period 2500 cal a BP to present (AD 1950) with a 5-point running mean (black line). The average $\delta^{18}O$ from the mean for the periods in which events occurred is calculated for each 2σ age range.

The correlation of warmer autumn seasons and higher precipitation with tsunami events in historical times could suggest that increased temperature, and likely increased rainfall, exerts a control on the frequency of landslides in Vaigat. On the long-term scale, rigorous testing of these hypotheses is not possible because of the uncertainties inherent to the ^{14}C dating technique. However, given the timing of the AD 2000 and AD 1952 events on the eve of winter, we tentatively suggest that seasonal freeze-thaw cycles, particularly at the start of the winter season (e.g. Phillips and Newlands, 2007), provides the final trigger mechanism responsible slope failure and tsunami generation in Vaigat. Future warming will drive an increase in active permafrost layer thickness and soil water storage that could contribute to increased landslide-tsunami risk in Vaigat and the wider Arctic.

6. Conclusions

We present the results of an investigation into the local frequency and minimum run-up height of landslide-generated tsunami in Vaigat, west Greenland. Our approach uses a combination of litho-, bio- and chronostratigraphic methods to reconstruct tsunami history for the past c. 2350 yrs from an Arctic freshwater lake. The main conclusions from this study are as follows:

The lake stratigraphy contains a record of tsunami frequency for the central portion of the Vaigat Strait for the past c. 2350 yrs. Evidence of likely five tsunamis, (indicated by marine diatom taxa, medium to coarse sand deposits, intraclasts of eroded gyttja and occasional black laminae suggesting anoxic conditions due to stagnating saline lake bottom waters) indicates an average return period of c. 600 yrs. This is more frequent than previous estimates that suggested an average of one event per thousand years. The most recent event was in AD 2000, while evidence of the smaller AD 1952 tsunami has not been identified. In our record, three large tsunami events occurred in the past c. 1000 yrs, indicating an average of c. 330 yrs for the last millennium.

The estimated frequency of events is a minimum because of a number of issues: i) low absolute abundances of objective marine microfossil evidence, ii) potential erosion of older lake sediments and thus older event signatures, iii) reduced probability of wave impact with age because of the lower position of RSL and, iv) potential changes to the coastal geometry at the study site.

The minimum run-up height of the AD 2000 tsunami has been calculated (4.95 m) by analysing the vertical position of the tidal cycle at the time of the Paatuut landslide in relation to the height of the basin sill. Minimum run-up heights for the remaining four historical and palaeotsunami have been determined by considering the height of RSL at the time of wave impact.

The timing of tsunami events compared to a local instrumental air temperature (°C) record indicates that the two most recent tsunami events occurred in periods of above average seasonal temperatures. In the long-term, there is some evidence that palaeotsunami occurred in above average periods of $\delta^{18}O‰$. These observations suggest that warmer air temperatures likely exert a positive control on the origin of slope failure and tsunami in Vaigat.

References

Aebly, F.A. and S.C. Fritz. 2009. Paleohydrology of Kangerlussuaq, West Greenland during the last ~8000 yr. *The Holocene* **19**: 91-104.

Andersen OGN. 1981. The annual cycle of temperature, salinity, currents and water masses in Disko Bugt and adjacent waters, West Greenland. Meddelelserom Grønland, Bioscience **5**, 1–36.

Andresen, C. and McCarthy, D. and Dylmer, C. and Seidenkrantz, M-S., Kuijpers, A., Lloyd, J. 2011. Interaction between subsurface ocean waters and calving of Jakobshavn Isbræ during the Late Holocene. *The Holocene* **21** (2). 211-224.

Atwater, B.F. and Hemphill-Haley, E., 1997, Recurrence intervals for great earthquakes of the past 3,500 years at northeastern Willapa Bay, Washington: *U.S. Geological Survey Professional Paper* **1576,** 108 p.

Barlow, L.K., 2001. The time period AD 1400–1900 in Central Greenland ice cores in relation to the North Atlantic sector. *Climatic Change* **48**, 101–119.

Bondevik, S., Svendsen, J.I., Mangarud, J. 1997a. Tsunami sedimentary facies deposited by the Storegga tsunami in shallow marine basins and coastal lakes, Western Norway. *Sedimentology* **44**, 1115-1131.

Ramsey, C. 2008. Deposition models for chronological records. *Quaternary Science Reviews* **27**(1-2), 42-60.

Bronk Ramsey, C. 2009a. Bayesian analysis of radiocarbon dates. *Radiocarbon*, **51**(1), 337-360.

Buchwal A, Szczuciński W, Strzelecki M, Long AJ (2015) Tree-ring structure of *Salix glauca* reveals evidence of a 2000 AD tsunami event in west Greenland: implications for Arctic paleotsunami and paleoecological studies. Polish Polar Res 36: 51-65

Corner, G.D., Yevzerov, V.Y., Kolka, V.V., Moller, J.J., 1999. Isolation basin stratigraphy and Holocene relative sea-level change at the Norwegian-Russian border north of Nikel, northwest Russia. *Boreas* **28**, 146-166.

Czernik J., Goslar T., 2001. Preparation of graphite targets in the Gliwice Radiocarbon Laboratory for AMS 14C dating. *Radiocarbon* **43**, 283-291.

Dahl-Jensen, T., Larsen, L.M., Pedersen, S.A.S., Pedersen, J., Jepsen, H.F., Pedersen, G.K., Nielsen, T., Pedersen, A.K., Platen-Hallermund, F.V., Weng, W. 2004. Landslide and tsunami 21 November 200 in Paatuut, West Greenland. *Natural Hazards*, **31**, 277-287.

D'Andrea, W., Y. Huang, S.C. Fritz, N.J. Anderson. 2011. Abrupt climate change as a factor in human migration in West Greenland. *Proceedings of the National Academy of Sciences* **108**: 9765-9769, doi/10.1073/pnas.1101708108.

Davies, P., Haslett, S.K. 2000. Identifying storm or tsunami events in coastal basin sediments. *Area* **32**(3), 335-336.

DMI. 2012. Danish Meteorological Institude. Illulissat tides. Retreived June 2012 [http://www.dmi.dk/en/groenland/]

Eronen, M. 1983: Late Weichselian and Holocene shore displacement in Finland. In Smith, D. E. & Dawson, A. G., (eds.): Shorelines and Isostasy. Institute of British Geographers, Special Publication 16, 183–207.

Gilks, W., Richardson, S., Spiegelhalter, D. (Eds.) 1996. Markov Chain Monte Carlo in Practice. Chapman & Hall, London.

Grootes, P.M., and M. Stuiver. 1997. Oxygen 18/16 variability in Greenland snow and ice with 10-3- to 10-5-year time resolution. Journal of Geophysical Research 102:26455-26470.

Hansen BU, Elberling B, Humlum O, Nielsen N (2006) Meteorological trends (1991–2004) at Arctic Station, Central West Greenland (69°15') in a 130 year perspective. Dan J Geog 106: 45-55

Hartley, B. 1996. An Atlas of British Diatoms. Ed: Sims, P.A. Biopress Ltd, London.

Henriksen N, Higgins AK, Kalsbeek F, et al. 2000. Greenland from Archaean to Quaternary: Descriptive Text to the Geological Map of Greenland 1:2,500,000 *Geology of Greenland Survey Bulletin* **185**.

Hopper, M. 2006. WXTide32 (Version 4.7) [Computer software]. Retrieved March 2014, from http://wxtide32.com.

Hutchinson, I., Guilbault, J.P., Clauge, J.J., Borbrowski, P.T. 2000. Tsunamis and tectonic deformation at the northern Cascadia margin: a 3000 year record from Deserted Lake, Vancouver Island, British Columbia, Canada. *The Holocene* **10**(4), 429-439. Hutchinson, U., Clague, J.T., Mathewes, R.W. 1997. Reconstructing the tsunami record on an emerging coast: A case study of Kanim Lake, Vancouver Island, British Columbia. *Journal of Coastal Research* **13(**2), 543-553.

Jankaew, K., Atwater, B.F., Sawai, Y., Choowong, M., Charoentitirat, T., Martin, M.E., Prendergast, A. 2008. Medieval forewarning of the 2004 Indian Ocean tsunami in Thailand **455**, 1228-1231. doi:10.1038/nature07373.

Kelsey, H.M., Nelson, A.R., Hemphill-Haley, E., Witter, R.C. 2005. Tsunami history of an Oregon coastal lake reveals a 4600 yr record of great earthquakes on the Cascadia subduction zone. *Geological Society of America Bulletin* **117**(7-8), 1009-1032, doi: 10.1130/B25452.1.

Larsen, J.G. & Pulvertaft, T.C.R. 2000: The structure of the Cretaceous-Palaeogene sedimentary-volcanic area of Svartenhuk Halvø, central West Greenland. *Geology of Greenland, Survey Bulletin* **188**, 40.

Leonard, G.S.; Johnston, D.M.; Gregg, C.E. 2013. Warning systems. IN: Bobrowsky, P. (ed.) Encyclopedia of natural hazards. Springer

Long, A.J., Roberts, D.H., Wright, M.R. 1999. Isolation basin stratigraphy and Holocene relative sea-level change on Arveprinsen Ejland, Disko Bugt, West Greenland. *Journal of Quaternary Science* **14**(4), 323-343.

Long, A.J., Woodroffe, S.A., Milne, G.A., Bryant, C.L., Wake, L.M., 2010. Relative sea level change in West Greenland during the last millennium. *Quaternary Science Reviews* **29**, 367-383.

Long, A.J., Woodroffe, S.A., Roberts, D.H., Dawson, S. 2011 Isolation basins, sea-level changes and the Holocene history of the Greenland Ice Sheet. *Quaternary Science Reviews* **30**, 3748-3768.

Miller, D.J. 1960. Giant Waves in Lituya Bay, Alaska, Geological Survey Professional Paper 345-C, US Government Printing Office, Washington.

Mosbech, A., Anthonsen, K.L., Blyth, A., Boertmann, D., Buch, E., Cake, D., Grondahl, L., Hansen, H., Kapel, S., Nielsen, S., Nielsen, N., Von Platen, F., Potter, S., Rasch, M. 2000. Environmental Oil Spill Sensitivity Atlas for the West Greenland Coastal Zone. Internet-version. *The Danish Energy Agency, Ministry of Environment and Energy*. 341.

Meese, D.A., A.J. Gow, P.M. Grootes, P.A. Mayewski, M. Ram, M. Stuiver, K.C. Taylor, E.D. Waddington, and G.A. Zielinski. 1994. The accumulation record from the GISP2 core as an indicator of climate change throughout the Holocene. Science 266:1680-1682

Nanayama, F., Satake, K., Furukawa, R., Shimokawa, K., Atwater, B.F., Shigeno, K. & Yamaki, S. 2003. Unusually large earthquakes inferred from tsunami deposits along the Kuril trench, Nature **424**, 660-663.

Nelson, A.R., Shennan, I., Long, A.J. 1996. Identifying coseismic subsidence in tidal-wetland stratigraphic sequences at the Cascadia subduction zone of western North America. *Journal of Geophysical Research* **101**(B3), 6115-6135.

Palmer, A.J.M., Abbott, W.H. 1986. Diatoms as indicators of sea-level change. *IN*: Van de Plassche, O. (ed.), *Sea-level Research: a Manual for the Collection an Evaluation of Data*, 457–488. Geo Books, Norwich.

Pedersen, S.A.S., Larsen, L.M., Dahl-Jensen, T., Jepsen, H.F., Pedersen, G.P., Nielsen, T., Pedersen, A.K., Platen-Hallermund, F.V., Weng, W. 2002. Tsunami-generating rock fall and landslide on the south coast of Nuussuaq, central West Greenland. *Geology of Greenland Survey Bulletin* **191**, 73-83.

Plafker, G., 1965, Tectonic deformation associated with the 1964 Alaska earthquake. *Science* **148**, 1675-1687.

Rasch, M., 2000. Holocene relative sea level changes in Disko Bugt, West Greenland. *Journal of Coastal Research* **16**, 306-315.

Reimer, P.J., Bard, E., Bayliss, A., Beck, J.W., Blackwell, P.G., Bronk Ramsey, C., Buck, C.E., Cheng, H., Edwards, R.L., Friedrich, M., Grootes, P.M., Guilderson, T.P., Haflidason, H., Hajdas, I., Hatte, C., Heaton, T.J., Hoffman, D.L., Hogg, A.G., Hughen, K.A., Kaiser, K.F., Kromer, B., Manning, S.W., Niu, M., Reimer, R.W., Richards, D.A., Scott, E.M., Southon, J.R., Staff, R.A., Turney, C.S.M., van der Plicty, J. 2013. Intcal13 and Marine13 radiocarbon age calibration curves 0-50,000 years cal BP. *Radiocabon* **55**(4) 1669-1667.

Riis, T., Sand-Jensen, K. (1997) Growth reconstruction and photosynthesis of aquatic mosses: influence of light, temperature and carbon dioxide at depth. *Journal of Ecology* **85**, 359-37.

Romundset, A., Bondevik, S., 2011. Propagation of the Storegga tsunami into ice-free lakes along the southern shores of the Barents Sea. *Journal of Quaternary Science* **26**, 457-462.

Romundset, A., Lohne, O.S., Mangerud, J., Svendsen, J.I., 2009. The first Holocene relative sea-level curve from the middle part of Hardangerfjorden, western Norway. *Boreas* **39**, 87-104.

Smith, D.E., Dawson, A.G. (Eds.), Shorelines and Isostasy. Academic Press, London, 183-207.

Szczuciński, W., Kokociński, M., Rzeszewski, M., Chagué-Goff, C., Cachao, M., Goto, K., Sugawara, D., 2012a. Sediment sources and sedimentation processes of 2011 Tohoku-oki tsunami deposits on the Sendai Plain, Japan - insights from diatoms, nannoliths and grain size distribution. *Sedimentary Geology* **282**, 40-56.

Szczuciński, W., Rosser, N.J., Strzelecki, M.., Long, A.., Lawrence, T., Buchwal, A., Chagué -Goff, C., Woodroffe, S., 2012b. Sedimentary Record and Morphological Effects of a Landslide-Generated Tsunami in a Polar Region: The 2000 AD Tsunami in Vaigat Strait, West Greenland. *American Geophysical Union Fall Meeting, San Francisco*, 3-7.12.2012, CONTROL ID: 1479941.

Ten Brink, N.W., Weidick, A., 1975. Holocene history of the Greenland Ice Sheet based on radiocarbon-dated moraines in West Greenland. *Grønlands Geologiske Undersøgelse Bulletin* **114**, 1-44.

Vinther, B. M., K. K. Andersen, P. D. Jones, K. R. Briffa and J. Cappelen, Extending Greenland Temperature Records into the late 18th Century, doi:10.1029/2005JD006810, *J. Geophys. Res., 111*, D11105

Vos, P.C. de Wolf, H. 2003. Diatoms as a tool for reconstructing sedimentary environments in coastal wetlands; methodological aspects. *Hydrobiologia* **267/270**, 285-296.

Wagner, B., Bennike, E, O., Klug, M., Cremer, H. 2007. First indication of Storegga tsunami deposits from East Greenland. *Journal of Quaternary Science* **22**(4), 321-325.

Wanamaker, A.D., Butler, P.G., Scourse, J.D., Heinemeir, J., Eiriksson, J., Knudsen, K.L., Richardson, C.A. 2012. Surface changes in the North Atlantic Meridional overturning circulation during the last millennium. *Nature Communications* **3:899**, doi: 10.1038/ncomms1 901.

Willemse, N.W., Tornqvist, T.E. 1999. Holocene century-scale temperature variability from West Greenland lake records. *Geology* **27**, 580-584.

5

Sedimentary evidence for a mid-Holocene iceberg-generated tsunami in a coastal lake, west Greenland

1. Introduction

Most tsunamis are generated on active plate boundaries, triggered by earthquake-generated rapid vertical sea-bed movement (e.g. Subarya et al. 2006; Ozawa et al. 2011). Other, less common sources include submarine landslides (e.g. Dawson et al. 1988), subaerial rockfalls or landslides that enter in the sea (e.g. Dahl-Jensen et al. 2004; Fritz et al. 2009), volcanic eruptions (e.g. Nishimura 2008), rapid large-scale air pressure disturbances - called also meteotsunami (e.g. Monserrat et al. 2006; Tappin et al. 2013) and, most rarely, cosmic asteroid impact (e.g. Wünnemann and Weiss 2015).

Icebergs provide a further potential source of tsunami in polar regions. Here we use the term "iceberg-generated tsunami" to capture the range of potential iceberg motions (e.g. rocking, capsizing, rolling, collapsing) that can generate waves. Tsunamis generated by icebergs are frequently observed in parts of Antarctica and Greenland, where they routinely have wave heights of 2 m or so (MacAyeal et al. 2009; Amundson et al. 2008; 2010). However, their occurrence and geomorphic significance over longer (Holocene) timescales have not previously been studied.

As part of a study reconstructing relative sea-level (RSL) changes in the Innaarsuit area of Disko Bugt, west Greenland (Fig. 5.1), Long et al. (2003) identified an anomalous sand unit within lake muds, deposited a few centuries after basin isolation from the sea by RSL fall. Here we re-appraise this sand unit with a focus on its potential significance as a palaeo-indicator of a past iceberg-generated tsunami. We consider this re-analysis is timely for several reasons. First, there is a growing awareness of the potential impact of iceberg-generated waves (due to rolling and breaking) on human activity on land and sea. This has been aided by some spectacular amateur video footage shot from Greenland (e.g. https://www.youtube.com/watch?v=_2NvwlnKVtU). Second, a recent acceleration in calving flux from many Greenland glaciers (e.g. Rignot and Kanagaratnam 2006; Velicogna 2009) has been accompanied by several direct measurements of several long waves caused by iceberg generation / roll (Amundson et al. 2008; 2010), although no evidence of their sedimentary impact on coastal lakes has been reported to date. Third, recent reports from Antarctica have speculated on the wider potential contribution of iceberg tsunami in accelerating the break-up of large ice shelves, including Larsen B and Wilkins ice shelves (MacAyeal et al. 2003; Scambos et al. 2009; Levermann 2011). Fourth, as discussed below, coastal lakes are excellent repositories of evidence for tsunami generated by a subduction

earthquakes and submarine landslides (e.g. Bondevik et al. 1997a,b; Hutchinson et al. 2002); as such they have a proven potential to do the same with regard to iceberg-related processes.

We present a new suite of field and laboratory analyses that help to characterise the lake deposit and establish approximate minimum tsunami wave run-up using the rate of mid-Holocene RSL fall. We review other isolation basin records within Disko Bugt and conclude that local tsunami-impact may have been more frequent than previously thought. We conclude by reflecting that global warming will lead to increased calving, at a time when human use of the polar coast will also grow. Iceberg-generated tsunami will become a growing hazard in polar coastal waters, especially in areas adjacent to large, fast flowing marine-terminating ice streams that are close to human populations or infrastructure.

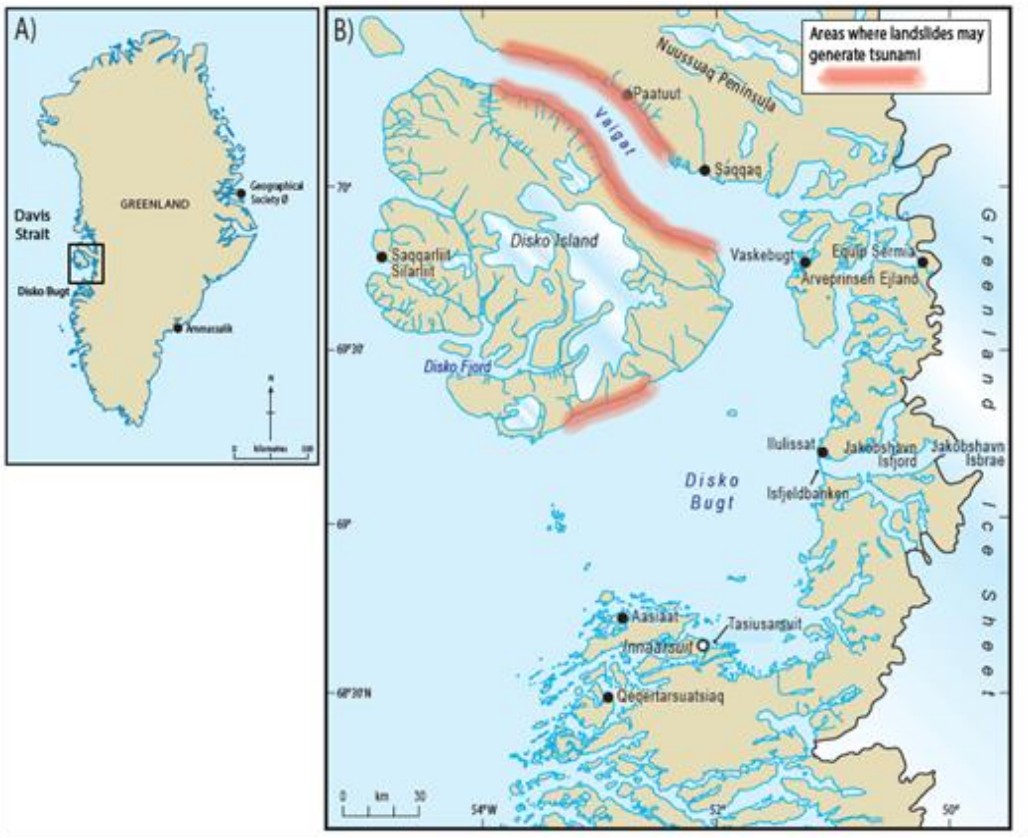

Figure 5.1. Location map of Greenland and Disko Bugt, showing place names mentioned in the text and areas of potential landslide-generating tsunamis (from Dahl-Jensen et al. 2004). The Innaarsuit study site is located on the south coast of Disko Bugt.

2. Previous work

2.1 Iceberg-generated tsunami

When an iceberg tilts, rocks, capsizes, rolls or disintegrates, it will generate waves the dimensions of which will depend on the size and geometry of the iceberg, the direction and speed of the rotation, as well as the water depth at the point of rotation and the wider local bathymetry. Based on these parameters, MacAyeal et al. (2011) developed a simple rule of thumb that relates tsunami wave height to iceberg thickness. This predicts that the open-water tsunami height has an upper limit of $0.01H$ where H is the initial iceberg thickness. Thus, a tsunami with a solitary surface wave amplitude of 10 m in open water could be caused by the rolling of an iceberg with a thickness of 1000 m. MacAyeal et al. (2011) note that icebergs of this size, with tsunami waves of approximately this amplitude, have been observed in the vicinity of Jakobshavn Isbrae (Sermeq Kujalleq), a large marine-terminating ice stream in west Greenland and one of the most prodigious generators of icebergs on the planet (e.g. Amundson et al. 2008).

Icebergs generated from thick ice tongues, such as those associated with marine-terminating glaciers in Greenlandic fjords, have a greater potential for generating large tsunami than the generally thinner ice shelves that are common in Antarctica (MacAyeal et al. 2011). However, even relatively small icebergs have the potential to generate large tsunamis, especially where the seabed bathymetry and coastal topography act to amplify wave height (e.g. Didenkulova and Pelinovsky 2011).

2.2 Tsunami hazard in Greenland

Iceberg-tsunamis are a well-known coastal hazard in parts of Greenland. Indeed, on the outskirts of the town of Ilulissat (west Greenland), which stands at the mouth of the Jakobshavn Isfjord (Kangia), public notices draw attention to the regular threat to life of iceberg-tsunami (Fig. 5.2). But icebergs are not the only source of tsunami that may impact Greenland and other polar regions, where two other processes can also be important: those associated with terrestrial landslides that terminate in the sea, and far-field tsunamis that are generated by an earthquake or submarine landslide, for instance the early-Holocene Storegga slide tsunami that originated from offshore of Norway and which impacted Norway, Scotland, northeast England, as well as east Greenland (Dawson et al. 1988; Wagner et al., 2007).

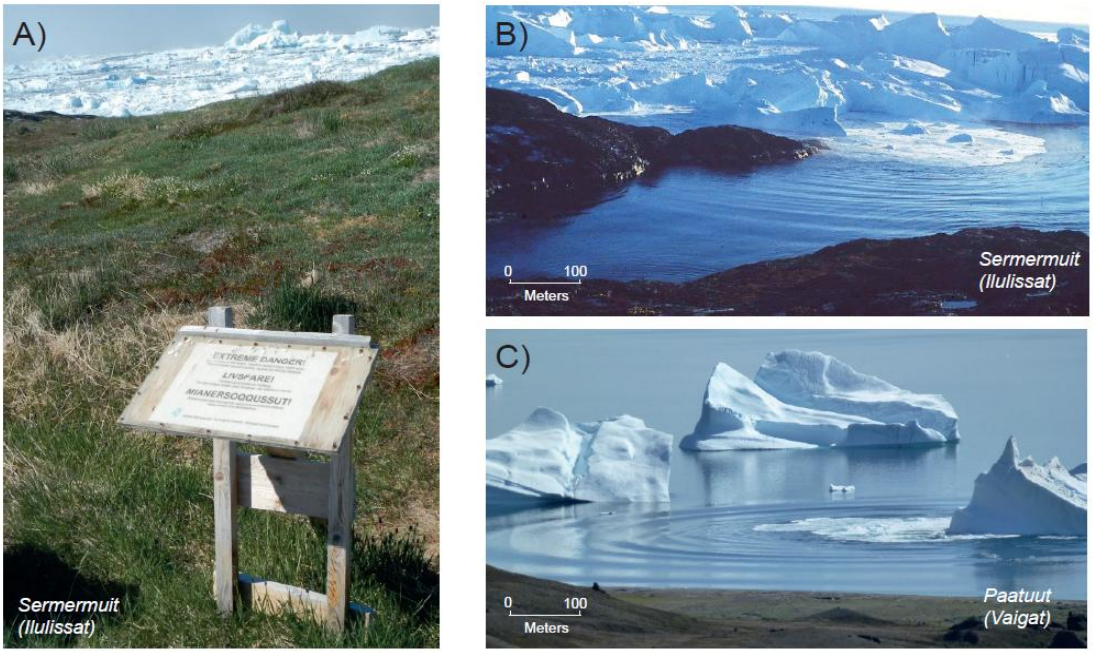

Figure 5.2. Iceberg tsunami hazard in Disko Bugt, west Greenland. (A) Public warning notice of the threat of iceberg-generated tsunami, posted by the Ilulissat Municipality. Sign reads "EXTREME DANGER! Do not walk on the beach. Death or serious injury might occur. Risk of sudden tsunami waves, caused by calving icebergs". (B) Example of small iceberg-generated waves from Ilulissat (close to site of A, credit Dr David Roberts)) and from near to Paatuut (C).

In many parts of Greenland, a combination of geological setting, permafrost, glacier ice, steep ground and freeze-thaw cycles contribute to high terrestrial landslide risk. This is especially so in the Nuussuaq Basin in central west Greenland (Fig. 5.1), where a sequence of weakly consolidated Cretaceous sediments are capped by Palaeogene basalts (Pederson et al. 2001). These geological conditions mean that certain areas of Disko Island, Nuussuaq and Svartenhuk Halvø are strongly affected by landslides (rock falls, slides and rock avalanches) that can generate large tsunami (Fig. 5.1).

The most recent landslide-triggered tsunami in Disko Bugt happened in the mid-afternoon of November 21st 2000, when residents of the coastal village of Saqqaq, located in Vaigat (northern Disko Bugt, Fig. 5.1) noted abnormal waves in the harbour. A subsequent survey by Pederson et al. (2001) and Dahl-Jensen et al. (2004) revealed that the waves were caused by a landslide that entered the sea c. 40 km northwest at Paattut. The escarpment that failed at the head of the slide reached c. 1400 m above sea level (asl), delivering an estimated 30 million m^3 of sediment into the sea. Photographs taken after the event indicate

a dark stripe along the coast where low-lying snow, below about 50 m asl, was washed away by the tsunami. Locally the resulting tsunami had a height of 50 m. Several icebergs were washed inland and stranded 300–700 m from the coast, with debris (sediment and icebergs) scattered across an alluvial fan up to 800 m. The tsunami was the largest reported in Vaigat during at least the last 500 years and field observations show the impact of the event was limited to the U-shaped Vaigat fjord (Dahl-Jensen et al. 2004). Buchwal et al. (2015) suggest that climatic factors likely had a role in influencing the event, with the highest precipitation and thickest permafrost active layer on record observed in the months leading up to the event.

2.3 The stratigraphic signature of tsunami in coastal lakes

Coastal lakes have the potential to act as quiet-water depositories within which evidence for past tsunami can be preserved. In British Columbia, for example, Hutchinson et al. (2000) record three layers of sand within a sequence of muddy gyttja in a core collected from Deserted Lake, located close to present sea level at the head of a fjord on the central west coast of Vancouver Island. The authors attribute these sands to tsunamis created by earthquakes at the Cascadia subduction zone, c. 2600, 1600 and 300 years ago. Other examples from active plate boundaries of modern and Holocene tsunami deposits identified in coastal lakes include those from Canada (Witter et al. 2012), Japan (Sawai et al. 2008) and Chile (Kempf et al. 2015). On the passive coastal margins of northwest Europe, stratigraphic evidence for the AD 1755 Lisbon tsunami is described from a coastal pond on the Scilly Isles (southwest English Channel) by Foster et al. (1993), whilst inundation of coastal lakes by the early-Holocene Storegga landslide is reported from a number of sites in Norway (e.g. Bondevik et al. 1997b; Romundset et al. 2011).

The early-Holocene Storegga tsunami, triggered by a large (3000 km^3) submarine landslide off southwest Norway, is dated to 8120-8175 cal a BP (Bondevik et al. 2012). Tsunami models predict that it would have struck the east coast of Greenland with a run-up of 3 to 5 m (Harbitz, 1992). Wagner et al. (2007) report evidence of the Storegga tsunami impacting what was, at the time of the event, a marine basin with water depths of 15-35 m located in NE Greenland. The sedimentary evidence of the tsunami comprises a 0.72 m thick sandy layer with an erosive base and distinct variations in grain-size distribution. In addition, in a study of lake stratigraphies in the Ammassalik area of SE Greenland, Long et

al. (2008) record a distinct sand unit within coastal lake stratigraphy that was deposited around the time of the Storegga tsunami.

The abrupt inundation of quiet-water lacustrine settings can have a significant impact on the nature of the pre-existing sediment body, and cause the deposition of a complex range of deposits associated with the tsunami and the immediate post-tsunami period. Bondevik et al. (1997a) developed an erosional and depositional model for tsunami, based on their analysis of the impact of the Storegga tsunami as it inundated coastal basins in Norway. We use this model as a baseline against which we compare the stratigraphic signature of potential tsunami in Greenland lakes.

The typical stratigraphic signatures of tsunami deposits in lakes, as described by Bondevik et al. (1997a), include;

1. An erosional unconformity underlies the tsunami deposit. Typically the erosion increases towards the seaward part of the basin, due to high lee-side turbulence as the tsunami crossed the shallow lake threshold resulting in high lake-bed shear velocities. These processes may erode lake sediments accumulated during several thousand years prior to the event.

2. The lowermost tsunami sand is typically a graded or massive sand, suggesting rapid deposition from suspension, and may also contain marine microfossils. The sand thins and fines in a landward direction.

3. Above the sand can be coarse organic detritus with rip-up clasts, termed an "organic conglomerate", and finer organic detritus. Some of this is derived from the lake bed itself, and some is inwashed from the surrounding area (e.g. Bondevik et al. 2012). After the final withdrawal of the tsunami, fines settle out from suspension and this may lead to deposition of a thin, laminated silt above the main tsunami deposits. This deposit is thought to have formed in anoxic bottom-water conditions with reduced bioturbation caused by salt-water remaining in the basin for a period after the tsunami.

4. Basins that are higher above sea-level at the time of the event typically record only one sand unit, whereas lower basins may record several sand units separated by organic detritus, reflecting distinct wave trains that impact lower basins.

5. In the case of the Norwegian basins, the typical Storegga tsunami sand thickness is 20-100 cm.

Bondevik et al. (1997a) also consider alternative explanations for these types of lake deposits. They note that the overall geometry of the basin stratigraphy precludes flash flood deposits or sediment slumping from the lake sides, whilst the presence of marine microfossils indicates a marine origin for the deposits. Moreover, they observe that storm surge deposits normally reach only a small height above normal tide levels and cannot explain the inundation of basins that lie many meters above the contemporary sea level.

It is important to note, however, that the stratigraphic model described above is developed from a large, sea-floor generated tsunami. This model may differ to one applicable to a tsunami generated by an iceberg or a local landslide that reached the sea. Tsunami modelling suggests that the Storegga tsunami had a wavelength of c. 600-800 km (Bondevik et al. 2005). In contrast, iceberg-generated tsunami differ because the of the lower amount of energy released. The origin of these waves is usually in relatively shallow water, so the wavelengths are shorter than in large earthquake-generated tsunamis. This means that wave energy dissipates rapidly and their impacts tend to be recorded only relatively close to the tsunami source. However, sea bed topography has the potential to amplify tsunami height at the local scale, especially on polar coasts that are typically characterised by areas of high relief. Landslide-generated tsunami are also capable of generating large waves, notably where they enter the sea in topographically restricted areas. Thus, in the case of the Paatuut tsunami, local residents at Saqqaq recorded multiple waves for nearly 2.5 hours. The long duration of the waves must have been due to reflection on multiple occasions by the steep sides of the Vaigat fjord (Dahl-Jensen et al. 2004).

There are other factors that may also mean that the stratigraphic model of Bondevik et al. (1997a) requires adaption for Greenland. For example, the sedimentary signal of a tsunami will vary depending on local ground conditions, including whether there is lake and/or sea ice, or whether the ground is frozen or snow-covered. Romundset and Bondevik (2011) note that these factors could reduce a tsunami's erosive capability and hence the availability of sediment for erosion from nearshore and possibly beach shoreface sources. Rip-up clasts from terrestrial sources would not be expected in such conditions. Tsunami grain size differences might also be expected for a winter tsunami strike; tsunami sediment

deposited on ice would melt out in a complex manner, with variable sediment thicknesses and more irregular grading to the tsunami sand (Romundset and Bondevik 2011).

Another characteristic of Greenland coastal lakes is that they typically have low sedimentation rates compared with Norwegian lakes, and this will influence the stratigraphic signature of a tsunami. Low sedimentation rates in Greenland caused by low organic productivity partly reflect the length of seasonal ice-cover and frozen catchments, and also low lake temperatures and nutrient availability. Bindler et al. (2001) and Malmquist et al. (2003) use ^{210}Pb and ^{137}Cs to determine typical sedimentation rates of between 0.12 to 3.7 mm yr for lake deposits accumulated in the last 100-150 years. Over Holocene timescales, Fredskild (1983) states that typical Greenland lake sedimentation rates are between 0.13 and 0.37 mm yr (similar values are also provided by Eisner et al. (1995) and Bennike (2000)). Greenland lake deposits are therefore often thin and can also be very soft, with a high water content.

3. Study site

The study site of Innaarsuit is located on the south shores of Disko Bugt, a large marine embayment on the west coast of Greenland (Fig. 5.1). At the Last Glacial Maximum, the ice sheet extended across the entire bay. At or shortly after the start of the Holocene (c. 11,700 cal a BP) the ice sheet margin was located at the eastern mouth of Disko Bugt, before retreating rapidly to reach the eastern shores of the bay by c. 11,000-10,000 cal a BP (e.g. Long et al. 2003; Kelley et al. 2013; 2015; Young et al. 2011). Several large marine-terminating ice streams, including Jakobshavns Isbrae, discharged icebergs into the bay during this retreat phase and throughout the remainder of the Holocene. Jakobshavn Isbrae presently discharges 25 to 50 km^3 of icebergs into Jakobshavn Isfjord each year (Joughin et al. 2004; Rignot and Kanagaratnam 2006). Amundson et al. (2008) observed icebergs calving from the ice stream terminus with a thickness of c. 900 m, a kilometre in lateral width and several hundred meters in the flow direction. Each iceberg rotated 90° within 5 minutes, displacing up to c. 0.5 km^3 of water. These icebergs travel 45 km along the Isfjord and must then cross into Disko Bugt via the Isfjeldsbanken (Fig. 5.1), a shallow bank (50–300 m water depth) that forms a significant topographical barrier to the large icebergs (Hogan et al. 2011). The depth of the wider Disko Bugt varies between 200 and 400 m (Brett and Zarudski 1979; Chalmers et al. 1999), defining an upper limit to iceberg size in coastal water of Disko Bugt. Once in Disko Bugt proper, most icebergs drift into Davis Strait via the

Vaigat strait (north Disko Bugt) or along the southern coast of Disko Island. Some icebergs also drift towards or into southern Disko Bay from Davis Strait due to the onshore component of ocean currents to the west of Aasiaat.

Following deglaciation, land uplift caused RSL to fall across Disko Bugt during the early- and mid-Holocene (Long et al. 2011). At Innaarsuit, which became ice-free early in the Holocene, RSL fell from a local marine limit (the highest occurrence of marine deposits) of c. 108 m at 10,300–9900 cal a BP (calibrated years before present) to reach the present sea level at c. 3500 cal a BP (Long et al. 2003). Here, a prominent inlet, Tasiusarsuit (Fig. 5.1), extends southward 5 km from the open waters of Disko Bugt (Fig. 5.3) and the isolation basins studied by Long et al. (2003) are located on the western margin of this inlet. The present-day tidal range is c. 2.5 m and mean high water is c. 1.1 m above mean sea level (MSL).

Tasiusarsuit is connected to Disko Bugt by a shallow and narrow eastern sill and a deeper western sill that has a present width of c. 150 m. Icebergs from Disko Bugt entering Tasiusarsuit via this entrance are restricted in size by this sill. Present water depths across this sill are >23 m (Fig. 5.3) but would have been c. 20 m deeper deeper in the mid-Holocene, when RSL was higher (see below, Fig. 5.6). This means that there was any iceberg entering Tasiusarsuit c. 6000 cal a BP had a maximum thickness of c. 45 m. Inland of the sill, water depths deepen again into Tasiusarsuit proper, and offshore from the study site lakes are presently c. 50 m deep (implying a water depth of c. 70 m at c. 6000 cal a BP).

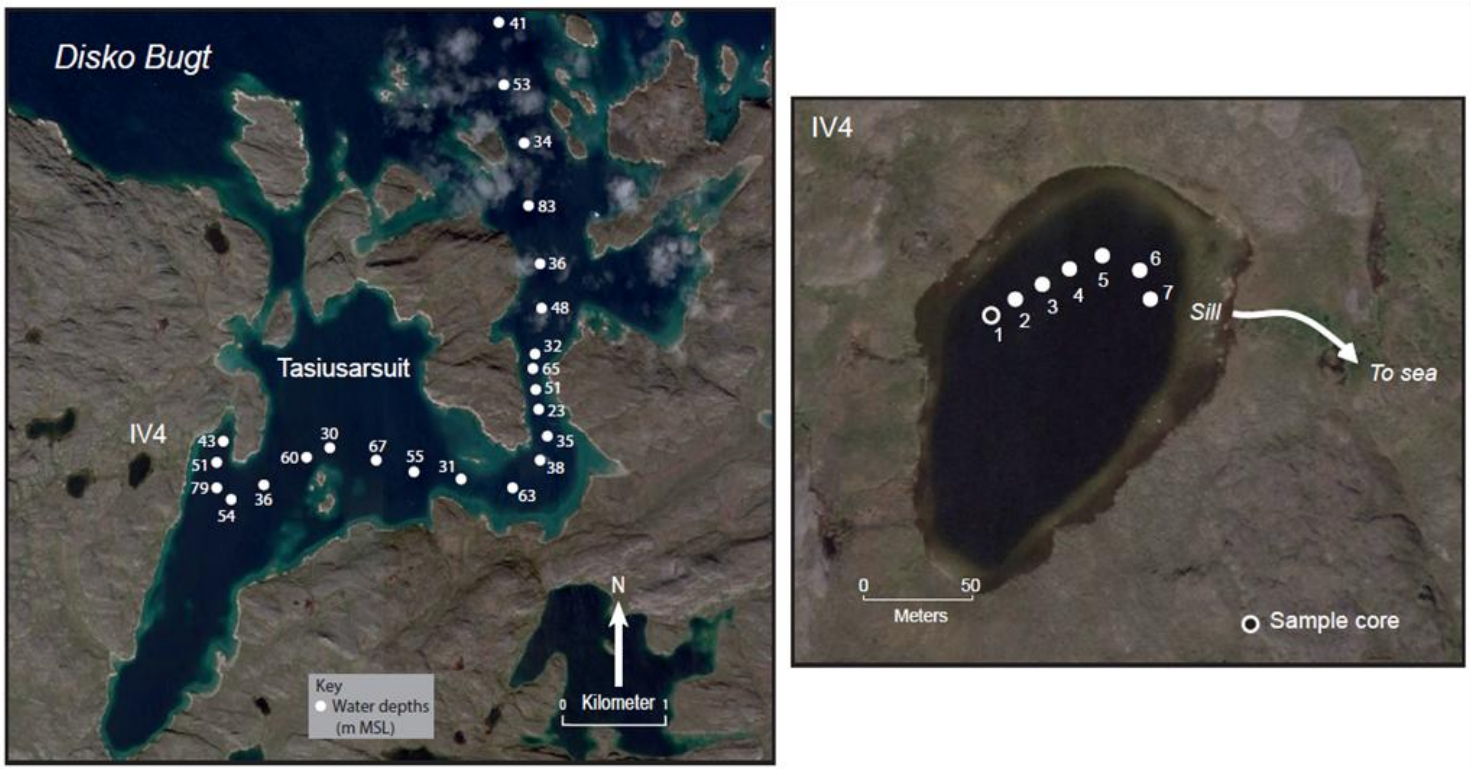

Figure 5.3. The Innaarsuit study area showing lakes cored as part of the relative sea-level study of Long et al. (2003). Lake IV4 is the focus of this chapter. The numbers annotated on the left-hand panel indicate water depths (m above MSL).

Long et al. (2003) collected stratigraphic data from six lakes at Innaarsuit. Lake IV4, an isolation basin that is the focus of this study, is a kidney-shaped lake, c. 270 m long and 170 m wide and located c. 21 m above present MSL (Fig. 5.3). Water-depths in the lake are c. 6 m, with a sediment thickness between c. 1 to 1.5 m. A stratigraphic transect of 7 hand cores (Figs. 5.3 and 5.4) identified a grey-blue silty sand in the base of the lake that was deposited under marine conditions, which fines upward into a laminated, brackish-water, organic silty clay. Overlying the silty organic clay is a dark brown to grey, freshwater silty gyttja (an organic lake mud). Diatoms through this sequence record the basins' gradual isolation from the sea, which was dated to 5440 ± 60 BP (6212-6447 cal a BP) (Table 5.1).

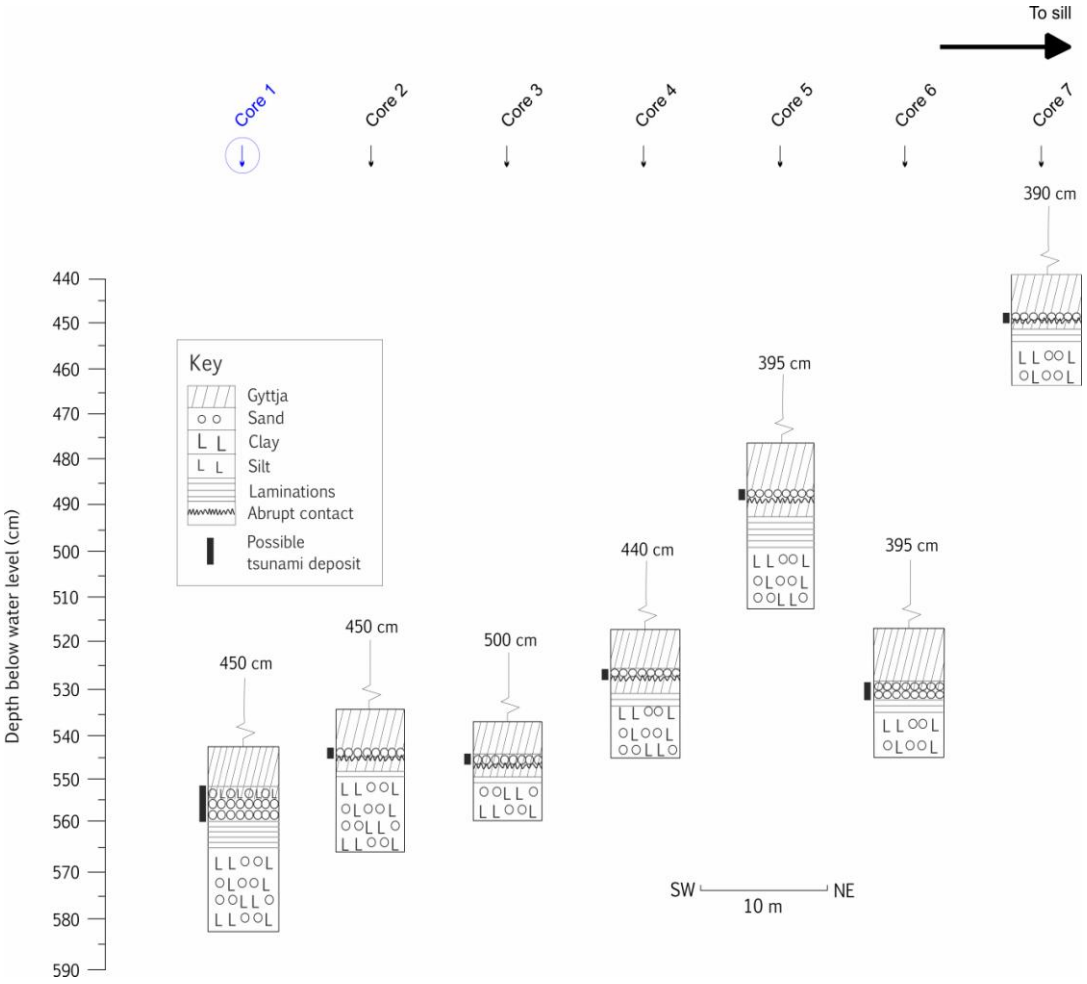

Figure 5.4. The lithostratigraphy of lake IV4, identifying the anomalous deposit and the sample core (core 1) used for detailed analysis. Only the lowermost part of the stratigraphy in each core is shown; the uppermost lake gytjja deposit in each core extended up to lake bed at the depth indicated.

Shortly after its isolation from the sea there was a brief incursion of saltwater into the basin, as indicated by diatom data. The incursion was accompanied by erosion of the underlying gyttja and the deposition of a thin (1- to 4-cm-thick) sheet of sand across the lake bed. The depth of erosion increases toward the north (seaward end) of the lake. A radiocarbon date from immediately above this anomalous sand layer yielded a date that, when calibrated, overlapped with the age of basin isolation at the 2σ age range (5620 ± 60 BP, 6292-6530 cal a BP). Long et al. (2003) briefly considered the origin of this deposit, suggesting that because the basin faces east and has a relatively protected aspect, the most obvious candidates for this incursion were either a storm surge or an exceptional wave caused by an iceberg roll-generated tsunami, or landslide-generated tsunami.

4. Methods

The original sample core was collected in July 2000 using a modified piston corer, from a small inflatable boat tethered to the lake shore. Half of the core was sampled for the initial study of Long et al. (2003), with the other half wrapped in plastic and refrigerated. The latter provided the basis for the new data described in this paper.

We used a GEOTEK Multi-Sensor Core Logger (MSCL) system based in the Geography Department at Durham University to quantify a suite of geophysical measurements from the IV4 sample core. The core image was captured using a Geotek GEOSCAN IV line-scan camera. We use magnetic susceptibility to assess the degree of magnetization of a material in response to an applied magnetic field. Measurements were made with a Bartington loop sensor (MS2C), using a low intensity (approx. 80 A/m RMS) non-saturating, alternating magnetic field (0.565 kHz), with values cited in SI units. The sampling interval for magnetic susceptibility was 0.2 cm.

Samples for diatom analysis were prepared using standard methods (Palmer and Abbott, 1986), identified with reference to Hartley (1996) and grouped according to the halobian classification scheme of Vos and de Wolf (1988; 1993), with minimum counts of 200 diatom valves. The original sampling interval for diatom analysis of 1 cm intervals is increased to 0.25-0.5 cm throughout the key sections of core. Summary diatom data are presented in Fig. 5.5, and full data are shown in Appendix 1, Fig. S1.

The original chronology for the sequence was based on two bulk AMS radiocarbon dates on lake gyttja that dated the basin isolation from the sea and the start of gyttja sedimentation following the deposition of the anomalous sand layer. Plant macrofossils are rare in the core and so here we report a further 4 AMS dates on bulk sediment, pre-treated using standard methods (e.g. Czernik and Goslar 2001) and dated at the Poznan Radiocarbon Laboratory in Poznan, Poland. Ages are calibrated (IntCal13; Reimer et al. 2013) and given as 2σ ranges (Table 5.1). With one exception the dates are in age sequence. We use Bayesian age modelling software OxCal 4.1 (Bronk Ramsey 2009a), utilising the *P_sequence* function which allows for random fluctuations in deposition rate. The model builds prior densities for each point (priors) before building posterior (modelled) densities for each point using stratigraphic information, Bayesian algorithms and a Monte Carlo Markov Chain random sampling approach (Gilks et al. 1996). Model agreement is provided by an "agreement index" (AI), with AI >60% the accepted threshold for good agreement (Bronk Ramsey 2008). Our age model carries an agreement index of 89%, indicating

excellent internal agreement, and enables us to generate modelled ages for key stratigraphic levels (Table 5.2).

Grain size analysis was performed on one sample from the anomalous sand deposit, using a Malvern Mastersizer 2000 Particle Analyser on material pre-treated with hydrogen peroxide to remove organic matter, and with sodium hexametaphosphate and ultrasound prior to the analyses to avoid aggregation. Grain size statistics were calculated using the logarithmic method of moments with GRADISTAT software (Blott and Pye 2001). Organic content is expressed as percentage loss on ignition (LOI) determined by combustion of 1-cm thick sediment slices at 550°C for a minimum of four hours.

5. Results

We present the combined physical property, diatom data and age model for the sample core in Fig. 5.5. Diatom diversity was relatively low with 19 taxa identified. Overall, the sequence records four discreet episodes of environmental change that reflect the control of both short- and long-term RSL fluctuations on basin sedimentation. Below, we discuss these four episodes in turn, from older to younger.

Table 5.1. List of radiocarbon ages from the sample core in lake IV4, Innaarsuit, Disko Bugt (west Greenland). All dates are on 1-cm thick bulk sediment samples. Dates are calibrated using Calib version 7.1.

Code	Mid sample depth (cm)	Laboratory code	Radiocarbon age BP, ±1σ	Calibrated age BP, ±2σ	Source
IV4-1	532.5	Poz-53393	5730 ± 40	6415-6637	This paper
IV4-2	531.5	AA-39652	5540 ± 60	6212-6447	Long et al. (2003)
IV4-3	527.5	Poz-53392	5350 ± 40	6000-6272	This paper
IV4-4	526	AA-39651	5620 ± 60	6292-6530	Long et al. (2003)
IV4-5	525	Poz-53391	5210 ± 40	5903-6174	This paper
IV4-6	518	Poz-53629	4665 ± 35	5313-5570	This paper

Table 5.2. Modelled ages of the main events recorded in the IV4 stratigraphy based on the use Bayesian age modelling software OxCal 4.1 (Bronk Ramsey 2001) – see text for details and Figure 4 for the age model itself. IV4-4 is not in age sequence and is excluded from the analysis.

Code	Mid sample depth (cm)	Mean calibrated age BP	95% probability age range (cal yr BP)	68% Probability age range (cal yr BP)
IV4-1	532.5	6487	6403-6614	6412-6525
IV4-2	531.5	6303	6205-6405	6236-6397
Basin isolation	530.5	6256	6138-6388	6179-6311
IV4-3	527.5	6112	6000-6261	6021-6192
Base of sand	527.25	6087	5963-6242	6000-6143
Top of sand	525.5	5984	5910-6104	5930-6010
IV4-5	525	5957	5900-6093	5924-5985
IV4-6	518	5420	5315-5575	5322-5567

Marine (544-534 cm)

The base of the IV4 sequence between 544-534 cm (16-26 cm core depth) comprises a blue-grey, silt-sand associated with low LOI (3%) and moisture content (34%) (Fig. 5.5). Diatom data show a marine origin for the deposit, with samples dominated by *Navicula digitoradiata*. Lesser assemblage contributions are provided by *Gyrosigma balticum*, *Nitzschia sigma* and *Nitzschia apiculata*. Sediment magnetic susceptibility is high, reflecting a relatively low content of diamagnetic substances (calcite, quartz, water, or organic matter). These are interpreted to be marine sediments that were deposited prior to the basins' final isolation from the sea.

Basin Isolation (533-530.5 cm)

Between 533-531 cm (12.5-16 cm core depth) the sediment is a brown, organic silt-clay with

black laminations that are slightly inclined, likely a result of the coring and subsequent extrusion of the sediment from the piston sample tube. Diatoms within this unit record the basins' gradual isolation from the sea, with marine taxa becoming replaced by increased frequencies of freshwater species. Key freshwater taxa include *Mastogloia ovata, Rhopalodia musculus, Fragilaria virescens* and *Fragilaria pinnata*. We define the basins' final isolation from the sea by the last occurrence of marine taxa at 530.5 cm, dated in our age model to 6388-6138 cal yr BP (Table 5.2). Up-core, moisture content and LOI increases across the isolation contact, indicating a switch from minerogenic to organic deposition. Conversely, sediment magnetic susceptibility undergoes a gradual decrease.

Freshwater (530.5-528 cm)

Between 531-528 cm the sediment is a dark brown-grey, silty-gyttja. Diatoms within the gyttja are dominated by fully freshwater taxa, as indicated by an assemblage dominated by the freshwater-indifferent *Fragilaria construens, Fragilaria virescens, Fragilaria pinnata* and *Fragilaria brevistriata*. LOI is relatively high (>10%) while magnetic susceptibility of sediments is low, likely reflecting increased organic matter content. Moisture content is the highest encountered in the sequence (55-60%).

"Anomalous deposit" (527.5-526)

Overlying the freshwater gyttja between 527.5-526 cm is an anomalous deposit. The base comprises a thin (5 mm-thick) yellow-white silty medium sand (89.6 % of sand) rich in quartz and mica. Mean grain size is within the fine sand class (2.29 phi), the principal mode is in medium sand (1.49 phi), the sediment is poorly sorted, very fine skewed and characterised by a leptokurtic distribution. LOI sharply decreases within the sand. Immediately overlying the sand is 1-cm of silty gyttja. Diatom analysis shows a mixed-salinity assemblage that is dominated (95%) by the taxa encountered in the freshwater gyttja and across the isolation contact (see above). However, a notable minor assemblage contribution (10%) of *Navicula digitoradiata* and *Mastogloia ovata* supports a marine origin of the deposit. The top of the sequence is constrained by a single black laminae that we interpret reflects a return to quiet-water sedimentation. Magnetic susceptibility undergoes an abrupt increase across the entire anomalous deposit, but also extends up-core by a further 1.5 cm. In our age model (Fig. 5.5, Table 5.2), the base of the medium sand ('base of deposit') is

dated to 6242-5963 cal yr BP, while the black laminae ('top of deposit') is dated to 6104-5910 cal yr BP, which defines a mathematical age range of 6242-5910 for the anomalous deposit (2σ modelled age range).

Freshwater (518-525 cm)

The upper 7 cm of the section is comprised of dark brown-grey, silty-gyttja, recording a return to organic-dominated sedimentation and final return to freshwater conditions. Overall, the diatoms encountered are identical those observed in the lower gyttja between 531-528 cm, while LOI and moisture content is also similar, averaging 15% and 59% respectively.

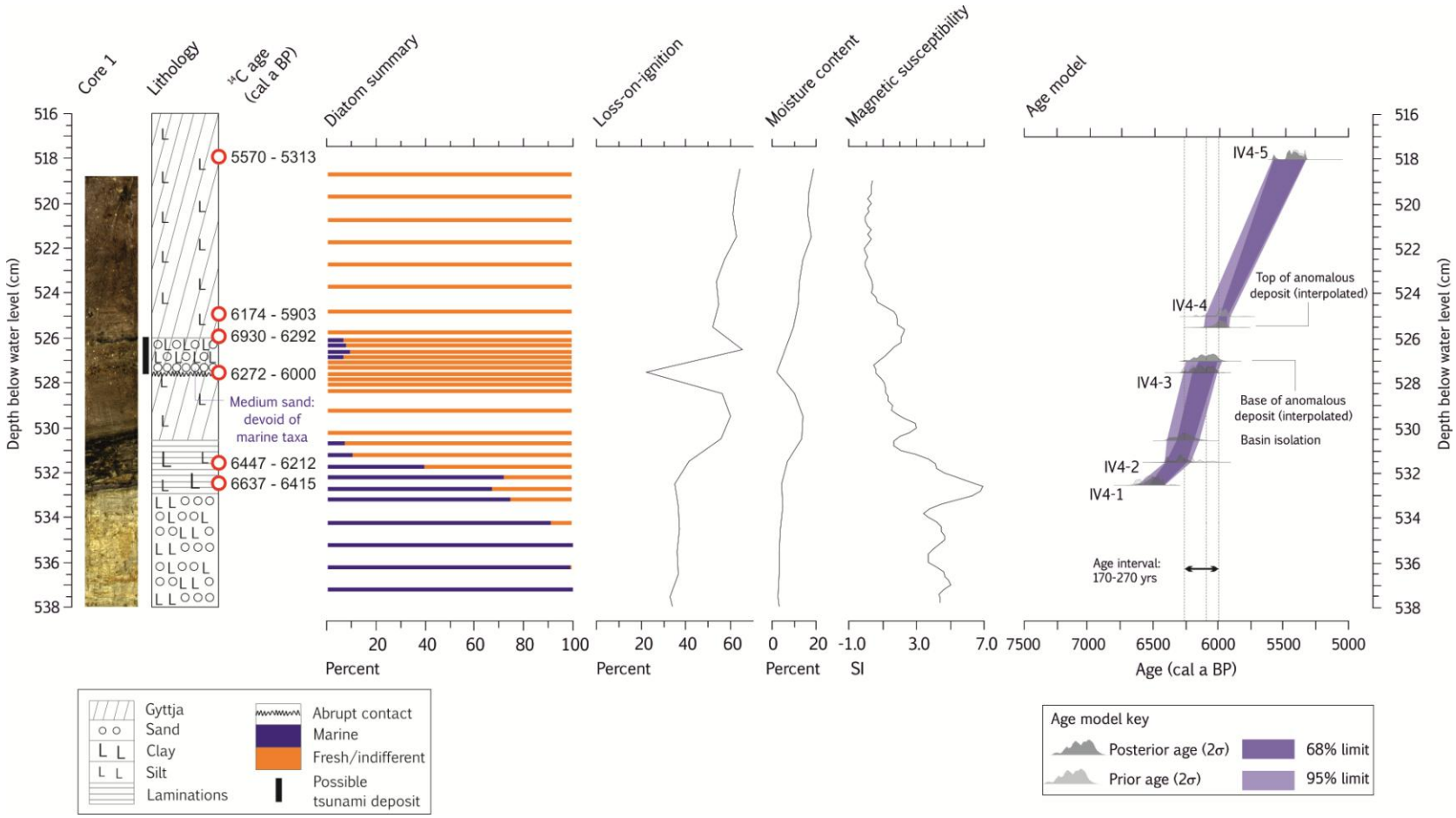

Figure 5.5. Litho-, bio- and chronostratigraphic data from IV4 sample core (core 1). The anomalous deposit is highlighted with calibrated radiocarbon dates on the left (2σ age ranges) and modelled ages on the right. The original radiocarbon dates and the modelled ages are detailed in Tables 1 and 2 respectively.

6. Discussion

6.1 Estimation of minimum flooding run-up height

The starting point of our discussion is to quantify the minimum run-up of sea-water inundation required to deposit the anomalous sand unit observed in the IV4 lake, which we do by combining our new age model for the sequence with what we know about RSL changes at the time of the event. The rate of RSL fall during the mid-Holocene at Innaarssuit is well-constrained by data from this site and from an adjacent site to the west; Queqertarsuatsiaq (Fig. 5.6) (Long and Roberts 2002). They show that RSL (MSL) fell from 31 m at c. 7.7 k cal a BP to 20.3 m by 6.2 k cal a BP (the date for isolation in IV4) and then continued to fall to reach c. 2 m by 3.9 k cal a BP. This is equivalent to a rate of RSL fall of c. 0.81 cm yr. We use this estimated rate of RSL fall to infer the run-up required to re-flood the IV4 basin.

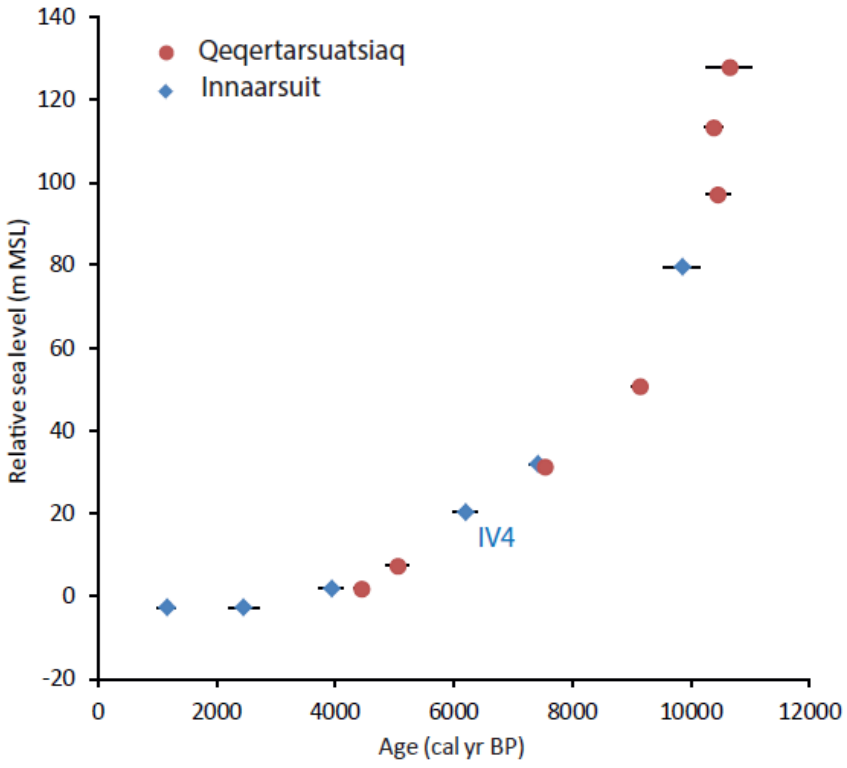

Figure 5.6. Relative sea-level history of Innaarsuit and Qeqertarsuatsiaq (original data are from Long et al. (2003) and Long and Roberts (2003)). The x-error uncertainties are the 2σ calibrated age range of each radiocarbon date, and the y-axis errors are less than the symbol sizes (see original publications for details).

The best-estimate age for basin isolation and sand deposition in IV4 have mean modelled ages of 6256 and 5984 cal a BP respectively (Table 5.2), hence there was an interval of c. 270 years between the two events. During this interval, RSL fell by c. 2.2 m (i.e. 270 years x 0.0081 m yr), meaning the wave must have had a run-up of at least this size to ingress the basin. This estimate assumes that event struck at the same point in the tidal cycle as existed when the basin was isolated (i.e. mid-way between Highest Astronomical Tides and Mean High Water of Spring Tides, c. 1.05 ± 0.59 m above MSL). Given that this level is high in the tidal frame and only reached by some of the highest tides of the year, it is more likely that the event struck at a lower tide position. This would increase the run-up required to inundate the basin. For example, if we assume that the event occurred at a point mid-way through the tide cycle, then the run-up would have been closer to 3.3 m. These estimates are also based on median age estimates. Utilizing the full 95% probability age estimates (modelled using OxCal), then the estimated maximum / minimum run-up range (assuming a mid-tide cycle event) would have been c. 5.0 / 1.3 m.

6.2 Depositional origin of the sand layer in IV4

The original interpretation by Long et al. (2003) of the anomalous sand in IV4 was equivocal regarding its depositional origin. They dismissed a non-marine origin (e.g. freshwater runoff or a slump within the lake) and noted that the most likely explanation was that it formed by either a storm surge or an exceptional wave caused by an iceberg roll-generated tsunami, or a landslide-generated tsunami.

We think an exceptional storm is unlikely as the cause of the sand unit observed in lake IV4 for several reasons. First, this is a low tidal range, protected coastal setting. The field site at the time of the event was located at the western end of a quiet-water inlet, with a maximum wind fetch (from the east) of about 3 km (Fig. 5.3). Direct observations of storm surge heights in Disko Bugt are not available, but wind speed data are available from several sites in the bay (e.g. Hansen et al. 2006). These show that the highest wind speeds each year are recorded in the winter months, when strong easterly air flow from the Greenland Ice Sheet dominates. In contrast, wind speeds are generally significantly lower in the summer months and are recorded with easterly and westerly directions. Strong winter winds coincide with low air temperatures that cause sea ice to freeze, especially in protected embayments, such as the study area. Therefore, the strongest winter winds are not able to generate large wave set-up because of the frozen sea and lake surfaces in winter months. A

combination of limited wave fetch, low tidal range and weak summer winds when open waters exist suggest that a large storm surge is an improbable mechanism to explain the sand deposit in IV4.

We now assess the stratigraphic evidence for the anomalous sand unit in IV4 having been formed by a tsunami, using the five criteria described by Bondevik et al. (1997a) from the Storegga tsunami.

1. An erosional unconformity underlies the sand in all cores in IV4. The amount of erosion is greatest close to the sill of the basin and decreases inland, where it is recorded at progressively higher levels within the stratigraphic sequence. In core 6, for example, close to the sill, the sand lies unconformably above the laminated sediments of the isolation contact, indicating the likely erosion of sediments that accumulated during several centuries. This pattern suggests greater turbulence near the sill and lee-side erosion caused by the erosive impact of the tsunami as it flooded over the basin sill.

2. The sand is a medium sand composed mainly of quartz and mica, suggesting rapid deposition from suspension. Its composition likely represents local beach conditions (the source of sediment) and shows that the coast was not affected by large storm waves. Beaches within the region of the study area that are commonly affected by storms are typically characterised by much coarser sandy and gravel sediments (e.g. Drewniak et al. 2014).

3. Immediately above the reworked gyttja in the cores 1, 3 and 6, we observe a faintly laminated unit that contains marine diatoms. We interpret this unit as forming as a result of salt water remaining in the basin following inundation, causing a period of anoxic bottom-water conditions and reduced bioturbation. A radiocarbon date from a sample just above the sand unit is not in chronological order, suggesting that it includes older, reworked organic matter. It likely contains some of the fine-grained sediments eroded by the tsunami and deposited after the inundation that deposited the sand layer.

4. We did not sample a staircase of vertically closely-spaced basins (they do not exist), which might have enabled identification of one or more sand units. Within IV4 there is a single sand unit with no intervening organic detritus, suggesting that a single wave inundated the basin or the period between successive waves was too brief to allow permanent deposition.

5. In contrast to the Norwegian examples, the tsunami deposit package is thin. The IV4 tsunami deposit sand unit itself is <3 cm thick, whilst the laminated sediments that formed after the event are found over only a further 1-3 cm. This may partly reflect the relatively small size of the wave but it may be also be due to a limited source of local sediment (the present-day intertidal zone adjacent to IV4 is rocky with little beach).

On the basis of the above comparison, we interpret the anomalous sand horizon in IV4 as having been formed by a tsunami, generated by either a landslide entering the sea or the rolling of an iceberg. We note that there are no existing stratigraphic criteria to distinguish between these potential mechanisms, and instead rely on our interpretation of the topographic setting of the study site, as well as what we presently know about the magnitude and frequency of landslide- and iceberg-related events in Disko Bugt.

In Disko Bugt, the prime source areas of landslides that terminate in the sea are Vaigat and the south coast of Disko Island (Fig. 5.1) (Pederson et al. 2001; Dahl-Jensen et al. 2004). A large landslide in Vaigat is unlikely to direct a tsunami of sufficient size across Disko Bugt to impact in the Innaarsuit area. For example, the Paatuut tsunami was recorded at Saqqaq, 40 km east of the landslide by local residents who filmed unusual waves arriving onshore. Although the initial waves were not observed, those that were recorded were only c. 1.5 m in height (Dahl-Jensen et al. 2004). This suggests that wave refraction within Vaigat acts to significantly reduce tsunami size in Disko Bugt proper. Landslides generated from the south coast of Disko Island provide an alternative potential source of landslide-generated tsunami although there is no record of landslide-generated tsunami from this location. The area is directly opposite the Innaarsuit field site, but any wave would have had to overcome both the small skerries and islands that lie offshore of Tasiusarsuit, where it would likely amplify, but would then have been dissipated within the deeper waters of Tasiusarsuit as it approached the shore adjacent to the IV4 lake. We therefore consider a landslide-tsunami, originating from Vaigat or the south coast of Disko Island, an unlikely source for the anomalous sand unit observed in lake IV4.

The second possibility is that the sand unit in IV4 originated by a tsunami that was generated by a local iceberg rolling within Tasiusarsuit. Icebergs enter Tasiusarsuit today and would have done so more freely in the middle Holocene, when RSL was higher than present. Based on the depth of the Tasiusarsuit inlet, the largest icebergs that were able to drift into Tasiusarsuit were probably rather small, with a maximum height of c. 45 m at the time of the event. Based on the simple rule of thumb proposed by MacAyeal et al. (2011), were an iceberg of this size to roll it would generate a tsunami with a wave height of c. 45

cm in open water, but this could have been significantly amplified in the restricted waters of the Tasiusarsuit inlet. This simple calculation supports several lines of evidence that suggest the tsunami was relatively small (> 3 m run-up height), including the inferred run-up from the RSL data, the thinness of the sand unit and the limited erosion of the underlying lake sediment. We also note that the IV4 sand unit is the only evidence for marine inundation during the c. 200 year time interval when RSL fall meant that a tsunami had the chance to reach the lake. The likelihood of a local iceberg roll as the cause of this tsunami is higher than that of a landslide-generated event, since the latter happen relatively infrequently. Indeed, as noted above, the Paatuut landslide was the largest event in at least 500 years and its impact was modest beyond Vaigat with, for example, little evidence for wave disturbance at Ilulissat, a distance of c. 130 km from the tsunami source (Dahl-Jensen et al. 2004). The south coast of Disko Bugt is c. 70 km from Innaarsuit and any landslide-generated wave would likewise dissipate energy crossing the bay and then entering Tasiusarsuit.

6.3 Stratigraphic and morphological evidence for iceberg-generated tsunami elsewhere in Disko Bugt

The potential for iceberg-generated tsunami is recognised elsewhere in Disko Bugt in sedimentological studies from the south coast of Disko Island, and in beach geomorphology adjacent to the marine-calving glacier Equip Sermia (Fig. 5.1). In a description of the coastal geomorphology of three cuspate forelands at Saqqrlitt Ilorlitt (Fig. 5.1), Rasch et al. (1997) describe the stratigraphy of several small coastal lagoons which comprise coarse sand layers within finer-grained sandy-clayey silts. The authors suggest that some of these sand layers might have resulted from "a short but dramatic event like a washover caused by a storm, calving of a large iceberg or a tsunami".

At Equip Sermia (Fig. 5.1), a large marine calving glacier in the north of Disko Bugt, Nielsen (1991) describes a coarse boulder beach located 2.5 km from, and directly opposite, the calving front. The site is located within the inner part of a fjord system where fetch is restricted and normal waves are typically very small. Nielsen (1991) concludes that "large waves generated by glacier calving, and/or sea-ice action, are therefore the only processes that can explain the geomorphology and clast distribution of this coastal feature". The Equip Semia example is not directly comparable to the situation in our study of IV4, since the proposed mechanism of wave generation is the collapse of the calving ice front of the glacier. However, icebergs are frequent in front of the Equip Sermia and it would seem likely that they, as well as direct ice face collapse, have the potential to generate waves in

this setting. Moreover, it is possible that the Innaarsuit wave was generated by the collapse of a grounded iceberg, as oppose to an iceberg roll – we cannot differentiate between these potential causes.

Our re-analysis of the IV4 stratigraphy, and the observations by Rasch et al. (1997) and Nielsen (1991), prompt us to re-analyse the stratigraphy of previously cored isolation basins elsewhere in Disko Bugt in order to assess whether there is evidence in any of these lakes for potential tsunami deposits. Arveprinsens Eijland is located in the northeast of Disko Bugt (Figs. 5.1 and 5.7) and was the site for a RSL study by Long et al. (1999). It is an ideal site to examine evidence of iceberg-generated tsunami due to the position of the sampled lakes immediately adjacent to Vaskebugt (Arveprinsens Eijland, Figs. 5.1 and 5.7), a deep fjord that harbours large icebergs that drift into the bay en route from the ice sheet towards the Vaigat and Davis Strait.

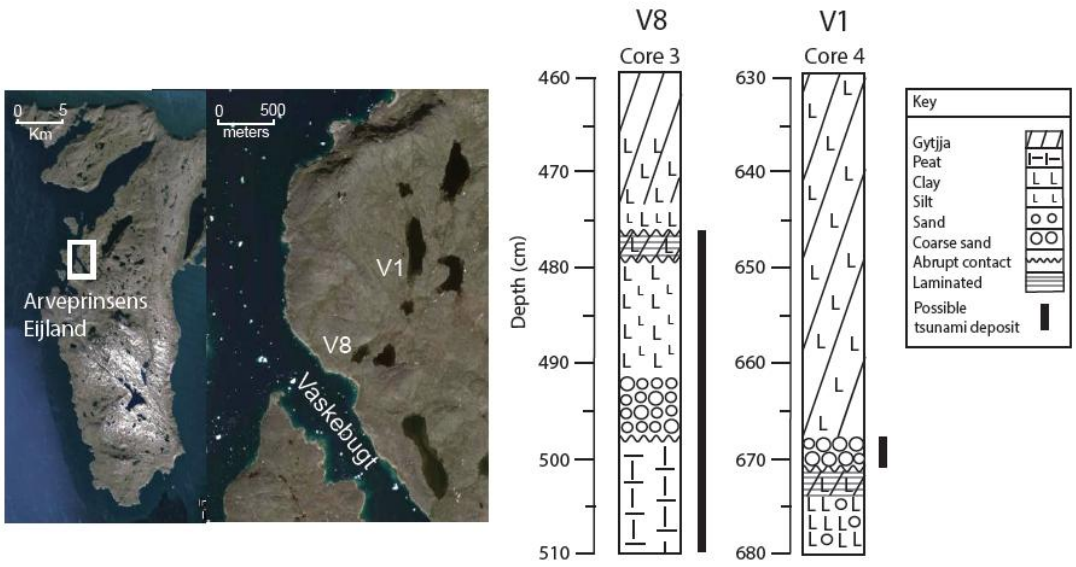

Figure 5.7. Location map and representative core stratigraphies from two isolation basins sampled on Arveprinsens Eijland (Long et al. 1999). The core numbers refer to those reported in the original study. The potential tsunami deposits are highlighted.

Several of the lakes sampled in this area may indeed contain evidence for tsunami inwash, evidence that Long et al. (1999) originally attributed to sediment slumping (e.g. Fredskild 1995). For example, the basal lake sediments of basin V8 (lake sill c. 14 m asl, core 3) comprise a deposit of dark red/brown *turfa* (rooted remains of herbaceous plants) with some detrital herbaceous matter that overlie an impenetrable substrate (Fig. 5.7). This is abruptly overlain by a sequence of interbedded organic silts and sands, which grade up into a

homogenous lake gyttja that extends to lake bed. In two of the deeper cores, a thin, faintly laminated silt gyttja is recorded above the silts and sand. This silt gyttja unit may record anoxic conditions in the basin after a marine incursion, similar to that observed in the IV4 core and also described from Norwegian lakes following the Storegga tsunami (Bondevik et al. 2005). The disturbed nature of the stratigraphy in this basin, including the presence of *turfa* in the stratigraphy of V8, suggests reworking of terrestrial vegetation and lake deposits by a marine incursion that flooded the basin and the adjoining land surface.

In a higher lake that was isolated in the early Holocene (V1, lake sill c. 61 m asl, isolated c. 9000 cal BP), Long et al. (1999) observed close to the transition between the lower marine silts and sands and the overlying freshwater gyttja a prominent horizon of coarse sand and angular gravel, between 2 cm and 0.5 cm thick (Figure 5.7). In some instances the coarse horizon is recorded immediately above the marine sediments, whilst in several cores it occurs within the base of the gyttja. Diatom data from core 2 (not shown) indicate a subtle marine influence in the sand. Viewed together, the V1 stratigraphy resembles elements of the tsunami sediment model described by Bondevik et al. (1997a), including the erosive base to the sand and the presence of marine diatoms in the sand.

A re-analysis of the stratigraphic data from two isolation basins on Arveprinsens Eijland suggests that they may have been impacted by tsunami during or shortly after their isolation from the sea. Arveprinsens Eijland is located close to the Nassuaq Peninsula, a known source of landslide-triggered tsunami (Pederson et al. 2001). However, the site is protected from the open coast to the west by a large bedrock ridge, meaning that the most likely cause of tsunami here are local icebergs. We have studied well over a hundred isolation basins in various RSL studies in Disko Bugt and elsewhere in Greenland (see Long et al. 2011). Reviewing these records we observe that only a small number have potential tsunami deposits within them. Those lakes that may preserve such evidence tend to be located adjacent to deep water and close to a source of icebergs. Our sampling strategy for RSL studies normally avoids these locations, by focussing on quiet, protected settings where a staircase of basins exists within a small geographical area. A more targeted sampling strategy towards basins located in favourable settings in Greenland or other polar regions would, we suspect, identify many more potential iceberg-generated tsunami sequences.

The potential for iceberg tsunami is likely to be higher during periods of large iceberg production, such as when marine-based portions of ice-sheets retreat rapidly. One such period would have been after the Last Glacial Maximum as the ice sheets retreated across their continental shelves. Evidence for equivalent events might be expected, therefore,

in lake basins in Greenland and elsewhere that were deposited close to the marine limit and which were isolated from the sea shortly after deglaciation. Such periods would potentially include iceberg-generated waves as well as those caused by direct calving from the ice sheet margin into the sea, as described from Equip Sermia (Nielsen 1991). However, more extensive sea-ice at this time may have reduced wave heights by dissipating wave energy. Indeed, there is a trade-off between the rate of RSL change and the potential to record tsunami, because a rapidly falling RSL will quickly put many meters, or even tens of meters, between an isolation basin and sea level. For these reasons, we hypothesise that some of the best records of iceberg-generated tsunami are likely preserved in low-lying coastal basins that developed during periods when RSL was changing slowly, yet when there were still sufficient icebergs to generate tsunami. There are many such lakes along the margins of the Greenland Ice Sheet, adjacent to large marine-terminating ice streams that have been active throughout the mid and late Holocene, that have the potential to record such events.

7. Conclusions

Iceberg tsunamis are a potentially significant coastal hazard in Arctic areas, especially where icebergs roll in topographically restricted settings and where the resulting waves can be amplified. We present, for the first time, a detailed stratigraphic study of a sedimentary record of an iceberg-generated tsunami from a field site in Disko Bugt. Our key conclusions are:

1. Relative sea-level fell quickly during the early- and mid-Holocene in Disko Bugt, isolating shallow embayments and rock-bound basins from the sea and converting them into lakes. This process resulted in a distinctive stratigraphic record that at its simplest comprises a marine deposit that is overlain by a mixed salinity transitional unit and then wholly freshwater lake gytjja. Departures from the long-term trend of RSL fall, by an abrupt event such as a storm or tsunami, has the potential to disrupt this sequence and create a distinctive stratigraphic signal.

2. Analysis of a lake basin stratigraphy (IV4) at Innaarsuit, located in a protected inlet on the south shore of Disko Bugt, reveals evidence for a distinct sand unit that interrupts the tripartite isolation basin stratigraphy noted above. The stratigraphic characteristics of this

sand, and its adjacent deposits, are similar to those described by Bondevik et al. (1997a) based on their analysis of the sedimentary signature created by the impact of the early Holocene Storegga tsunami on coastal lakes in Norway. We use the background trend in RSL to estimate a wave run-up of c. 3.3 m, assuming the event happened at mid tide cycle.

3. We note that there are no sedimentary criteria that uniquely separate a tsunami generated by an icerberg roll or a landslide that enters the sea. In this case, however, several site factors favour an iceberg- over a landslide-origin for the tsunami, including: i) the low frequency of large landslides in the past within Disko Bugt and an absence of any known local landslide sources within the Innaarsuit study area, ii) the limited propagation of landslide generated waves from their main source area in Disko Bugt (Vaigat), iii) the large distance between potential landslide source areas in Disko Bugt and the Innaarsuit study area, iv) an abundance of icebergs in Disko Bugt that, under a higher than present relative sea level during the mid-Holocene, could have entered the Tasisusarsuit study area, and v) the known ability of even relatively small icebergs to generate locally large waves in topographically restricted settings.

4. Suitable conditions for iceberg roll, and the generation of a sedimentary record of a resulting tsunami, include an ample supply of icebergs, deep water close to the shore, a protected depositional setting, and a coastal configuration that has the potential to amplify small waves as they shallow and impact the coast.

5. We conclude by reflecting that global warming will lead to increased calving, at a time when human use of the Arctic coast will also grow. We predict, therefore, that iceberg-generated tsunami will become a growing hazard in Arctic coastal waters, especially in areas adjacent to large, fast flowing marine-terminating ice streams that are close to human populations or infrastructure.

References

Amundson JM, Fahnestock M, Truffer M, Brown J, Lüthi MP, Motyka RJ (2010) Ice mélange dynamics and implications for terminus stability, Jakobshavn Isbræ, Greenland. J Geophys Res 115: DOI: 10.1029/2009JF001405

Amundson JM, Truffer M, Lüthi MP, Fahnestock M, West M, Motyka RJ (2008) Glacier, fjord, and seismic response to recent large calving events, Jakobshavn Isbra, Greenland. Geophys Res Lett 35: L22501: 10.1029/2008GL035281

Bennike O (2000) Palaeoecological studies of Holocene lake sediments from west Greenland. Palaeogeog Palaeoclim Palaeoecol 155: 285-304

Bindler R, Renberg I, Appleby PG, Anderson NJ, Rose NL (2001) Mercury accumulation rates and spatial patterns in lake sediments from west Greenland: a coast to ice margin transect. Environ Sci Technol 35: 1736-1741

Blott SJ, Pye K (2001) GRADISTAT: a grain size distribution and statistics package for the analysis of unconsolidated sediments. *Earth Surf Proc Land* 26: 1237-1248

Bondevik S, Svendsen JI, Mangerud J (1997a) Tsunami sedimentary facies deposited by the Storegga tsunami in shallow marine basins and coastal lakes, western Norway. Sedimentology 44: 1115-1131

Bondevik, S., Svendsen, J.I., Johnsen, G., Mangerud, J., Kaland, P.E., 1997b. The Storegga tsunami along the Norwegian coast, age and runup. Boreas 26, 29–53.

Bondevik S, Løvholt F, Harbitz C, Mangerud J, Dawson A, Svendsen JI (2005) The Storegga Slide tsunami - comparing field observations with numerical simulations. Mar Petrol Geol 22: 195-208

Bondevik S, Stormo SK, Skjerdal G (2012) Green mosses date the Storegga tsunami to the chilliest decades of the 8.2 ka cold event. Quat Sci Rev 45: 1-6

Brett CP, Zarudzki EFK (1979) Project Westmar: a shallow marine geophysical survey on the West Greenland shelf. Rap Grøn Geol Unders 87: 1-27

Bronk Ramsey C (2009a) Bayesian analysis of radiocarbon dates. Radiocarbon 51: 337-360

Buchwal A, Szczuciński W, Strzelecki M, Long AJ (2015) Tree-ring structure of *Salix glauca* reveals evidence of a 2000 AD tsunami event in west Greenland: implications for Arctic paleotsunami and paleoecological studies. Polish Polar Res 36: 51-65

Chalmers JA, Pulvertaft TCR, Marcussen C, Pedersen AK (1999) New insight into the structure of the Nuussuaq Basin, central West Greenland. Mar Petrol Geol 16: 197-224

Czernik J, Goslar T (2001) Preparation of graphite targets in The Gliwice Radiocarbon Laboratory for AMS 14C dating. Radiocarbon 43: 283-291

Dahl-Jensen T, Larsen LM, Pedersen SAS, Pedersen J, Jepsen HF, Pedersen GK, Nielsen T, Pedersen AK, Von platen-Hallermund F, Weng W (2004) Landslide and tsunami 21 November 2000 in Paatuut, west Greenland. Nat Hazards 31: 277-287

Dawson AG, Long D, Smith DE (1988) The Storegga Slide: evidence from eastern Scotland for a possible tsunami. Mar Geol 82: 271-276

Didenkulova I, Pelinovsky E (2011) Runup of tsunami waves in U-shaped bays. Pure Applied Geophys 168: 1239-1249

Drewniak M, Strzelecki M, Szczuciński W (2014) Factors controlling beach development in Vaigat Strait, West Greenland - insights from automated grain size analysis. In: Migała K (ed) Diversity and state of polar ecosystems. Results of the 35th Polar Symposium Wrocław, 5-7 of June 2014 University of Wroclaw, pp 189-203

Eisner WE, Törnqvist TE, Koster EA, Bennike O, van Leeuwen JFN (1995) Paleoecological studies of a Holocene lacustrine record from the Kangerlussuaq (Søndre Strømfjord) region of West Greenland. Quat Res 43: 55-66

Foster IDL, Dawson AG, Dawson S, Lees J, Mansfield L (1993) Tsunami sedimentation sequences in the Scilly Isles, southwest England. Sci Tsunami Haz 11: 35-46

Fredskild B (1983) The Holocene vegetational development of the Godthåbsfjord area, west Greenland. Medd. Gronl. Geosci 10: 1–28

Fredskild B (1995) Palynology and sediment slumping in a high arctic Greenland lake. Boreas 24: 345–354

Fritz HMF, Mohammed A, Yoo J (2009) Lituya Bay landslide impact generated mega-tsunami 50th anniversary. Pure App. Geophys. 166: 153-175

Gilks WR, Richardson S, Spiegelhalter DJ (1996) Markov chain monte carlo in practice. London, Chapman and Hall

Hansen BU, Elberling B, Humlum O, Nielsen N (2006) Meteorological trends (1991–2004) at Arctic Station, Central West Greenland (69°15') in a 130 year perspective. Dan J Geog 106: 45-55

Harbitz CB (1992) Model simulation of tsunamis generated by the Storegga Slides. Marine Geol 105: 1–21

Hartley B, Barber HG, Carter JR, Sims PA (1996) An Atlas of British Diatoms. Biopress, Bristol, England, 601 pp

Hill J, Collins GS, Avdis A, Kramer SC, Piggott MD (2014) How does multiscale modelling and inclusion of realistic palaeobathymetry affect numerical simulation of the Storegga Slide tsunami? Ocean Modelling 83: 11-25

Hogan KA, Dix JK, Lloyd JM, Long AJ, Cotterill CJ (2011) Seismic stratigraphy records the deglacial history of Jakobshavn Isbrae, West Greenland. J Quat Sci 26: 757-766

Hutchinson I, Clague JJ, Mathewes RW (1997) Reconstructing the tsunami record on an emerging coast: a case study of Kanim Lake, Vancouver Island, British Columbia, Canada. J Coastal Res 13: 545-553

Joughin I, Abdalati W, Fahnestock M (2004) Large fluctuations in speed on Greenland's Jakobshavn Isbrae glacier. Nature 432: 608-610

Kelley SE, Briner JP, Young NE (2013) Rapid ice retreat in Disko Bugt supported by 10Be dating of the last recession of the western Greenland Ice Sheet. Quat Sci Rev 82: 13-22

Kelley SE, Briner JP, Zimmermann SR (2015) The influence of ice marginal setting on early Holocene retreat rates in central West Greenland. J Quat Sci 30: 271-280

Kempf P, Moernaut J, Van Daele M, Vermassen F, Vandoorne M, Pino W, Urruttia R, Schmidt S,. Garrett E,. De Batist M. (2015) The sedimentary record of the 1960 tsunami in two coastal lakes on Isla de Chiloé, south central Chile. Sedimentary Geol. 328: 73-86

Levermann A (2011) When glacial giants roll over. Nature 472: 43-44

Long AJ, Roberts DH (2003) Late Weichselian deglacial history of Disko Bugt, West Greenland, and the dynamics of the Jakobshavns Isbrae ice stream. Boreas 32: 208-226

Long AJ, Roberts DH, Wright MR (1999) Isolation basin stratigraphy and Holocene relative sea-level change on Arveprinsen Eijland, Disko Bugt, West Greenland. J Quat Sci 14: 323-345

Long AJ, Roberts DH, Rasch M (2003) New observations on the relative sea level and deglacial history of Greenland from Innaarsuit, Disko Bugt. Quat Res 60: 162-171

Long AJ, Roberts DH, Simpson MJR, Dawson S, Milne GA, Huybrechts P (2008) Late Weichselian relative sea-level changes and ice sheet history in southeast Greenland. Earth Plan Sci Letts 272: 8-18

Long AJ, Woodroffe SA, Roberts DH, Dawson S (2011) Isolation basins, sea-level changes and the Holocene history of the Greenland Ice Sheet. Quat Sci Rev 30: 3748-3768

MacAyeal DR, Okal EA, Aster RC, Bassis JN (2009) Seismic observations of glaciogenic ocean waves (micro-tsunamis) on icebergs and ice shelves. J Glaciol 55: 193-206

MacAyeal DR, Scambos TA, Hulbe CL, Fahnestock MA (2003) Catastrophic ice-shelf break-up by an ice-shelf-fragment capsize mechanism. J Glaciol 49: 22-36

MacAyeal DR, Abbot DS, Sergienko OV (2011) Iceberg-capsize tsunamigenesis. Ann Glaciol 52: 51-56

Malmquist C, Binder R, Remberg I, van Bavel B, Karlsson E, Anderson NJ, Tysklind M (2003) Time trends of selected persisent organic pollutants in lake sediments from Greenland. Environ Sci Tech 37: 4319-4324

Monserrat S, Vilibic I, Rabinovich AB (2006) Meteotsunamis: atmospherically induced destructive ocean waves in the tsunami frequency band. Nat Hazards Earth Syst Sci 6: 1035-1051

Nielsen N (1991) A boulder beach formed by waves from a calving glacier; Eqip Sermia, West Greenland. Boreas 21:159-168

Nishimura Y (2008) Volcanism-induced tsunamis and tsunamiites. In: Shiki T, Tsuji Y, Yamazaki T, Minoura K (eds) Tsunamiites-Features and Implications. Elsevier Science, Amsterdam, Oxford, pp 163-184

Ozawa S, Nishimura T, Suito H, Kobayashi T, Tobita M, Imakiire T (2011) Coseismic and postseismic slip of the 2011 magnitude-9 Tohoku-Oki earthquake. Nature 475: 373-376

Palmer AJM, Abbott WH (1986) Diatoms as indicators of sea-level change, in: Van de Plassche O (ed.), Sea-Level Research: A Manual for the Collection and Evaluation of Data, Geo Books, Norwich, pp. 457–488

Pedersen SAS, Dahl-Jensen T, Jepsen H, Larsen LM, Pedersen GK, Nielsen T, Pedersen AK, Weng W (2001) Fjeldskred ved Paatuut. Rep. 2001/99, Geological Survey of Denmark and Greenland, Copenhagen

Rasch M, Jakobsen BH, Nielsen N (1997) Geomorphology and sedimentary record of three cuspate forelands as indicators of late Holocene relative sea-level changes, Disko, West Greenland. Danish J Geog 97: 33-46

Reimer PJ, Baillie MGL, Bard E, Bayliss A, Beck JW, Blackwell PG, Ramsey CB, Buck CE, Burr GS, Edwards RL, Friedrich M, Grootes PM, Guilderson TP, Hajdas I, Heaton TJ, Hogg AG, Hughen KA, Kaiser KF, Kromer B, McCormac FG, Manning SW, Reimer RW, Richards DA, Southon JR, Talamo S, Turney CSM, van der Plicht J, Weyhenmeye CE (2009) IntCal09 and Marine09 radiocarbon age calibration curves, 0-50,000 years cal BP. Radiocarbon 51: 1111-1150

Rignot E, Kanagaratnam P (2006) Changes in the velocity structure of the Greenland Ice Sheet. Science 311: 986-990. DOI: 10.1126/science.1121381

Romundset A, Bondevik S (2011) Propagation of the Storegga tsunami into ice-free lakes along the southern shores of the Barents Sea. J Quat Sci 26: 457-462

Sawai Y, Fujii Y, Fujiwara O, Kamataki T, Komatsubara J, Okamura Y, Satake K, Shishikura M (2008) Marine incursions of the past 1500 years and evidence of tsunamis at Suijin-numa, a coastal lake facing the Japan Trench. The Holocene 18: 517-528

Scambos TA, Fricker HA, Liu CC, Bohlander J, Fastook J, Sargent A, Massom R, Wu AM (2009) Ice shelf disintegration by plate bending and hydro-fracture: Satellite observations and model results of the 2008 Wilkins Ice Shelf break-ups. Earth Plan Sci Letts 280: 51-60

Subarya C, Chlieh M, Prawirodirdjo L, Avouac J-P, Bock Y, Sieh K, Meltzner AJ, Natawidjaja DH, McCaffrey R (2006) Plate-boundary deformation associated with the great Sumatra-Andaman earthquake. Nature 440: 46-51

Tappin DR, Sibley A, Horsburgh K, Daubord C, Cox D, Long D (2013) The English Channel 'tsunami' of 27 June 2011: a probable meteorological source. Weather 68: 144-152

Wagner B, Bennike O, Klug M, Cremer H (2007) First indication of Storegga tsunami deposits from East Greenland. J Quat Sci 22: 321-325

Weiss R, Lynett P, Wünnemann K (2015) The Eltanin impact and its tsunami along the coast of South America: insights for potential deposits. Earth Plan Sci Letts 409: 175-181

Witter RC, Zhang Y, Wang K, Goldfinger C, Priest GR, Allan JC (2012) Coseismic slip on the southern Cascadia megathrust implied by tsunami deposits in an Oregon lake and earthquake-triggered marine turbidites. J Geophys Res 117: B10303. doi: 10.1029/2012JB009404

Wünnemann K, Weiss R (2015) The meteorite impact-induced tsunami hazard. Phil. Trans. R.

Soc. Lond. A 373: 20140381.http://dx.doi.org/10.1098/rsta.2014.0381

Velicogna I (2009) Increasing rates of ice mass loss from the Greenland and Antarctic ice sheets revealed by GRACE. Geophys Res Letts 36: L19503, doi:10.1029/2009GL040222

Vos PC, de Wolf H (1988) Methodological aspects of paleoecological diatom research in coastal areas of the Netherlands. *Geol en Mijnb* 67: 31-40

Vos PC, de Wolf H (1993) Diatoms as a tool for reconstructing sedimentary environments in coastal wetlands; methodological aspects. Hydrobiol 267/270: 285-296

Young NE, Briner JP, Stewart HA, Axford Y, Csatho B, Rood DH, Finkel RC (2011) Response of Jakobshavn Isbræ, Greenland, to Holocene climate change. Geology 39: 131-134

Appendix 3

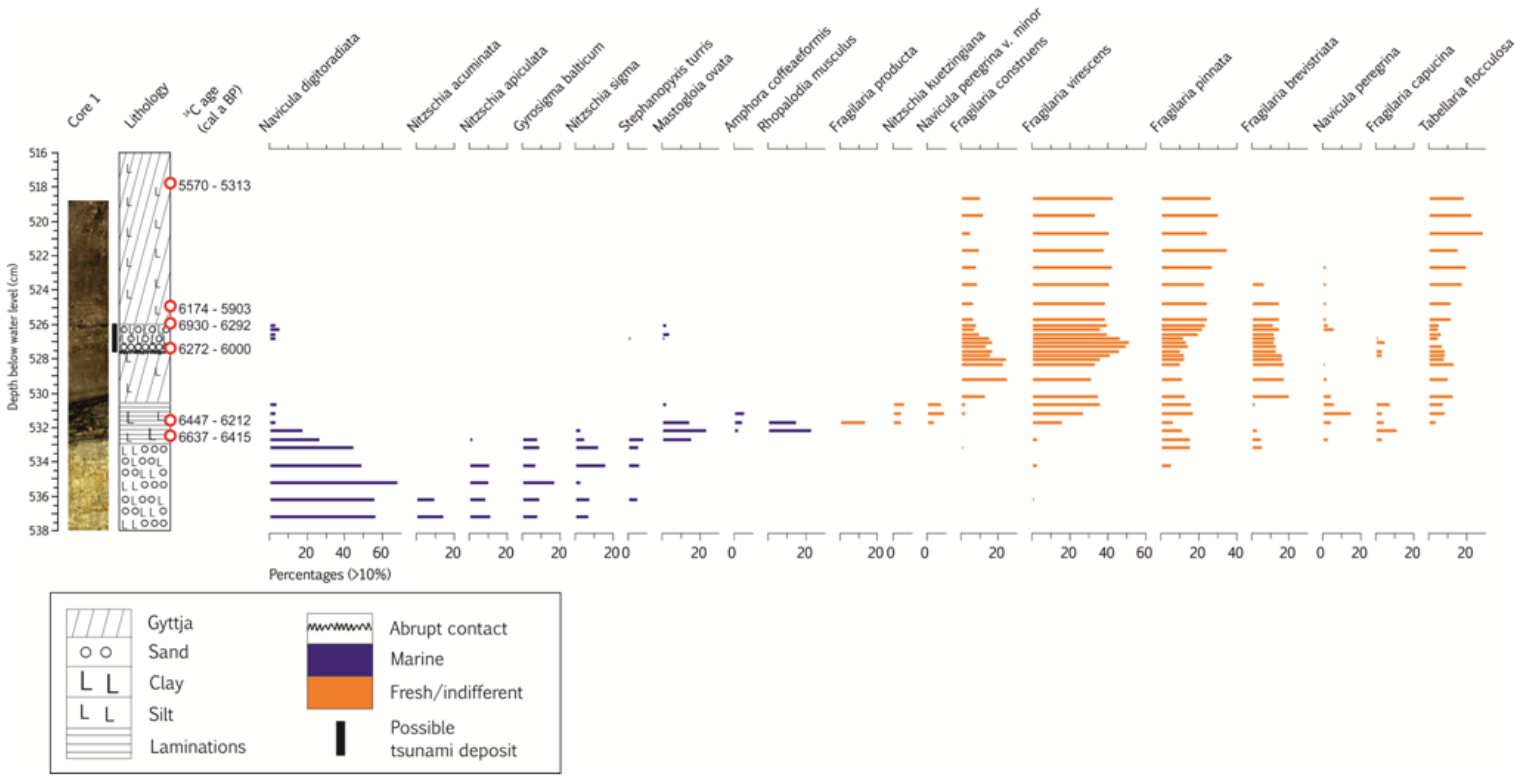

Fig. S1. Full diatom diagram from the sample core at IV4.

6

Discussion

6.1 Introduction

In the previous four chapters I have developed records of abrupt RSL change from a range of depositional contexts at two near-field settings; one a presently active glacial environment and the other an ice-free setting since the late glacial. In this chapter, I begin by interpreting an "event chronology" of tsunami activity for Vaigat by holistically appraising the findings presented in the standalone studies outlined in Chapters 3 (nearshore sedimentary records) and 4 (lake stratigraphic record). Second, I assess the challenges and opportunities with regards to reconstructing episodes of rapid RSL change in near-field settings using the knowledge acquired from all studies (addressing Objective 5). Finally, I examine the wider significance of RSL records, once developed.

6.2 The late Holocene tsunami history of Vaigat Strait, west Greenland

This thesis has assessed the stratigraphic evidence of abrupt events in Vaigat with two separate analyses, with each focusing on two contrasting types of depositional environment. The first presented an array of records from nearshore sedimentary environments (Chapter 3), while the second presents a coastal freshwater lake record (Chapter 4). Within these individual chapters, interpretations have been drawn based solely on the observations specific to each chapter. To provide a more holistic interpretation of Vaigat tsunami history, the following considers the observations from Chapters 3 and 4 together. This holistic interpretation is based on a synthesis of the data outlined in Table 6.1.

Table 6.1 Synthesis of abrupt sea-level events in Vaigat, west Greenland. Ages are with respect to AD unless otherwise stated. In simple terms, landslide tsunami events are inferred from the lake record (as the lake is placed altitudinally beyond the range of storm events - both past and present). Landslide tsunami are also likely where deposits of similar age are found in two geographically distinct areas, while those that are localised to single sites more likely reflect inundation by iceberg tsunami and/or minor landslide tsunami.

Lake VA1		**Sandstone Point**		**Moss Cliff**		**Interpretation**
Age	**Deposit**	**Age**	**Deposit**	**Age**	**Deposit**	
AD 2000* (TE-1)	Cap of coarse sand	**AD 2000***	Cap of coarse sand	**AD 2000***	Cap of coarse sand	Major landslide tsunami
		1953-2006	Sandy peat	**1897-1956**	Sandy peat	Major landslide tsunami
		1953-2011	Sandy peat	**1951-1959**	Coarse sand	
1358-1944 (TE-2)	Coarse sand	**1752-1955**	Sandy peat	No equivalent	Sandy peat	Possible landslide tsunami(s) or iceberg roll(s)
		1813-1910	Sandy peat	No equivalent	Sandy peat	
		1640-1680	Sandy peat	No equivalent		Iceberg roll event
1018-1172 (TE-3)	Coarse sand	**423-1056**	Silty clay	**686-1167**	Organic mud	Major landslide tsunami
356-570 (TE-4)	Coarse sand	No equivalent	No equivalent	No equivalent	No equivalent	Possible minor landslide tsunami
2338-2149 cal yr BP (TE-5)	Coarse sand	No equivalent	No equivalent	**2107-1807 cal yr BP**	Onset of peat accumulation	Possible minor landslide tsunami
* Assumed age on the basis of sample stratigraphic position (i.e. recent deposition)						

To recap, the nearshore sedimentary record contains evidence of five abrupt events within the past 1000-1500 yrs. The most recent two occurred at AD 2000 and AD 1952 and are attributed to landslides (Dahl-Jensen et al., 2004). The third most recent event occurred at AD 1811-1905, evidence for which is found at only one of two widely spaced sites (Sandstone Point). Accordingly, in Chapter 3 I attributed this event to a small landslide, iceberg-roll or storm event. The deposit of an event at AD 1640-1680 has no chronological equivalent in the study area and was also attributed to a small landslide, iceberg-roll or storm event. A final event occurred at AD 661-1048 and is present at both sites, albeit the evidence is equivocal at Sandstone Point. For this event, I ruled out the potential of iceberg-roll and storm events as emplacement mechanisms, concluding that a landslide-tsunami was the most probable responsible driving mechanism.

Similarly, the lake stratigraphic record also contains evidence of five separate episodes of marine inundation. The most recent reflects the landslide-tsunami in AD 2000 (TE-1), while earlier events occurred at AD 1358-1944 (TE-2), AD 1018-1172 (TE-3), AD 356-570 (TE-4) and 2338-2149 cal yr BP (TE-5). Given the protected setting of the lake, storm events were ruled out as the mechanisms responsible for the emplacement of these deposits. Further, it is unlikely that they record iceberg-roll events. Given the current RSL position, a run-up height of an iceberg-tsunami of a minimum 4.95 m is required to ingress basin VA1. It is unlikely that iceberg-rolls can generate tsunami of this magnitude (Chapter 5). In addition, the probability of ingression into VA1 is systematically reduced with extension into the late Holocene when RSL was lower. Thus, on the whole, I speculated that the majority of the deposits within the lake stratigraphic record reflect the inundation of large landslide-tsunami.

The correlation of deposits within the two different types of record enables better assessment of the driving mechanisms of Vaigat tsunami events. First, both depositional contexts contain evidence of the AD 2000 landslide-tsunami event, while evidence of the AD 1952 landslide-tsunami is restricted to the nearshore records. This either implies that, i) the run-up height of the AD 1952 event was insufficient to ingress the basin or, ii) that the event was not identified within the lake sequence because it occurred during winter; at a time when reconstructing tsunami events is challenging (see discussion in Section 6.3). Second, TE-2 coincides with the third most recent event within the nearshore record (AD 1811-1905), but evidence for this was restricted to Sandstone Point (i.e. no evidence present at Moss Cliff). Given the overlap of ages, it is logical to interpret that these record the same landslide-tsunami event, however given the relatively wide uncertainty attached to the age estimate from the lake (falling within a pronounced plateau within the ^{14}C calibration curve),

it remains possible that these record two separate iceberg-rolls or small landslide events. Third, the event at AD 1640-1680 was found in a single section local to the fjord-side of Sandstone Point. No further evidence of this was found within the lake record, supporting the initial interpretation that it reflects localized deposition by an iceberg-roll. Fourth, TE-3 overlaps in timing with the fifth and final event in the nearshore records at AD 661-1048, pointing to a landslide as the most probable driving mechanism. Finally, the base of the lake sequence records TE-5 but this contains no equivalent deposit within the terrestrial environment. It is interesting to note however that it preceded the onset of peat accumulation in Section J at Moss Cliff by a minimum of a few decades (2107-1807 cal yr BP) (Section 4.3.3), which could reflect erosion of pre-existing substrate and the subsequent delayed onset of peat accumulation following the event at Moss Cliff (e.g. Bondevik et al., 1997b; Smith et al., 2004).

In summary, there are trade-offs between the type of environment used in the reconstruction of abrupt RSL changes. The soft sediments within quiet-water depositional settings (lakes) are susceptible to disturbance by high-magnitude events such as landslide-tsunami, making it difficult to interpret stratigraphic history without a detailed program of dating and microfossil analyses, both of which are laborious and costly to implement. Lake environments however provide precise chronologies as short-lived material becomes inwashed and incorporated into the stratigraphy. Dating these has the potential to shave considerable uncertainty off reconstructed age estimates. However, ages based on bulk sediment slices can be anomalously old because of the basin 'hardwater' effect (Section 6.3.5.1). This is not a problem in the nearshore environment where bulk sediment slices appear to produce accurate and sometimes relatively precise ages. In contrast, nearshore chronologies can be negatively impacted where downward penetrating root material is sampled. Short-lived macrofossils such as seeds can also undergo significant post-depositional movement through widely-spaced rhizomes of Arctic shrubs (Section 6.3.5.1). A final important trade-off to consider reflects the application of microfossil analyses in order to identify marine deposits. It is significantly more challenging to identify marine taxa within diverse freshwater lake sequences than it is nearshore records characterized by low diversity assemblages.

6.3 Near-field coastal processes: challenges and opportunities

6.3.1 Climate and event timing

The processes that operate in near-field coastal environments undergo large-scale shifts from

season to season. Fundamentally, near-field settings are characterised by the operation of a distinct group of seasonal coastal processes; shoreline development in winter is impacted by distinctly "cold processes" - sea-ice formation, subsequent reduced wave-activity and the resistance of frozen surfaces to erosion and thus deposition. In contrast, summer months are characterised by inherently "warm processes" – warming leads to ice melt, the defrosting of surfaces, enhanced sediment supply and changes to patterns of erosion and deposition. Consequently, the dynamics of cold environments are strongly controlled by external climate forcing (Knight and Harrison, 2009; Strzelecki et al., in press), presenting challenges to reconstructing abrupt episodes of RSL change.

6.3.2 Reconstructing winter events

The reconstructions from both the Vaigat nearshore sedimentary and lake environments have shed important light on the many ways in which seasonality can impact reconstruction potential of an abrupt event – particularly those that occur in winter. Critically, the two most recent tsunami events in Vaigat – AD 2000 and AD 1952 – occurred in winter, enabling some assessment of the criteria for identifying winter tsunami deposits. This builds on the work of Romundset and Bondevik (2011), who list criteria for the potential identification of winter tsunami deposits in lake settings by logically inferring the potential patterns of erosion and deposition during winter (Chapter 4).

The post-winter thaw of frozen surfaces, both lacustrine and terrestrial (nearshore) presents the most significant challenge to identifying a proposed tsunami deposit with full confidence. In the Vaigat nearshore record the AD 2000 tsunami deposit is characteristically variable, reflecting irregular deposition during the event and modification of the associated tsunami deposit by post-depositional processes (Chapter 3, section 5.2). The same deposit within the lake environment is patchily preserved as a single grain-thick layer of coarse sand, supporting the earlier logic of Romundset and Bondevik (2011) in their assumption that irregular melting of lake ice will lead to irregular deposition of tsunami sediment. Material reworked by fluvial activity (snowmelt streams) from the adjacent lake banks further contributes to irregular patterns of deposition, while aeolian processes will rework fine- to coarse-grained material. The signatures of tsunami in nearshore records however, are typically strongly overprinted by post-depositional processes that occur in spring-summer months. For example the AD 1952 tsunami deposits are characteristically very thin and well-incorporated into under- and overlying tsunami soil (Section 5.1.2). The rapid spring recovery of densely-rooting hardy Arctic herbs and plants such as *Empetrum nigrum* and

Salix glauca initially promotes the stabilization of tsunami deposits and protects them from erosion, but eventually they are disturbed beyond the point of identification by bioturbation. Similar finds have been made on tropical coasts where coastal ecosystems thrive on extreme conditions (e.g. Szczuciński, 2012). Most deposits encountered were found unevenly incorporated into over- and underlying tsunami soils. Thus, post-depositional reworking of tsunami sediments make the signatures of winter events unclear and therefore very difficult to reconstruct with conventional methods used to reconstruct lower latitude events.

Despite the evidence that post-depositional reworking exerts a prime control on the marked thinness of tsunami deposits in Vaigat, other factors may also contribute, in particular the role of sea-ice. In winter months, fast ice ('landfast' ice) anchors itself to the sea-bed and can, dependent on shelter from prevailing winds and local bathymetry, extend between hundreds of metres to several hundreds of kilometers offshore (Kovacs and Mellor, 1974; Eicken et al., 2005). Studies from the Russian and Canadian Arctic illustrate that fast ice influences submarine coastal geomorphology by promoting the formation of shallow submarine benches in approximately 2 m water depth (Nalimov, 1995; Reminitz, 2000). If present in Greenland, how then, does fast ice, in addition to pack ice, impact the shoaling and sediment transport-capacity of a tsunami as it inundates the coastal zone? These questions are difficult to answer in the absence of tsunami modelling and/or pre- and post-tsunami monitoring studies, but it is reasonable to speculate that sea-ice affects wave power; including its sediment entrainment and transport capacity, in addition to its erosive ability as it shoals at the coast. Local variability in sea-ice thickness and extent could also dampen/enhance wave run-up, leading to localised variations in wave run-up height and inundation extent.

6.3.3 Tsunami frequency in near-field areas: climate-driven?

Coastal evolution in near-field regions is strongly influenced by climatic controls. In a classic paper, Forbes et al. (1995) proposed five key factors as critical in the evolutional development of paraglacial coasts, of which climate ranks fourth in the list: i) physiographical and geological setting, ii) RSL change, iii) glacigenic sediment supply, iv) climate and v) tides and river discharge. However, this paper was developed using examples from 'late-stage' (mature) paraglacial coasts such as Ireland and Atlantic North America. In paraglacial regions that are relatively 'early-stage' such as coastal west Greenland, sediment fluxes can vary markedly in response to climate-led glacier fluctuations (Nielsen, 1992; Mercier and Laffly, 2005; Ziaja et al., 2009; Zagorski et al., 2012). In turn, it is reasonable to

propose that high-amplitude fluctuations in sediment supply driven by upstream glacier changes will exert a strong control on coastal evolution, particularly on short centennial timescales (Strzelecki, 2012; Strzelecki *et al*., in press). Indeed the impact of climate in Vaigat is reflected in the stratigraphic record of Lake VA1 as a traceable litho- and biostratigraphic shifts (Figs. 4.4, 4.5 and 4.7). Evidence of the same event is also present in the nearshore records, albeit equivocally (Chapter 3, section 5.4).

The notion that climate exerts a strong positive control on coastal evolution might also be applicable on shorter interannual timescales. In Vaigat, tsunamis are primarily sourced from landslides that terminate in the sea. Dahl-Jensen et al. (2004) hypothesised that air temperature fluctuations and repeated freeze-thaw cycles was the causal mechanism of the landslide at Paatuut on 21 November AD 2000. Air temperatures in the days leading up to the event were uncharacteristically variable, with swings by 5-6 degrees (Dahl-Jensen et al., 2004). Climate as a causative control on the event was explored further by Buchwal et al. (2015), who, in Vaigat, interpreted injuries to the 2000-2001 growth rings of the *Salix glauca* shrub as evidence for solifluction induced by an over-saturated active layer. Indeed, their analysis of temperature and precipitation records revealed that AD 2000 was exceptionally warm and was the wettest since the year 1990 (Hansen et al., 2006). Hence, it is reasonable to propose two causative factors of the Vaigat landslide-tsunami, reflecting two important timescales: i) repeated freeze-thaw weathering; this requires uncharacteristically high-amplitude air temperature fluctuations (day-weekly timescales), ii) high-amplitude air temperature and precipitation changes, occurring on interannual-decadal timescales. Indeed the highest-amplitude temperature changes occur in the early/late winter months. It is interesting to note that the AD 1952 and AD 2000 landslides occurred in such months where there is greater amplitude of daily variation. I therefore propose the potential of "a winter window of opportunity", whereby repeated mechanical weathering (freeze-thaw) over a short time-window (days) promotes rock instability. In turn this increases the likelihood of landslide-tsunami strike in early/late winter months. This appears to be consistent with the winter patterns of deposition in the lake and nearshore records (Chapter 4, section 5.1; Chapter 3; section 5.1.2). As the climate of Arctic areas is thought to undergo major change over the next few decades in response to Arctic amplification feedbacks (e.g. Overland et al., 2013), the probability of climate-induced mass movements will likely grow.

It is plausible that iceberg-generated tsunami might also be strongly seasonally-controlled. Glacial and paraglacial coastal margins are constrained by sea-ice in winter months that 'lock' icebergs discharged from upstream glaciers into position. Melting is highly dependent on temperature, wave action, water currents, bubble release and wind

forcing (Diemand, 2001; Stern et al., 2015), parameters that in colder months would be dampened. In addition, sea-ice would dissipate wave energy and, at the coast, act as an important barrier to icebergs travelling from deeper waters. I therefore propose the potential of a "summer window of opportunity", whereby iceberg rollover events are restricted to warmer months (mainly summer). Indeed, the deposit interpreted to record and iceberg-tsunami in lake IV4 demonstrates a uniform pattern of deposition (Chapter 5, section 6.2). which is in contrast to the winter tsunami deposits recorded in Vaigat. With decreased sea-ice thickness, extent and increased glacier calving under a scenario of future warming (e.g. Wang and Overland, 2009; Nick et al., 2009; Rignot et al., 2010), it is also reasonable to propose that the future risk of iceberg-generated tsunami will increase.

6.3.4 Terrestrial processes

As discussed above, an overarching theme is that climate exerts a first-order control on coastal change in near-field areas by changing modes and patterns of sediment supply. In this regard, the continuity of a sequence and therefore its efficacy as a record of both long- and short-term coastal change is shaped by climate fluctuations occurring across a range of temporal scales.

Terrestrial processes influence the nearshore records in Vaigat. In Arctic areas, geomorphic activity is caused by the impact of precipitation on solifluction, frost weathering and active layer development (e.g. Cogley and McCann, 1976; Rouse et al., 1997; Lønne I, Lyså A, 2005). The slopes surrounding the study site on the south coast of Vaigat are strongly influenced by periglacial processes, including solifluction and frost heave (Buchwal et al., 2015). These processes deliver new sediment to the coastal zone from up-slope sources and modify the stratigraphic integrity of existing deposits. In this study, flame structures in the basal part of Section J indicate minor frost heaving (Chapter 3, section 4.3.1). Aeolian processes can also rework coastal and terrestrial sediments and result in the deposition of sand and silt within coastal sequences, although their study has been beyond the scope of this project.

The accumulation history of a lake sequence is driven fundamentally by the production of in situ organic material, and to a lesser extent, via the inwashing of allochthonous minerogenic material. This presents a number of key challenges with regard to reconstructing records from Greenland lakes. First, background accumulation rates are typically low because organic productivity is relatively low. Fredskild (1983) report typical accumulation rates of

0.13 and 0.37 mm/yr over the Holocene. This impacts the precision and temporal resolution of reconstructed records. Second, climate exerts an indirect control on stratigraphic development via influencing organic productivity. Climate-led changes to organic productivity can impart significant lithological and biostratigraphic changes (Fig. 4.5). Third, near-field areas are typically less well-vegetated rendering lake stratigraphies susceptible the inwashing of allochthonous material by fluvial activity. Indeed, average sediment accumulation rates in core 10A from Lake VA1 are higher than average at 0.73 mm/yr (Fig. 4.6). This probably reflects a greater composition of coarse-grained material within this small basin derived from the partly unvegetated slopes that surround the site by fluvial activity (e.g. Fig. 4.4). Finally, fluvial activity is strongly controlled by seasonality and climate such that climate exerts a second indirect control on record development. The benefit from this, however, is that when discovered in widely spaced cores or sites, climate-driven litho- and biostratigraphic changes can be used as useful chronostratigraphic markers to aid correlations. For example, a lake-wide litho- and biostratigraphic change in Lake VA1 reflects climate-related changes to lake productivity (e.g. Fig. 4.7). Dating the key transition reveals an apparent synchroneity with lake-wide stratigraphic shifts elsewhere in west Greenland records that have also been attributed to reflect regional climatic variability (Willemse and Tornqvist, 2008; Aelby and Fritz, 2009).

Deriving tsunami histories from small, shallow lakes such as VA1 is a challenge because the variable supply of coarse-grained sediment from the terrestrial environment obscures the search and identification of tsunami deposits. An opportunity might arise where larger, deeper lake sequences are targeted. For example, the stratigraphy of Lake IV4 contains minimal coarse-grained material within the fine-grained terrestrial portion of the sequence (Fig. 5.4). This enables preliminary interpretations to be made regarding the source of an anomalous deposit prior to it being sampled for further analysis, which has been a key mode of operating in studies of tsunami elsewhere (e.g. Kelsey et al., 2005; Hemphill-Haley, 1996). By contrast, understanding the significance of anomalous deposits in a smaller water body such as VA1 depends strongly on further primary analyses, particularly ^{14}C dating and high-resolution microfossil analyses, techniques that are costly and time-consuming.

It is clear from the Greenland studies discussed above that sediment supply is highly variable, mostly climate-led but unique to location, reflecting the control of a range of terrestrial processes. The Blair's Croft sequence in the Cree Estuary is, to my knowledge, the fastest accumulating depositional sequence ever observed for the short centennial-scale time period leading up to the 8.2 event. This is an important strength to the study because it leads to a highly resolved sedimentary record, but it also raises questions pertaining to the source

of sediment supply, as it is clear that Blair's Croft was a uniquely accumulating depositional setting in the early Holocene.

It is likely that the paraglacial nature of the Cree estuary in the early Holocene contributed to the high sediment supply and hence the eventual development of the high-resolution RSL record in two ways: i) an abundance of fine-grained sediment was delivered via fluvial activity from the recently deglaciated catchment and, ii) the reworking of relic glacial landforms at the coast promoted coarse-clastic barrier development. This back-barrier setting offered an ideal environment for net accumulation, offered a sheltered quiet-water setting away from the influence of strong tidal processes and wave action.

6.3.5 Dating near-field sequences

Chronological control provides an important means to validate the significance of event stratigraphies via the process of local to regional and, in some instances, global correlation. As the evidence for abrupt RSL change can initially appear equivocal, ensuring that stratigraphic events are accurately interpreted as regional in their RSL significance or whether they represent a manifestation of some localised terrestrial event requires tight dating control that is both accurate *and* precise. To this end, in studies of abrupt change in lower latitudes, dating has been recognized as a critical means to assess the wider significance of deposits inferred from 'spot sites', or single stratigraphies, when viewed alongside other criteria for the evidence of abrupt change (e.g. Nelson et al. 1996).

6.3.5.1 Absolute dating

As previously discussed, the near-field examples here are unlike those developed from lower latitude settings in that there is a distinct lack of clear criteria for the identification of abrupt events. Dating therefore becomes paramount in determining the wider significance of event stratigraphies, more so than in lower latitudes where interpretations are accompanied by a holistic range, or 'toolkit', of identification criteria (e.g. Chague-Goff et al., 2011).

The dating of near-field sequences is a non-trivial task for several reasons. First, low organic productivity in Greenland reflect a combination of the length of seasonal ice-cover and frozen catchments, low lake temperatures and nutrient availability. For instance, Bindler et al. (2001) and Malmquist et al. (2003) use ^{210}Pb and ^{137}Cs to determine typical sedimentation rates of 0.12 to 3.7 mm/yr for lake deposits accumulated in the last 100-150

years. Bulk sediment samples represent long centennial-scale time periods (thus, are imprecise but accurate) due to the averaging of several hundreds of years worth of organic material during the ^{14}C dating process. Nevertheless, as previously discussed, the close coupling of terrestrial processes and climate in near-field regions can generate lithological changes that can be traced over wide areas. In such cases these offer scope for use as chronostratigraphic markers.

Second, material suitable for dating in near-field areas is often scarce. Deposition is restricted to highly localised centres reflecting the importance of shelter, sediment supply, aspect and topography for vegetation growth and sediment accumulation. Plant macrofossils dated in this study from the shores of Vaigat, such as seeds, can produce anomalously old ages due to their post-depositional movement through widely-spaced rhizomes of cold-tolerant shrubs (thus, are inaccurate but precise) (Table 3.2). The problem remains therefore of dating allochthonous, rather than in situ material, as in the case in lower latitudes. In addition, some studies of west Greenland lakes report erroneously old ages based on ^{14}C dated bulk sediment slices (e.g. Kaplan et al., 2002; Bennike et al., 2010). Outlying ages are likely an indication of the basin 'hard-water effect' in areas rich in carbonate rocks. This has been reported to increase the age of freshwater radiocarbon age by several hundred years (e.g. Philippsen, 2013).

The Vaigat tsunami deposits are mostly too thin to incorporate in-washed organic material that can be dated and confirmed as older reworked (i.e., confirming transport by wave or other abrupt event). This eliminates the use of this criterion in the study of tsunami deposits (e.g. Bondevik et al. 1997b). Similarly, thin deposits exclude the opportunity to target a specific horizon for dating. In the rare instances where event deposits are sufficiently thick with well-defined upper and lower contacts, anomalously old ages indicate erosion, similar to lower latitudes (e.g. Dawson et al., 1988; Bondevik et al., 1997b; Romundset and Bondevik, 2011; Srinivasalu et al., 2009; Srisutam and Wagner, 2010). By contrast, the swift recolonization of Arctic vegetation types within years of the event in places (Buchwal et al., 2015) means that upper contacts, if well-defined, offer potential as a key dating horizon. In Norway, Bondevik et al. (1997b) noted that ages from the upper contact of the Storegga tsunami deposits in lake sequences were older than equivalent ages from terrestrial sequences in Scotland (e.g. Smith et al., 2004), reflecting a delayed onset of peat accumulation on top of the tsunami deposit.

Similarly, within the Cree Estuary stratigraphy, the 8.2-related meltwater pulses are marked by sudden switches from organogenic to minerogenic sediment accumulation. Minerogenic sediment is devoid of organic material and therefore difficult to date. Despite

the presence of dateable fossil foraminifera within these units (Smith et al., 2003), uncertainties associated with local ocean reservoir corrections far outweigh the precision of the underlying chronology by an order of magnitude, rendering ages based on marine material unsuitable in these contexts and on these timescales. Overall, therefore 'event horizons' are themselves mostly devoid of suitable organic material that can be ^{14}C dated. This challenge of dating abrupt RSL changes will proliferate as long as the ^{14}C dating technique remains the primary method of dating such events.

6.3.5.2 The Storegga tsunami example

The largest tsunami event of the prehistoric era, the North Sea Storegga tsunami, offers a useful opportunity to assess the effectiveness of a range of different strategies used to date a known tsunami event. An age 'best-estimate' of the event is 8176-8032 cal yr BP (7277 ± 20) based on age estimates from moss fragments ripped up and deposited by the tsunami in a tidal inlet in Norway (Bondevik et al., 2012), highlighting that it impacted paraglacial shorelines during the coldest decades of the 8.2 event. The database of ages from circum-North Sea sites thus provides a potential analogue for dating a near-field abrupt event, enabling a statistical assessment of: a) the *dating horizons* that yield the most accurate and precise ages when dating a near-field abrupt event, and b) the *types of material* that provide the most accurate and precise ages.

I assimilated 139 radiocarbon ages and their ± 1σ lab uncertainties from 29 studies of a range of depositional environments (isolation basins, freshwater bogs, estuaries and wetlands) from circum-North Sea sites (Norway; Bondevik et al., 1997b; 2003; 2005; 2012; Bondevik, 2003; Romundset and Bondevik, 2011; Vasskog et al., 2013), Eastern Scotland (Chisholm, 1971; Morrison, 1981; Smith et al., 1980; 1983; 1992, 1999; 2004; Birnie, 1981; Haggart, 1982; Robinson, 1982; 1993; Wordsworth, 1985; Smith, 1993; Smith and Cullingford, 1985; Dawson and Smith, 1997; 2000), Northern England (Horton et al., 1999; Boomer et al., 2007), East Greenland (Wagner et al., 2007) and the Faroe Islands (Grauert et al., 2001). In summary, the analysis pools all ages together by randomly sampling the probability distributions of each age about their means (μm) and uncertainties (σ). The same ages were then grouped into one of seven sub-groups according to: sample stratigraphic position and type of organic material dated. Finally, I derived descriptive statistics and confidence intervals for the full dataset and each of the sub-groups. I then compared these statistics in order to assess the relative importance of the type of material used and stratigraphic position of an age in reconstructing the timing of the Storegga event.

Ages are based on sample material from one of three horizons: i) within 1 cm of the upper contact of the tsunami deposit, ii) within the tsunami deposit itself, and iii) within 1 cm of the lower contact of the tsunami deposit. Samples that had the potential to be anomalously young or old were removed; including two dates from marine shell (TUa-832, TUa-859; Bondevik et al., 1997b, KIA-27662; Wagner et al., 2007), three containing rhizomes or roots (TUa-1672, TUa-1673, Bondevik, 2003, TUa-3425; Bondevik et al., 2005), one anomalously young age of 3815 ± 45 (Smith, 1993) and one sample based on mixed material from both the upper and lower lithological contacts (SRR-1565; Smith et al., 1983). Further, I conservatively chose not to include the 'best-estimate' moss ages (n=6) of Bondevik et al. (2012) given that these were taken from a stratigraphically superior, geologically unique context, to avoid data skew. I then expressed each age symmetrically about their means and uncertainties (n=125; all distributions assumed normal), using random sampling to produce 500 new 'iterations' for each age. I then derived the 25th and 75th percentiles and 95% probability range of the dataset using these iterations. This process was repeated after grouping each sample according to, i) its sampled stratigraphic position (i.e., lower contact, within, upper contact) and, ii) according to the type of material dated; leaves and seeds (Group 1), twigs (Group 2), bulk ages (both conventionally and AMS dated; Group 3) and wood (Group 4).

Figure 6.1 plots the 25th and 75th percentiles for the full dataset and each of its sub-groups, alongside their associated 95% probability ranges (data presented in Table 6.2). The mean timing of the Storegga tsunami inferred by all ages is 7328 ± 439 (median 7292), with upper and lower confidence bounds (95%) of 8291 and 6456, respectively. Despite the spread in the data, the median age is well-aligned with the best-estimate of Bondevik et al. (2012) of 7277 ± 20 (stippled blue vertical line).

Table 6.2. Age probability ranges of the Storegga tsunami, inferred by random sampling radiocarbon ages grouped by stratigraphic position and dating material type.

	Upper 95% confidence limit	**75th percentile**	**Median**	**25th percentile**	**Lower 95% confidence limit**
All data	8291	7579	7297	7079	6456
Upper contact	7885	7344	7136	6912	5303
Within deposit	8469	7911	7506	7299	6969
Lower	9574	7695	7365	7128	5724

contact					
Group 1	9643	7529	7294	7188	6916
Group 2	8351	7622	7338	7202	6981
Group 3	8431	7680	7300	6838	5618
Group 4	7945	7705	7371	7127	6675

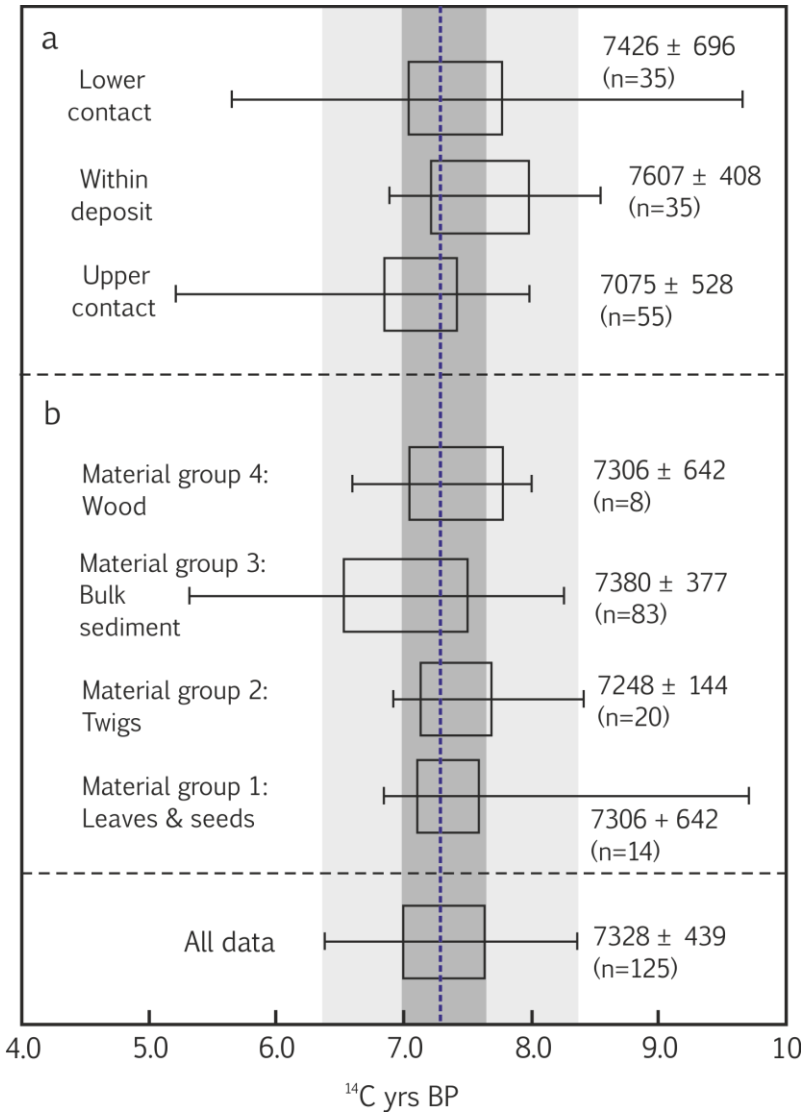

Figure 6.1. Box and whisker plots detailing the timing of the Storegga tsunami inferred by random sampling. Samples are grouped by stratigraphic position and dating material types. Stippled blue line indicates the 'best-estimate' mean age of Bondevik et al. (2012) (7277 yrs). Shading highlights the "full dataset" ages, to which the sub-group ages are compared against.

I explored the relative accuracy and precision of ages by comparing the descriptive statistics of each sub-group to those of a common benchmark dataset, in this case the full dataset values. Table 6.3 plots the differences between the ages of the sub-group values and the full dataset, with negative values (red) and positive values (blue) indicating age over- and undershoots, respectively. Here, these differences are termed 'age deviations'. With respect to the median values, the age deviations for the samples grouped according to stratigraphic position are: upper contact; 160 yrs younger, ages from within the tsunami deposit; 209 yrs older, ages from lower contact; 68 yrs older. For samples grouped according to material dated, the age deviations are: group 1 (leaves and seeds); 3 yrs younger, group 2 (twigs); 41 yrs older, group 3 (bulk ages); 4 yrs older, group 4 (wood); 74 yrs older.

The age deviations in Table 6.3 shed light on the importance of adopting a dating strategy after carefully considering the key variables that might influence the efficacy of a radiocarbon age. First, I assess the effectiveness of ages in relation to their stratigraphic position. Ages from the upper contact yield the most precise ages, as reflected by the narrowest interquartile range, although there is a tendency to produce anomalously young ages. This principally reflects a time/depositional lag between the end of the event and the start of organic accumulation (Bondevik et al. 1996; 1997b). This time lag is likely to be reflected more strongly in lake settings where accumulation rates are typically low (e.g. Fredskild, 1983). Indeed, ~60% of the upper contact sub-group is comprised of ages taken from above the tsunami deposit in Norwegian lakes whereas, in contrast, upper contact ages from the estuarine deposits of Scotland provide ages that are slightly closer to the median value, highlighting typically higher rates of terrestrial (non-lacustrine) accumulation.

Table 6.3. Deviations of age estimates for sub-grouped data, relative to the mean value of the full dataset. Blue values indicate young ages offsets, while red values highlight older deviations.

Age group	**Upper 95% confidence limit**	**75th percentile**	**Median**	**25th percentile**	**Lower 95% confidence limit**
All data	*8291*	*7579*	*7297*	*7079*	*6456*
Upper contact	407	234	161	167	1153
Within deposit	-178	-332	-209	-220	-514

Lower contact	-1283	-116	-68	-49	731
Group 1	-1352	50	3	-109	-460
Group 2	-60	-43	-41	-123	-526
Group 3	-139	-101	-4	241	838
Group 4	346	-126	-74	-48	-219

In terms of median values, lower contact ages are most accurate but have a tendency to generate both anomalously young and old ages. Anomalously old ages reflect erosion to pre-existing substrate (e.g. Dawson et al., 1988). The most conceivable mechanism for younger ages from the lower contact is that material transported by downward root penetration has been sampled (e.g. Garrett et al., 2014). Nonetheless the interquartile range of this sub-group coincidences closely with that of the full dataset, highlighting the potential as an effective dating horizon providing that care is taken to reduce the probability of sampling heavily eroded sequences or sections impacted by the downward penetration of younger material.

Ages taken from within the tsunami deposit are consistently older than the values of the full dataset by a few hundred years. This pattern extends beyond a simple comparison of median values; it is consistent when considering the full probability range of the data. Clearly, this reflects the encasement of reworked older material into tsunami deposits. Nevertheless, ages from this stratigraphic position offer potential to provide precise ages of the event if care is taken to sample short-lived macrofossils such as minor twigs, leaves and seeds (e.g. Romundset and Bondevik, 2011).

Second, I now assess the effectiveness of the different types of sample material in dating the Storegga tsunami. Based on an assessment of median values alone, material sub-group 1 (leaves and seeds) provide ages with the greatest accuracy. This form of sample material is widely used in studies of abrupt change in lower latitudes on the grounds that material is highly delicate; any reworking will likely cause it to disintegrate (e.g. Kemp et al., 2013; Dura et al., 2014). However the relatively long extrusion of the upper 95% confidence limit indicates that this type of material can produce anomalously old ages. This highlights that macrofossils from near-field settings may not decay as effectively as those in lower latitudes where soil processes are generally more active (e.g. Nichol and Kench, 2008; Szczuciński et al., 2007; Szczuciński, 2012). Alternatively, this might indicate the time delay

related to the resettling of reworked detrital macrofossils from suspension (e.g. Bondevik et al., 1997b). Further, it is interesting to find that in Vaigat, dating this material can generate anomalously young ages because of the apparent ability of younger material to move downward through the rhizomes of thickly-rooted Arctic shrubs. This indicates the positive influence of vegetation cover and surface roughness on the accuracy of a radiocarbon age.

In contrast, samples from bulk slices are associated with a relatively wide interquartile range that is skewed towards the younger end of the timescale. Although it is reasonable to propose that this reflects the inclusion of younger material in the sampling of a bulk slice, it is more likely that this is influenced by a sampling bias. Indeed 54% of the sample population is based on upper contact samples, which have a tendency to produce anomalously young ages (see above). An important point also concerns the sampling of bulk ages from lake systems within areas that are rich in ancient calcium carbonates. This basin 'hard-water effect' can increase the age of a freshwater radiocarbon age by several hundred years (e.g. Olssen, 1986; Wohlfarth et al., 1993; Philippsen, 2013). This phenomenon however, is not evident within the Storegga data. Overall the strong overlap between the median values of bulk ages with those of the full dataset indicates an averaging process whereby the accuracy is increased with the inclusion of more ages, albeit at the minor expensive of dating precision. Hence, it is recommended that bulk ages can reasonably constrain the timing of an event deposit, providing that multiple ages are used in the reconstruction and bulks based on aquatic material are avoided.

Despite the potential to produce anomalously old ages, dates from twigs are among the most accurate and precise types of ages. Almost all of the twigs sampled are from the studies of Norwegian coastal lakes. These studies illustrate that accurate and precise ages can be generated if based on the smallest, most non-robust samples. In contrast, larger wood fragments generally produce older ages, reflecting their decreased rate of decay and ability to remain longer in the terrestrial environment upon being deposited.

To summarise the lessons from this analysis, each dating strategy is associated with its own set of opportunities and challenges. All three stratigraphic contacts have the potential to infer effectively the timing of an event deposit, but ages from the upper and lower contacts are generally the most accurate and precise. In addition, all types of sample material show promise, but the most accurate and precise ages are those from leaves, seeds and other short-lived plant macrofossils, including minor twigs. These can however generate ages that are both anomalously young and old. In this regard ages from bulk slices offer potential when there is a minor dating program in place (i.e., one based on few ages), as produce relatively accurate ages, albeit at the expense of precision. Overall, the preferred strategy is

to base a chronology on several samples of plant macrofossils from all three dating horizons. As Bondevik et al. (2012) demonstrate, age modelling that incorporates the stratigraphic position of samples can then be used to shave further uncertainty off the final estimate. Finally, the accuracy and precision of ages are influenced by a range of factors related to the nature of environment at the time of the event, the depositional context and rates of accumulation, extent of erosion and type/amount of vegetation cover. Developing a dating strategy that will effectively reconstruct the timing of an event will depend strongly on site-specific, careful consideration of all of these variables.

6.3.5.3 Age modelling

Age modelling abrupt event stratigraphies in near-field settings is faced with a number of opportunities and challenges. The best age models are constructed from continuous accumulation histories, i.e. those without sedimentary hiatuses, as these permit accurate interpolation of ages between ^{14}C dated boundaries. The incorporation of an abrupt event into an age model, regardless of the global position of the site concerned, relies to some extent on *a priori* judgments and perceptions of the timescale under which deposition occurred, as well as the inferred continuity of deposition, with some events being deposited instantaneously and others near-instantaneously.

As noted above, the Cree Estuary is a good example of an environment with high 'background' sedimentation rates, promoting conditions conductive to 'punctuation' events such as transient episodes of rapid RSL rise. This continuity in sedimentation across the observed meltwater event(s) enables continuous age modelling and the confident age interpolation of horizons between ^{14}C dated tie-points. In this regard, paraglacial coasts experiencing uniquely high rates of sediment delivery from glacigenic sources should be viewed as potential targets where continuous records might be found.

Where abrupt RSL changes can be tied to climate-driven ice-sheet changes as recorded in other non-coastal and coastal proxy records, there is potential to extract chronostratigraphic markers from existing climate records for use in age modelled chronologies. As a hypothetical example, if the climatic signal of the 8.2 event was measured within the Cree stratigraphy (core BC421), the age modelled chronology would benefit from the inclusion of age constraints of the event from close-by proxy records (e.g. Vincent et al., 2011; northwest England). However, this would require careful consideration of potential pitfalls as adopting such an approach would render the chronology non-independent. For instance, the 8.2 event is globally non-synchronous (time-transgressive) (e.g. Rohling and Palike, 2005; Wiersma et al., 2011). Overall though, near-field records are

positioned closer to ice-sheets, making them sensitive to climate-driven ice-sheet changes. This increases their potential to record climatic signals and hence climate-related abrupt RSL changes.

In contrast, 'instantaneous' examples of abrupt change such as the thin tsunami and storm deposits of Vaigat are difficult to age model (e.g. Fig. 3.3). By their nature they record abrupt deposition that may or may not be associated with erosion. In contrast, thicker tsunami deposits offer potential to be targeted more precisely for different types of dating material (e.g. Fig. 3.6). The ability to produce a reliable age model reflects the amount of sediment supply, the rate of RSL change and the nature of the abrupt event in question; whether it is instantaneous or near-instantaneous.

6.3.5 Microfossil analyses

Given the inability to robustly test for evidence of contrasting tsunami signatures (because of the thinness of deposits); the focus shifts to confirming whether the deposit in question has a marine origin. Microfossil analysis thus provides the only objective evidence of marine inundation within an otherwise terrestrial environment. In the lake records it is difficult to identify marine taxa within assemblages dominated by freshwater species. Davies and Haslett (2000) found that the probability of recovering a single marine specimen deposited by a high-energy event into a freshwater lake is exceptionally low. To avoid missing rare occurrences of marine taxa, this study adopted a sampling strategy to increase the chance of discovering rare marine taxa. In particular upon exceeding the standard count of 200-300 specimens, the remainder of the diatom slide(s) was scanned for marine taxa. In most cases, however, this could not improve the statistical significance of the frequencies of marine taxa; indeed these remained almost always statistically non-significant (e.g. Fig. 4.4). Hence, a great degree of care is required to assess the potential significance of the find by assessing other factors, in particular the stratigraphic continuity of the assemblage (i.e., can it be laterally traced?) and the nature of the accompanying sedimentology (e.g. coarse- or fine-grained?). Despite the high diversity of freshwater assemblages, however, biostratigraphic studies of nearshore records are aided by less diverse assemblages comprising ubiquitous taxa (e.g. Chapter 3, section 4.3.2).

6.4 Near-field reconstructions: scaling stratigraphic records

6.4.1 West Greenland

Separating local from non-local (regional) RSL signals relies largely on the extrapolation, or up-scaling, of local stratigraphic records. In the context of palaeoseismology, Nelson et al. (1996) outlined five key criteria for identifying evidence of cosiesmic subsidence in local stratigraphic records. On passive coastal margins such as Greenland, two of these original criteria remain applicable: 1) the lateral extent of tsunami deposit, 2) synchronicity of deposits across widely-spaced sites. Is it possible to confidently separate non-regional from regional signals from local stratigraphic records, using these criteria alone? Although the thinness of tsunami deposits has precluded a robust assessment of their sedimentological signatures, they could be traced laterally on the basis of age. To this end, dating has provided the only means to link to fragmentary and widely-spaced deposits, permitting some assessment of their potential emplacement mechanisms (Chapters 3 and 4). The two criteria outlined above are thus closely coupled; age control provides the means to identify the lateral extent of deposits across widely-spaced sites.

When encountering an anomalous deposit confirmed by dating and microfossil analyses to record marine inundation, the next step is to infer the source mechanism of its emplacement (e.g. Hutchinson et al., 1997). A challenge identified in this thesis is that at present there are no clear stratigraphic criteria that can distinguish between the various potential mechanisms. In the case of the Innaarsuit iceberg-roll example, we dismiss a possible landslide-generated tsunami as the cause for the basin ingression on the basis that: i) there is no local landslide capable of generating such a tsunami; ii) the south coast region of Disko Bugt is over 100 miles away and there is no reported evidence for landslides terminating in the sea in this area; iii) any tsunami sourced from this area would have to cross Disko Bugt, pass through the shallow shoals that lie at the mouth of the Tasiusarsiaq inlet and then reach the protected study site. In contrast, the likelihood of a local iceberg roll source is more probable, based on the abundance of large icebergs in Disko Bugt.

In Vaigat, there are strong reasons to attribute at least some of the recorded tsunamis to landslide-triggered events. The challenge is that even the deposits of the known Vaigat AD 2000 and 1952 events, supported by local testimony as being triggered by landslides, bear resemblance to those interpreted to be iceberg-tsunami and storm deposits (VA5 peninsula and lake IV4). Likewise, the iceberg-generated tsunami deposits in basin IV4 differ little from the Storegga submarine landslide deposits found in circum-North Atlantic lake settings (e.g. Wagner et al., 2007; Bondevik et al., 1997b; Romundset and Bondevik,

2011). This problem represents the latest example of the wider challenge in regard to isolating the mechanism of emplacement where two or more potential candidates involved (e.g. Foster et al., 2001; Morton et al., 2007; Switzer et al., 2005; Switzer and Jones, 2008), although differentiation has been possible in some instances (e.g. Komatsubara et al., 2008). Notwithstanding these issues, the Vaigat studies have revealed that exceptionally subtle deposits from different sites can be correlated on the basis of their age. The mechanism of their emplacement can then be narrowed down further by considering the environmental context of the site (Goff et al., 2011). For example, where iceberg tsunami are local processes affecting relatively small (<1 km) areas, the extent of landslide-tsunami is more likely to be more pronounced (>5 km). This suggests that regional interpretations can be derived from 'spot-site' stratigraphic data. However, this is a somewhat tentative process involving assumptions and speculation in the absence of criteria to distinguish between different types of event deposits. Nevertheless, future studies should take care not to dismiss fine-scale stratigraphic detail.

6.4.2 The Cree Estuary

Compared to reconstructing singularities of sea-level rise such as tsunamis, up-scaling decadal-centennial scale RSL records developed from single sites represents a greater challenge. There are a greater number of interrelated processes that drive the RSL signal on these timescales, including: eustatic and isostatic (GIA) components, dynamical effects (halo- and thermosteric changes), tectonics, geoidal and rotational contributions (continental levering and ocean siphoning) (Shennan and Horton, 2002; Tamisiea et al., 2001; Shennan, 2015). This makes extrapolating local stratigraphies to form wider interpretations of global sea-level history a non-trivial task. Arguably, however, the Cree Estuary example has shed light on the greater potential of near-field coasts as archives of high-magnitude (metre-scale) RSL changes, particularly in the early Holocene, compared to sites from lower latitudes.

The greater role of GIA in near-field areas makes it easier to distinguish abrupt RSL changes. In the case of the Cree estuary, crustal rebound in response to the removal of ice provides an offsetting effect whereby the typically rapid rates of early Holocene eustatic rise are dampened. These lower background rates of rise have made it possible to distinguish metre-scale RSL changes. This is in contrast to lower latitude sites where the eustatic component dominates the RSL signal. Metre-scale inflexions occurring on decadal-centennial timescales are not able to be discerned within the uncertainties of coral-based reconstructions (e.g. Fairbanks, 1989; Bard et al., 1996; 2010; Chappell and Pollach, 1991),

while there is an argument that coastal-peat based records are also insensitive (e.g. Hijma and Cohen, 2010). In addition, paraglacial coasts experiencing GIA-induced crustal subsidence will be equally as unsuitable, despite offering greater scope for higher-resolution reconstructions. As an example, rates of early Holocene RSL rise between 9-8 ka in the south of England, an area experiencing forebuldge-related coastal subsidence, were on the order of 8-9 mm/yr (e.g. Jennings et al., 1998; Massey et al., 2008). Records from these areas at this time are thickly minerogenic, reflecting permanent subtidal conditions. In contrast, background RSL was rising at rates of 3-4 mm/yr at the same time. The Cree record is characterised by peat-mud couplets that reflect gradual marsh recovery. Thus, it is possible that paraglacial salt-marsh records offer more promise in constraining global sea-level histories compared to that of lower latitude sites, providing that background rates of RSL change have been well constrained by millennial-scale RSL records. These can either be modelled estimates (in areas where GIA models are well-resolved, such as the case in this study), or from additional observational datasets based on the collection and analysis of sea-level index points (e.g. Gehrels, 1999; Shennan et al., 2000; Donnelly et al. 2004).

Coupled with the benefit of land uplift (the 'ideal' amount of which will vary dependent on the timescale and magnitude of the abrupt event under consideration), high rates of sediment supply promote the conditions necessary to record abrupt sea-level changes. Net sediment accumulation will keep pace with the new availability of accommodation space as long as there is a net surplus of sediment supply (e.g. Jennings et al., 1998).

The reworking and delivery of glacial sediment in the Cree estuary was significant in the development of the Cree RSL record for two reasons. First, the main postglacial transgression in the estuary at ~10-8 kyr BP reworked large volumes of glacial material and led to the development of coarse-clastic, drift-aligned barrier structures. The back-barrier stratigraphy has been documented at two of these; the first is Blair's Croft (this study; Smith et al., 2003) and the second at Baltersan at the opposite side of the estuary (Smith et al., 2003). Both sequences record peat-mud couplets of similar age, reflecting estuary-wide stratigraphic changes. Orford et al. (1991) recognized that the first phase of barrier development on paraglacial coasts is the formation of small-scale drift aligned structures at the leading edge of the erosional front (i.e., the rising RSL). These are analogous to the Barrier at Blair's Croft. Similar features, termed 'proto-barriers', are found on paraglacial coasts of North America (FitzGerald et al., 1994; Buynevich & FitzGerald, 2003; Hein et al., 2014). Critically, the back-barrier setting would have acted as important depocentre for large quantities of fine-grained sediment transported from upstream. This facilitated rapid

accumulation and hence the development of the high time-resolution stratigraphy in the back-barrier area.

Finally, because of the strong climatic control on coastal paraglacial sediment supply over centennial-scale timescales, there is a greater possibility for accumulation history and hence age model development to be climate-driven in turn. This could present a problem when attempting to develop RSL records from paraglacial coasts, particularly when these are accompanied by strong climatic expressions such as the 8.2 event. However, the potential of these areas is provided by the fact that changes to RSL, sediment supply and local coastal morphodynamics often demonstrate a close coupling (e.g. Shaw and Forbes, 1990; Long and Innes, 1993; Jennings et al., 1998).

References

Aebly, F.A. and S.C. Fritz. 2009. Paleohydrology of Kangerlussuaq, West Greenland during the last ~8000 yr. *The Holocene* 19: 91-104.

Bard, E., Hamelin, B., Arnold, M., Montaggioni, L., Cabioch, G., Faure, G., Rougerie, F. 1996. Deglacial sea-level record from Tahiti corals and the timing of global meltwater discharge. Nature 282, 241-244.

Bard, E., Hamelin, B., Delanghe-Sabatier, D. 2010. Deglacial meltwater pulse 1B and Younger Dryas sea levels revisited with boreholes at Tahiti. Science, 327, 5970, 1235-1237.

Bennike, O., Anderson, N.J., McGowan. S. Holocene palaeoecology of southwest Greenland inferred from macrofossils in sediments of an oligosaline lake. Journal of Paleolimnology 43, 4, 787-798.

Bindler R, Renberg I, Appleby PG, Anderson NJ, Rose NL (2001) Mercury accumulation rates and spatial patterns in lake sediments from west Greenland: a coast to ice margin transect. Environ Sci Technol 35: 1736-1741

Birnie, J., 1981. Environmentalchanges on Shetland since the end of the last glaciation. Ph.D. Thesis, University of Aberdeen (542pp).

Bondevik S, Løvholt F, Harbitz C, Mangerud J, Dawson A, Svendsen JI (2005) The Storegga Slide tsunami - comparing field observations with numerical simulations. Mar Petrol Geol 22: 195-208

Bondevik, S., Mangerud, J., Dawson, S., Dawson, A.G., Lohne, O., 2003. Record-breaking height for 8000-year-old tsunami in the North Atlantic. Eos, Transactions, American Geophysical Union 84 (31), 291–292.

Bondevik, S., Stormo, S.K., Gudrun, S. 2012. Green mosses date the Storegga tsunami to the chilliest decades of the 8.2 ka cold event, *Quaternary Science Reviews* 45, 1-6. doi:10.1016/j.quascirev.2012.04.020.

Bondevik, S., Svendsen, J.I., Johnsen, G., Mangerud, J., Kaland, P.E., 1997b. The Storegga tsunami along the Norwegian coast, age and runup. Boreas 26, 29–53.

Boomer, I., Waddington, C., Stevenson, T., Hamilton, D. 2007. Holocene coastal change and geoarchaeology at Howick, Northumberland, UK. The Holocene 17 (1): 89– 104.

Buchwal A, Szczuciński W, Strzelecki M, Long AJ (2015) Tree-ring structure of *Salix glauca* reveals evidence of a 2000 AD tsunami event in west Greenland: implications for Arctic paleotsunami and paleoecological studies. Polish Polar Res 36: 51-65

Buynevich, I. V. & FitzGerald, D. M. 2003. High resolution subsurface (GPR) profiling and sedimentology of coastal ponds, Maine, USA: implications for Holocene back-barrier evolution. Journal of Sedimentary Research, 73, 559–571.

Chague-Goff, C., Schneider, J-L., Goff, J.R., Dominey-Howes, D. & Strotz, L. 2011. Expanding the proxy toolkit to help identify past events: Lessons from the 2004 Indian Ocean Tsunami and the 2009 South Pacific Tsunami. Earth-Science Reviews 107, 107-122 - See more at: http://www.ansto.gov.au/ResearchHub/StaffProfiles/CHAGUE-GOFF-CATHERINE#sthash.WuX8n4FZ.dpuf

Chappell, J., Polach, H. 1991. Post-glacial sea-level rise from a coral record at Huon Peninsula, Papua New Guinea *Nature* 349, 147 – 149.

Chisholm, J.I., 1971. The stratigraphy of the post-glacial marine transgression of NE Fife. Bulletin of the Geological Survey of Great Britain 37, 91–107.

Cogley. J. G. & McCann, S. B. (1976) An exceptional storm and its effects in the Canadian High Arctic. Arctic and Alpine Res.H, 105-110

Dahl-Jensen, T., Larsen, L.M., Pedersen, S.A.S., Pedersen, J., Jepsen, H.F., Pedersen, G.K., Nielsen, T., Pedersen, A.K., Platen-Hallermund, F.V., Weng, W. 2004. Landslide and tsunami 21 November 200 in Paatuut, West Greenland. *Natural Hazards*, 31, 277-287.

Davies, P., Haslett, S.K. 2000. Identifying storm or tsunami events in coastal basin sediments. *Area* 32(3), 335-336.

Dawson, A.G., Long, D., Smith, D.E. 1988. The Storegga slides: evidence from eastern Scotland of a possible tsunami. Marine Geology, 82. 271-276.

Dawson, S., Smith, D.E., 2000. The sedimentology of middle Holocene tsunami facies in northern Sutherland, Scotland, UK. Marine Geology 170, 69–79

Diemand, D. 2001. Icebergs. p. 1255-1264 In: Origins and spatial distribution. Academic Press, doi:10.1006/rwos.2001.0002.

Donnelly, J.P., Cleary, P., Newby, P., Ettinger, R. 2004. Coupling instrumental and geological records of sea-level change: Evidence from southern New England of an increase in the rate of sea-level rise in the late 19th century. Geophysical Research Letters, 31, L0523

Dura, T., Cisternas, M., Horton, B.P., Ely, L.L., Nelson, A.R., Wesson, R.L., Pilarczyk, J.E. 2014. Coastal evidence for Holocene subduction-zone earthquakes and tsunamis in central Chile, Quaternary Science Reviews 113, 93-111.

Eicken, H., I. Dmitrenko, K. Tyshko, A. Darovskikh, W. Dierking, U. Blahak, J. Groves, H. Kassens (2005) Zonation of the Laptev Sea landfast ice cover and its importance in a frozen estuary. Global Planet. Change, 48, 55-83.

Fairbanks, R.G. 1989. A 17,000-year glacio-eustatic sea level record: influence of glacial melting rates on the Younger Dryas event and deep-ocean circulation. Nature 342, 637-641.

FitzGerald, D. M. & van Heteren, S. 1999. Classification of paraglacial barrier systems: coastal New England, USA. Sedimentology, 46, 1083–1108.

Forbes, D.L., Orford, J.D., Carter, R.W.G., Shaw, J., Jennings, S.C. 1995a. Morphodynamic evolution, self-organisation, and instability of coarse-clastic barriers on paraglacial coasts. Marine Geology 126, 63–85.

Foster I.D.L., Dawson A.G., Dawson, S., Lees, J., Mansfield, L. 1993. Tsunami sedimentation sequences in the Scilly Isles, southwest England. Sci Tsunami Haz 11: 35-46

Fredskild B (1983) The Holocene vegetational development of the Godthåbsfjord area, west Greenland. Medd. Gronl. Geosci 10: 1–28

Garrett, E., Shennan, I., Woodroffe, S.A., Cisternas, M., Hocking, E.P., Gulliver, P. 2014. Reconstructing paleoseismic deformation, 2: 1000 years of great earthquakes at Chucalen, south central Chile. Quaternary Science Reviews, 113, 112-122.

Gehrels, W.R., 2000. Using foraminiferal transfer functions to produce high-resolution sea-level records from saltmarsh deposits, Maine, USA. The Holocene 10, 367-376.

Goff, J., Catherine, Chagué--Fogg, Nichol, S., Jaffe, B., Dominey-Howes, D. 2011. Progress in palaeotsunami research. Sedimentary Geology 243-244, 70-88

Grauert, M., Bjork, S., Bondevik, S. 2001. Storegga tsunami deposits in a coastal lake Suduroy, the Faroe Islands, Boreas, 30, 263-271.

Haggart, B.A., 1982. Flandrian sea-level changes in the Moray Firth area. Unpublished Ph.D. Thesis, University of Durham.

Hansen BU, Elberling B, Humlum O, Nielsen N (2006) Meteorological trends (1991–2004) at Arctic Station, Central West Greenland (69°15') in a 130 year perspective. Dan J Geog 106: 45-55

Hein, C.J., Fitzgerald, D.M., Buynevich, I.V., Van Heteren, S., Kelley, J.T. Evolution of paraglacial coasts in response to changes in fluvial sediment supply. In: Martini, I. P.&Wanless, H. R. (eds). 2014. Sedimentary Coastal Zones from High to Low Latitudes: Similarities and Differences. Geological Society, London, Special Publications, 388, http://dx.doi.org/10.1144/SP388.15

Hemphill-Haley, E., 1996. Diatoms as an aid in identifying late-Holocene tsunami deposits. The Holocene 6 (4), 439–448.

Hijma, M.P and Cohen, K.M. 2010. Timing and magnitude of the sea-level jump precluding the 8200 yr event, *Geology* 38, 3, 275-278.

Horton, B.P., Innes, J.B., Shennan, I., Gehrels, W.R., Lloyd, J.M., McArthur, J.J., Rutherford, M.M., 1999. In: Bridgland, D.R., Horton, B.P., Innes, J.P. (Eds.), The Quaternary of North- East England. Field Guide, Quaternary Research Association, pp.146–165.

Hutchinson I, Clague J.J., Mathewes, R.W. 1997. Reconstructing the tsunami record on an emerging coast: a case study of Kanim Lake, Vancouver Island, British Columbia, Canada. J Coastal Res 13: 545-553

Jennings, S., Orford, J.D., Canti, M., Devoy, R.J.N., Straker, V. The role of relative sea-level rise and changing sediment supply on Holocene gravel barrier development: the example of Porlock, Somerset, UK. The Holocene, 8, 2, 165-181.

Kaplin, M.R., Wolfe, A.P., Miller, G.H. 2002. Holocene environmental variability in Southern Greenland inferred from lake sediments. Quaternary Research 58, 149-159.

Kelsey, H.M., Nelson, A.R., Hemphill-Haley, E., Witter, R.C. 2005. Tsunami history of an Oregon coastal lake reveals a 4600 yr record of great earthquakes on the Cascadia subduction zone. *Geological Society of America Bulletin* 117(7-8), 1009-1032, doi: 10.1130/B25452.1.

Kemp, A.C., Horton, B.P., Vane, C.H., Bernhardt, C.E., Corbett, D.R., Engelhart, S.E., Anisfeld, S.C., Parnell, A.C., Cahill, N., 2013. Sea-level change during the last 2500 years in New Jersey, USA. Quat. Sci. Rev. 81, 90e104.

Knight, J., & Harrison, S. 2009. Periglacial and Paraglacial Processes and Environments. Geological Society, London, Special Publications, 320.

Komatsubara, J. & O. Fujiwara (2007): Overview of Holocene tsunami deposits along the Nankai, Suruga, and Sagami Troughs, southwest Japan. In: Pure and Applied Geophysics 164: 493–507.

Kovacs, A., Mellor. M. 1974. "Sea ice morphology and ice as a geologic agent in the Southern Beaufort Sea". In" Reed. J.C. and Sater, J.E. (eds). *The coast and Shelf of the Beaufort Sea*. Va. USA.

Long, A. J. & Innes, J. B. 1993. Holocene sea-level changes in Romney Marsh and Southeast England, U.K. *Proceedings of the Geologists' Association*. 104:223-237

Lønne I, Lyså A. 2005. Deglaciation dynamics following the Little Ice Age on Svalbard: Implications for 542 shaping of landscapes at high latitude. *Geomorphology* **72**: 300-319

Malmquist C, Binder R, Remberg I, van Bavel B, Karlsson E, Anderson NJ, Tysklind M (2003) Time trends of selected persisent organic pollutants in lake sediments from Greenland. Environ Sci Tech 37: 4319-4324

Massey, A. C., Gehrels, W. R., Charman, D. J., Milne, G. A., Peltier, W. R., Lambeck, K. and Selby, K. A. 2008. Relative sea-level change and postglacial isostatic adjustment along the coast of south Devon, United Kingdom. *J. Quaternary Sci.*, Vol. 23 pp. 415–433

Mercier, D., & Laffly, D. 2005. Actual paraglacial progradation of the coastal zone in the Kongsfjorden area, western Spitsbergen (Svalbard). In: Harris, C., & Murton, J.B. (eds.) Cryospheric systems: glaciers and permafrost. Geological Society, London, Special Publication 242, 111–117.

Morrison, J., Smith, D.E., Cullingford, R.A., Jones, R.L., 1981. The culmination of the Main Postglacial Transgression in the Firth of Tay Area, Scotland. Proceedings of the Geologists' Association 92 (3), 197–209.

Morton, R.A., Gelfenbaum, G., Jaffe, B.E. 2007. Physical criteria for distinguishing sandy tsunami and storm deposits using modern examples, Sedimentary Geology, 200, 184-207.

Nalimov, Yu.V., 1995. The ice thermal regime at front deltas of rivers of the Laptev Sea. Rep. Polar Res. 176, 55 – 61.

Nelson, A.R., Shennan, I., Long, A.J. 1996. Identifying coseismic subsidence in tidal-wetland stratigraphic sequences at the Cascadia subduction zone of western North America. *Journal of Geophysical Research* 101(B3), 6115-6135.

Nichol, S.J., & Kench, P.S. 2008. Sedimentology and preservation potential of carbonate sand sheets deposited by the December 2004 Indian Ocean tsunami: South Baa Atoll, Maldives. Sedimentology, 55: 1173–1187

Nick, F., Vieli, A., Howat, I.M., Joughin, I. 2009. Large-scale changes in Greenland outlet glacier dynamics triggered at the terminus. *Nature Geoscience* 2, 110 - 114 (2009)

Nielsen, N. 1992. A boulder beach formed by waves from a calving glacier: Eqip Sermia, West Greenland. Boreas 21, 159 – 168.

Orford, J.D., Carter, R.W.G., Forbes, D.L. 1991a. Gravel barrier migration and sea-level rise: some observations from Nova Scotia. Journal of Coastal Research 7, 477–490.

Overland, J. E., M. Wang, J. E. Walsh, and J. C. Stroeve (2013), Future Arctic climate changes: Adaptation and mitigation time scales, Earth's Future, 2, doi:10.1002/2013EF000162.

Philippsen, B. 2013. The freshwater reservoir effect in radiocarbon dating. Heritage Science 1, 24.

Reimnitz, E., 2000. Interactions of river discharge with sea ice in proximity of Arctic Deltas: a review. Polarforschung vol. 70, pp. 123 – 134.

Rignot, E., Koppes, M., Velicogna, I. Rapid submarine melting of the calving faces of West Greenland glaciers. *Nature Geoscience* 3, 187 – 191.

Robinson, M., 1982. Diatomanalysis of Early Flandrian lagoon sediments from East Lothian, Scotland. Journal of Biogeography 9, 207–221.

Robinson, M., 1993. Microfossil analyses and radiocarbon dating of depositional sequences related to Holocene sea-level change in the Forth Valley, Scotland. Transactions of the Royal Society of Edinburgh: Earth Sciences 84, 1–60.

Rohling, E.J. & Palike, H. Centennial-scale climate cooling with a sudden cold event around 8,200 years ago. Nature 434, 975-976.

Romundset, A., Bondevik, S., 2011. Propagation of the Storegga tsunami into ice-free lakes along the southern shores of the Barents Sea. *Journal of Quaternary Science* 26, 457-462.

Rouse, W.R., Douglas, M.S.V., Hecky, R.E., Hershey, A.E., Kling, G.W., Lesack, L., Marsh, P., McDonald, M., Nicholson, B.J., Roulet, N.T., Smol, J.P. 1997. Effects on climate change on the freshwaters of Arctic and subarctic North America. Hydrol. Process., 11: 873–902.

Shaw, J. & Forbes, D.L. 1990. Relative sea-level change and coastal response, northeast. Newfoundland. Journal of Coastal Research, 6(3), 641-660.

Shennan, I. 2015. Handbook of sea-level research: framing research questions. In: Shennan, I., Long, A.J., Horton, B.P. Handbook of Sea-level Research, Wiley, London.

Shennan, I., Horton, B.O., Innes, J., Gehrels, R., Lloyd, J., McArthur, J., Rutherford, M. 2000, Late Quaternary sea-level changes, crustal movements and coastal evolution in Northumberland, UK. Journal of Quaternary Science 15, 3, 215-237.

Shennan, I., Horton, B.P., 2002. Holocene land- and sea-level changes in Great Britain. J. Quat. Sci. 17, 511e526.

Smith, D.E., 1993. Norwick, Unst; Burragarth, Unst; Sullom Voe, Mainland. In: Birnie, J., Gordon, J., Bennett, K., Hall, A. (Eds.), The Quaternary of Shetland. Quaternary Research Association Field Guide, pp. 52–56.

Smith, D.E., Cullingford, R.A., Brooks, C.L., 1983. Flandrian relative sea level changes in the Ythan valley, northeast Scotland. Earth Surface Processes and Landforms 8, 423–438.

Smith, D.E., Cullingford, R.A., Haggart, B.A., 1985. A major coastal flood during the Holocene in eastern Scotland. Eiszeitalter und Gegenwart 35, 109–118.

Smith, D.E., Firth, C.R., Brooks, C.L., Robinson, M., Collins, P.E.F., 1999. Relative sea-level rise during the Main Postglacial Transgression in NE Scotland, UK. Transactions of the Royal Society of Edinburgh: Earth Sciences 90, 1–27

Smith, D.E., Firth, C.R., Turbayne, S.C., Brooks, C.L., 1992. Holocene relative sea-level changes and shoreline displacement in the Dornoch Firth area, Scotland. Proceedings of the Geologists' Association 103, 237–257.

Smith, D.E., Morrison, J., Jones, R.L., Cullingford, R.A., 1980. Dating the main postglacial shoreline in the Montrose area, Scotland. In: Cullingford, R.A., Davidson, D.A., Lewin, J. (Eds.), Timescales in Geomorphology. Wiley, Chichester, pp. 225–245.

Smith, D.E., Shi, S., Cullingford, R.A., Dawson, A.G., Dawson, S., Firth, C.R., Foster, I.D.L., Fretwell, P.T., Haggart, B.A., Holloway, L.K., Long, D. 2004. The Holocene Storegga slide tsunami in the United Kingdom. Quaternary Science Reviews 23, 2291-2321.

Smith, D.E., Wells, J.M., Mighall, T.M., Cullingford, R.A., Holloway, L.K., Dawson, S., Brooks, C.L. 2003a. Holocene relative sea levels and coastal changes in the lower Cree valley and estuary, SW Scotland, UK. *Transactions of the Royal Society of Edinburgh: Earth Sciences*, 93, 301-331.

Srinivasalu, S., N. Rajeshwara Rao, N. Thangadurai, M.P. Jonathan, P.D. Roy, V. Ram Mohan & Saravanan, P. 2009. Characteristics of 2004 tsunami deposits of the northern Tamil Nadu coast, southeastern India. In: Boletín de la Sociedad Geológica Mexicana 61 (1): 111–118.

Srisutam, C. & F.-F. Wagner (2010): Tsunami sediment characteristics at the Thai Andaman coast. In: Pure and Applied Geophysics 167: 215–232.

Stern, A.A., Johnson, E., Holland, D.M., Wagner, T.J.W., Wadhams, P., Bates, R., Abrahamsen, E. P., Nicholls, K.W., Crawford, A., Gagnon, J., Tremblay, J.E. 2015 Wind-driven upwelling around grounded tabular icebergs. *Journal of Geophysical Research: Oceans*, 120 (8). 5820-5835

Strzelecki, M.C. 2012. 2012. High Arctic Paraglacial Coastal Evolution in Northern Billefjorden, Svalbard, Durham theses, Durham University. Available at Durham E-Theses Online: http://etheses.dur.ac.uk/7363/

Strzelecki, M.C. and Long, A.J. and Lloyd, J.M. (in press). Post-Little Ice Age development of a High Arctic paraglacial beach complex. *Permafrost and periglacial processes.*

Switzer, A., Pucillo, A. Haredy, R.A., Jones, B.G., Bryant, E.A. 2005. Sea level, storm, or tsunami: Enigmatic sand sheet deposits in a sheltered coastal embayment from southeastern New South Wales, Australia. *Journal of Coastal Research* 21, 655-663.

Switzer, Adam, and Brian G. Jones. "Setup, Deposition, and Sedimentary Characteristics of Two Storm Overwash Deposits, Abrahams Bosom Beach, Southeastern Australia." *Journal of Coastal Research*(2008): 189-200.

Szczucinksi, W., Niedzielskip, K.L., Frankowski, M., Ziola, A., Lorenc, A. 2007. Effects of rainy season on mobilization of contaminants from tsunami deposits left in a coastal zone of Thailand by the 26 December 2004 tsunami. *Environmental Geology* 53: 253-264

Szczucinski, W. 2012. The post-depositional changes of the onshore 2004 tsunami deposits on the Andaman Sea coast of Thailand. *Natural Hazards 60, 115-133.*

Tamisiea ME, Mitrovica JX, Milne GA, Davis JL. 2003. Long wave length sea level and solid surface perturbations driven by polar ice mass variations: fingerprinting Greenland and Antarctic Ice Sheet flux. *Space Science Reviews* (108) 81–93.

Vasskog K, Waldmann N, Bondevik S, et al. (2013) Evidence for Storegga tsunami run-up at the head of Nordfjord, western Norway. Journal of quaternary science 28: 391-402.

Wagner, B., Bennike, O., Klug, M., Cremer, H. 2007. First indication of Storegga tsunami deposits from East Greenland, Journal of Quaternary Science, 22(4), 321-325.

Wang, M., and J. E. Overland (2009), A sea ice free summer Arctic within 30 years? Geophys. Res. Lett., 36, L07502, doi:10.1029/2009GL037820.

Wiersma, A.P., Roche, D.M., and Renssen, H. 2011. Fingerprinting the 8.2 ka climate response in a coupled climate model, *Journal Quaternary Science* 26, 1, 118-127.

Willemse, N.W., Tornqvist, T.E. 1999. Holocene century-scale temperature variability from West Greenland lake records. *Geology* 27, 580-584.

Wohlfarth, B., Bjork, S., Possnert, G., Lemdahl, G., Brunnberg, L., Ising, J, Olsson, S., Svensson, N.O. 1993. AMS dating Swedish varved clays of the last glacial interglacial transition and the potential difficulties of calibration Late Weichselian 'absolute' chronologies. Boreas 22, 113-128.

Wordsworth, J., 1985. The excavation of a Mesolithic horizon at 13–24 Castle Street, Inverness. Proceedings of the Society of Antiquaries of Scotland 115, 89–103.

Zagorski, P., Gajek, G., Demczuk, P. 2012a. The influence of glacier systems of polar catchments on functioning of the coastal zone (Recherchefjorden, Svalbard). Zeitschrift fur Geomorfologie 56 Suppl. 1, 101-122.

Ziaja, W., Maciejowski, P., Ostafin, K. 2009. Coastal Landscape Dynamics in NE Sorkapp Land (SE Spitsbergen), 1900–2005. Ambio 38, 201-208.

7

Conclusions

7.1 Introduction

This chapter concludes this thesis by summarizing the main findings of the work in the context of the original aims and objectives set out in Chapter 1. It finishes with some recommendations for future work on abrupt RSL changes in near-field settings.

The overarching aim of this thesis was to **reconstruct abrupt, high-magnitude sea-level changes from near-field settings.** I have targeted two, temporally distinct types of high-magnitude RSL changes for reconstruction: i) sub-centennial scale episodes of rapid RSL rise (attributed to meltwater-induced accelerations in global SLR) and, ii) singularities of RSL rise on the order of minutes to hours (namely tsunamis and storms). To achieve this aim, this thesis addressed the following objectives:

- To determine; using litho-, bio- and chronostratigraphy of raised salt-marsh and estuarine deposits, the timing and magnitude of sea-level changes in the Cree Estuary, SW Scotland, between a critical time period of 9000 to 8000 cal yr BP.
- To compare the timing and magnitude of sea-level changes in the Cree record with those in a range of coastal and non-coastal archives from around the globe, in order to assess the drivers responsible for such changes.
- To assess the evidence for abrupt singularities of RSL rise (storm events, iceberg- and landslide-generated tsunami) using litho-, bio- and chronostratigraphy of coastal lakes and nearshore sedimentary sequences in west Greenland.
- To assess whether the patterns and signatures of deposition associated with abrupt RSL change can be used to infer driving (source) mechanisms.
- To reflect on the opportunities and challenges with regards to reconstructing abrupt RSL change in near-field settings and identify future research directions.

The following details how these objectives were addressed and the key findings from this work.

7.2 Key findings

To determine; using litho-, bio- and chronostratigraphy of raised salt-marsh and estuarine deposits, the timing and magnitude of sea-level changes in the Cree Estuary, SW Scotland, between a critical time period of 9000 to 8000 cal yr BP

Long-term millennial-scale RSL changes in the Cree Estuary were reported by Smith et al. (2003). This paper provided the impetus for the work presented in this Chapter 2. At Blair's Croft, one of the sites that contributed sea-level data to the Smith et al. (2003) record, radiocarbon dating of raised estuarine and saltmarsh deposits revealed a sequence marked by unusually high rates of sediment supply dated to 9.0 to 8.0 kyr BP. Given the close coincidence with the timing of the 8.2 event and sea-level jumps observed elsewhere in the North Atlantic, this thesis investigated the potential of the sedimentary record to contain evidence for abrupt RSL change(s) associated with the 8.2 ka event. Chapter 2 investigates the Blair's Croft stratigraphy in more detail with fifty hand- and piston-cores, high-resolution microfossil (diatom) analysis and radiocarbon dating.

The stratigraphy at Blair's Croft records a gradually rising RSL of 6-5 mm/yr between 8.8 to 7.8 kyr BP, superimposed upon which are three decimetre-metre scale inflexions ('jumps') in the rate of RSL rise. These occurred within a short 500 yr time interval leading up to 8.2 kyr BP. The first episode registered a RSL rise of 0.38 ± 0.19 m at 8680-8610 cal yr BP, the second 0.88 ± 0.19 m (8550-8450 cal yr BP) and the third 0.22 ± 0.22 m (8231-8163 cal yr BP). The site stratigraphy and topography suggest that local barrier morphodynamics may have influenced sediment supply and hence record development. To resolve the potential importance of local versus global drivers, I compared the timing of the Cree RSL jumps with other episodes of abrupt change observed in a range of coastal and non-coastal archives from around the North Atlantic (below).

To compare the timing and magnitude of sea-level changes in the Cree record with those in a range of coastal and non-coastal archives from around the globe, in order to assess the drivers responsible for such changes

The Cree RSL jumps overlap in timing with abrupt events recorded in various proxy records from the North Atlantic Ocean and fringing coastal environments. These abrupt events are unique in the Holocene RSL record. A comparison of ages reveals three distinct time periods in the centuries prior to 8.2 kyr BP where the age of events overlap, but with mid-points separated by up to two centuries. In particular, all three of the Cree RSL jumps overlap in timing with three notable episodes of enhanced ice-sheet retreat documented within an exceptionally resolved near-field sea-bed record of LIS activity (Jennings et al.,

2015). There is also significant overlap in timing with RSL jumps documented in two key RSL records from the western Netherlands (Hijma and Cohen, 2010) and southern USA (Li et al., 2011). The final age group includes the onset of the 8.2 event as recorded in Greenland ice-core records. However, the radiocarbon dating technique is currently unable to resolve the short time periods between events. As a result, the observations are unable to validate but strongly support the hypothesis that the LIS retreated in a non-linear fashion during the early Holocene (Carlson et al., 2008) and that this contributed to the onset of the 8.2 event (e.g. Barber et al., 1999). In light of the dating limitations, future work should focus on sequencing events into plausible, testable scenarios. To this end, I finish Chapter 2 by speculating on the underlying source mechanisms responsible for each freshwater discharge event and their role in forcing the 8.2 event, from which I propose a three-event model of freshwater release involving proglacial lake drainage events and dynamical ice-sheet contributions in the 500 yr time window prior to 8.2 kyr BP.

To search for evidence of abrupt singularities of RSL rise (storm events, iceberg- and landslide-generated tsunami) using litho-, bio- and chronostratigraphy of coastal lakes and nearshore sedimentary sequences in west Greenland

Chapter 4 presents the litho-, bio- and chronostratigraphy of Lake VA1, a coastal freshwater lake situated ~5m above present MSL in Vaigat, west Greenland. The biostratigraphic record of the lake contains evidence of five separate marine inundation events in the past c. 2300 yrs, implying an average return period of one event per c. 600 yrs. In the last millennium the average return period of events increases to c. 330 yrs. Similarly evidence from nearshore sedimentary records from two sites situated c. 3.5 km apart imply an average frequency of one event per 250-500 yrs (Chapter 3). This is more frequent in comparison to a previous estimate of one event per 1000 yrs inferred from geomorphological mapping of landslide back-scars on the northern coast of Vaigat Strait (Dahl-Jensen et al., 2004), although the examples in this thesis reflect both landslide- and iceberg-driven tsunami deposition, in addition to possible storm deposition. Determining the precise mechanism of emplacement that is responsible for each deposit however, is difficult given a lack of clear criteria to uniquely separate abrupt event deposits. Where landslides provide a chance to map and directly date sources, for iceberg and storms the drivers no longer exist and one relies on attributing “orphan” events to processes based on a range of less diagnostic criteria, such as site context.

Chapter 5 presents the first record of iceberg-generated tsunami from west Greenland based on high-resolution biostratigraphy and new radiocarbon dating of isolation basin deposits from Lake IV4 at Innaarsuit, Disko Bugt. This builds on initial stratigraphic analyses of Long et al. (2003). The site is situated in a sheltered fjord setting c. 100 miles to the southeast of Vaigat where it is beyond the influence of landslide-generated tsunamis. Furthermore, wave set-up in the fjord is limited which enables the ruling out of storm inundation as a candidate for deposition. The stratigraphic characteristics of the marine deposits are similar to those noted by Bondevik et al. (1997b) based on their analysis of the sedimentary record of the early Holocene Storegga tsunami within Norwegian coastal lakes. Assuming a mid-tide event and considering the height of basin with respect to RSL at the reconstructed time of the event, the tsunami attained a vertical run-up height of 5.0 – 1.3 m. The work demonstrates the potential for iceberg-related processes to influence coastal processes in near-field settings.

To assess whether the patterns and signatures of deposition associated with abrupt RSL change in west Greenland can be used to infer driving (source) mechanisms

A major outcome of this thesis is that at present there are no clear stratigraphic criteria that can distinguish between the various potential driving mechanisms of tsunami in west Greenland (Chapters 3, 4, and 5). While local testimony in Vaigat supports a landslide source for the AD 1952 and AD 2000 events, the associated deposits offer no clear distinction when compared to iceberg-tsunami or storm deposits reported from Innaarsuit and elsewhere in Vaigat. Likewise, the iceberg-tsunami deposit at Innaarsuit offers no clear distinction between the Storegga tsunami deposits found in the circum-North Atlantic (e.g. Bondevik et al., 1997b). Inferring the likely driving mechanism of an event is restricted to considering less diagnostic criteria, in particular the spatial extent of the deposit, site context and the perceived maximum extents of different types of tsunami.

To reflect on the opportunities and challenges with regards to reconstructing abrupt RSL change in near-field settings

Chapter 6 discusses the challenges and opportunities with regards to reconstructing abrupt RSL change in near-field areas. A key theme is that stratigraphic records are highly variable because sediment delivery to near-field coasts is strongly variable, reflecting the influence of both local and non-local processes. In particular sediment delivery is controlled locally by

paraglacial processes (reworking of glacial deposits), geomorphic activity (solifluction and mass movements) and non-locally by upstream glacier fluctuations. In turn these processes are strongly influenced by both short- and long-term climatic fluctuations. The opportunity that can be drawn from this however is that these dynamic, albeit often transient sources of sediment supply that are inherent to near-field environments can, at times, deliver large volumes of fine-grained sediment to the coastal zone, facilitating the high sediment accumulation rates required to develop high resolution records.

7.3 Concluding remarks

To conclude, this thesis has explored how near-field areas can act as both sources and depositories of abrupt RSL change. Whilst the fundamental controls on coastal evolution are the same in near-, intermediate- and far-field coastal environments, there are a number of additional processes in operation that are unique to near-field regions. Near-field coasts are innately dynamic; experiencing rapid rates of GIA, RSL change and sediment supply. In contrast to lower latitude sites where high-magnitude events are preserved as stand-alone 'punctuation' events within the stratigraphic record, equivalent events occur at a higher frequency in near-field regions. In contrast, intermediate-field coasts are less dynamic; experience slower rates of RSL change, reduced sediment supply, more vegetation and organic productivity. These provide excellent conditions for reconstructing ice-equivalent volume RSL changes with high resolution, albeit at the temporal limit of the mid to late Holocene (e.g. US East coast salt marshes; Kemp et al., 2011). Hence, most intermediate-field sites are unable to resolve early Holocene RSL changes. Similarly far-field regions produce excellent coral-based records for the deglacial but are too imprecise to reconstruct lower-magnitude ice-equivalent sea-level changes from the early Holocene to present. Accordingly, near-field paraglacial regions offer scope to bridge the temporal gap by further extending the application of high resolution RSL reconstruction techniques into the early Holocene.

7.4 Future research

Much of this work was completed against the backdrop of little or no baseline data to compare against, and I hope this thesis will provide the stimulus for future work in near-field regions, specifically in regard to the study of abrupt RSL change. Although there are clear limitations related to near-field reconstructions of abrupt change (as discussed in each

chapter), there are also exciting opportunities. Borne out of this thesis, the following is a range of potential avenues for further work.

Isolation basin constraints on the timing and magnitude of 8.2-related meltwater pulses: western Scotland

This PhD research has identified that episodes of non-linear meltwater release in the 500 yrs prior to the 8.2 event equated, once corrected, to a combined ~2 m of global sea-level rise. This represents an amount that could be constrained by isolation basin records from western Scotland. A notable record is from Arisaig, which has been used to constrain deglacial RSL changes and the timing and magnitude of MWP-1A (Shennan et al., 2005). Interestingly, this record demonstrates metre-scale variability around 8.2 kyr BP (basins at ~8 m above present MSL). In this part of Scotland, RSL was rising more slowly compared to the farther south in the Cree Estuary because of the greater influence of GIA; ideal background conditions for reconstructing the 8.2-related sea-level jumps. A region of potential interest is the Isle of Skye where isolation basins form dense networks of staircases (e.g. Selby and Smith, 2007). Thus, this area offers good potential to develop a long-term record similar to that of Arisaig, from which it might be possible to constrain the timing and magnitudes of deglacial and early Holocene meltwater pulses.

Isolation basin constraints on iceberg roll events: Scotland

The Arisaig record demonstrates that RSL in western Scotland fell rapidly from ~30-10 m above present MSL between ~16-10 kyr BP. As glacier retreat would have fed large volumes of terrestrial ice into Scottish coastal waters, there is high potential that many of these icebergs would have become trapped in constrained topographical settings. Scottish isolation basins might therefore harbour evidence of iceberg roll during the deglacial period.

Evidence of Scottish isolation basins as potential abrupt event depositories is illustrated by Shennan et al. (1999), who recognized numerous thin (sub millimetre-thick), discrete coarse-grained laminae within the isolation basin stratigraphy of Rumach VI, Morar, western Scotland. These were unlikely to have been deposited by an iceberg roll event as Rumach VI isolated late into the Holocene at ~7 kyr BP. However, Shennan et al. (1999) attempted to resolve the origin of the deposit using high resolution microfossil sampling at 1

mm resolution across the critical section of core. Results were deemed inconclusive as no marine microfossils were found (Shennan et al., 1999).

The results from this study support the conclusions of Davies and Haslett (2000) who, in a simple model, quantify that there is an exceptionally low probability of recovering marine microfossils within freshwater lake sequences. In this thesis microfossil slides from the two lakes sampled required complete scanning to identify marine taxa as these were exceptionally rare and obscured by the freshwater assemblage. I suspect that a similar sampling strategy applied to the deposits in Rumach VI would lead to the identification of marine microfossils, thereby confirming a marine origin of deposits. It is likely that this approach will need to be applied consistently in the study of abrupt events in Scottish isolation basins.

Developing a fully integrated climate and sea level record for the Cree Estuary

Elucidating the relationships between sea-level and climate is difficult because interpretations always rely on the assumption that independent chronologies are accurate (e.g. Rohling et al., 2014). Against the inability to assess the accuracy of independent chronologies with full confidence, one way to circumvent this issue is to develop fully integrated records of climate and RSL change from single stratigraphic sequences. As mentioned previously in this chapter, the minerogenic deposits that comprise large sections of the Cree stratigraphy contain fossil foraminifera (calcareous forms). A growing body of work is beginning to illustrate that benthic foraminifera from shallow water settings can be successfully used as environmental proxies with stable isotope analysis (e.g. Debenay et al., 2000; Duchemin et al., 2005, Murray, 2006), albeit often demonstrating severe spatial and temporal variability (e.g. Murray and Alve, 2000; Buzas et al., 2002). Despite the potential for variability, there is also potential to 'correct' these records using other environmental proxies in a modern analogue approach (e.g. Diz et al., 2009). It would therefore be interesting to analyze calcareous foraminifera preserved within the Cree record for stable isotopes in order to assess the evidence of a wider climate signal. If stable isotope concentrations reflect wider climatic changes then the 8.2 signal will be registered within the event stratigraphy, facilitating more robust assessment of the interrelationship of climate and sea level during this critical phase of the Holocene.

Isolation basin constraints on mid Holocene RSL change and iceberg roll events: west Greenland

The characteristic 'j-shaped' RSL history of west Greenland is marked by three notable outliers between 7-5 kyr BP that appear to give the impression of a slowdown in the rate of RSL fall. These are from widely spaced sites; a first is from Avreprinsens Eijland (Long et al., 1999), the second from Disko Fjord (southern Disko Island; Long et al., 2011) and the third from Qivitutt (also southern Disko Island; Bennike, 1995). Long et al. (2011) provided reasons to discount the notion of a real RSL slowdown in the mid Holocene. Plausibly, these basins contain disturbed stratigraphies (Long et al., 2011). A potential candidate for the cause of this disturbance is an iceberg-generated tsunami. Nevertheless, the clustering of three outliers within the same c. 1000 yr window is an interesting find. Resolving the reasons behind these outlying points is important given that a mid Holocene slowdown in the rate of RSL rise would signify the existence of an unknown GIA mechanism, pointing to either a local (Greenland) or non-local (Canadian) ice-sheet response (Long et al., 2009). Interestingly, the mid Holocene period constitutes a period of climate variability in Greenland (e.g. Funder and Hansen, 1996; Eisner et al., 1995).

During the summer 2012 field season I encountered a sloping, shore-parallel bedrock ramp, protected at its seaward extent by a bedrock buttress. The stratigraphy of the ramp comprises a ~50 cm deep intercalated sequence formed of two separate peat-clay couplets. Vertically the sequence is positioned ~8-15 m above present MSL. If these sediments were deposited at or near sea level then their elevations imply a mid Holocene origin. The fine-grained sediments are unique to this elevation and it is difficult to attribute their deposition to processes not related to sea level. Also encountered were relic barrier shorelines and raised beaches at the same elevation. This either implies that, a) the coastal zone received a large increase in sediment supply at this time or, b) that the coarse-clastic barrier structures and raised beaches formed during a period of relatively stable RSL. Indeed, Rasche and Nielsen (1995) describe similar morpho-sedimentary structures on the southern coast of Disko Island, near to where two of the three outlying sea-level index points were recovered. The sloping ramp sediments thus offer the opportunity to test the hypothesis of a mid Holocene RSL slowdown. If a sea level-sedimentary relationship can be confirmed with microfossil analyses, this would facilitate the development of a novel sea level reconstruction for the mid Holocene with unusually high resolution. RSL observations from

this time period will be important in constraining the local/regional response of the Greenland Ice Sheet to climate fluctuations within a period of known climatic instability.

References

Barber, D.C., Dyke, A., Hillaire-Marcel, C., Jennings, A.E., Andrews, J.T., Ker- win, M.T., Bilodeau, G., McNeely, G., Southon, J., Morehead, M.D., and Gagnon, J.-M. 1999. Forcing of the cold event of 8,200 years ago by catastrophic drainage of Laurentide lake: *Nature* 400. 344–348, doi: 10.1038/22504.

Bennike, O., 1995. Palaeoecology of two lake basins from Disko, West Greenland. Journal of Quaternary Science 10, 149-155.

Bondevik, S., Svendsen, J.I., Johnsen, G., Mangerud, J., Kaland, P.E., 1997b. The Storegga tsunami along the Norwegian coast, age and runup. Boreas 26, 29–53.

Buzas, M. A., Hayek, L.-A., Reed, S. A., and Jett, J. A.: Foraminiferal densities over five years in the Indian River Lagoon, Florida: A model of pulsating patches, J. Foramin. Res., 32, 68–93, 2002

Carlson, A.E., LeGrande, A.N., Oppo, D.W., Came, R.E, Schmidt, G.A., Anslow, F.S., Licciardi, J.M., Obbink, E.Z. 2008. Rapid early Holocene deglaciation of the Laurentide Ice Sheet. Nature Geoscience 1, 620-624.

Dahl-Jensen, T., Larsen, L.M., Pedersen, S.A.S., Pedersen, J., Jepsen, H.F., Pedersen, G.K., Nielsen, T., Pedersen, A.K., Platen-Hallermund, F.V., Weng, W. 2004. Landslide and tsunami 21 November 200 in Paatuut, West Greenland. *Natural Hazards*, 31, 277-287.

Davies, P., Haslett, S.K. 2000. Identifying storm or tsunami events in coastal basin sediments. *Area* **32**(3), 335-336.

Debenay, J.-P., Guillou, J.-J., Redois, F., and Geslin, E.: Distribution trends of foraminiferal assemblages in paralic environments: a base for using foraminifera as bioindicators, in: Environmental Micropaleontology. The application of microfossils to environmental geology, edited by: Martin, J. E., Topics in Geobiology, Kluwer Academic/Plenum Publishers, New York, USA, 39–67, 2000.

Diz, P., Jorissen, F. J., Reichart, G. J., Poulain, C., Dehairs, F., Leorri, E., and Paulet, Y.-M. 2009. Interpretation of benthic foraminiferal stable isotopes in subtidal estuarine environments, Biogeosciences, 6, 2549-2560, doi:10.5194/bg-6-2549-2009

Duchemin, G., Jorissen, F. J., Redois, F., and Debenay, J.-P.: Foraminiferal microhabitats in a high marsh: Consequences for reconstructing past sea levels, Palaeogeogr. Palaeocl., 226, 167– 185, 2005.

Eisner WR, Tornqvist TE, Koster EA, Bennike O, van Leeuwen JFN. 1995. Paleoecological studies of a Holocene lacustrine record from the Kangerlussuaq (Søndre Strømfjord) region of West Greenland. Quaternary Research 43: 55–66

Funder, S., Hansen, L., 1996. The Greenland ice sheet - a model for its culmination and decay during and after the last glacial maximum. Bulletin of the Geological Society of Denmark 42, 137e152.

Hijma, M.P and Cohen, K.M. 2010. Timing and magnitude of the sea-level jump precluding the 8200 yr event, *Geology* **38**, 3, 275-278.

Jennings, A., Andrews, J., Pierce, C., Wilson, L., Olfasdotttir, S. 2015. Detrital carbonate peaks on the Labrador shelf, a 13e7 ka template for freshwater forcing from the Hudson Strait outlet of the Laurentide Ice Sheet into the subpolar gyre, *Quaternary Science Reviews* **107**, 62-80. http://dx.doi.org/10.1016/j.quascirev.2014.10.022.

Kemp, A.C., Horton, B.P., Donnelly, J.P., Mann, M.E., Vermeer, M., Rahmstorf, S. 2011. Climate related sea-level variations over the past two millennia. Proceedings of the National Academy of Sciences 108, 27, 11017-11021.

Li, Y.X., Tornqvist, T.E., Nevitt, J.M., and Kohl, B. 2011. Synchronizing a sea-level jump, final lake Agassiz drainage and abrupt cooling 8200 years ago, *Earth and Planetary Science Letters* **315-316**, 41-50.

Long, A.J., Roberts, D.H., Rasch, M. 2003. New observations on the relative sea level and deglacial history of Greenland from Innaarsuit, Disko Bugt. Quat Res 60: 162-171

Long A.J,. Roberts, D.H., Wright, M.R., 1999. Isolation basin stratigraphy and Holocene relative sea-level change on Arveprinsen Eijland, Disko Bugt, West Greenland. J Quat Sci 14: 323-345

Long, A.J., Woodroffe, S.A., Roberts, D.H., Dawson, S. 2011. Isolation basins, sea-level changes and the Holocene history of the Greenland Ice Sheet. Quat Sci Rev 30: 3748-3768

Long, A.J., Woodroffe, S.A., Dawson, S., Roberts, D.H., Bryant, C.L. 2009. Late Holocene relative sea level rise and the Neoglacial history of the Greenland ice sheet. Journal Quaternary Science, 24, 4, 345-359.

Murray, J. W., and Alve, E. 2000. Major aspects of foraminiferal variability (standing crop and biomass) on a monthly scale in an intertidal zone, J. Foramin. Res., 30, 177–191.

Rasch M, Nielsen N. 1995. Coastal morpho-stratigraphy and Holocene relative sea-level changes at Tuapaat, southeastern Disko Island, central West Greenland. Polar Research 14: 277–289.

Rohling, E.J., Foster, G.L., Grant, K.M., Marino, G., Roberts, A.P., Tamisiea, M.E. and Williams, F. 2014. Sea-level and deep-sea temperature variability over the past 5.3 million years, *Nature* **508**, 477-482.

Selby, K.A., Smith, D.E. 2007. Late Devensian and Holocene relative sea-level changes on the Isle of Skye, Scotland, UK. Journal Quaternary Science, 22, 2, 119-139.

Shennan, I., Hamilton, S., Hillier, C., Woodroffe, S. 2005. A 16,000-year record of near-field relative sea-level changes. Northwest Scotland, United Kingdom. Quaternary International 133-134, 95-106.

Shennan, I., Tooley, M., Green, F., Innes, J., Kennington, K., Llloyd, J.,. Rutherford, M. 1999. Sea level, climate change and coastal evolution at Morar, northwest Scotland, *Geologie en Mijnbouw*, 77, 247-262.

Smith, D.E., Wells, J.M., Mighall, T.M., Cullingford, R.A., Holloway, L.K., Dawson, S., Brooks, C.L. 2003a. Holocene relative sea levels and coastal changes in the lower Cree valley and estuary, SW Scotland, UK. *Transactions of the Royal Society of Edinburgh: Earth Sciences*, **93,** 301-331.